TECHNICAL REPORT SL-88-37

STATIC TESTS OF SHALLOW-BURIED REINFORCED CONCRETE ARCHES

by

Frank D. Dallriva, Robert L. Hall

Structures Laboratory

DEPARTMENT OF THE ARMY
Waterways Experiment Station, Corps of Engineers
PO Box 631, Vicksburg, Mississippi 39181-0631

September 1988
Final Report

Defense Nuclear Agency
Washington, DC 20305

Unclassified

SECURITY CLASSIFICATION OF THIS PAGE

REPORT DOCUMENTATION PAGE

Form Approved
OMB No 0704-0188
Exp Date Jun 30, 1986

1a REPORT SECURITY CLASSIFICATION Unclassified	1b RESTRICTIVE MARKINGS
2a SECURITY CLASSIFICATION AUTHORITY	3 DISTRIBUTION / AVAILABILITY OF REPORT Approved for public release; distribution unlimited.
2b DECLASSIFICATION / DOWNGRADING SCHEDULE	
4 PERFORMING ORGANIZATION REPORT NUMBER(S) Technical Report SL-88-37	5 MONITORING ORGANIZATION REPORT NUMBER(S)
6a NAME OF PERFORMING ORGANIZATION USAEWES Structures Laboratory 6b OFFICE SYMBOL (If applicable) CEWES-SS-R	7a NAME OF MONITORING ORGANIZATION
6c ADDRESS (City, State, and ZIP Code) PO Box 631 Vicksburg, MS 39181-0631	7b ADDRESS (City, State, and ZIP Code)
8a NAME OF FUNDING / SPONSORING ORGANIZATION Defense Nuclear Agency 8b OFFICE SYMBOL (If applicable)	9 PROCUREMENT INSTRUMENT IDENTIFICATION NUMBER
8c ADDRESS (City, State, and ZIP Code) Washington, DC 20305	10 SOURCE OF FUNDING NUMBERS PROGRAM ELEMENT NO / PROJECT NO / TASK NO / WORK UNIT ACCESSION NO 100

11 TITLE (Include Security Classification)
Static Tests of Shallow-Buried Reinforced Concrete Arches

12 PERSONAL AUTHOR(S)
Dallriva, Frank D., and Hall, Robert L.

13a TYPE OF REPORT	13b TIME COVERED	14 DATE OF REPORT (Year, Month, Day)	15 PAGE COUNT
Final Report	FROM _____ TO _____	September 1988	236

16 SUPPLEMENTARY NOTATION
Available from National Technical Information Service, 5285 Port Royal Road, Springfield, VA 22161.

17 COSATI CODES			18 SUBJECT TERMS (Continue on reverse if necessary and identify by block number)
FIELD	GROUP	SUB-GROUP	See reverse.

19 ABSTRACT (Continue on reverse if necessary and identify by block number)

The determination of the loads on and behavior of shallow-buried arch structures is complicated by the geometry of the arch and by the existence of soil-structure interaction effects. A common approach to the analysis of buried arches is to idealize the structure as a lumped parameter single-degree-of-freedom (SDOF) system. The parameters which must be assumed for input into the SDOF model include a loading function and a structural resistance-deflection relationship.

The applied load on a buried arch due to overpressure at the ground surface includes a radial and a tangential component. The radial component can be measured experimentally; however, there seem to be no available transducers to measure the tangential component or interface friction.

(Continued)

20 DISTRIBUTION / AVAILABILITY OF ABSTRACT ☒ UNCLASSIFIED/UNLIMITED ☐ SAME AS RPT ☐ DTIC USERS	21 ABSTRACT SECURITY CLASSIFICATION Unclassified
22a NAME OF RESPONSIBLE INDIVIDUAL	22b TELEPHONE (Include Area Code) / 22c OFFICE SYMBOL

DD FORM 1473, 84 MAR 83 APR edition may be used until exhausted
All other editions are obsolete

SECURITY CLASSIFICATION OF THIS PAGE
Unclassified

18. SUBJECT TERMS (Continued).

Air blast simulation,
Arch structures
Concrete structures,
Hardened installation,
Shallow buried structures,
Soil arching
Soil structure interaction,
Static tests
Structural response
Survivability,
Underground structures,
Vulnerability.

19. ABSTRACT (Continued).

Two 1/12-scale model reinforced concrete arches were tested statically in a sand backfill. The arches were semicircular with an inside radius of 1 foot 9 inches and a thickness of 2 inches. One arch was covered with two layers of 1/32-inch-thick Teflon at the soil-structure interface to significantly reduce the interface friction, and the loading and behavior of the two arches were compared. Pretest finite element calculations were conducted to estimate the arch behavior.

Based on both the experimental data and posttest calculations, it appears that interface friction on a shallow-buried arch has an effect on its behavior, at least for the case of static loads. The load path at sections in the arch with a lower friction coefficient at the interface tended more toward pure compression than it did in the other arch.

SUMMARY

The determination of the loads on and behavior of shallow-buried arch structures is complicated by the geometry of the arch and by the existence of soil-structure interaction effects. A common approach to the analysis of buried arches is to idealize the structure as a lumped parameter single-degree-of-freedom (SDOF) system. The parameters which must be assumed for input into the SDOF model include a loading function and a structural resistance-deflection relationship.

The applied load on a buried arch due to overpressure at the ground surface includes a radial and a tangential component. The radial component can be measured experimentally; however, there seem to be no available transducers to measure the tangential component or interface friction.

Two 1/12-scale model reinforced concrete arches were tested statically in a sand backfill. The arches were semicircular with an inside radius of 1 foot 9 inches and a thickness of 2 inches. One arch was covered with two layers of 1/32-inch-thick Teflon at the soil-structure interface to significantly reduce the interface friction, and the loading and behavior of the two arches were compared. Pretest finite element calculations were conducted to estimate the arch behavior.

Based on both the experimental data and posttest calculations, it appears that interface friction on a shallow-buried arch has an effect on its behavior, at least for the case of static loads. The load path at sections in the arch with a lower friction coefficient at the interface tended more toward pure compression than it did in the other arch.

PREFACE

The research reported herein was sponsored by the Defense Nuclear Agency (DNA) under Subtask Y99QMXSC, Work Unit 100, "Shallow-Buried Structures." Mr. Jim Cooper, DNA, was Technical Monitor.

The construction and testing were conducted by personnel of the Structures Laboratory (SL), US Army Engineer Waterways Experiment Station (WES), under the general supervision of Messrs. Bryant Mather, Chief, SL, and J. T. Ballard, Assistant Chief, SL; and Dr. J. P. Balsara, Chief, Structural Mechanics Division (SMD), SL; and under the direct supervision of Dr. S. A. Kiger of the Research Group, SMD. This report was prepared by Mr. F. D. Dallriva, and Mr. R. L. Hall of the Research Group, SMD, and was edited by Mr. Bobby Odom, Information Technology Laboratory, under the Inter-Governmental Personnel Act.

COL Dwayne G. Lee, EN, is the Commander and Director of WES. Dr. Robert W. Whalin is the Technical Director.

CONTENTS

LIST OF ILLUSTRATIONS

CONVERSION FACTORS, NON-SI TO SI (METRIC)
UNITS OF MEASUREMENT

Non-SI units of measurement used in this report can be converted to SI (metric) units as follows:

Multiply	By	To Obtain
degrees (angle)	0.01745329	radians
feet	0.3048	metres
inches	2.54	centimetres
pounds (force)	4.448222	newtons
pounds (force) per square inch	6.894757	kilopascals
pounds (mass) per cubic foot	16.01846	kilograms per cubic metre

STATIC TESTS OF SHALLOW-BURIED REINFORCED CONCRETE ARCHES

SECTION 1

INTRODUCTION

1.1 BACKGROUND

Reinforced shallow-buried, concrete arch structures are often used in protective construction applications. Structures designed to resist the dynamic loads produced by nuclear detonations are expected to undergo significant inelastic deformations. The determination of the loads on buried structures is complicated by the geometry of the arch and by the existence of soil-structure interaction effects (SSI). Due to SSI the structure and the soil act as a synergistic unit, and it must be determined how the loads which act on the buried structure are influenced by this interaction between the structure and the surrounding soil. Advances in finite element methods (FEM) have resulted in improved design-analysis capabilities for complex systems such as this; however, to use the FEM to analyze and design every buried arch would be very expensive and impractical. A common approach to the analysis of buried arches is to idealize the structure as a lumped parameter single-degree-of-freedom (SDOF) system whose properties correspond to the mode of failure. The mode of failure of a particular structural element such as an arch can be determined by experimental testing and verified by the use of the FEM. The parameters which must be assumed for input into the SDOF model include a loading function and a structural resistance-deflection relationship. The resistance of an element is the internal force tending to restore the element to its unloaded static position and is defined in terms of the load distribution for which the analysis is made. The maximum resistance is the total load having the given distribution which the element could support statically.

The applied load on a buried arch due to overpressure at the ground surface normally includes a radial and a tangential component. These forces are not simply a function of the overpressure but are also related to the flexibility of the structure and the soil characteristics. The radial component of the load can be accurately measured experimentally by the use of interface pressure gages mounted flush with the structure surface at the soil-structure interface. The magnitude of the tangential component or skin friction, which

is a function of the normal force and the friction angle between the soil and the structure, is difficult to quantify experimentally. This is due to the nature of the frictional force, a shear force parallel to the surface of the arch at the soil-structure interface. The surface of any gage measuring this frictional force must have a surface similar to the surface of the surrounding structure. Previous attempts to accurately measure these frictional forces have, in general, been unsuccessful. At present there seems to be no available transducer to measure the interface friction accurately.

1.2 PREVIOUS ARCH TESTS

Very few arches have been tested to collapse; however, some have been tested well into the plastic range of response. Previous arch tests (References 1-3) indicate that buried arches subjected to overpressures applied to the soil surface appear to respond in a combination of a compressive mode and a symmetric bending mode. In most of these tests, flexural behavior resulted in positive bending (tension on the inside face) at the crown and negative bending (tension on the outside face) at about 45 degrees.*

Static and dynamic tests were conducted by Meyer and Flathau (Reference 1) on unreinforced concrete model arches buried in dry sand. The arches responded generally in a compressive mode. Internal moment in the arch rings was generally positive at the crown with an inflection point between 35 and 60 degrees and with negative moment from the inflection point down to the springline. Since there was no steel reinforcing in the arches and concrete is weak in tension, these arches would have failed at much lower pressures had the failure mode not been predominately compression.

Munn, Carre, and Kennedy (Reference 2) conducted static tests of steel circular arches buried in sand. The parameters which were varied included the footings, arch flexibility, and depth of burial. The modes of failure included buckling of the arch haunches in the thinner arches and arch crown buckling in the thicker arches. Arches which had narrow footings responded by the footing punching into the soil. The depth of burial had an influence on the required failure overpressure in that the greater the depth of burial, the higher the surface pressure required for failure.

---

* A table of factors for converting non-SI units of measurement to SI (metric) units is presented on page viii.

Meyerhof (Reference 3) conducted tests of steel model arches of different sizes, shapes, and stiffnesses buried in sand and clay fills with various strengths and depths of burial. The arches were subjected to a static, uniformly distributed load at the soil surface. At any given load the observed circumferential axial stresses and thus the corresponding thrust were fairly constant around the arches. As buckling failure was approached, the circumferential bending stresses in the arches were about one-fourth to one-half of the axial stresses. The vertical deflections of the crown of the arches at failure varied from about 1 to 4 percent of the span for the semicircular arches and about 3 to 8 percent of the major diameter for the three-centered arches.

Gill and Allgood (Reference 4) statically tested shallow-buried steel arches in a sand backfill. The two arches tested were identical except that one had footings twice as wide as the other. The objectives were to determine the deflection, thrust, and moment distributions; to learn something of the interface pressure distribution; and to investigate the phenomenon of soil arching. Wiehle (Reference 5) defines soil arching as the ability of the soil, by virtue of its shear strength, to redistribute the stress in the vicinity of an inclusion. For a soil mass undergoing large strains, a relatively stiff structure would be subjected to a total stress greater than the free-field stress while a relatively soft structure would be subjected to a total stress less than the free-field stress. For complex structures it is a combination of the two types, and the total stress may be greater or less than the free-field stress. Reference 4 indicates that for a dry granular backfill, the static behavior is primarily dependent upon the soil density, the footing width, the radius of the arch, the depth of cover over the crown, and the stiffness of the structure. The deflection of both arches under surface loading consisted primarily of a downward body motion with some bulging of the sides and flattening of the top. As the overpressure increased, the flattening of the top continued, but the outward movement of the sides stopped. Although the deflection of the narrow footings was much greater than that of the wide footings, the crown deflection relative to the footings was nearly the same for both arches. The peak moment in both arches developed in the vicinity of 5 degrees from the horizontal. At corresponding overpressures, the peak moment in the arch with wide footings was approximately a factor of 4 larger than the peak moment in the arch with narrow footings. The thrusts in

both structures were much the same at the crown but differed markedly in the vicinity of the footings.

1.3 CURRENTLY USED ANALYSIS PROCEDURES

Haltiwanger (Reference 6) presents equations for the resistance of shallow-buried arches. The arch is assumed to respond in two modes, a uniform compression and a flexural mode as shown in Figure 1. The uniform compression mode is characterized by uniform ring compression under a constant uniform radial pressure, and the flexural mode is a side sway, moving inward on one side and outward on the other, with a point of zero moment at the crown. The assumed loading in the flexural mode is uniform and acts radially inward on one-half of the arch and radially outward on the other half. These loadings do not include any interface friction forces. It appears from the previously discussed tests that the asymmetric mode of response is very unlikely because the soil confines the arch ring and restricts its ability to deflect outward. The symmetric flexural mode, observed in some of the tests, is a higher order mode than the asymmetric mode and, therefore, results in a stiffer structure. The resistance function for the compression mode is assumed to be bilinear as shown in Figure 2 with a constant resistance beyond the elastic limit. The maximum resistance for a concrete arch is given by

$$q_{y_c} = (0.85\ f'_c + 0.9\ p_t\ f_y)\ Ac/12r \qquad (1)$$

where

q_{y_c} = ultimate resistance per unit roof area, psi*
f'_c = concrete strength, psi
p_t = total steel ratio
f_y = steel yield strength, psi
Ac = cross-sectional area of concrete (square inches) per longitudinal of arch length
r = arch radius, feet

The weight of the soil over the arch is subtracted from this value to obtain the net maximum resistance. Haltiwanger gives an equation for the natural

---

* For convenience, symbols and abbreviations are listed in the Notation (Appendix C).

period T of the arch in this mode and the stiffness k can be obtained from the relationship

$$T = 2\pi \frac{m}{k} 0.5 \qquad (2)$$

where m is the mass of the system. The resistance given for the compression mode of response is an upper bound solution, i.e., if the arch responded in the compression mode only, it would carry the greatest amount of load.

Flathau, Bryant, and Mlakar (Reference 7) present an SDOF model which assumes a simplified loading condition and response mode shown in Figure 3. The assumed resistance corresponding to this response mode is shown in Figure 4. As shown, the horizontal stress is equal to the vertical stress multiplied by the factor K . The factor K is assumed to increase with increasing load. The resistance function is based on the assumption that the arch will respond in the compression regime, i.e., between the balance point and the point of pure compression on the arch moment-thrust interaction diagram. For a fixed-end arch, it is initially assumed that the moment-thrust path will approach the balance point of the interaction diagram. When the moment capacity at the spring line is exceeded, plastic hinges form, and the arch is considered to act as a two-hinged arch. For the two-hinged arch, the maximum moment occurs at 25 degrees up from the spring line; however, the crown is also very close to maximum capacity and with a slight increase in load, a hinge also forms at the crown. The stiffness of the arch decreases, and as the load and K increase, the moment capacity at a critical section is reached. However, the constraint supplied by the soil is assumed to prevent collapse of the arch due to the formation of hinges at 25 degrees. A hinge is assumed, however, to form at the crown, and the arch now behaves as a three-hinged arch. The value of K increases with the load, and at some appropriate value of K and load, the moment capacity of the arch at 30 degrees from the spring line is exceeded. With each hinge development, the arch ring becomes less stiff and is capable of more centerline deflection even though K , which helps to stiffen the arch, increases.

Past experiments and analyses of shallow-buried cylindrical structures provide useful information for the study of buried arches. These structures can include culverts, pipelines, tunnel liners, and fuel tanks. Elling (Reference 8) states that evaluation of stresses and deformations in buried

cylinders must, in many instances, account for the relative slip between the soil and the cylinder as well as for a partial debonding of the interface surface because of a limited tensile capacity of the soil. A study was conducted of the stresses in buried cylinders with imperfect boundaries through an alternative to the finite element method that uses assumed stress functions for the soil field as well as for the buried cylinder. The normal stresses and the shear stresses that exist at the soil-cylinder interface were also represented through shape functions. This solution was based on the use of linear constitutive laws for both the soil and cylinder; therefore, the results obtained may not be valid for large strains. The emphasis in the study was to determine the influence on cylinder stresses of interface boundaries subjected to tensile debonding and tangential slip. Results indicated that tensile debonding does not occur for most cases of practical interest, but that tangential slip does occur for most practical designs. The interface stress distribution was found to be sensitive to tensile debonding and friction as was the average tangential stress in the cylinder walls. In general, increased friction at the interface resulted in an increased peak value of mean tangential stress.

Katona (Reference 9) conducted an analytical study of the effects of friction on a pipe-soil interface. The computer code CANDE was used in the analysis. CANDE consists of three solution levels. Level 1 is a closed-form elasticity solution whereas levels 2 and 3 are based on finite element methods. Three values of Coulomb friction at the pipe-soil interface were considered: μ = infinity, 0.25, and 0.0. The Coulomb friction hypothesis implies the interface remains bonded wherever the interface shear traction is less than the maximum frictional resistance defined by the product of normal traction and friction coefficient. Thus, $\mu = 0$ allows free relative movement along the interface.

The friction study was applied to the following linear system: confined modulus = 4,000 psi; Poisson's ratio = 0.333; and a 66-inch-diameter pipe with 3- by 1-inch corrugation of 12-gage steel. The analytical study resulted in the following observations: the normal pressure distribution became more hydrostatic as friction decreased, and thrust distributions became more uniform with decreased friction due to the near hydrostatic normal pressure distribution. For $\mu = 0$, peak thrust values were reduced by 25 percent. Unlike thrust, moment distributions increased in amplitude with decreasing friction.

1.4 SOIL-STRUCTURE INTERFACE FRICTION EXPERIMENTS

Structures that are in direct contact with soil transmit forces through the contact surface or interface. Transmission of the forces through the interface constitutes the skin friction. In the analysis of structures subjected to interface skin friction, reasonable values of interface properties should be provided to reach a meaningful solution. According to Potyondy (Reference 10), the four major factors which determine skin friction are the moisture content of the soil, the roughness of the surface, the composition of the soil, and the intensity of normal load. Experiments were carried out by Potyondy to determine the magnitude of skin friction in which the following variables were considered:

1. Various construction materials: steel, wood, concrete.
2. For each material two surface conditions were used: rough and smooth.
3. Various types of soil.
4. Strictly controlled moisture content.
5. Variation of the normal load between the friction surfaces.

The test results for sand on concrete indicate that when the normal load was increased, the angle of skin friction and the angle of internal friction values generally slightly decreased. The internal friction value, however, was more sensitive to the load than the skin friction value. Proposed coefficients of skin friction for sand on concrete ranged from 0.76 to 0.98 for smooth to rough surfaces. The coefficient of friction is defined as the ratio of friction force to normal force on the slip surface at slip.

Brumund and Leonards (Reference 11) conducted interface friction tests using two types of sand referred to as 20-30 sand, of which 100 percent passed the 20 and was retained on the 30 US standard sieve, and 60-80 sand, of which 70 percent of the particles were retained between the 60 and 80 US standard sieves. Two of the structural materials used were smooth and rough mortar. The test configuration consisted of a cylinder of sand encased in a rubber membrane with a 1-1/8-inch-diameter, 14-inch-long rod located along its axis. By evacuating air from within the membrane, a normal stress was applied to the sand/rod interface. The rod was then caused to slip relative to the sand by gradually applying static forces to the rod in the axial direction. For the 20-30 sand and smooth mortar, the coefficient of friction was 0.60, and for the rough mortar, 0.76. For the 60-80 sand and the smooth mortar, the

coefficient of friction was 1.05, and for the rough mortar, 1.11. Some conclusions of the experiments were: the static coefficient of friction is markedly affected by the size, angularity, and surface texture of the sand grains; and when the sliding surface is rough in comparison to the grain size of the sand, the angle of wall friction exceeds the angle of shearing resistance of the sand and sand/sand slip occurs.

Kulhawy and Peterson (Reference 12) conducted skin friction tests in a Whdeham-Farrance strain-controlled direct shear machine using a 4-inch-square shear box, 2 inches deep. Four different concrete textures were examined. Three were precast blocks with smooth, intermediate, and rough textures while the fourth was cast in place in the shear box and cured with the desired soil density and normal stress. A uniform sand and a graded sand were used in the tests. The primary purpose of the study was to investigate the strength of the interfaces and their relative strength compared with the soil alone. The data obtained for the study were plotted in τ-σ space, and a least-squares best-fit linearization through the origin was used to obtain the respective interface friction angles δ and soil friction angles θ.

According to Reference 12, the resulting behavior of an interface depends primarily upon the gradations of the soil and the face of the structural component. It was found that the roughness of the soil or structural face could be described best as:

$$R = D_{60} \frac{D_{10}}{D_{50}} \tag{3}$$

where

R = roughness

D_{60}, D_{50}, D_{10} = respective particle sizes at 60, 50, and 10 percent finer

The relative roughness (R_R) of the interface can then be defined as:

$$R_R = \frac{\text{Rstructural face}}{\text{Rsoil}} \tag{4}$$

The relative roughness values included in the study ranged from 0 to 7.27. A soil-soil interface gives R_R as unity and would separate the smooth ($R_R < 1$) and rough ($R_R > 1$) interfaces.

The conclusions reached in the study included the following: for rough

interfaces, δ is equal to or greater than θ, which implies that the interface is stronger than the soil, leading to the conclusion that failure would occur in the soil out from the interface; and for smooth interfaces, $\delta = 0.8$ to $1.0\ \theta$ with an average δ equal to about $0.9\ \delta$. Interface shear should control failure in this case.

1.5 OBJECTIVES

The objectives of this study were to evaluate the effects of soil-structure interaction, including interface skin friction, on the normal load distribution and behavior of a shallow-buried reinforced concrete arch structure in a sand backfill.

1.6 SCOPE

Two 1/12-scale model, reinforced concrete arch structures were tested statically in a sand backfill at a depth of burial (DOB) of 7.5 inches which resulted in a depth-to-arch-diameter ratio of about 1:6. The arches were semicircular with an inside radius of 1 foot 9 inches and a thickness of 2 inches and were supported on continuous concrete footings. The arches were constructed as nearly identical as possible except that one arch was covered with two sheets of 1/32-inch-thick Teflon at the soil-structure interface to significantly reduce the interface skin friction. Since the frictional force is difficult to measure reliably, the use of Teflon on one arch provided a means of evaluating the effects of interface skin friction by comparing the test results with the arch without Teflon.

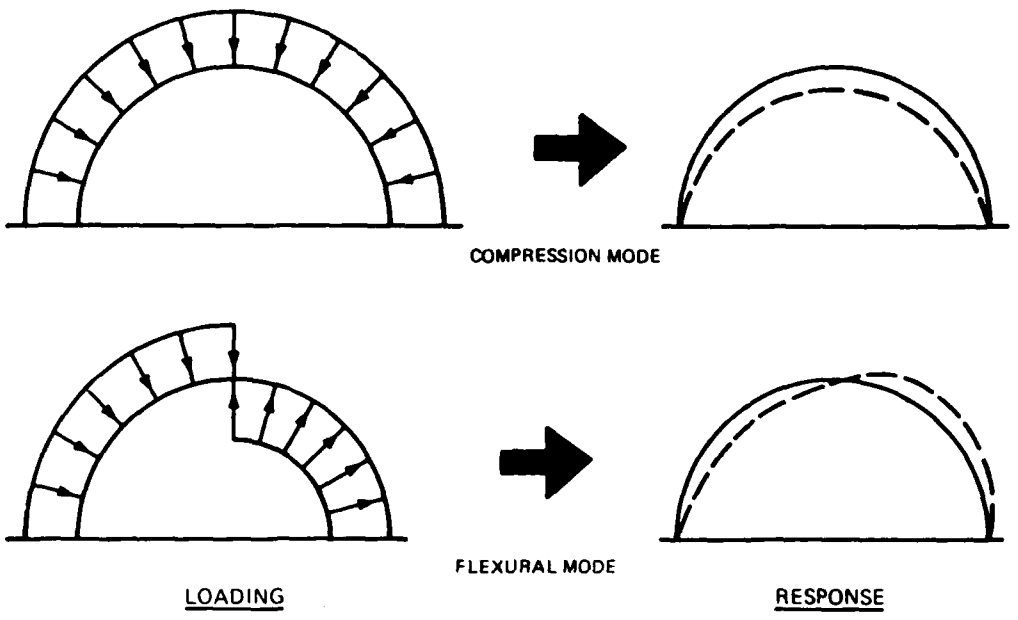

Figure 1. Haltiwanger's assumed loading and response modes.

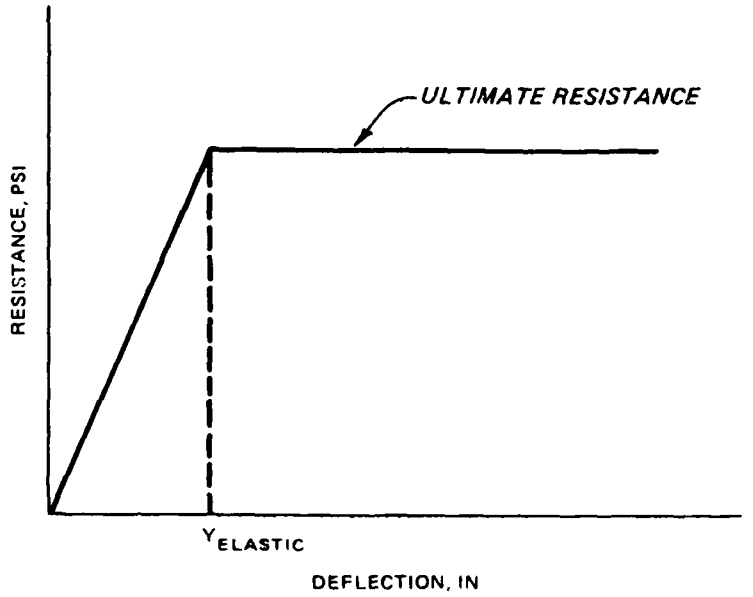

Figure 2. Bilinear resistance function for compression mode of response.

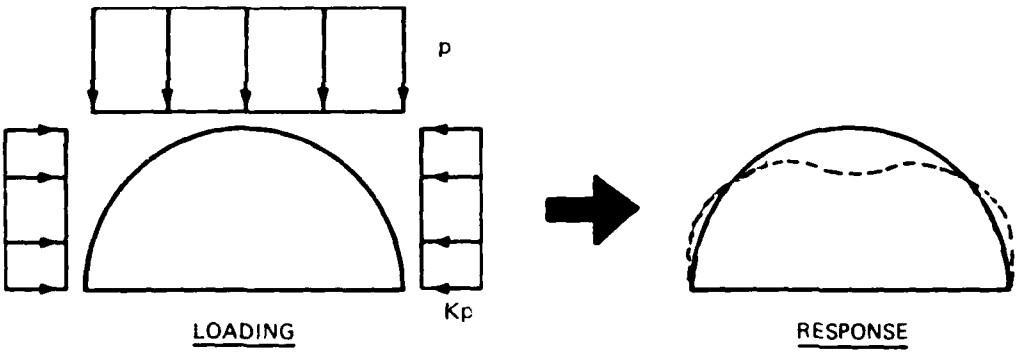

Figure 3. Flathau's assumed loading and response mode.

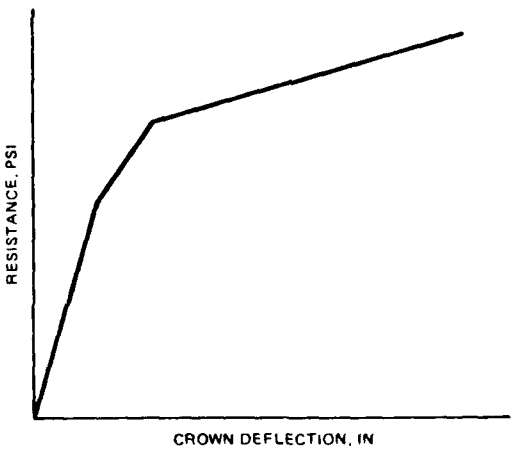

Figure 4. Resistance function for symmetric bending mode.

SECTION 2

EXPERIMENTAL INVESTIGATION

2.1 OVERVIEW

Two 1/12-scale reinforced concrete arch structures were constructed and tested statically in the laboratory at the US Army Engineer Waterways Experiment Station (WES). The first arch tested, which did not have Teflon at the soil-structure interface, was designated as arch S-1 and was tested on 16 June 1986. The arch with two Teflon layers at the soil-structure interface was designated arch S-2 and was tested on 27 June 1986. Arch construction details, test configuration and procedure, instrumentation and photography, and material properties are described in the following sections.

2.2 ARCH CONSTRUCTION DETAILS

Construction details and dimensions of the model arch structures are shown in Figure 5. The inside radius of the arches was 1 foot 9 inches and the thickness of the arch ring was 2 inches. Reinforcing steel in the radial direction consisted of D3 wire (area equals 0.0295 in^2) spaced at 2-1/4 inches on center in each face, which resulted in a principal reinforcing steel ratio of approximately 0.008 in each face. Longitudinal reinforcing consisted of D3 wire spaced at 8.5 degrees on center and was placed inside the radial steel. A concrete cover of 1/4 inch was maintained over the principal reinforcing steel. A photograph of the reinforcing steel for the arch rings prior to placing the concrete is shown in Figure 6.

The footings used to support the arch rings were constructed separately. The footings were overdesigned in an attempt to ensure that they did not fail prior to failure of the arch rings. Footing reinforcement consisted of D3 wire in the longitudinal direction in the top and bottom faces of the footings and D3 wire stirrups spaced at 1-1/2 inches on center as shown in Figure 5. A photograph of the footing reinforcing before concrete placement is shown in Figure 7.

Plywood form work was used for placement of the concrete for the arch rings and footings. Hardware was secured to the arch ring form work prior to concrete placement for use in installing soil-structure interface pressure gages immediately prior to testing the structures. After concrete placement

and removal of the form work, one of the arches received a 1/32-inch layer of Teflon. The Teflon was glued to the exterior surface and the edges of the arch ring. Figure 8 shows the arch rings after placement of the concrete and application of the Teflon to one arch.

2.3 TEST CONFIGURATION AND PROCEDURE

Figure 9 shows an illustration of the test device used to produce the static overpressure. The device is capable of developing pressures up to 3,000 psi. The test chamber, a cylinder 72 inches inside diameter (ID) and 72 inches high, has a piston-type lid that seals the top and rests on a steel plate with an O-ring to seal the bottom. The testing device is composed of platen, spacer blocks, test chamber, and upper bearing block. For testing, the device is rolled into a massive, posttensioned, prestressed concrete reaction structure designed to resist the large dynamic or static loads generated in the test chamber. An air-to-hydraulic multiplier is used to pressurize the test chamber. The pressure pushes the piston-type lid up until the upper bearing block makes full contact with the ceiling of the reaction structure. The upper bearing block and the platen distribute the load to the reaction structure. The test is then loaded by the water pressure supplied by the air-driven pump.

The test configuration is shown in Figure 10. Two layers of Teflon were placed on the inside face of the test chamber to reduce the amount of friction between the sand and the chamber. In each of the two tests, sand was placed to the proper height in the test facility in 6-inch lifts and compacted to provide a uniform support for the model structure. The precast concrete footings were set in place in the chamber, and a steel support for deflection gages was welded to embedded plates in the footings. The arch ring was then lowered into the chamber and placed in the proper position on the footings and grouted in. Transducers for measuring structure loading and response were then installed, and sand backfill was placed around and over the arch to a height of 7.5 inches above the arch crown. Steel endplates were used to close the ends of the arches. The ends of the arches and the steel plates were covered with Teflon to provide a Teflon-Teflon interface between the two, thereby reducing the effects of end support as the arches were loaded. A plastic pipe was installed which ran from the inside surface of the test chamber to a hole cut in one of the steel endplates. This pipe provided a

means of inserting an optical borescope through the endplate so that the inside of the arch could be inspected during the test.

After closing up the end of the arch, sand was placed in 6-inch lifts and compacted by making four passes with a 23-pound hand tamp having a 6-3/4- by 11-inch foot. Free-field soil stress gages were placed at specific locations as the backfilling process proceeded.

After backfilling, the top of the soil surface was leveled, and two 1/8-inch-thick neoprene rubber membranes were placed over the soil surface. The pressure lid, bearing plate, and bearing shell were then assembled, and the test device was rolled into the concrete reaction structure. In each test the data tape recorder was started immediately preceding the opening of the waterline valve used to fill the test device with water. The time required to fill the water chamber was approximately 20 minutes. A relief plug at the top of the water chamber indicated when the chamber was full at which time the waterline valve was closed to allow closing of the relief valve. The pump was then started, and the pressure in the water chamber was increased very slowly to load the soil surface. As each test proceeded, a plot of water pressure versus arch crown deflection was monitored to provide a means of determining when to terminate the test.

2.4 INSTRUMENTATION

Thirty channels of data were recorded on magnetic tape in each of the two tests on a 32-channel Sangamo Model III FM magnetic tape recorder. The data for each channel were later digitized, processed, and plotted. An instrumentation summary is presented in Table 1. The instrumentation layout for both tests is shown in Figure 11.

Two water-pressure gages (Kulite Model HKM-375) were used to record the pressure applied to the soil surface over the arches. Two gages were used so that if one malfunctioned, data from the backup gage could be used. One of the water-pressure gages was used as a reference channel against which all other data were plotted.

Nine interface pressure (IP) gages (Micro-Gage Model P-302) were mounted around the arch ring at approximately every 22.5 degrees to define the pressure distribution around the arch. The gages had a range of 1,000 psi. The gages were installed in mounting hardware, which was fabricated at WES, and installed in a sleeve that had been cast into the concrete arch ring. The

gages were placed flush with the outside surface of the arch ring.

Eight single-axis, metal film strain gages were mounted to principal (radial) reinforcing bars in the arch ring. Four were on interior bars (EI) and four on exterior or outer bars (EO). These gages (Micro-Measurements Model EA-06-250BF-350-W) were 0.25-inch, 350-ohm, temperature-compensated gages.

Two displacement (D) transducers (Celesco Model PT-101) with a range of 10 inches were used to record the vertical displacement of the arch ring at 0 and -45 degrees. The body of the transducers was mounted to a steel support which was welded to embedded plates in the footings.

Nine free-field soil stress (SE) gages (Kulite Model LQV-080-8U-H) were used in each test. Both vertical and horizontal stress measurements were made. In both tests a gage was placed 1.5 inches below one of the footings so that bearing pressures could be measured. In test S-1 (no Teflon) two gages were used to measure vertical free-field stress at the arch crown elevation to provide a backup. In test S-2, instead of using a backup gage at the arch crown, one gage was placed 1 inch above the top of one of the footings to provide a measurement of the approximate interface pressure at the top of the footing.

2.5 PHOTOGRAPHY

Photography provided during the arch construction phase and the posttest documentation phase included black-and-white photographs, color slides, and video recording. Posttest photography of structural damage provided a means of visually documenting and comparing the failure modes and degree of damage to each arch.

2.6 MATERIAL PROPERTIES

2.6.1 Concrete

The concrete mix for these tests was designed to have a 28-day compressive strength of 4,000 psi. The concrete was composed of a type I portland cement and was obtained from a local commercial supplier. The fine aggregate was a natural siliceous sand, and the coarse aggregate was pea gravel with a 3/8-inch maximum diameter. Five test cylinders were cast at the time of concrete placement of the arches. Cylinders were tested at 28 days and on the

day of each arch test. The average 28-day concrete strength was about 4,400 psi. Results of the compressive strength tests are presented in Table 2.

One of the cylinders was instrumented with strain gages to allow the constitutive relationships of the concrete under uniaxial compression to be evaluated. The modulus of elasticity and Poisson's ratio were determined for the concrete according to the American Society for Testing and Materials Standards (ASTM C469). The computed modulus of elasticity was 4.35E6, and Poisson's ratio was determined to be 0.14.

2.6.2 Reinforcing Steel

All reinforcing steel used in the arch rings and footings was ASTM A496 D3 deformed wire (Reference 13), which has a cross-sectional area of 0.0295 inch. The wire was heat-treated in an oven at WES until a yield strength of approximately 60,000 psi was reached. The yield strength before heat treatment was approximately 90,000 psi. Random samples of the reinforcement were tested to rupture in a tensile-testing apparatus. The yield and ultimate strengths of the reinforcement were computed by dividing the applied tensile force by the original cross-sectional area of the bar. Results of the tensile tests are presented in Table 2.

2.6.3 Backfill

The sand backfill was obtained locally from a commercial supplier. The sand was classified as poorly graded (SP) according to the Unified Soil Classification System (Reference 14). Laboratory tests were conducted on samples of the sand to determine its gradation, compaction characteristics, and angle of internal friction. Figure 12 shows the gradation curve, and Figure 13 shows the compaction curve. Results of the direct shear test are shown in Figure 14, which indicates an angle of internal friction for the sand of 38.5 degrees. As the backfill was being placed in 6-inch lifts, several water content and density readings were taken at each lift using a Troxler nuclear-testing device. The water content measurements in test S-1 ranged from 4.9 to 12.4 percent and averaged 7.4 percent while in test S-2 they ranged from 2.7 to 7.6 percent and averaged 5.9 percent. The dry density measurements in test S-1 ranged from 101.6- to 108.3-lb/ft^3 with an average of 105.4-lb/ft^3. The dry density measurements in test S-2 ranged from 99.2- to 109.1-lb/ft^3

with an average of 104.1-lb/ft^3. The results of the water content and density tests are shown in Figures 15 and 16.

Table 1. Instrumentation summary.

Gage	Location	Range	Manufacturer	Model
Interface pressure	IP-1 IP-2 IP-3 IP-4 IP-5 IP-6 IP-7 IP-8 IP-9	1,000 psi	Micro-Gage	P-302
Soil stress	SE-1 SE-2 SE-3 SE-4 SE-5 SE-6 SE-7 SE-8 SE-9	1,000 psi	Kulite	LQV-080-8U-H
Deflection	D1 D2	10 in	Celesco	PT-101
Strain	EI-1 EO-1 EI-2 EO-2 EI-3 EO-3 EI-4 EO-4	10,000 μin/in	Micro-Measurements	EA-06-250BF-350-W
Water pressure	WP-1 WP-2	1,000 psi	Kulite	HKM-375

Table 2. Concrete compressive test and steel tensile test results.

Wire size	Sample	Yield strength psi	Ultimate strength psi
		Reinforcing Steel	
D3	1	65,830	75,900
D3	2	65,400	75,300
D3	3	67,600	75,900
D3	4	57,030	65,770
D3	5	57,130	64,830
D3	6	57,630	65,570
	Average	61,770	70,550

Batch	28-Day compressive strength psi	Compressive strength on test day psi	Element age when tested days
		Concrete	
1	4,460	4,420 (S-1)	35
1		4,560 (S-2)	45
2	4,320	4,390 (S-1)	35

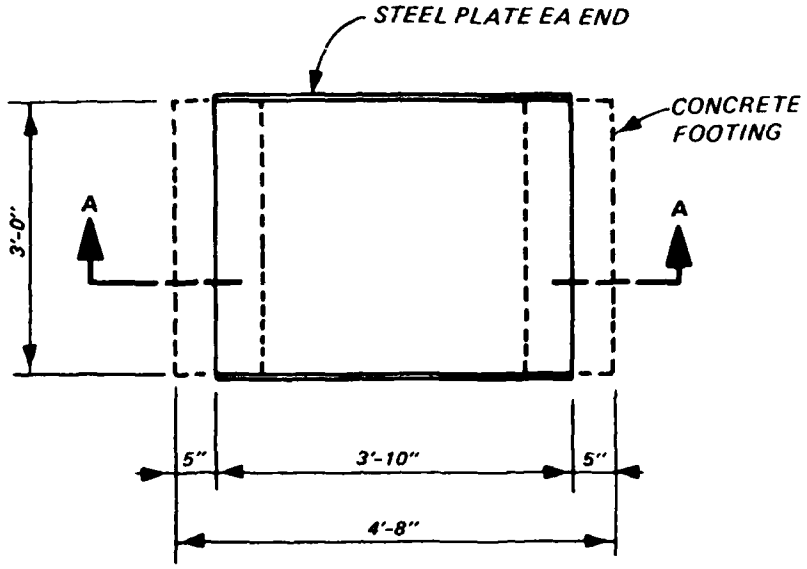

PLAN

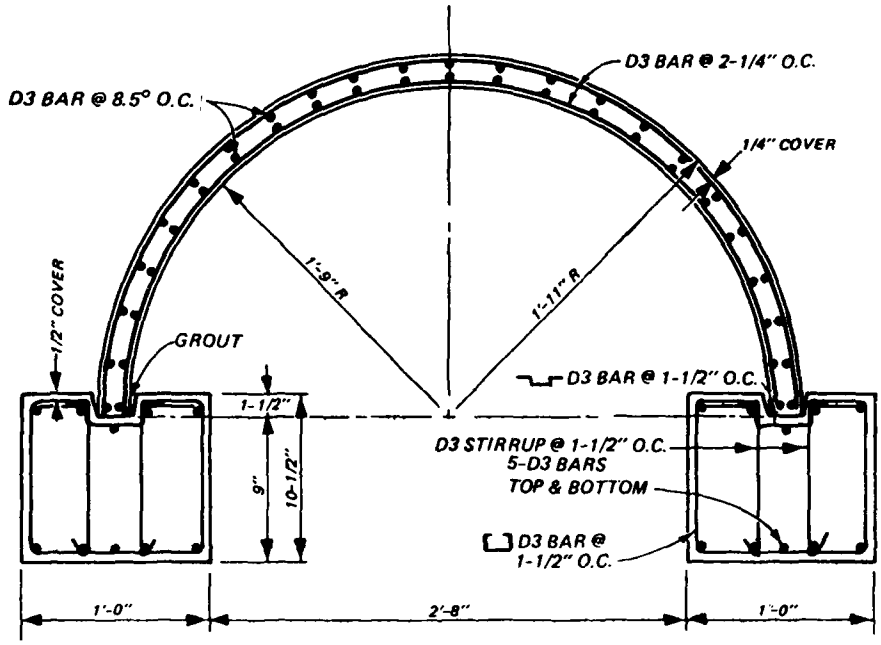

SECTION A-A

Figure 5. Construction details and dimensions.

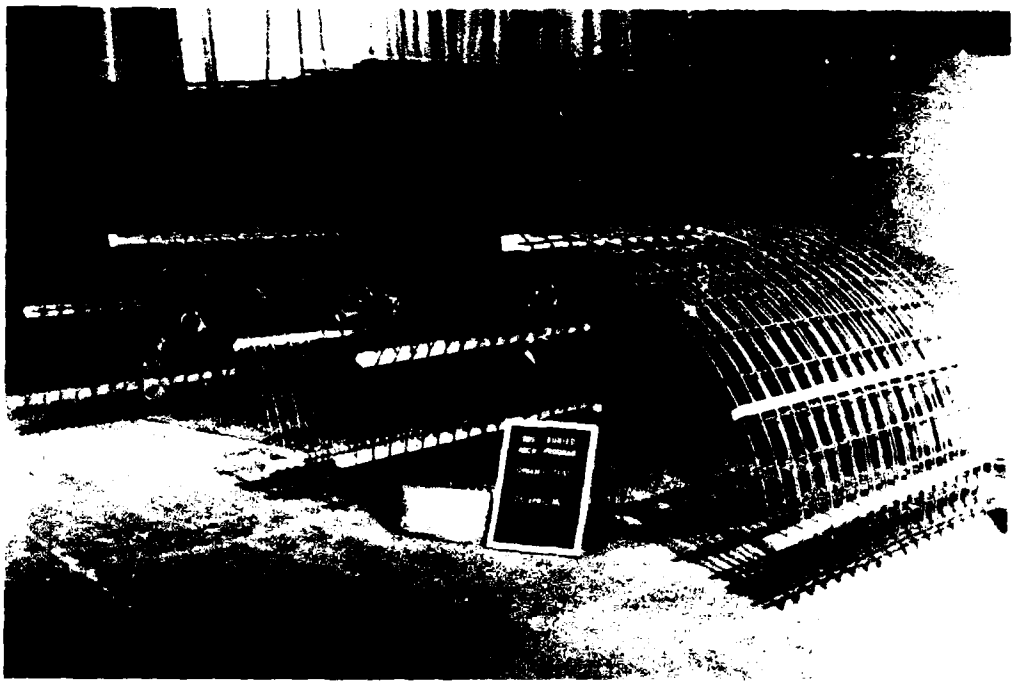

Figure 6. Arch ring reinforcing steel.

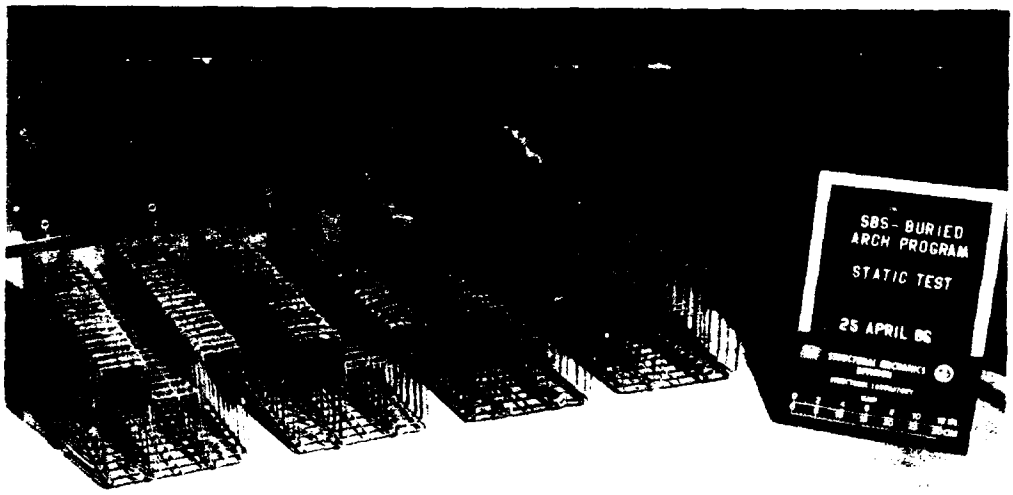

Figure 7. Footing reinforcing steel.

Figure 8. Completed arch rings.

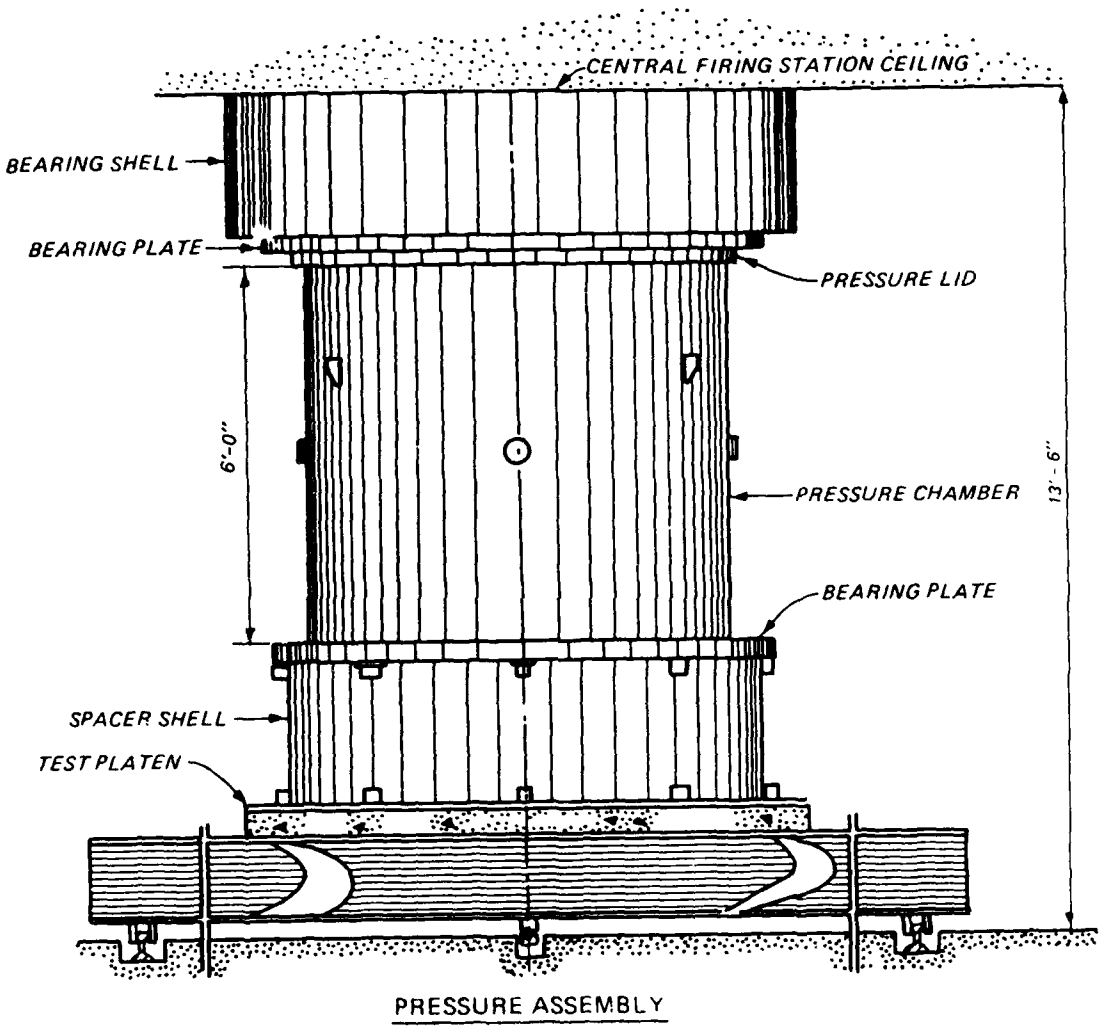

Figure 9. Static test device.

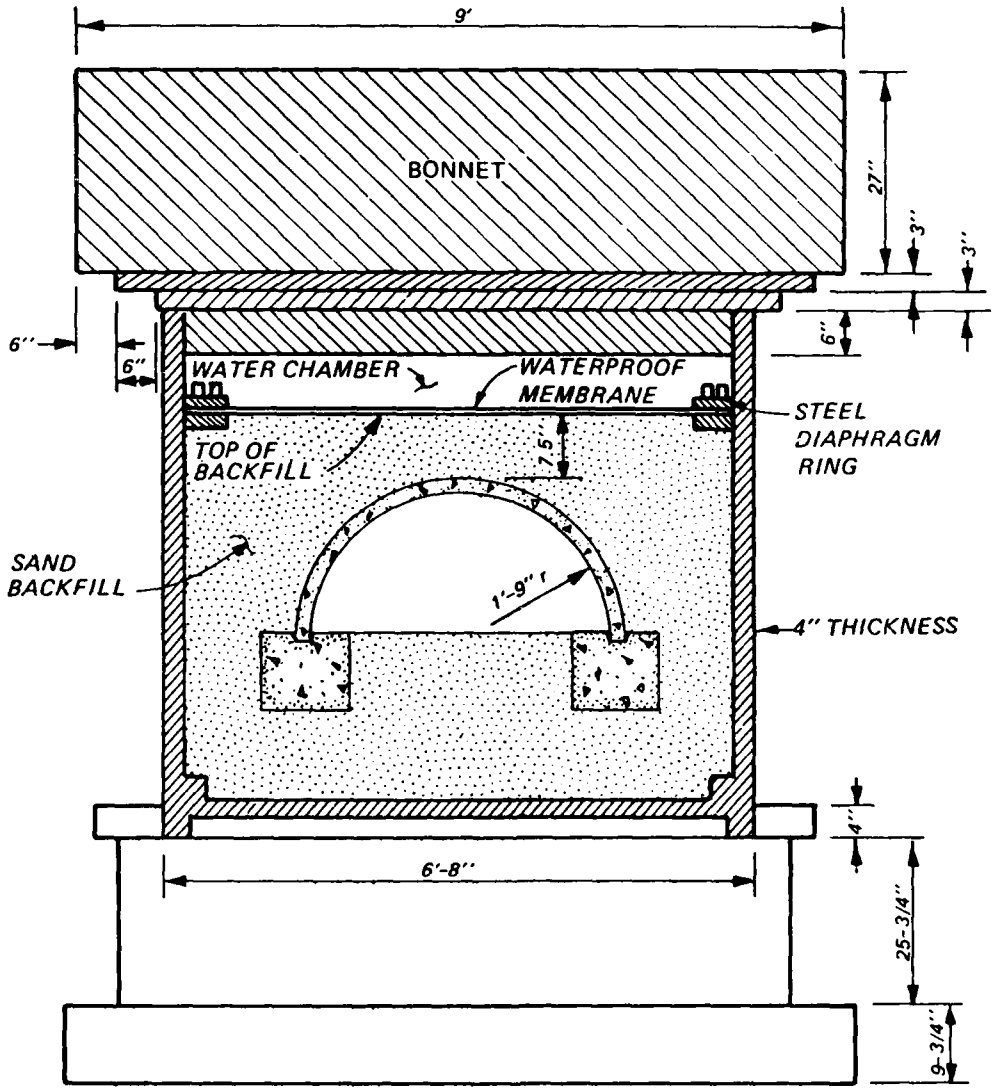

Figure 10. Test configuration.

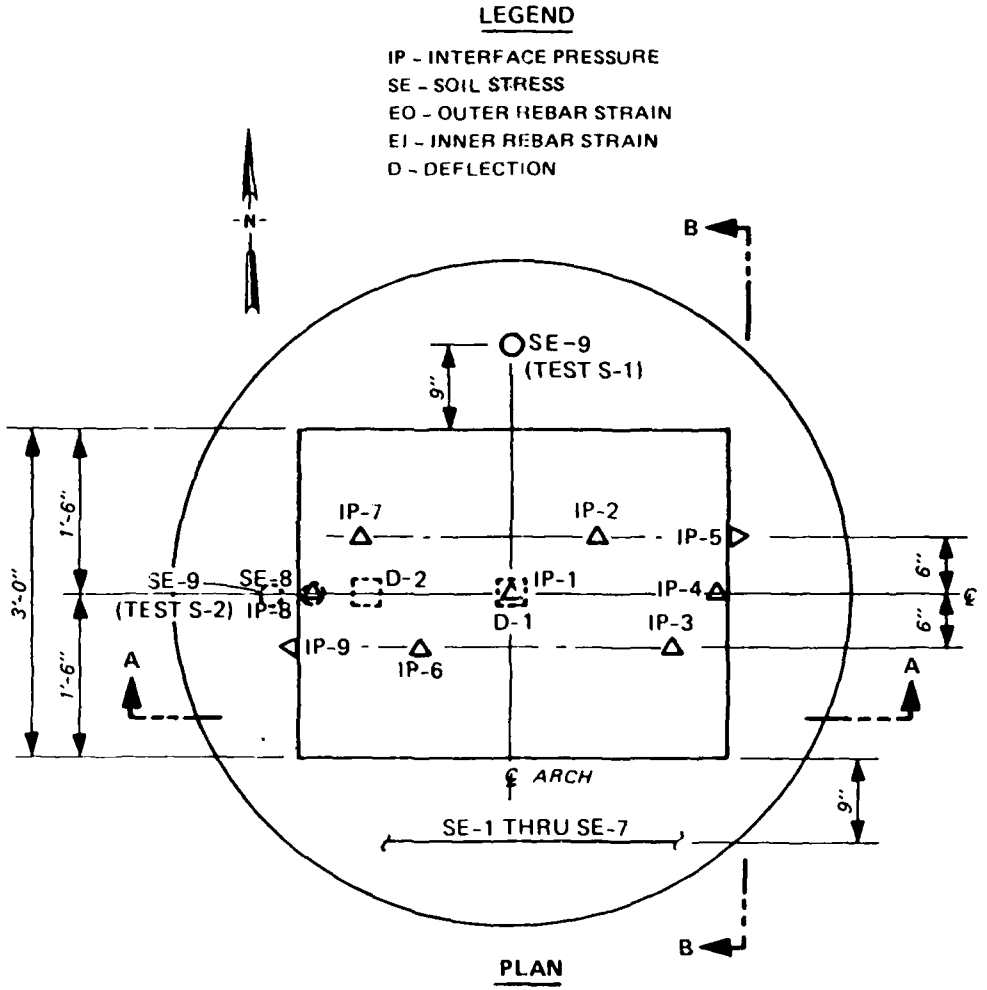

Figure 11. Instrumentation layout (Continued).

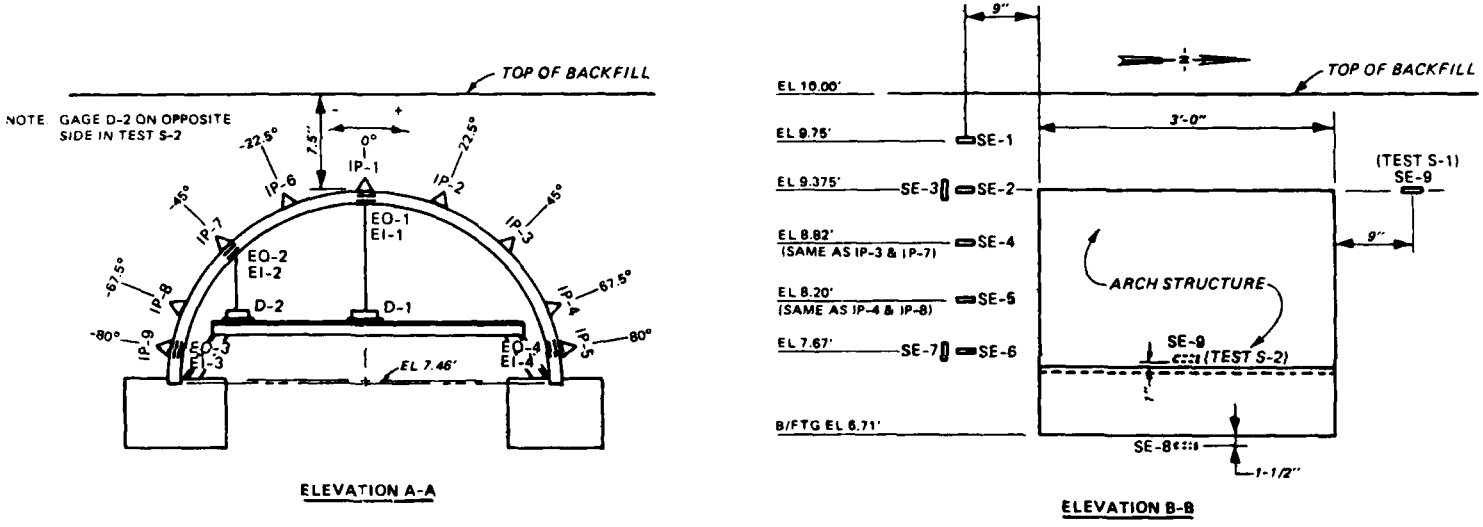

Figure 11. (Concluded).

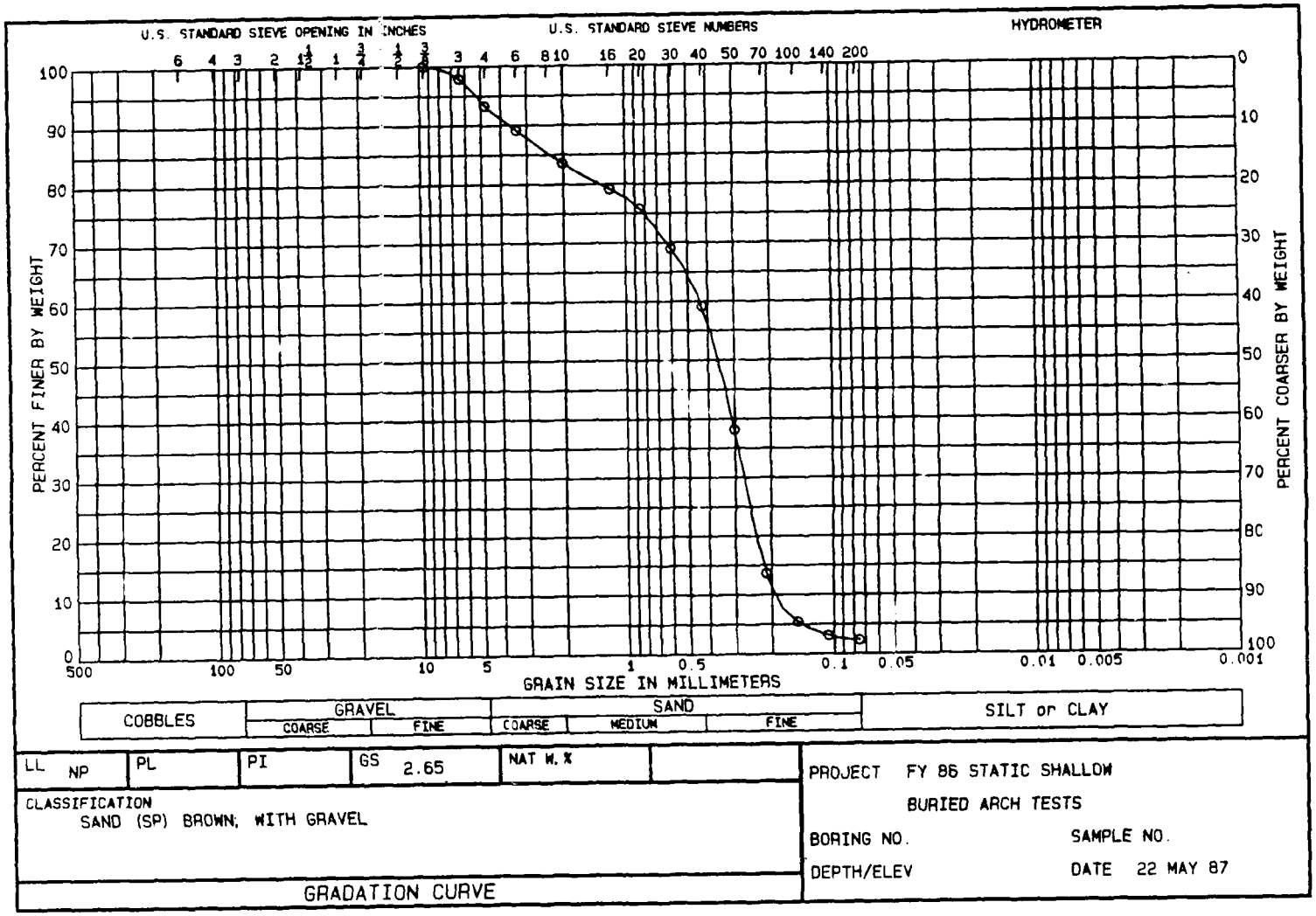

Figure 12. Gradation curve for sand backfill.

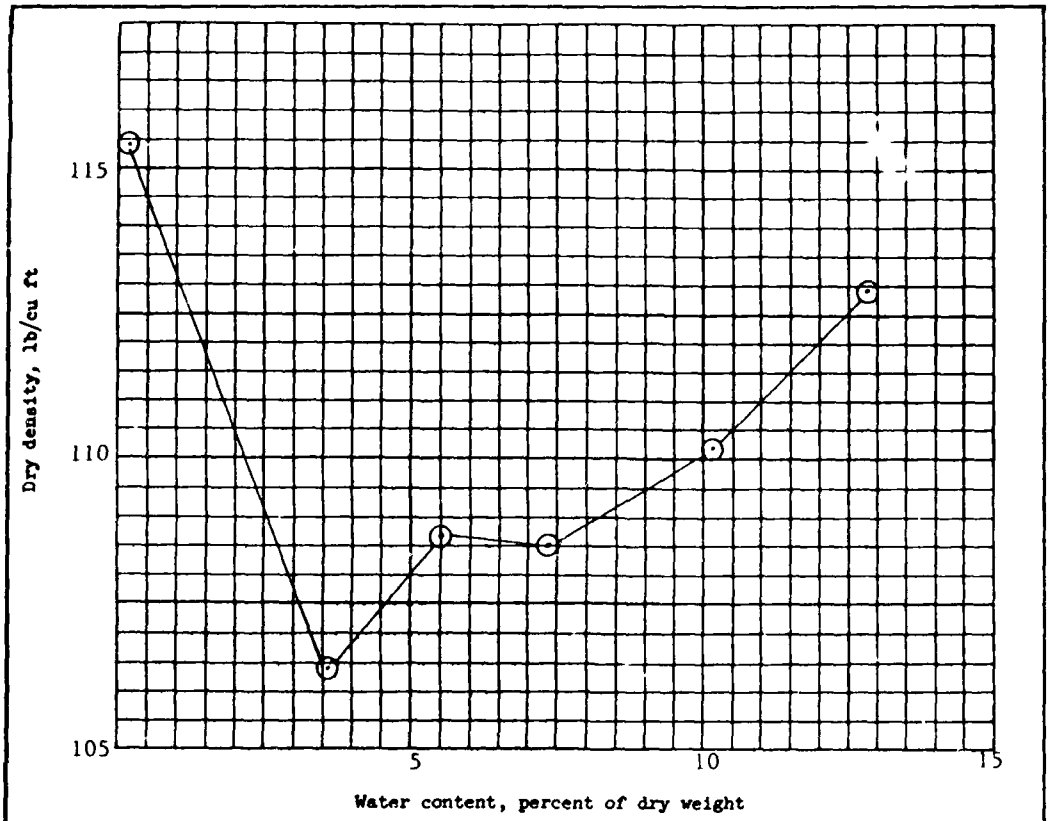

CE-55 compaction test

55 blows per each of 5 layers, with 10 lb sliding wt. rammer and 18 inch drop. 6 inch diameter mold

Sample No.	Elev or Depth	Classification	G	LL	PL	% > No. 4	% > 3/4 in.
		SAND (SP), BROWN; WITH GRAVEL	2.65				

Sample No.				
Natural water content, percent				
Optimum water content, percent				
Max dry density, lb/cu ft	115.4			

Remarks	Project FY 86 STATIC SHALLOW BURIED ARCH TESTS
Relative Density Test	
Max. Dry Den. 117.2 pcf	Area
Min. Dry Den. 101.6 pcf	Boring No. / Date 1 JUN 1987
	COMPACTION TEST REPORT

Figure 13. Compaction curve for sand backfill using CE-55 effort.

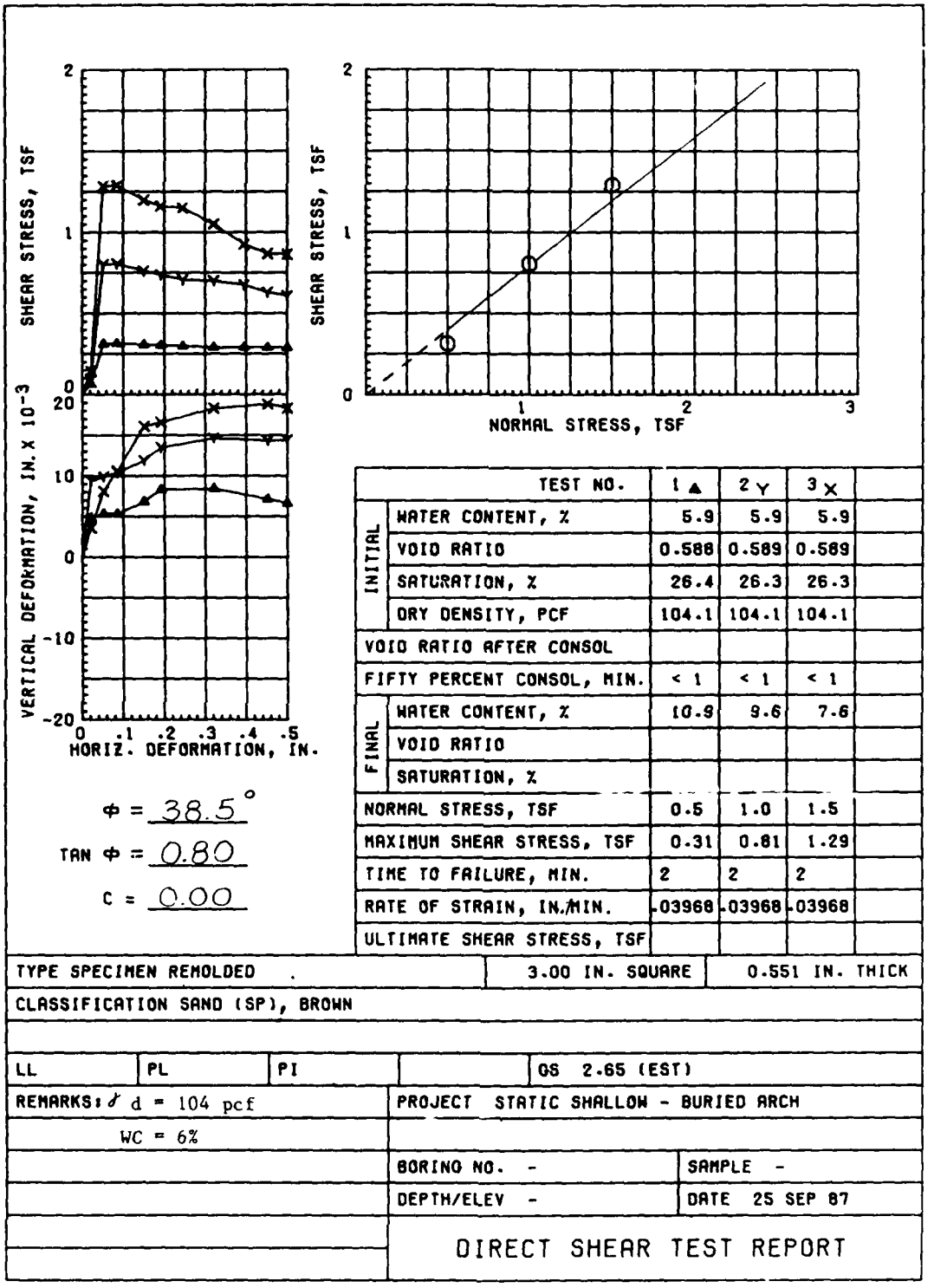

TEST NO.		1 ▲	2 Y	3 X
INITIAL	WATER CONTENT, %	5.9	5.9	5.9
	VOID RATIO	0.588	0.589	0.589
	SATURATION, %	26.4	26.3	26.3
	DRY DENSITY, PCF	104.1	104.1	104.1
VOID RATIO AFTER CONSOL				
FIFTY PERCENT CONSOL, MIN.		< 1	< 1	< 1
FINAL	WATER CONTENT, %	10.9	9.6	7.6
	VOID RATIO			
	SATURATION, %			
NORMAL STRESS, TSF		0.5	1.0	1.5
MAXIMUM SHEAR STRESS, TSF		0.31	0.81	1.29
TIME TO FAILURE, MIN.		2	2	2
RATE OF STRAIN, IN./MIN.		.03968	.03968	.03968
ULTIMATE SHEAR STRESS, TSF				

TYPE SPECIMEN REMOLDED . | 3.00 IN. SQUARE | 0.551 IN. THICK

CLASSIFICATION SAND (SP), BROWN

LL | PL | PI | | GS 2.65 (EST)

REMARKS: γ_d = 104 pcf
WC = 6%

PROJECT STATIC SHALLOW - BURIED ARCH

BORING NO. - | SAMPLE -

DEPTH/ELEV - | DATE 25 SEP 87

DIRECT SHEAR TEST REPORT

Figure 14. Sand backfill direct shear test results.

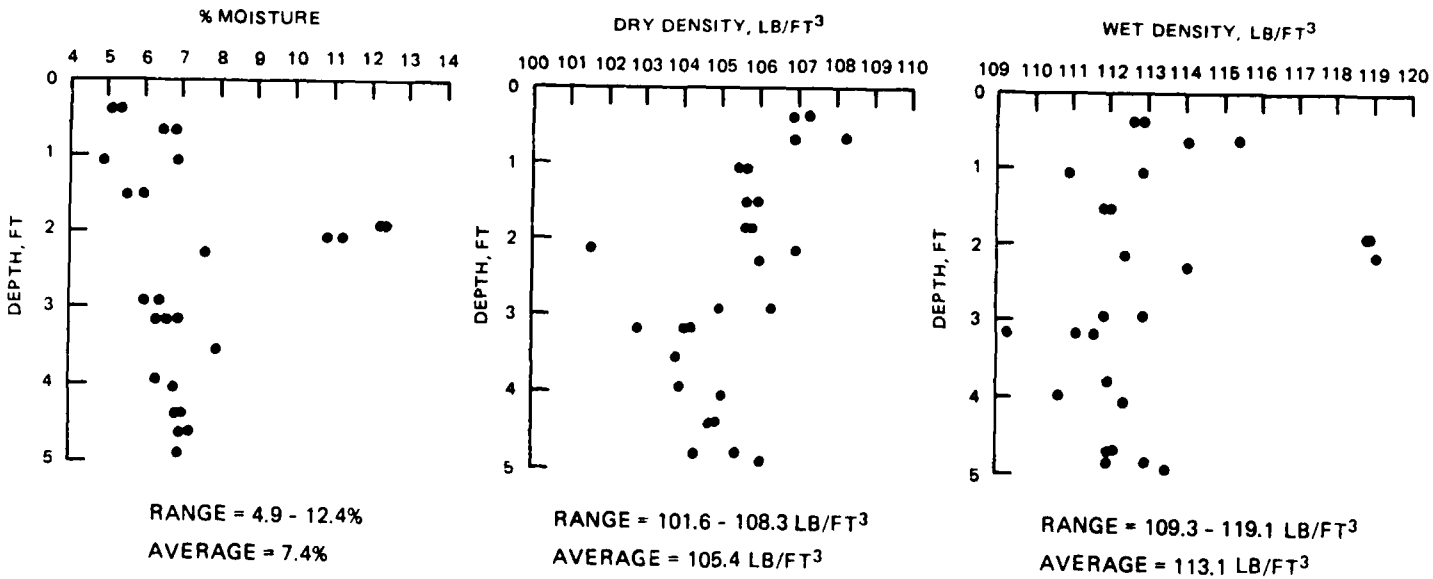

Figure 15. Water content and density measurements for sand backfill in test S-1.

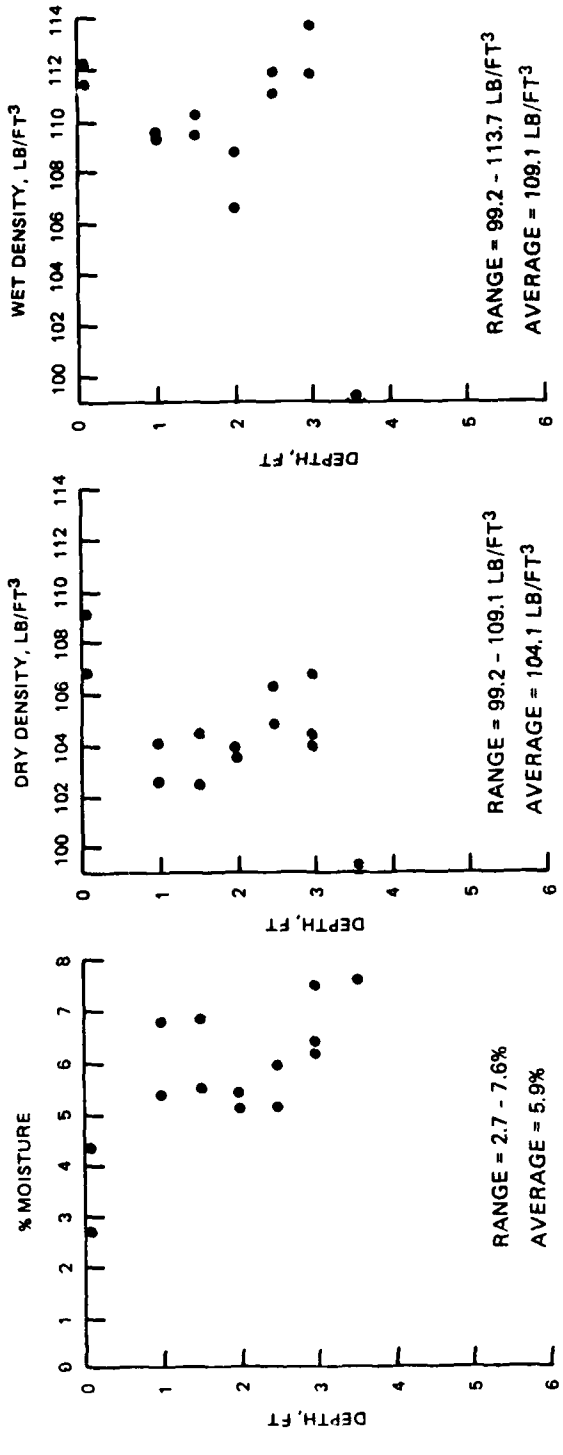

Figure 16. Water content and density measurements for sand backfill in test S-2.

SECTION 3

EXPERIMENTAL RESULTS

3.1 PRETEST ANALYSIS

Pretest linear elastic finite element (FE) calculations were conducted using the computer program ADINA (Reference 15) in an attempt to estimate the static overpressure required to produce severe damage in the arch ring. Figure 17 shows the two-dimensional plane strain FE model used. Since the arch structure is symmetrical, only half of it was modeled in the analysis. The arch portion of the structure was modeled with 12 linear elastic beam elements while the soil and footing were modeled with 268 two-dimensionsal isoparametric 4-node elements. The grid contained 299 nodes. The 4-node elements had 2 degrees of freedom (x-y translation) at each node, and the beam elements had 3 degrees of freedom (x-y translation and moment z-z) at each node. The soil nodes along each vertical surface were restrained against any lateral displacements, and those along the bottom horizontal surface were restrained against any vertical displacements. After the application of these boundary conditions, the FE model had a total of 501 degrees of freedom. Calculations were conducted for two different soil elastic moduli, 2,000 psi and 7,000 psi with a Poisson's ratio of 0.2.

Results of the FE analysis are shown in Figure 18 where the maximum moments and thrusts in the arch at various static overpressure levels are plotted on the arch moment-thrust diagram. Based on the results of FE analyses, it appeared that 500 psi was a conservative estimate of the maximum overpressure required to fail the arch. Based on this, maximum gage readings were predicted for setting the calibration steps. For arch S-1 (no Teflon), the interface pressure and soil-stress gages were set for a maximum gage reading of about 500 psi.

3.2 OBSERVATIONS

As the test of arch S-1 proceeded, water pressure versus crown deflection was closely monitored. When the water pressure reached about 550 psi, the crown deflection was only about 0.35 inch. To continue loading the arch at this point would likely have resulted in clipping any additional data since the calibration steps on most of the gages were set at 500 psi. Therefore,

the water pressure was lowered back down to zero, and the arch was visually inspected through the borescope. The data corresponding to the first load-unload sequence is designated test S-1. The only indication of any damage was some very small hairline cracks at the arch crown. At this point it was decided that the calibration steps would be reset to a higher value, and the structure would be reloaded. The water pressure was again slowly applied until it reached about 840 psi. At this point it was determined that the structure should be inspected for damage in case the deflection plot being viewed was in error. To view the arch through the borescope requires that the arch be unloaded first because if the arch were to fail catastrophically, water and sand under high pressures could be forced out through the opening used for the borescope possibly resulting in serious injury to anyone looking through the borescope. The water pressure, therefore, was decreased to zero. Data corresponding to this second load-unload sequence are referred to as test S-1A. The attempt to view the damage was not successful because rigid body displacement and footing rotation had caused sand to block the end of the borescope. At this point it was decided to reload the arch. The water pressure was again applied and reached approximately 700 psi at which time a decrease in pressure and an increase in crown deflection indicated failure of the arch. The test was terminated at this point. The data corresponding to the third loading is designated test S-1B.

The knowledge gained in testing arch S-1 resulted in better gage predictions for arch S-2. In this test only one loading sequence was conducted. The water pressure was applied slowly until a large increase in crown deflection and a decrease in pressure occurred at about 820 psi, which indicated that the arch had failed. After the pressure had been lowered to zero, visual inspection of the inside of the arch was made using the borescope. This inspection revealed that severe damage had occurred. The test was terminated, and the structure was excavated.

3.3 STRUCTURAL DAMAGE

Posttest photographs of arch S-1 are shown in Figures 19-25. The crown deflection relative to the footings was about 2-3/4 inches. The average rigid body displacement, obtained by averaging the downward displacement of the footings at the four corners of the structure, was about 1/4 inch. Each of the footings rotated inward about 1.5 degrees. As shown in Figures 19 and 20,

small tension cracks occurred on the outside, and crushing and spalling occurred on the inside of the arch ring at about +45 and -45 degrees and extended the entire length of the arch indicating flexural behavior at these locations. Figure 21 shows that on the west side a large crack ran the length of the arch. At the north end, the crack was located at about -30 degrees, and it ran downward in a zigzag pattern to the other end where it ended up at about -80 degrees. Some local buckling of the reinforcing bars was evident at this crack. At the north end of this crack (Figure 22), the arch ring appeared to have sheared through and slipped to where the two sections were overlapping. Figure 23 is a view of the south end of the arch. Figure 24 shows small tension cracks on the interior of the arch at the crown, and a small amount of concrete crushing was visible on the exterior indicating flexural displacement at the crown. As shown in Figure 25, near the arch-footing intersection, major concrete cracking and spalling occurred on both sides, and the arch was cracked all the way through its thickness. Large cracks in the footing ran from directly below the arch ring to the bottom of the footing.

Posttest damage photographs of arch S-2 are shown in Figures 26-31. The crown deflection relative to the footings was 5-1/4 inches on the north end and 1 inch on the south end. The average rigid body displacement was 3/8 inch. There was no measurable rotation of the footings. Figure 27 shows that on the south end, the arch ring crushed and sheared all the way through its thickness for slightly more than one-half its length. A large radial crack formed and ran across the arch to about -20 degrees where it turned and ran longitudinally to the south end of the arch. The arch segment, outlined by this continuous crack, deflected downward and was prevented from totally collapsing mainly by the reinforcing steel since most of the concrete was sheared through. Figures 30 and 31 show that at about +85 degrees (east side) near the arch-footing intersection, concrete crushing and buckling of the reinforcing bars took place. Some crushing and spalling of the concrete also occurred on the west side near the arch-footing intersection; however, it was not as severe as on the east side.

3.4 INSTRUMENTED DATA

All recovered analog data recorded from active instrumentation were digitized by computer, plotted versus water pressure, and are presented in

Appendix A. This provided a means of comparing the data between the two arches at the same static pressures. Comparisons of interface normal pressure, reinforcing bar strain, arch ring deflection, and soil stress were made between the two arches to determine variations in normal load distribution and arch behavior under the same loading conditions.

3.4.1 Interface Normal Pressure

A comparison of the interface radial or normal pressure around the arch ring was made between the two tests at 100-psi intervals. Figures 32-35 show the interface normal pressure profile around both arches at each interval. The recorded pressures were plotted and connected with straight lines. The recorded interface pressure around arch S-1 (no Teflon) was consistently lower than that around arch S-2, and the distribution around arch S-1 appeared to be more uniform although the pressure near the springline was significantly lower than that near the crown, especially at higher overpressures. The interface pressure near the crown of arch S-2 was consistently higher than the water pressure, indicating that passive soil arching may have been occurring, i.e., that the arch was attracting load from the free field. The interface pressure near the crown of arch S-1 was always lower than the water pressure, indicating active soil arching, i.e., that load was being arched to the free field. As the water pressure increased in test S-1, the pressure profile around the arch seemed to flatten out. Initially, the pressure at the crown was higher than the pressure at ±45 degrees; however, as the load increased, the relative pressures became approximately equal. At 500 psi, the pressure at the crown was lower than the pressure at 45 degrees. This was probably the result of the crown deflecting downward and some of the load being transmitted over through soil arching.

The unloading and reloading of arch S-1 appeared to have resulted in more active soil arching during the reloading. This is evident because the pressure around the arch at 500 psi during the first loading sequence (S-1) is of lower magnitude than at 600 psi during the second loading sequence (S1-A). This did not occur in test S-2 where no unloading and reloading was conducted.

3.4.2 Reinforcing Bar Strain

Comparisons of the experimental reinforcing bar strains are shown in Figures 36-38. The comparisons were made only for the first loading sequence in

test S-1 because the unloading resulted in strain reversals in the reinforcing. For this reason, comparisons are made up to 500 psi only.

The only strains which were tensile strains occurred in test S-1 (no Teflon) at pressures of 300 psi and below. All other strains in both arches were compressive throughout the loading sequences. Comparisons of the magnitudes of the strains between arches, for both inner and outer reinforcing bars, showed that the magnitudes of the strain in test S-1 were consistently slightly higher. The recorded strains were used to compute thrusts and moments in the arch, which are presented in Section 4.

3.4.3 Crown Deflection

A comparison of the recorded arch crown deflections is shown in Figure 39. Included in the comparison are the deflections corresponding to each load-unload sequence of arch S-1. When arch S-1 was unloaded, very little deflection was recovered. Upon reloading, the curve closely followed the unload curve up to about two-thirds the previous maximum load where it became less steep. In load sequence S1-B and in test S-2, the arch deflected suddenly, accompanied by a rapid pressure decrease due to the increase in volume in the test chamber. At this point the test was stopped. The curves show that the load-deflection relationship in tests S-1 (first load sequence) and S-2 were very similar up to about 300 psi, at which point the slope of the curve for test S-1 became less steep, i.e., more deflection was occurring for a given increase in water pressure. The maximum pressure reached for both arches was slightly over 800 psi; however, the deflection of arch S-1 was much greater at this pressure than was the deflection of arch S-2. It appears that this was not merely the result of unloading and reloading arch S-1 because the load-deflection curve for the initial loading shows arch S-1 to be less stiff than arch S-2. Possible reasons for the difference in the load-deflection curves may be seen more clearly in Section 4, which presents comparisons of the calculated moments and thrusts at specific locations in the arches.

3.4.4 Soil Stress

Comparisons of experimental soil-stress measurements are shown in Figures 40 and 41. In a static test, the vertical stress in the free field at any depth should theoretically be equal to the applied overpressure. As shown in the soil stress comparisons, the measured vertical soil stress varied

widely from gage to gage. The inside surface of the test facility was covered with two layers of Teflon and, therefore, should not have attracted significant friction forces from the soil. The outside surface of the steel endwalls on the arch were not covered with Teflon which may have resulted in some of the near field soil load being arched over to the endwall. This could account for the measured soil stresses being less than the applied overpressure; however, it should not have affected the arch response since the inside surface of the steel endwall and the ends of the arch ring were covered with Teflon, thereby prohibiting transfer of the friction force on the endplate to the arch itself. Ideally, soil stress gages are placed far enough from the test structure to obtain soil-stress measurements which are not affected by the presence of the structure. This was not possible in these tests because of the relative sizes of the test structures and the test facility.

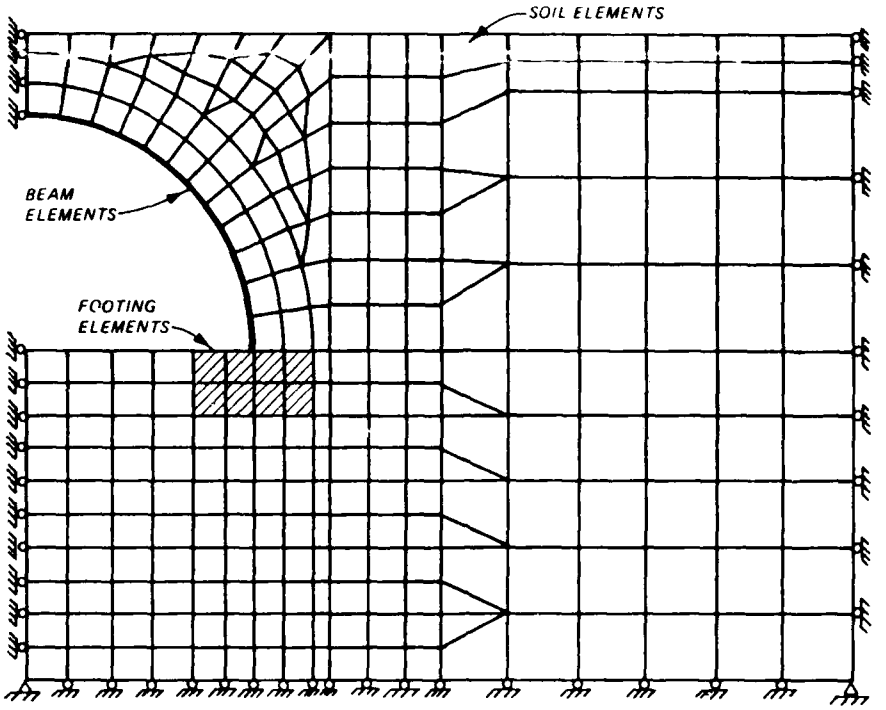

Figure 17. ADINA FE grid.

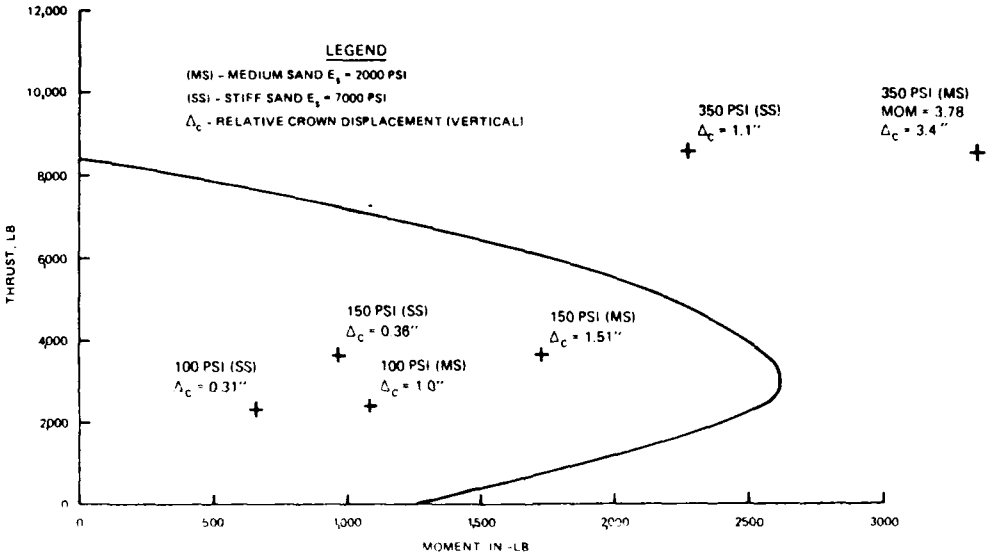

Figure 18. Moment and thrust from FE analyses.

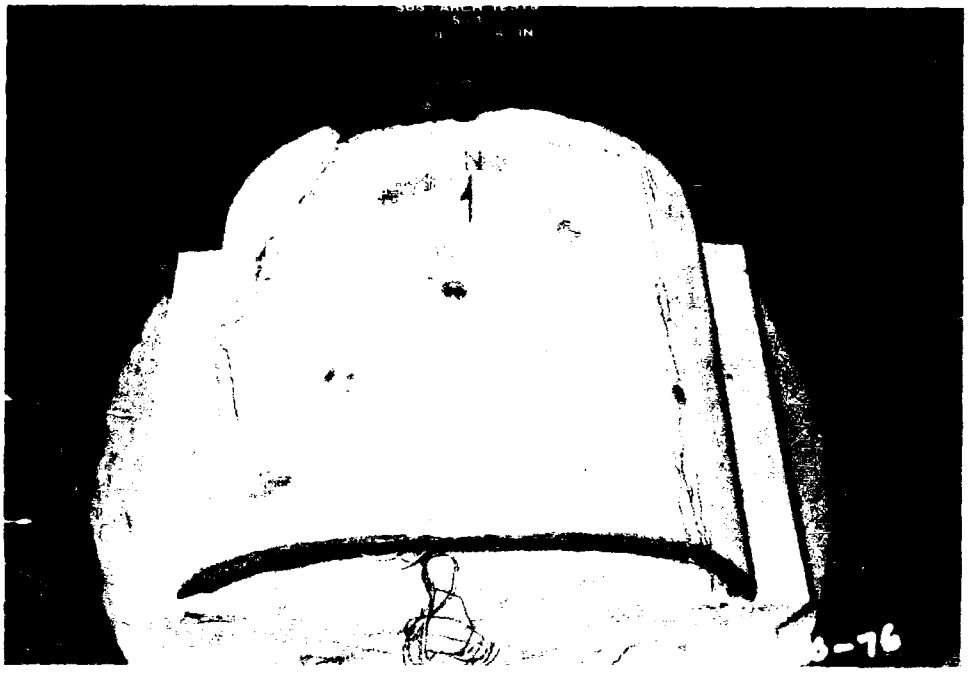

Figure 19. Posttest overall view of arch S-1.

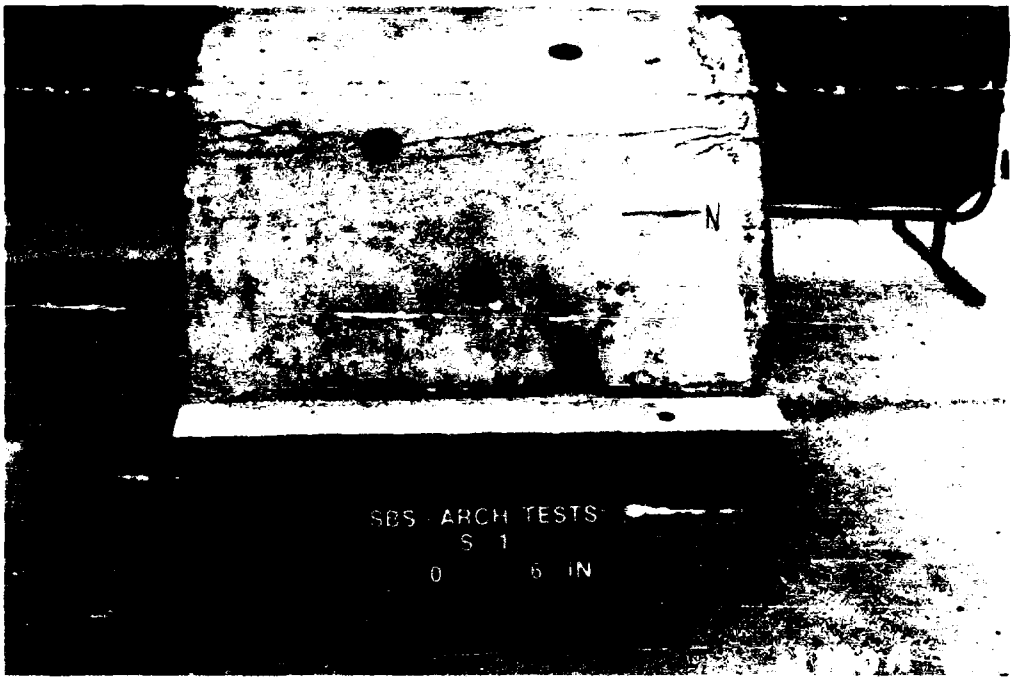

Figure 20. Posttest view of east side of arch S-1.

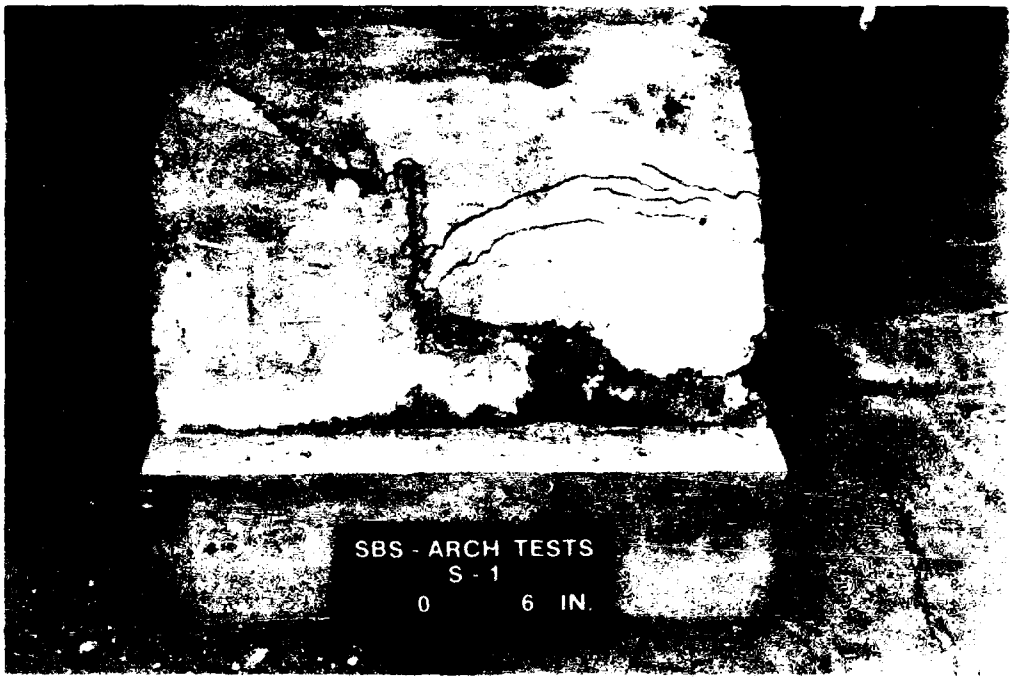

Figure 21. Posttest view of west side of arch S-1.

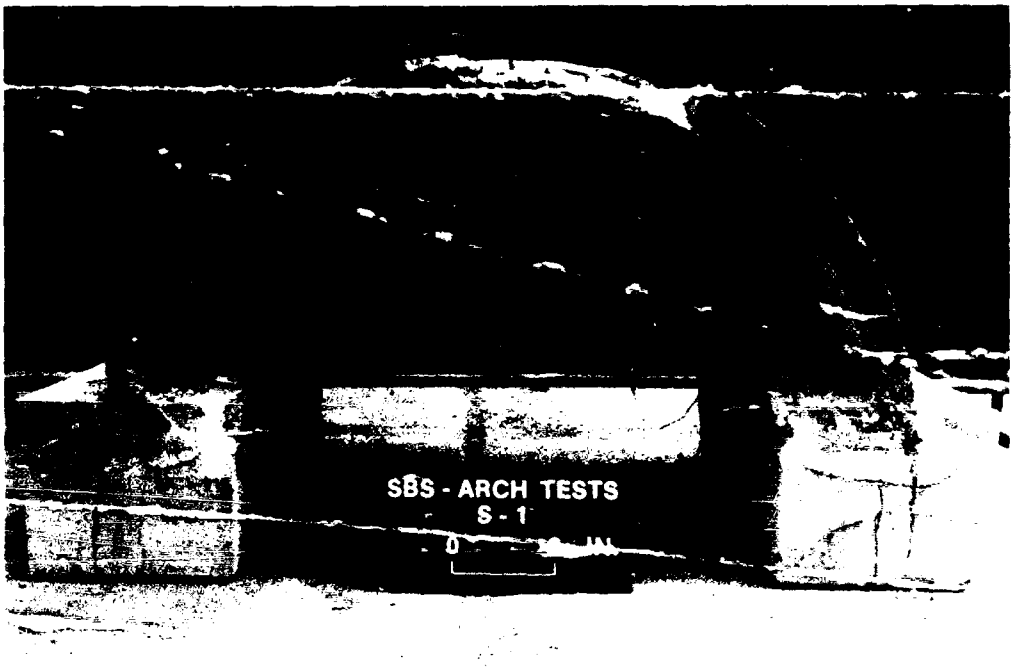

Figure 22. Posttest view of north end of arch S-1.

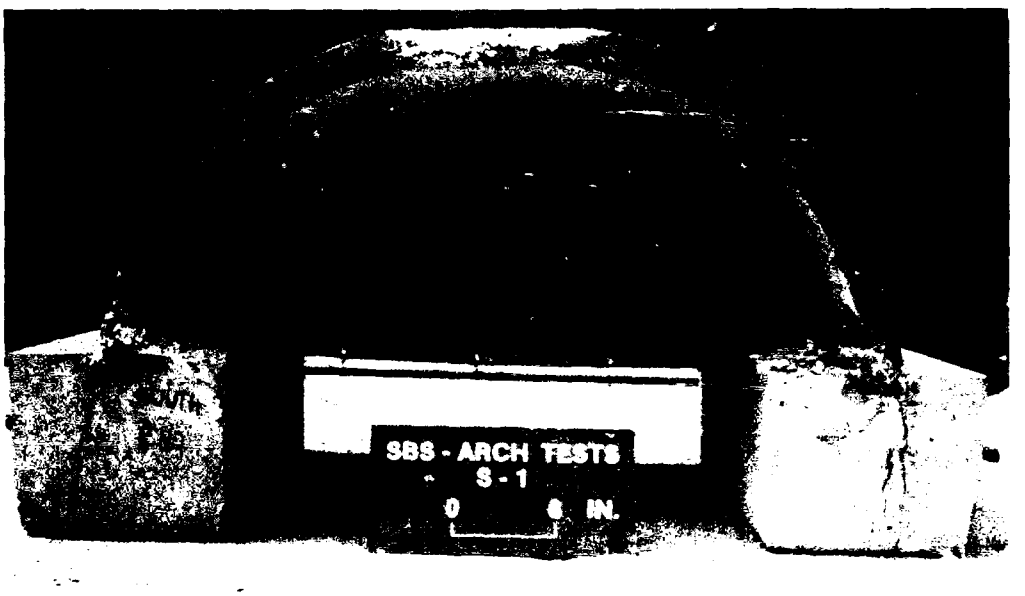

Figure 23. Posttest view of south end of arch S-1.

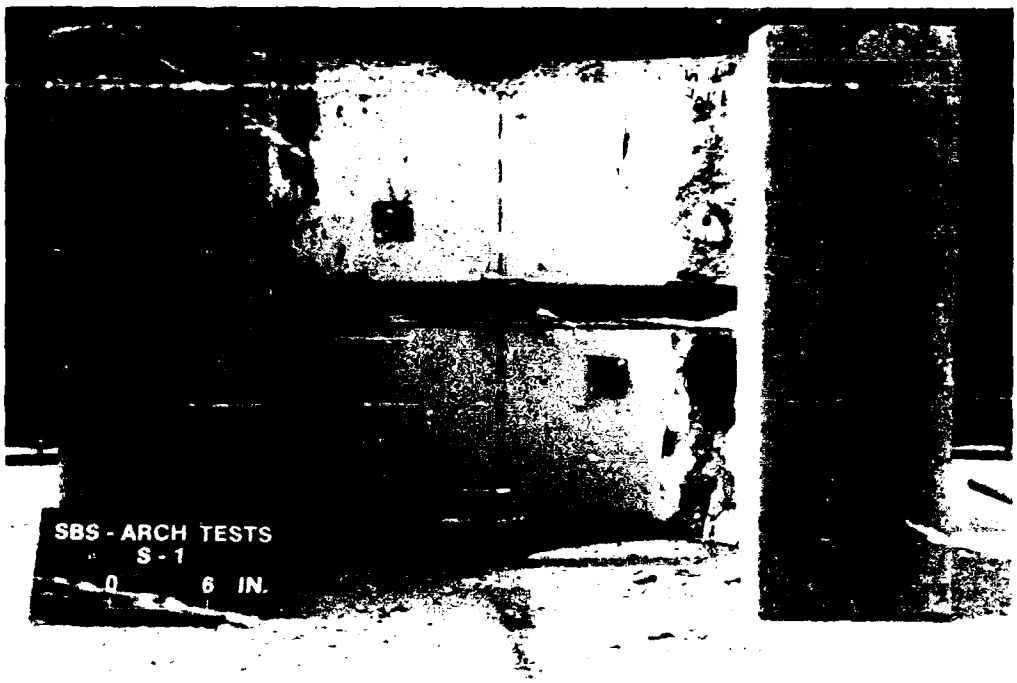

Figure 24. Posttest view of inner arch ring (S-1).

Figure 25. Closeup view of damage to arch S-1 near the footing.

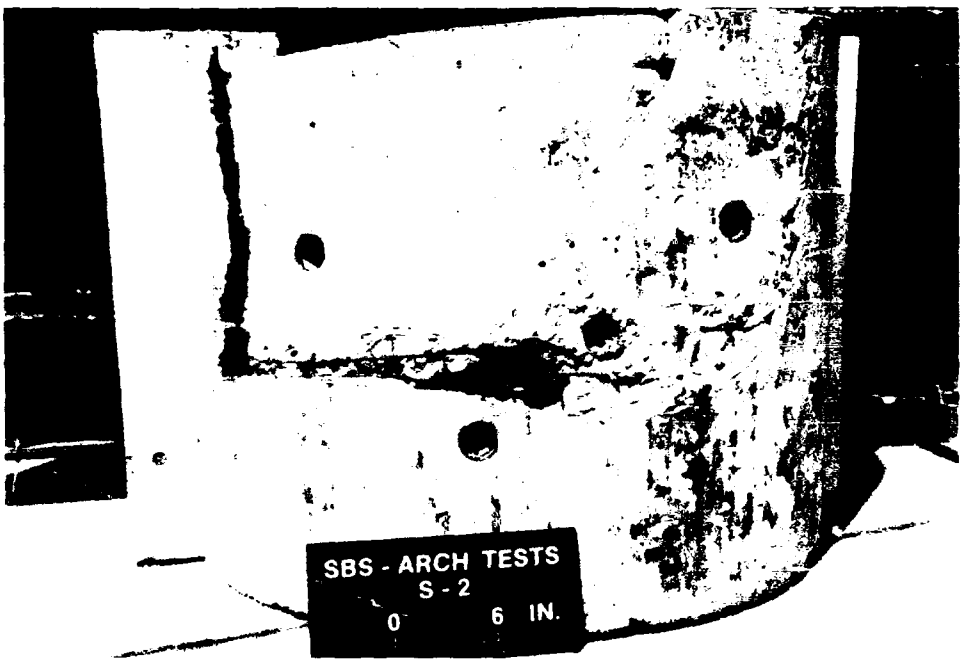

Figure 26. Posttest view of the top of arch S-2.

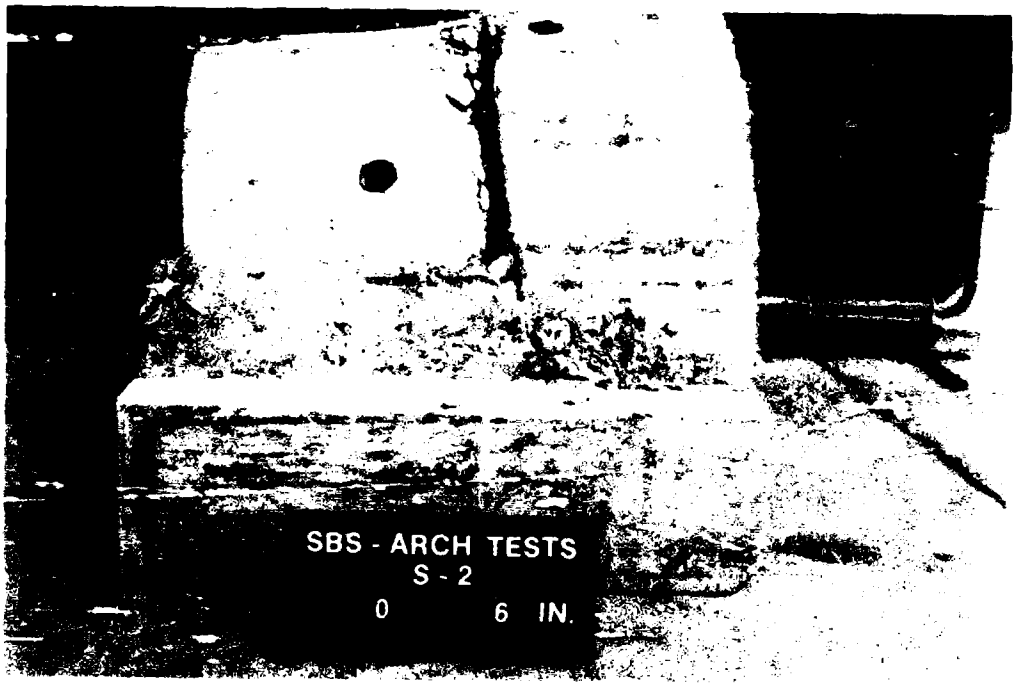

Figure 27. Posttest view of east side of arch S-2.

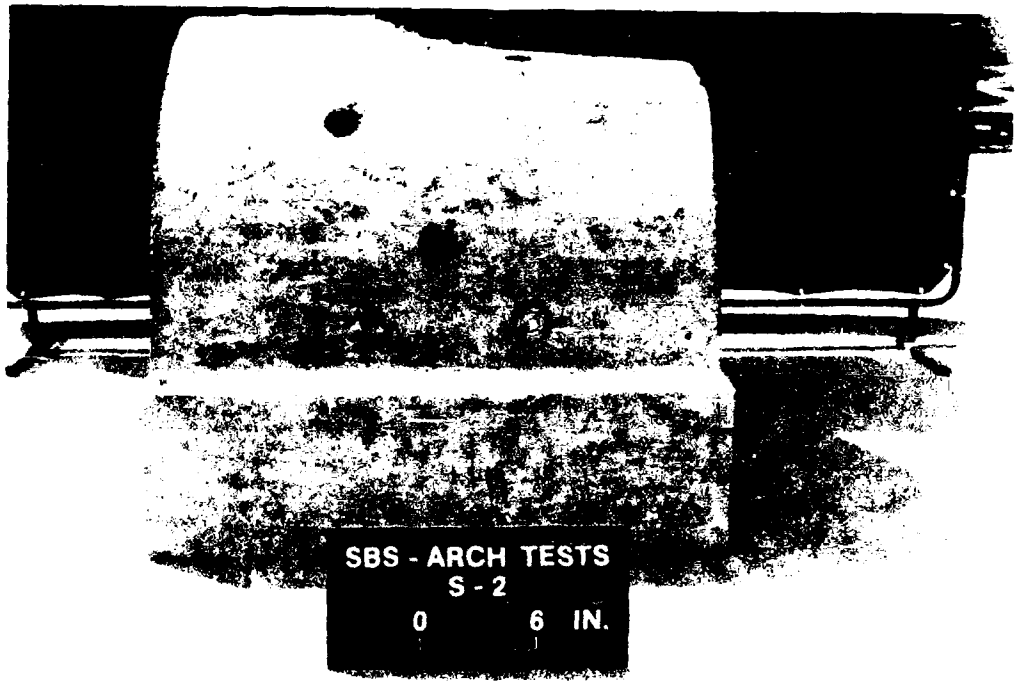

Figure 28. Posttest view of west side of arch S-2.

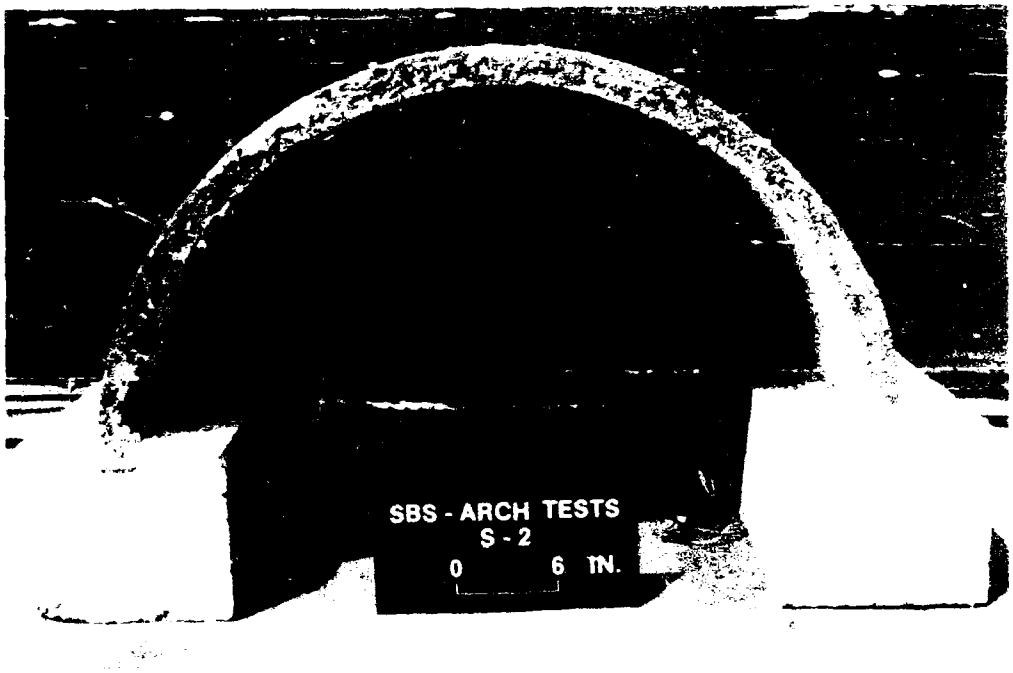

Figure 29. Posttest view of north end of arch S-2.

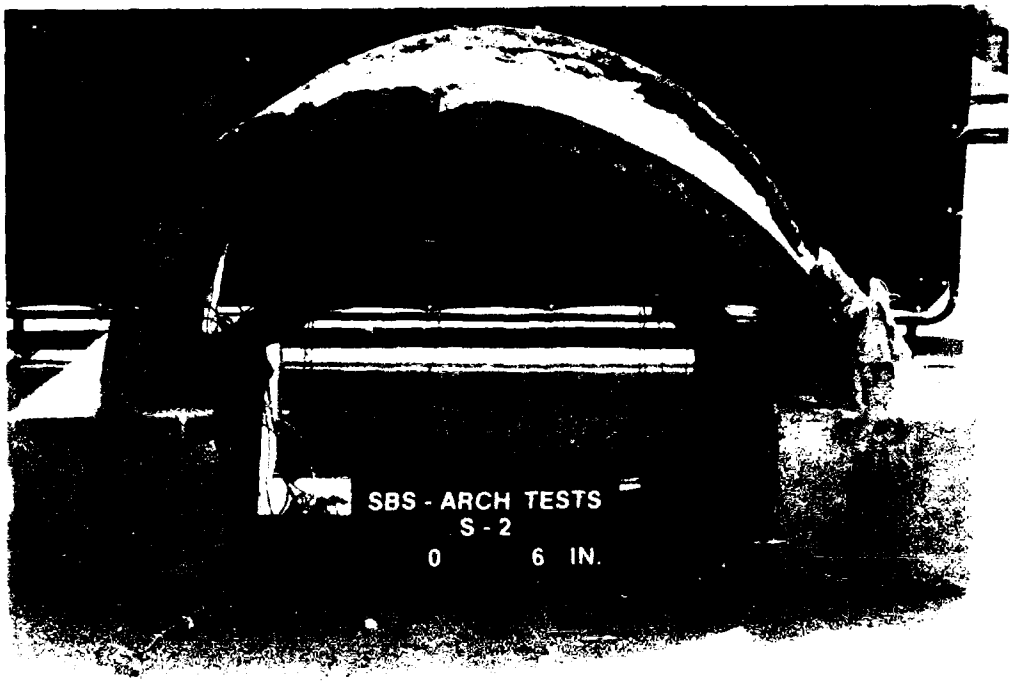

Figure 30. Posttest view of south end of arch S-2.

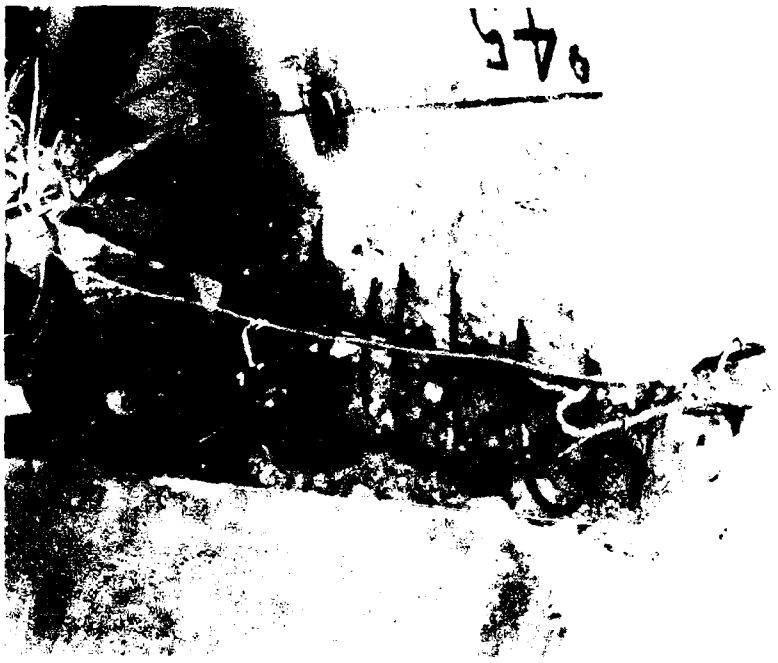

Figure 31. Closeup view of damage at south end near footing (S-2).

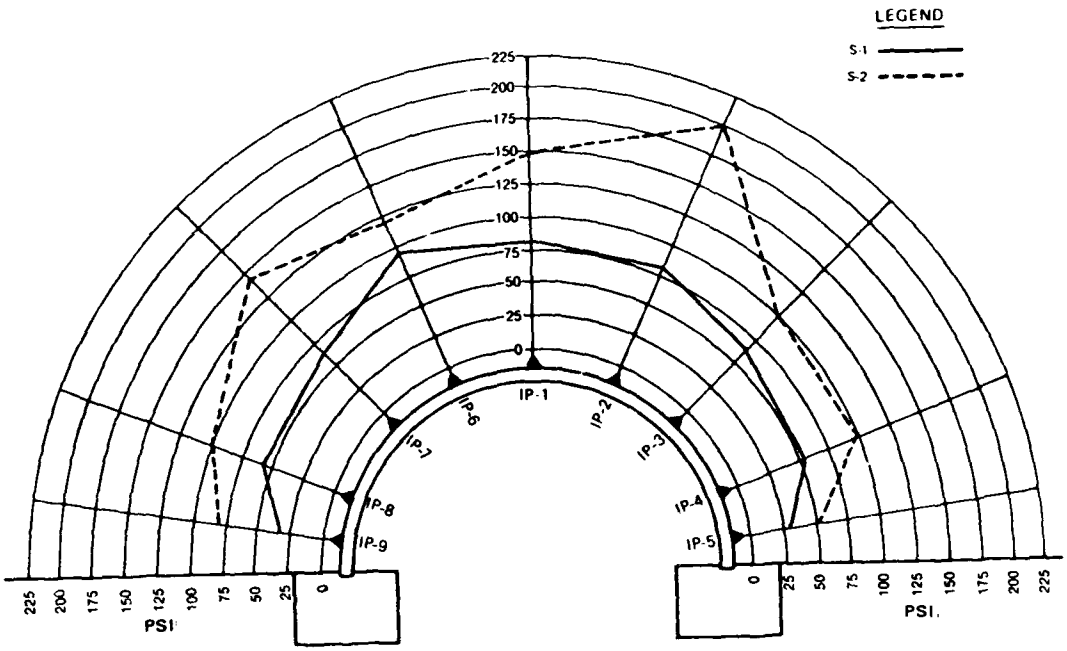

WP = 100 PSI

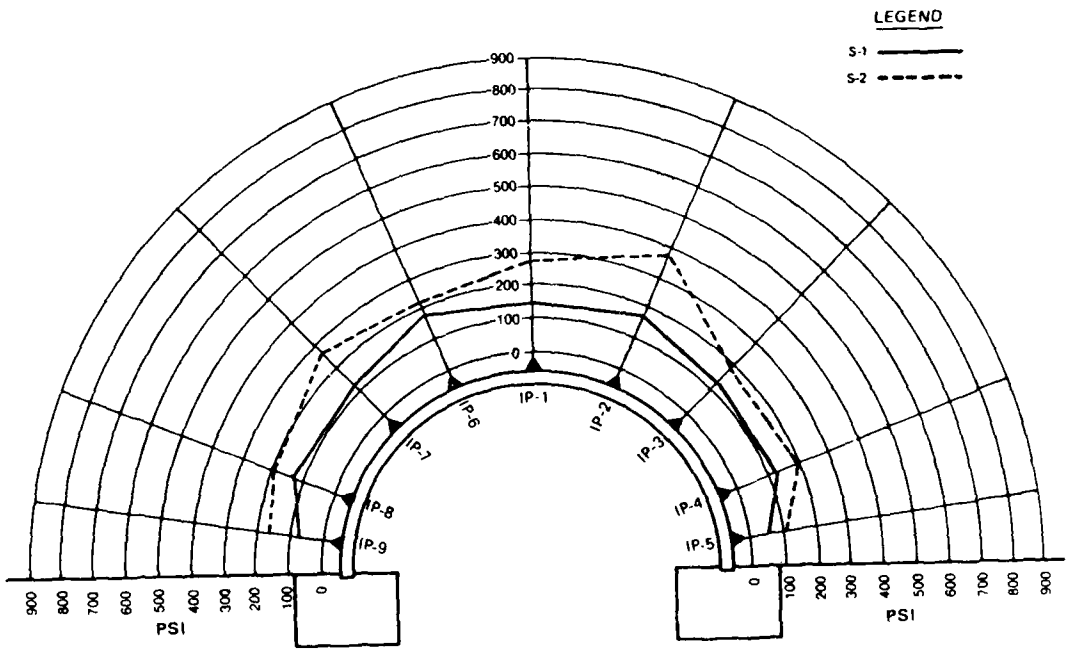

WP = 200 PSI

Figure 32. Interface normal pressure distribution at water pressure (WP) = 100 and 200 psi.

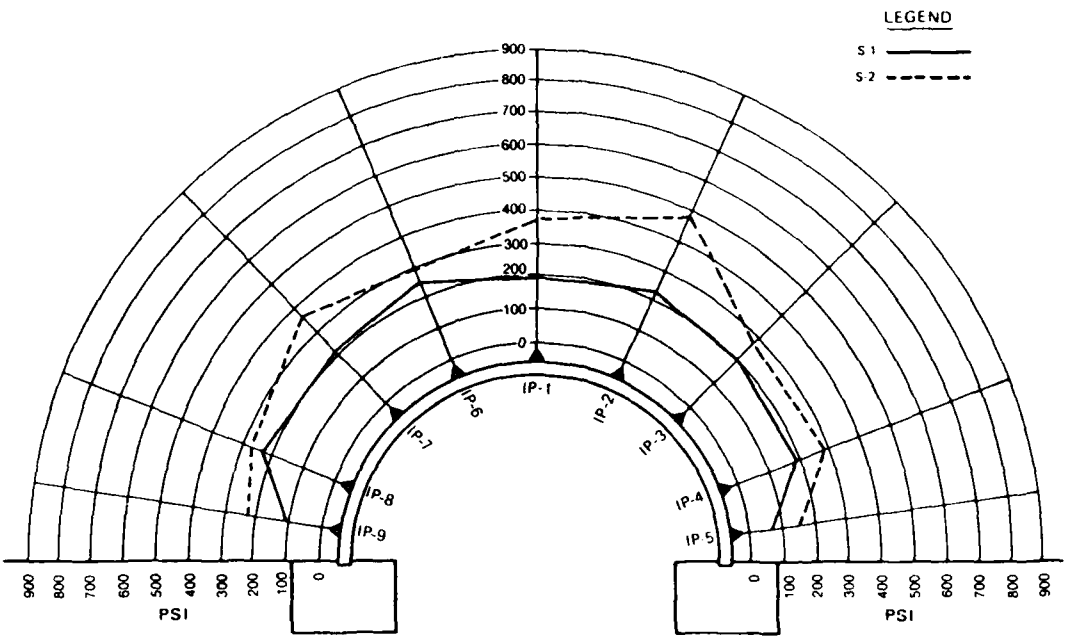

WP = 300 PSI

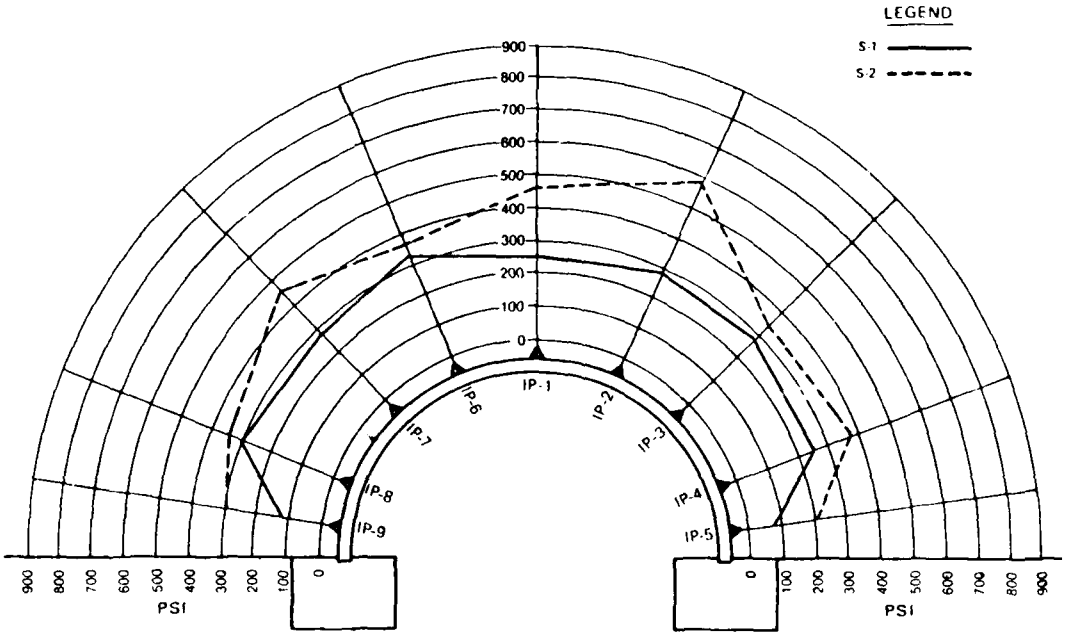

WP = 400 PSI

Figure 33. Interface normal pressure distribution at water pressure (WP) = 300 and 400 psi.

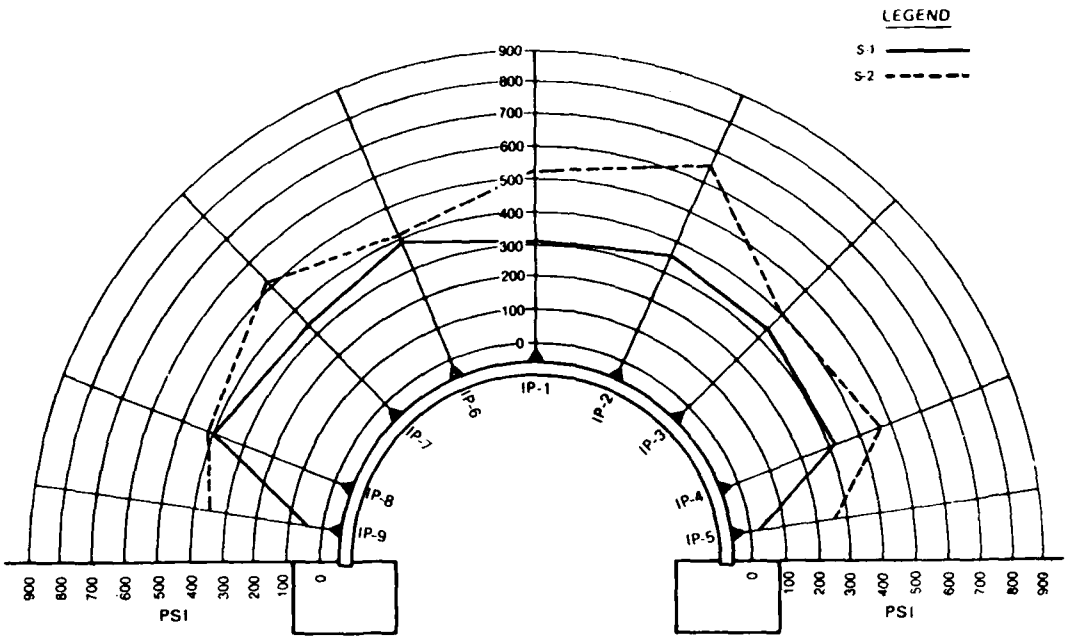

WP = 500 PSI

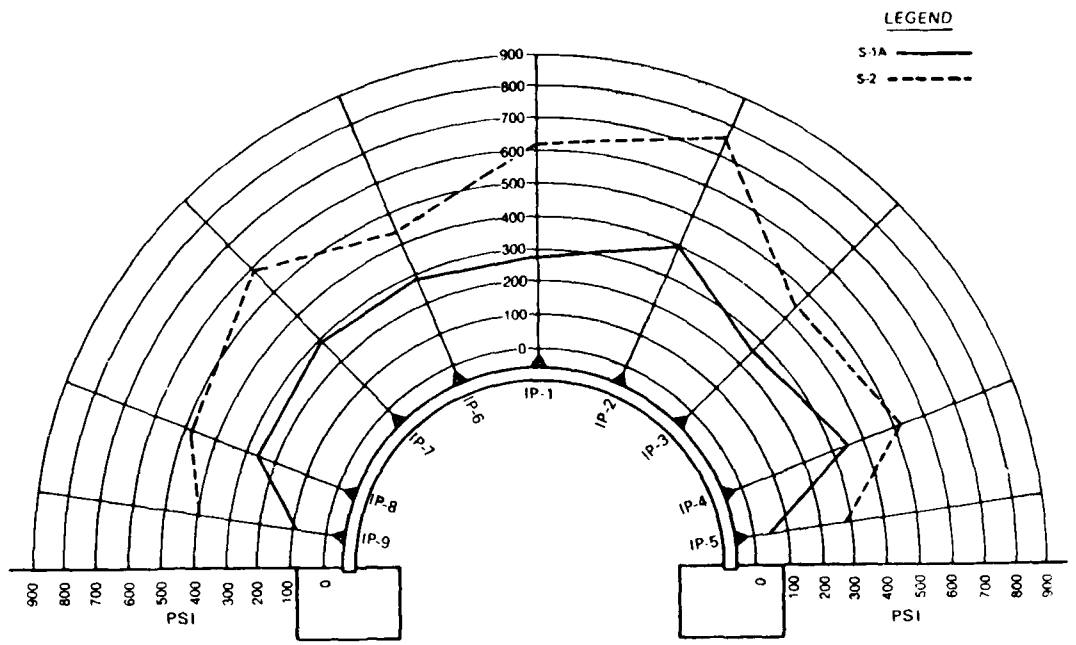

WP = 600 PSI

Figure 34. Interface normal pressure distribution at water pressure (WP) = 500 and 600 psi.

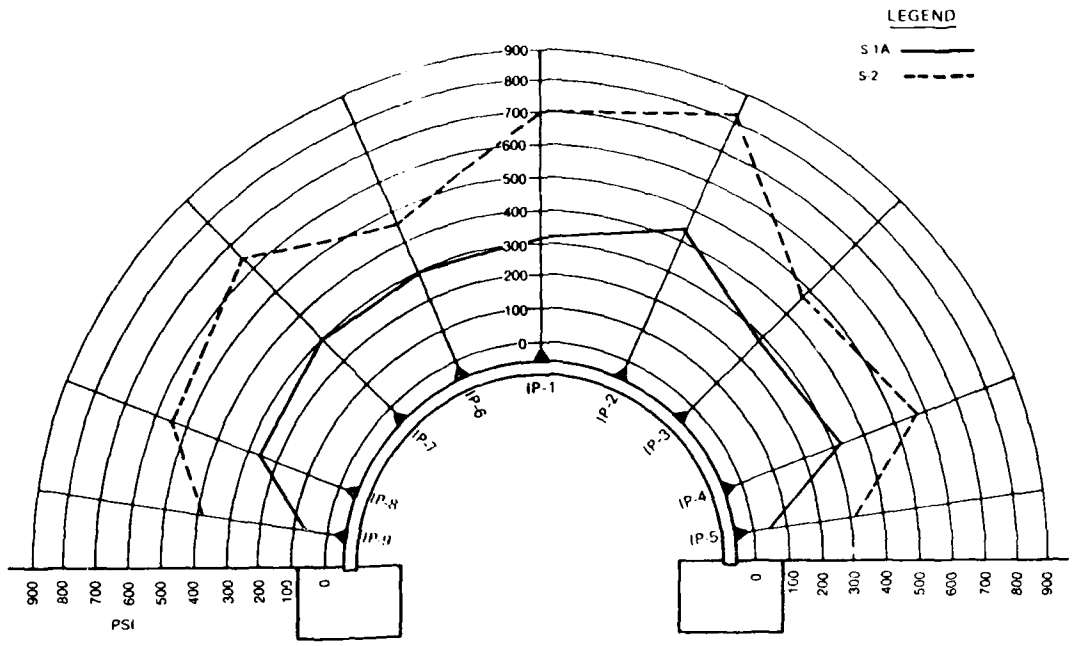

WP = 700 PSI

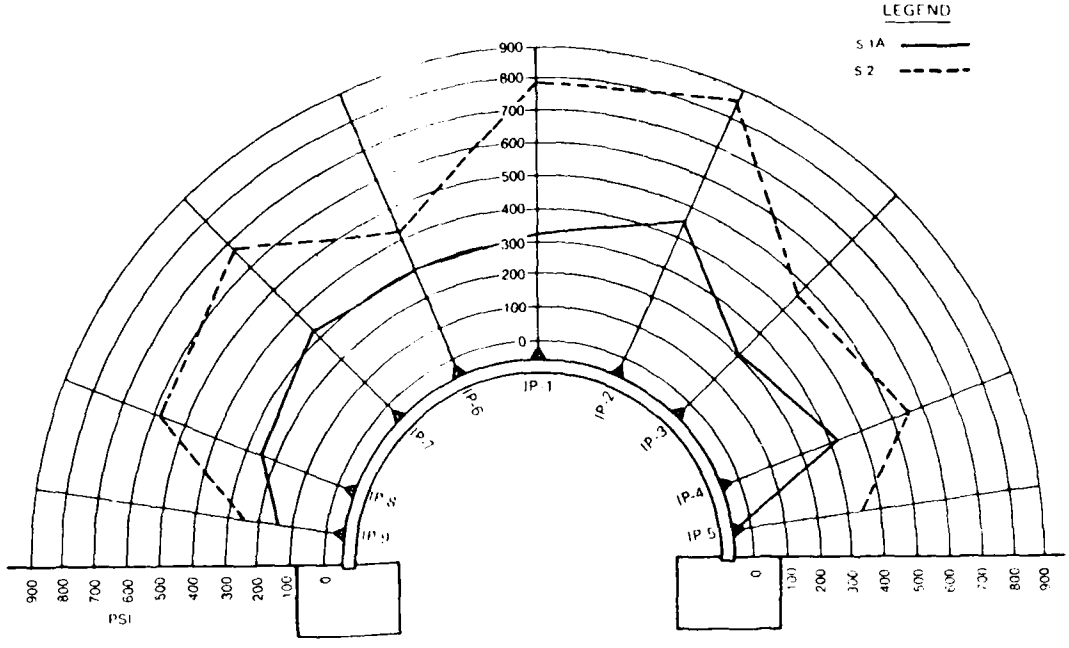

WP = 800 PSI

Figure 35. Interface normal pressure distribution at water pressure (WP) = 700 and 800 psi.

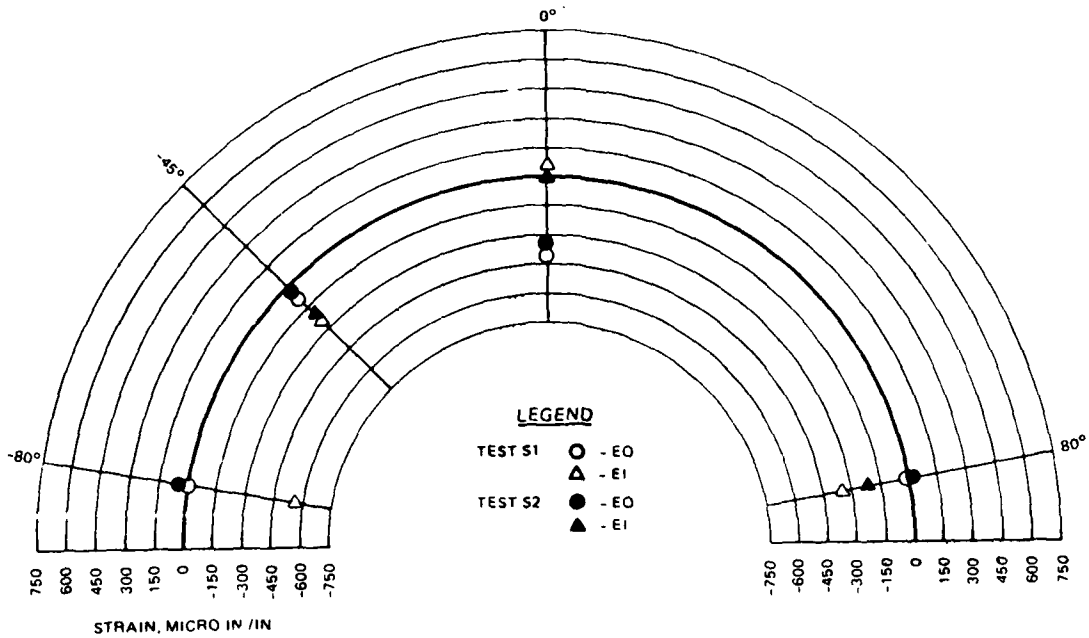

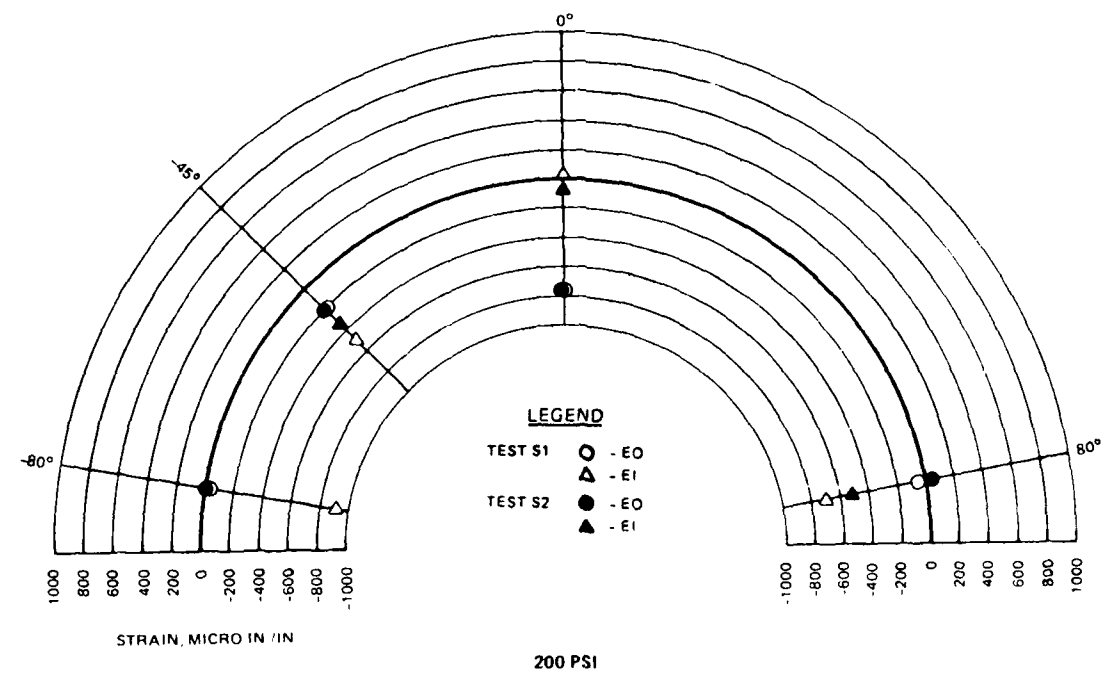

Figure 36. Experimental reinforcing bar strains at water pressure (WP) = 100 and 200 psi.

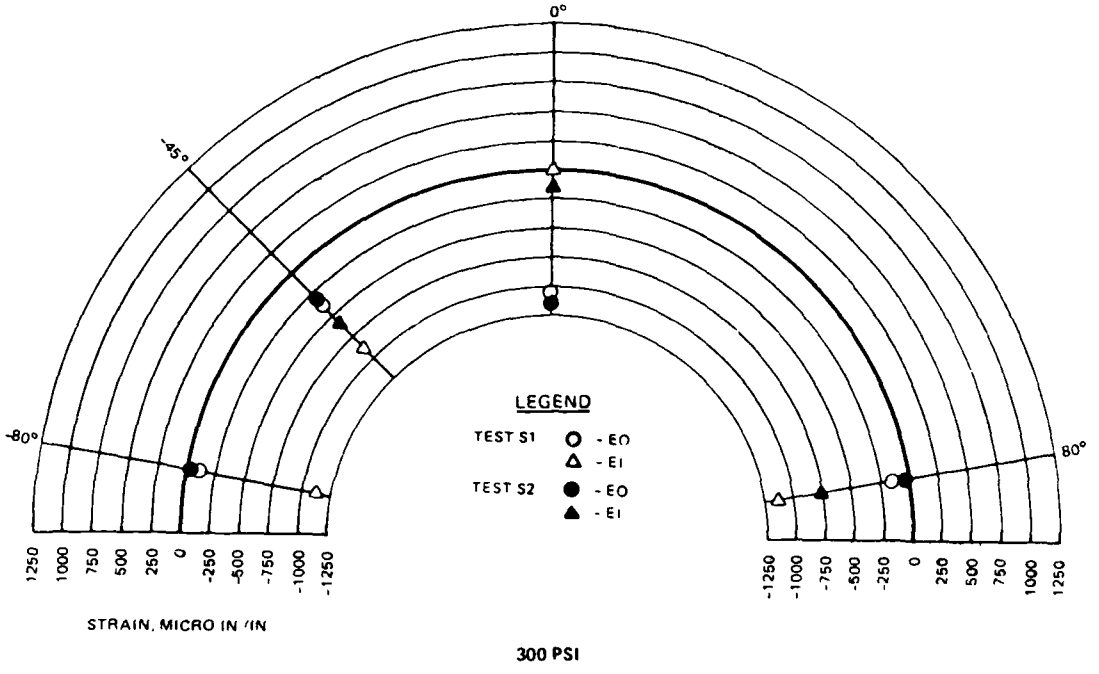

300 PSI

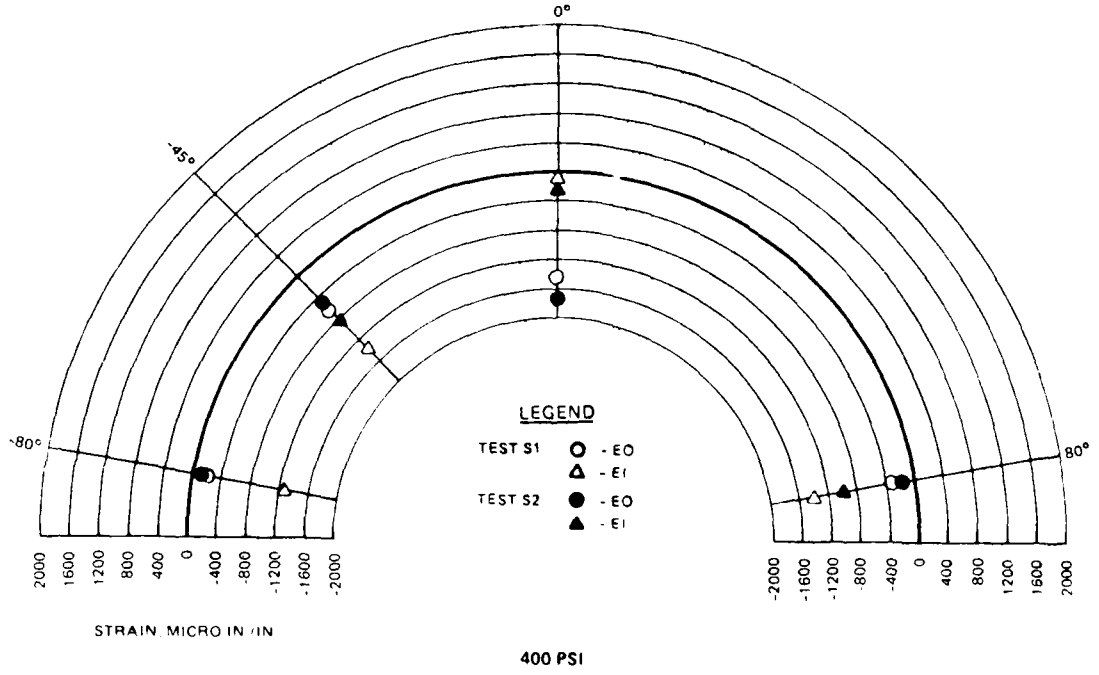

400 PSI

Figure 37. Experimental reinforcing bar strains at water pressure (WP) = 300 and 400 psi.

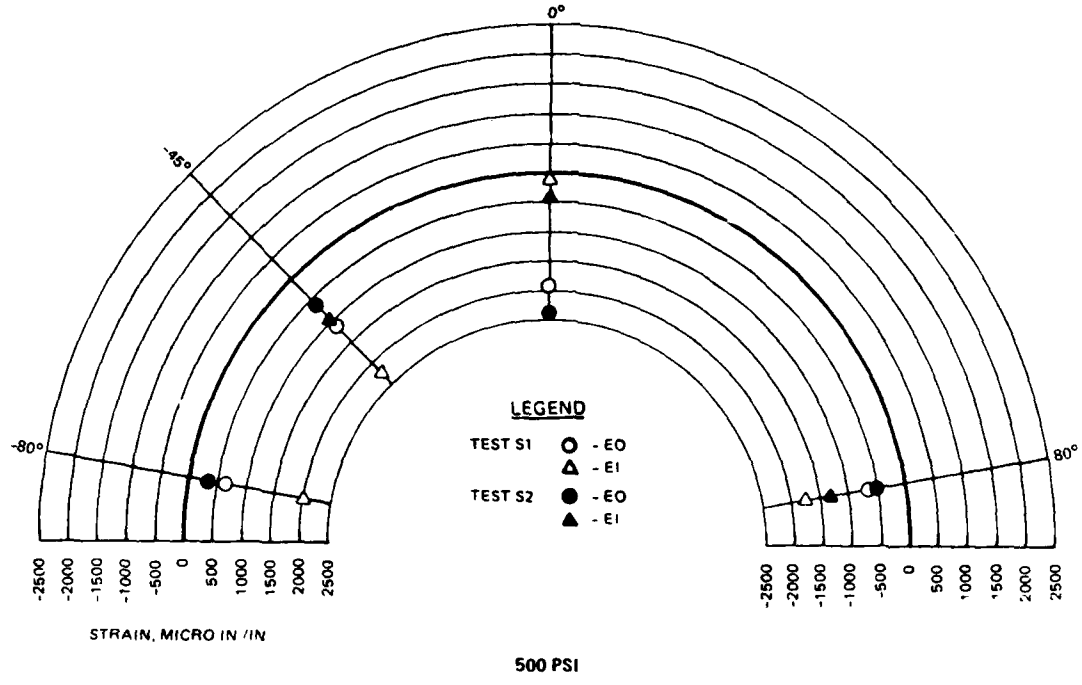

Figure 38. Experimental reinforcing bar strains at water pressure (WP) = 500 psi.

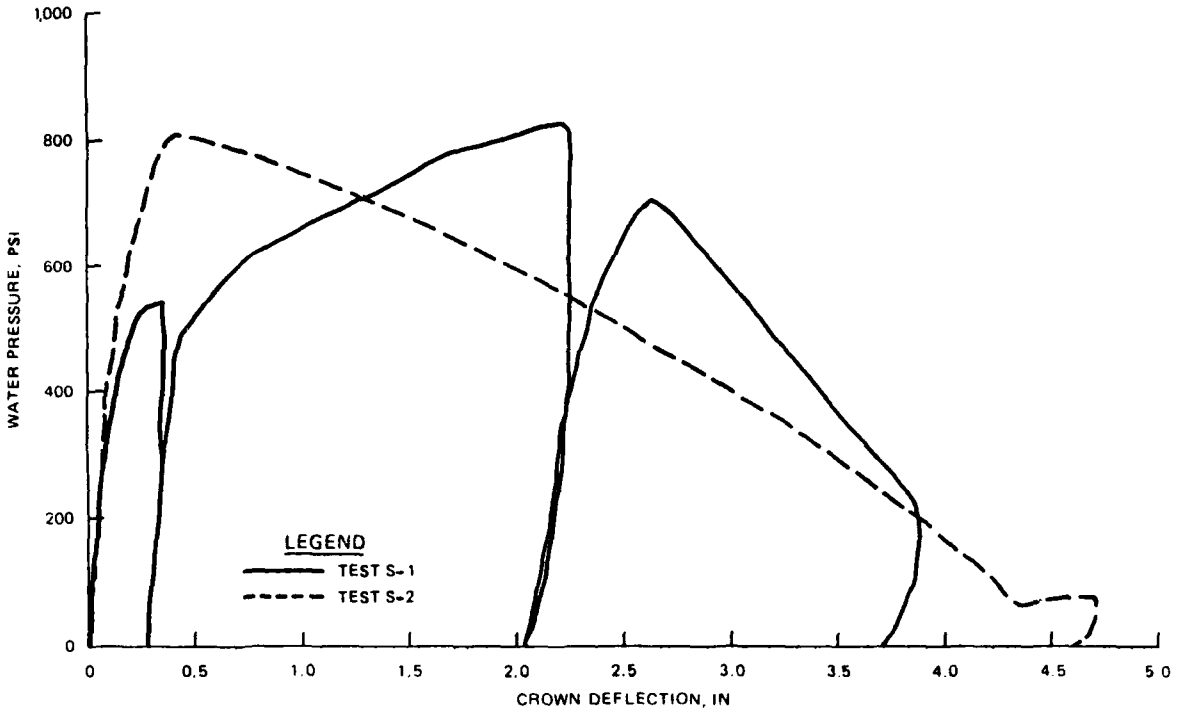

Figure 39. Measured arch crown deflection.

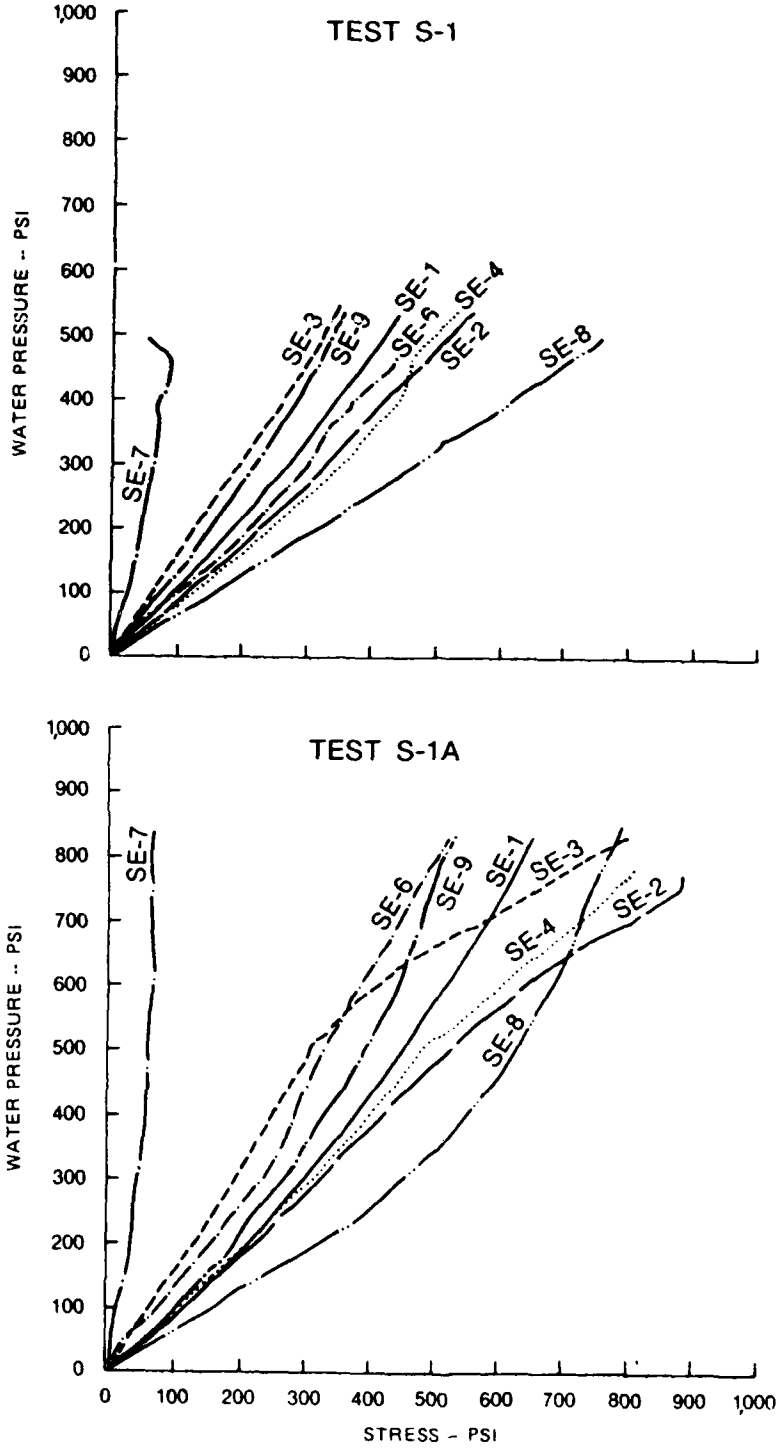

Figure 40. Soil-stress measurements, test S1 and S-1A.

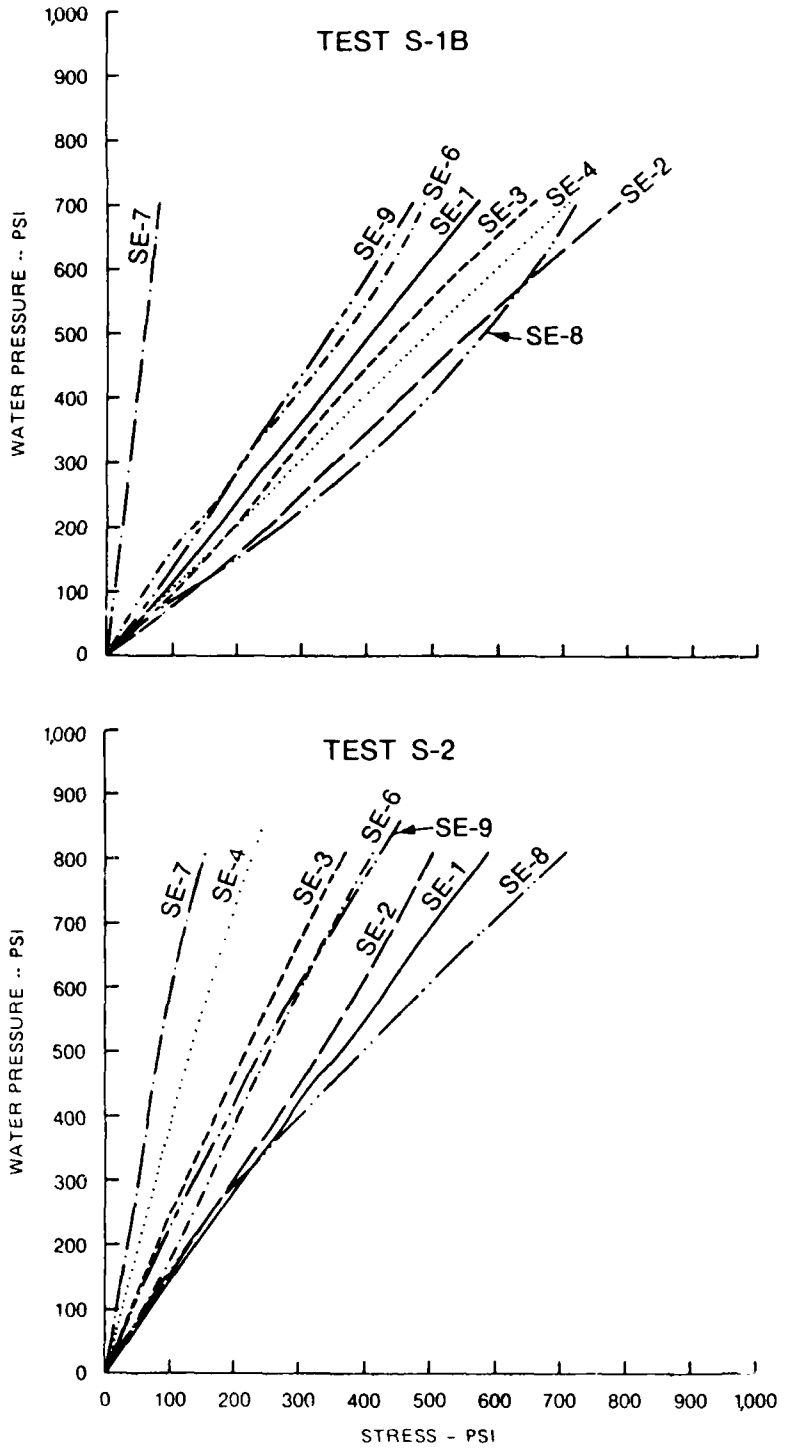

Figure 41. Soil-stress measurements, test S-1B and S-2.

SECTION 4

ANALYSIS

4.1 INTRODUCTION

Analysis of the test results included computations of experimental moments and thrusts in the arch rings using strain data recorded from gages placed on the inner and outer reinforcing bars at 0, -45, and 80 degrees from the crown. Comparisons made between the two arches included moment versus thrust, overpressure versus moment, and overpressure versus thrust.

4.2 EXPERIMENTAL MOMENTS AND THRUSTS

A computer program (Appendix B) was written to calculate the combined moments and thrusts in the arch ring using experimental strain data. The calculational procedure was based on the free-body diagram and the assumed linear strain distribution shown in Figure 42. The inner and outer experimental reinforcing bar strains were input, and a computed straight line through the two points defined the strain distribution across the section. The concrete stress across the section was calculated based on the Kent-Park stress-strain curve (Reference 16) shown in Figure 43. In region BC of the stress-strain curve ($0.002 < \varepsilon_c < \varepsilon_{20c}$):

$$f'_c = f'_c \, [1 - Z \, (\varepsilon_c - 0.002)] \qquad (5)$$

where

$$Z = 0.5/(\varepsilon_{50u} + \varepsilon_{50h} - 0.002)$$

ε_c = concrete strain

$\varepsilon_{50u} = (3 + 0.002 \, f'_c)/(f'_c - 1000)$

$\varepsilon_{50h} = 0.75 \, \rho_s \, (b''/s_h)^{0.5}$

ρ_s = ratio of volume of transverse reinforcement to volume of concrete core measured to outside of hoops

b'' = width of confined core measured to outside of hoops

s_h = spacing of hoops measurements

The parameter Z defines the slope of the assumed linear falling branch. The slope of the falling branch is specified by the strain when the stress has fallen to 0.5 f'_c . Since the arches in this test did not have stirrups, the

falling branch for unconfined concrete was used in the moment-thrust calculations.

The stress-strain curve used to compute the reinforcing steel stress is shown in Figure 44 and takes into account plastic strains. Once the stresses in the reinforcing steel and across the concrete section have been computed, the thrust and moment is calculated by

$$P = F_c + F'_s - F_s \tag{6}$$

$$M = [(P)(\frac{h}{2}) + (F_s)(d) - (F_c)(k_x) - (F'_s)(d')] \tag{7}$$

where

P = thrust

F_c = force in concrete

F'_s = force in compression steel

F_s = force in tensile steel

M = bending moment

h = overall height of the concrete section

d = depth to tension steel

k_x = distance from compression force to F_c

d' = depth to compression steel

Figures 45-48 show the moment in the arches at the strain gage locations (0, -45, and 80 degrees) corresponding to water pressures at 100-psi intervals. Figure 49 shows a comparison of the moment at each of these locations as a function of the water pressure. The moment in both arches was generally positive at 0 degrees (crown) and negative at -45 and 80 degrees although the moment at the crown of arch S-2 became negative at an overpressure of about 650 psi. At the crown of the arches, the moment-pressure plot for both tests is very similar up to about 400 psi where the difference in the magnitude of the moments starts to increase with that in test S-1 being greater than in S-2. At -45 degrees the moment in test S-1 is greater than in test S-2 from the beginning of the test to about 450 psi after which the moment in test S-1 undergoes a sharp decrease and falls below that in test S-2 at about 480 psi. This also occurred at 80 degrees although the moments at 80 degrees were significantly higher than at 45 degrees. This can be seen in Figure 50 which shows moment versus pressure at all three strain gage locations in each arch.

The moment-pressure plots for test S-2 show that from about 400 to 500 psi the moments in the arch reached their maximum value and began to decrease. At approximately 700 psi the moment at all three locations was near zero and the moment at 0 and 80 degrees changed signs. This indicates that the effects of soil-structure interaction tended to force the arch into its most favorable mode of response, that being the compression mode. Although the first loading sequence in test S-1 reached only about 500 psi, this same effect appears to be occurring in that all of the moments have peaked and are headed back toward zero.

Figures 51-54 show the thrust in the arches at 100-psi intervals. Figure 55 compares the thrust-pressure curves between the two arches at the three strain gage locations. Figure 56 compares the thrust-pressure curves between the three locations on the same arch for both tests. As can be seen, the thrust in test S-1 was generally higher than in test S-2 except for the 0-degree location where the opposite was true after the overpressure reached about 200 psi. In test S-1 the thrust was about equal at each of the three locations until the water pressure reached about 200 psi, after which the thrust at -45 degrees climbed at the highest rate and at 80 degrees at the lowest rate. In test S-2 the thrust at 0 degrees was the highest up to a water pressure of about 500 psi where it began to decrease. The thrust at -45 and 80 degrees continued to climb with increasing water pressure until at 80 degrees, it began to fall at about 650 psi. When arch S-2 failed, the thrust was highest at -45 degrees.

Figure 57 compares the load paths (moment-thrust interaction as the arches were being loaded) in both tests at each strain gage location along with the theoretical ultimate moment-thrust interaction diagram. The theoretical curve was computed assuming failure at a concrete compressive strain of 0.003. These plots show that at each of three locations in the arch ring, the ultimate strength of the section was reached in the compression regime of the moment-thrust diagram, i.e., above the point representing the condition of balance thrust. The location in both tests which had the highest ratio of thrust to moment throughout most of the loading was -45 degrees with 0 degrees having the lowest. Arch S-2 had higher thrust-to-moment ratios at all three locations than did arch S-1 throughout most of the loading, indicating that the behavior of the Teflon-covered arch was in more of a compression mode than the other arch. Figure 58 compares, separately for each test,

the load paths at the three strain gage locations.

Table 3 lists, for each of the three strain gage locations, the static overpressure when the theoretical ultimate capacity (ε_c = .003) of the section was reached at that location. This was obtained by reading the thrust values from the load paths at the point where they intersected the ultimate moment-thrust curve and by finding the corresponding pressure on the thrust-pressure plots. In both test S-1 and test S-2, the theoretical ultimate capacity at the crown was reached first followed by the 80-degree location. In test S-1 the overpressure, when the ultimate capacity at the crown was reached, was 390 psi, and in test S-2 it was 325 psi. In both tests, as the pressure increased after the ultimate capacity at the crown was reached, the moment started decreasing. In test S-2 the moment at the crown decreased to such an extent that the sign changed from positive to negative. This resulted in the moment and thrust at the crown decreasing below the ultimate capacity while the ultimate capacity was being reached at the other locations in the arch. Test S-1 appeared to be behaving similarly before the pressure was reduced to zero to recalibrate the gages. The moment-thrust plots in Figure 57 indicate that as the pressure increased after the ultimate capacity was reached at the strain gage locations, the moment at those locations tended to start reducing, resulting in the arch behaving more in compression. This had the effect of providing the arch with added load carrying capacity and was the result of the soil confining the arch ring.

4.3 ARCHING RATIOS

Global soil arching can be computed by dividing the total load applied directly above the arch by the vertical reactions at the arch springline. If this ratio is greater than one, then the arch is stiffer than the surrounding medium and is attracting load, which is known as active arching. If the ratio is less than one, then the arch is less stiff than the surrounding medium causing load to be arched to the soil, which is known as passive arching. The global arching ratios for each test were computed using the thrust-pressure plots computed from the strains near the springlines. Plots of arching ratio versus overpressure for both tests are shown in Figure 59 and were obtained from:

$$C_a = \frac{T}{(p)\left(\frac{D}{2}\right)} \qquad (8)$$

where

C_a = soil arching ratio

T = springline thrust for a unit length of arch

p = static overpressure

D = outside arch diameter

Figure 59 shows that in both tests active soil arching occurred throughout the loading. More arching occurred in test S-2 than in test S-1. In test S-1 the arching ratio was about 0.6 throughout the first load sequence. The arching ratio in test S-1 varied widely with overpressure. The minimum value was about 0.05 at 50-psi overpressure, and the maximum was about 0.6 at an overpressure of 630 psi where it began decreasing to about 0.25 at 800 psi. Although the normal pressure on the arch with Teflon (S-2) was greater than on the arch without Teflon for a given overpressure (Figures 32-39), the arching ratios indicate that there was less total load on the Teflon-covered arch than on the arch without Teflon. This is possible because the normal pressure on the Teflon-covered arch was approximately the total load since there should have been very little frictional loading, and the normal pressure on the arch without Teflon was only one component of the total load, the other component being the friction force.

4.4 INFLUENCE OF AXIAL LOAD ON CURVATURE DUCTILITY

A comparison between load-deflection curves corresponding to brittle and ductile behavior of a reinforced concrete member is shown in Figure 60. From Reference 14, the distributions of bending moment, shear force, and axial load in a statically indeterminate structure depend on the ductility of the members at the critical sections. A distribution of bending moments differing from that obtained from a linear elastic structural analysis can be achieved if moment redistribution can take place. Some sections may reach their ultimate resisting moments before others; however, if plastic rotation can occur there while the ultimate moment is maintained, additional load can be carried as the moments elsewhere increase to their ultimate value. However, the presence of axial load has been shown to have a significant effect on the curvature ductility of a reinforced concrete member.

Although it was developed as an upper bound solution, the bilinear resistance function shown in Figure 2, has a zero slope after ultimate

resistance, is not realistic. This resistance function assumed pure compression with no bending or shear stresses. As shown in Figure 39, once the arch reached its maximum resistance, the resistance decreased with increasing deflection. The combination of ultimate moment and thrust above the balance point in an unconfined concrete section results in brittle behavior. A study was conducted by Blume, Newmark, and Corning (Reference 17), which showed the relationship between curvature ductility and axial load in a column section having bars on two opposite faces. The balanced point in the column section studied occurred at $P/P_o = 0.31$. Figure 60 shows that the curvature ductility of the section is significantly reduced by the presence of axial load. Another investigation was conducted by Pfrang, Seiss, and Sozen (Reference 18) and dealt with inelastic deformations of reinforced concrete column sections. Moment-curvature curves were obtained for column sections with various levels of constant axial load, i.e., the column load was held constant at a particular level while the column was bent to failure. A set of these curves corresponding to a section with 1 percent reinforcing steel is shown in Figure 61. These curves illustrate again that at axial load levels greater than the balanced failure load, the curvature ductility is negligible.

Table 3. Water pressure at ultimate strength.

Test	Water Pressure, psi, at indicated location in arch ring, degrees		
	0	-45	80
S-1	390	410	420
S-2	325	530	580

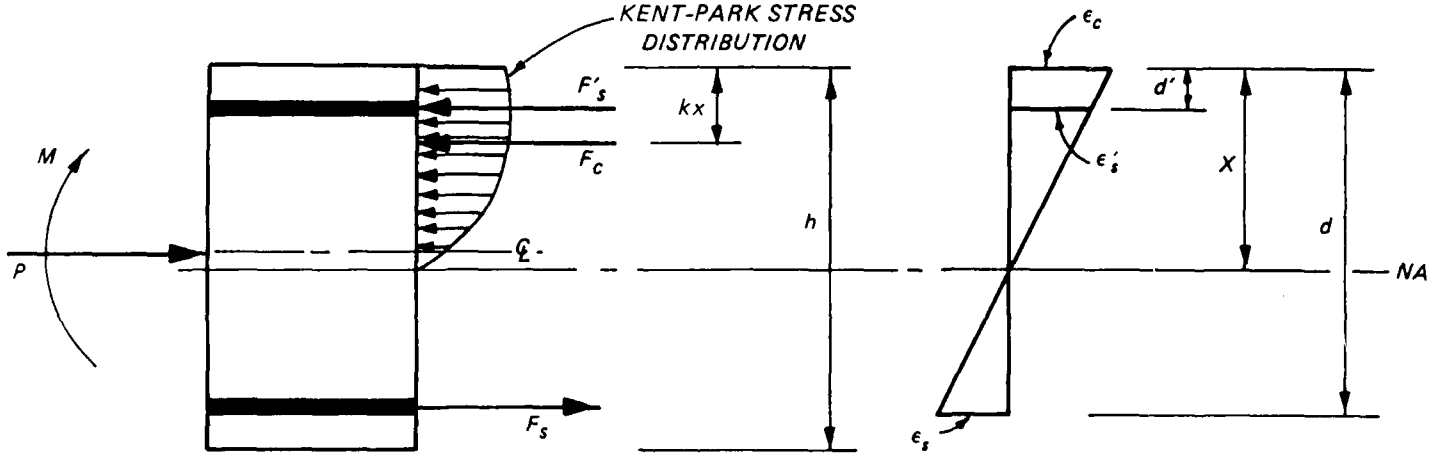

Figure 42. Concrete section free-body diagram and assumed strain distribution.

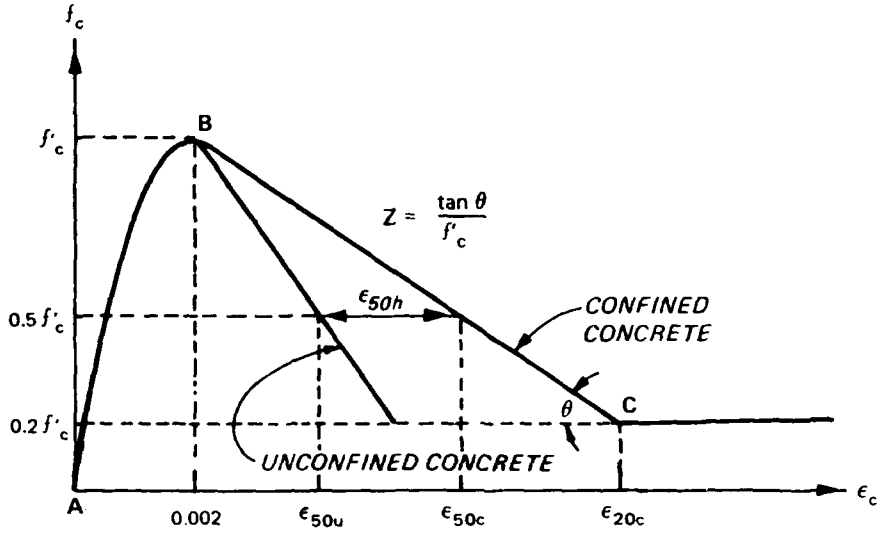

Figure 43. Kent-Park concrete model.

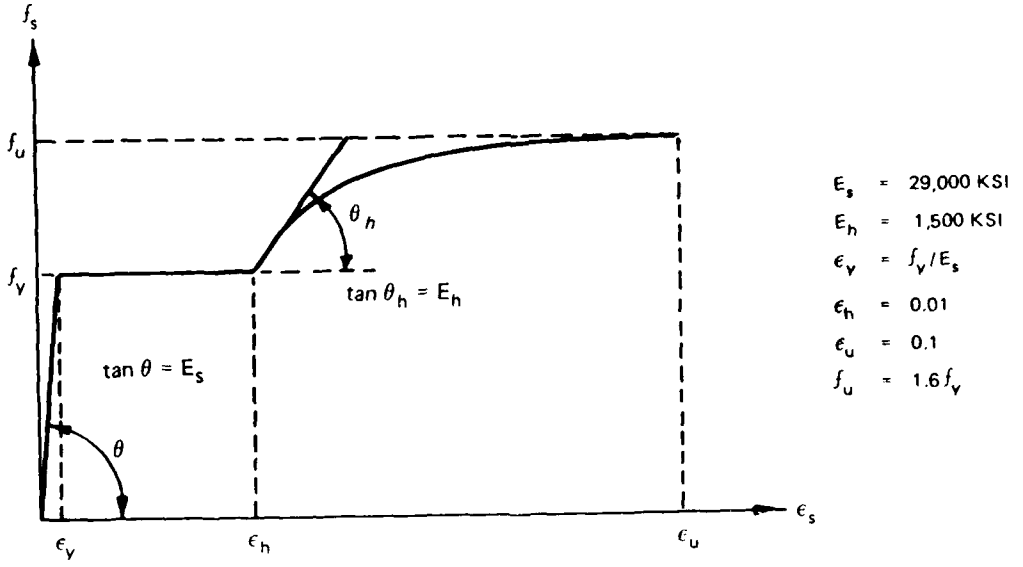

Figure 44. Reinforcing steel constitutive model.

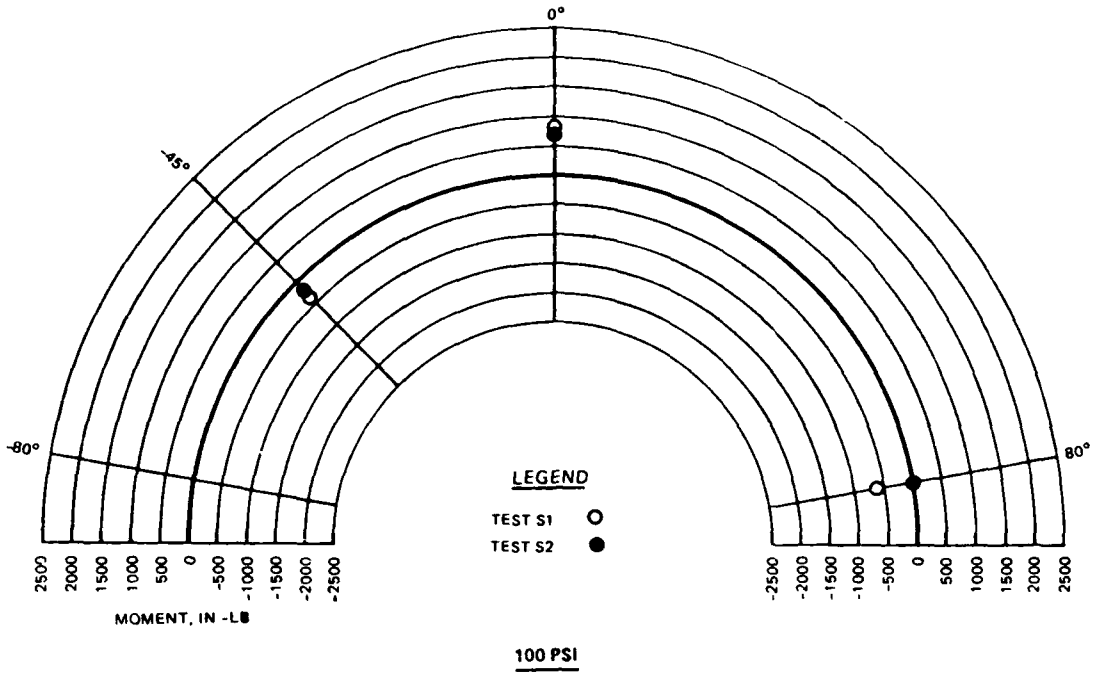

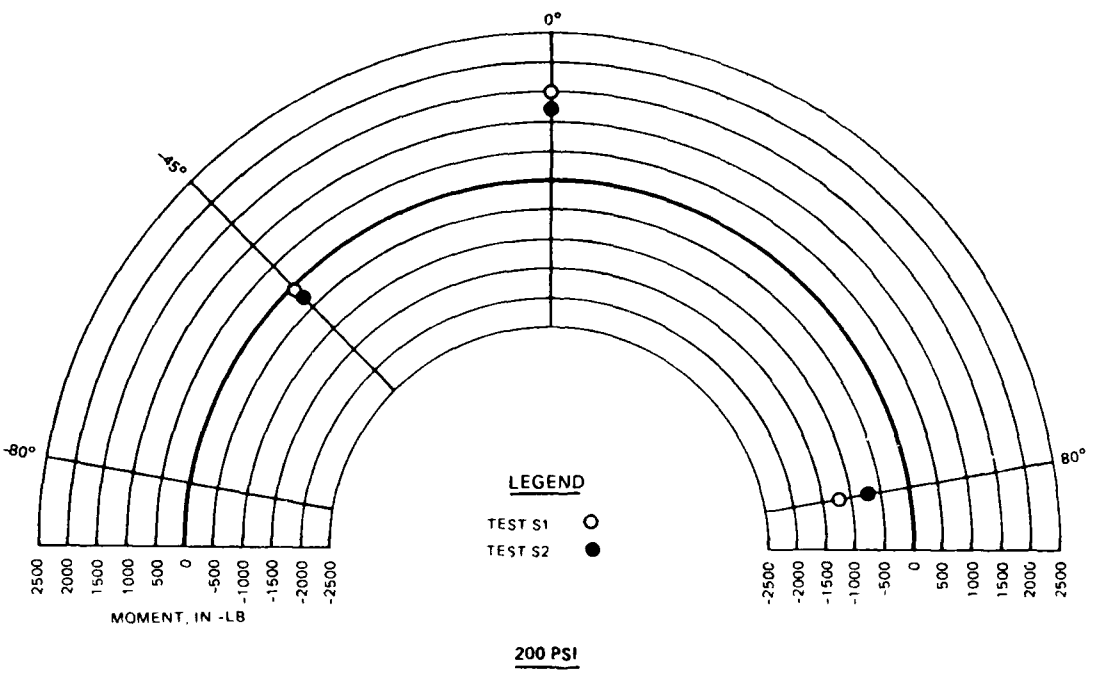

Figure 45. Experimental moments in arch ring at water pressure (WP) = 100 and 200 psi.

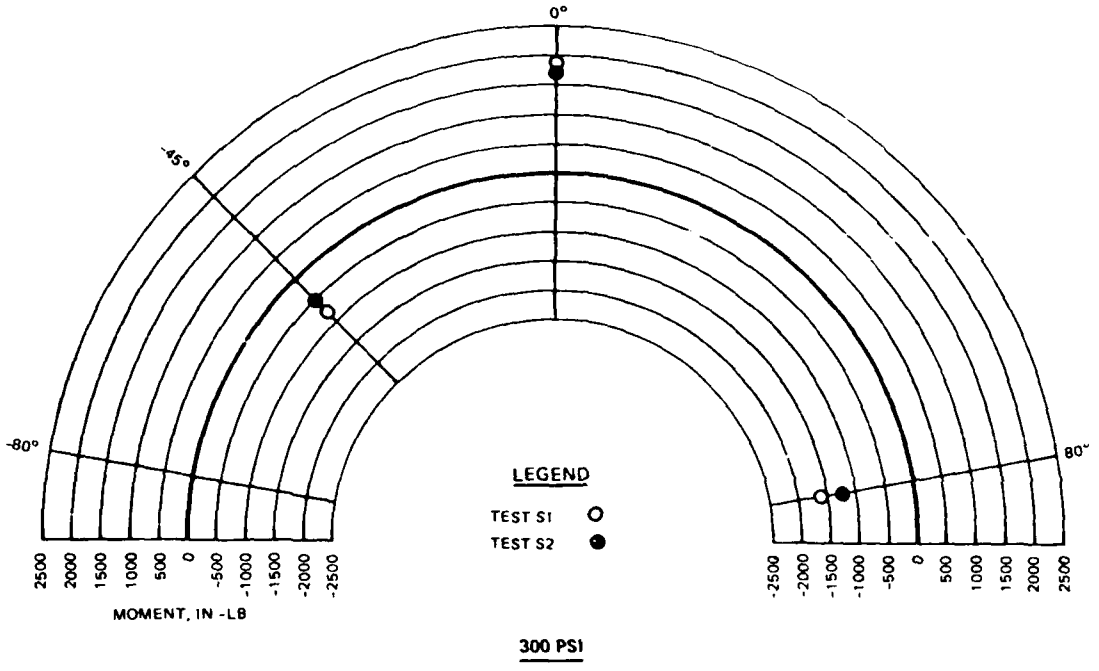

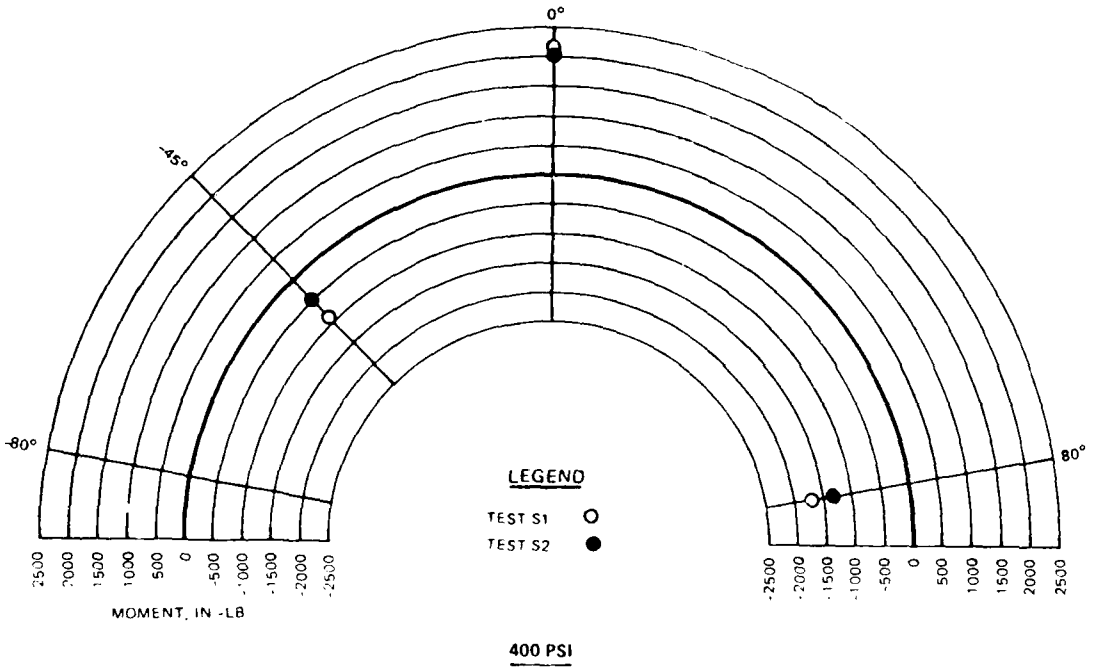

Figure 46. Experimental moments in arch ring at water pressusre (WP) = 300 and 400 psi.

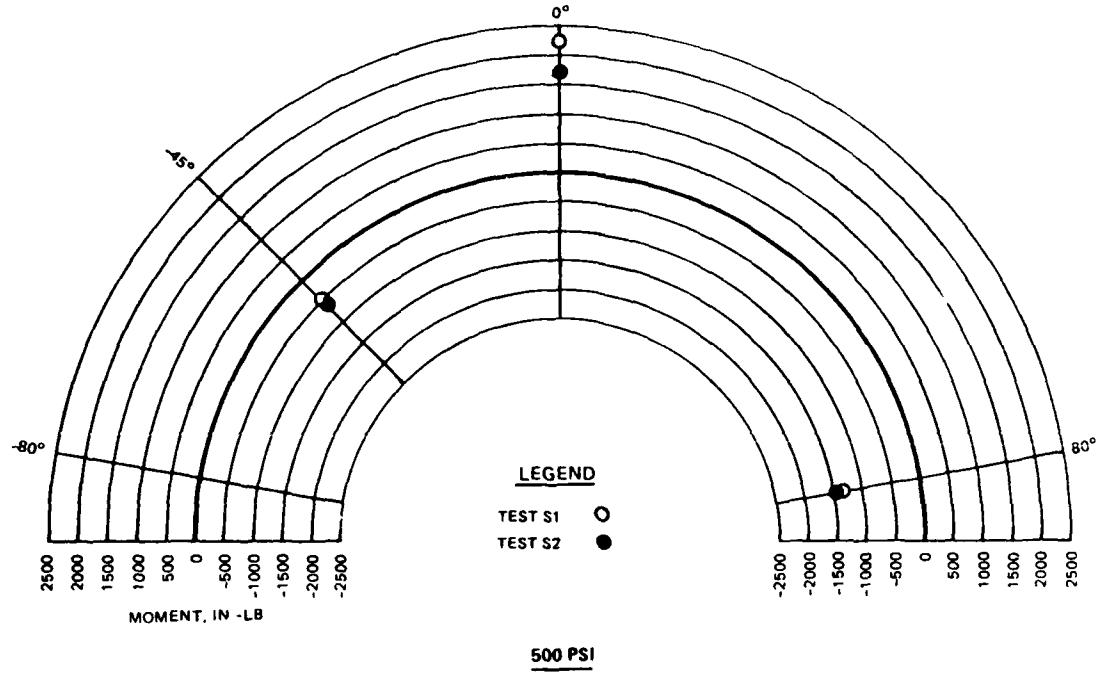

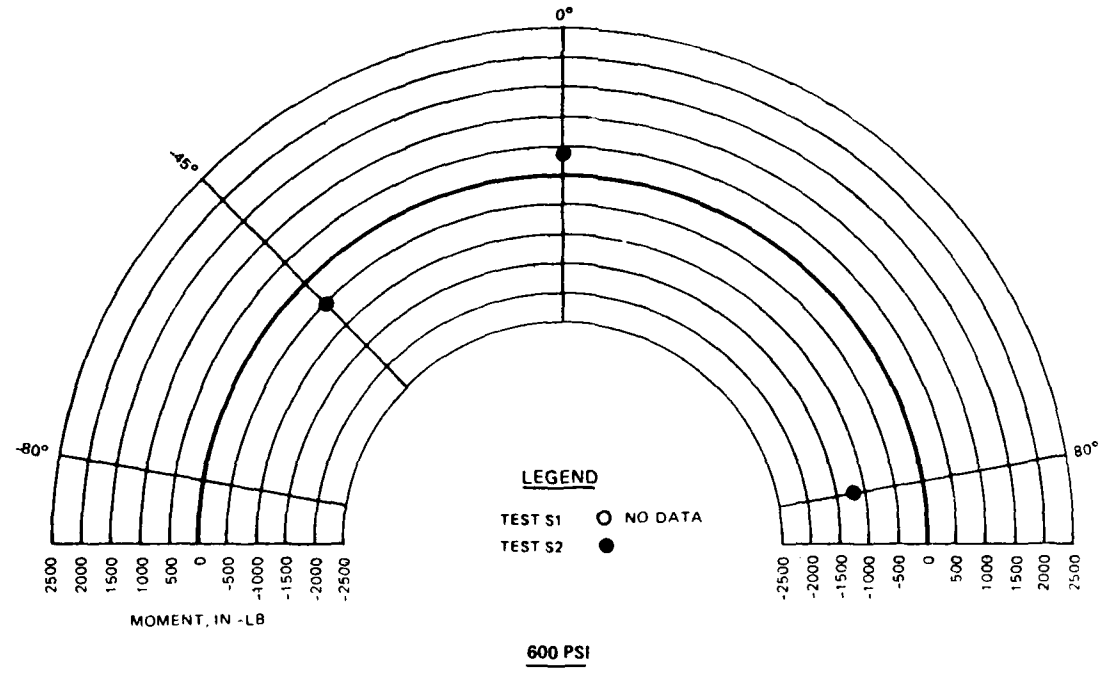

Figure 47. Experimental moments in arch ring at water pressure (WP) = 500 and 600 psi.

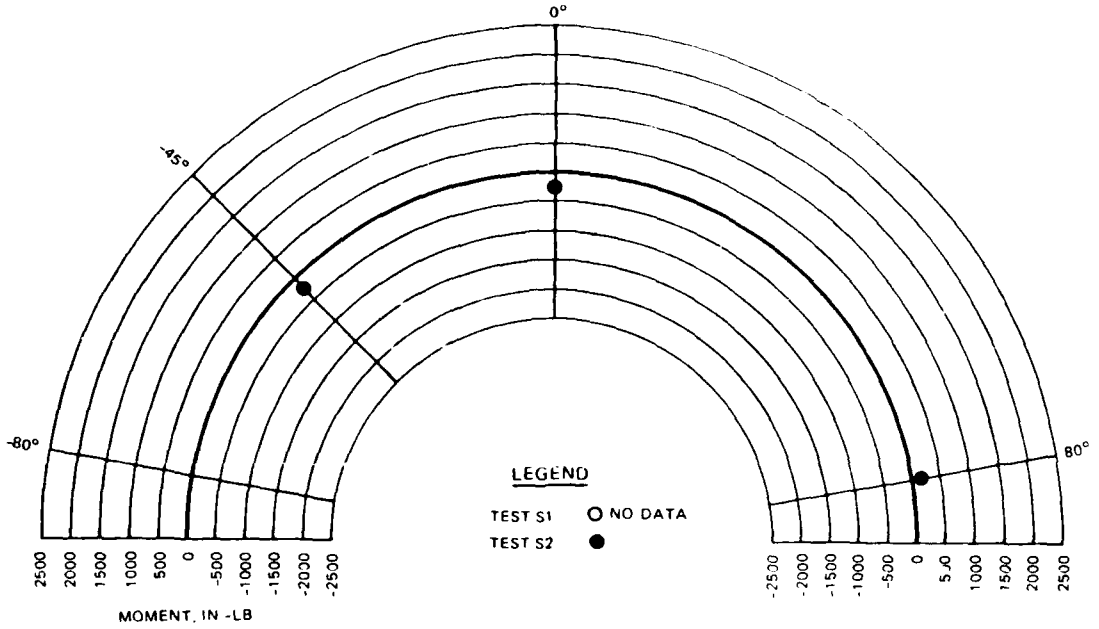

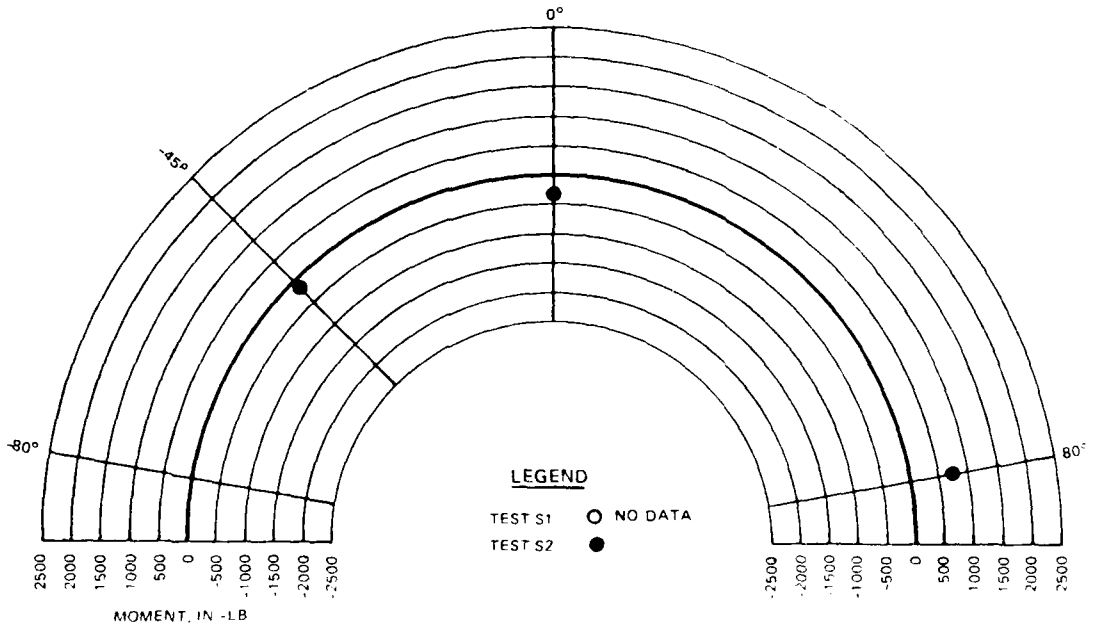

Figure 48. Experimental moments in arch ring at water pressure (WP) = 700 and 800 psi.

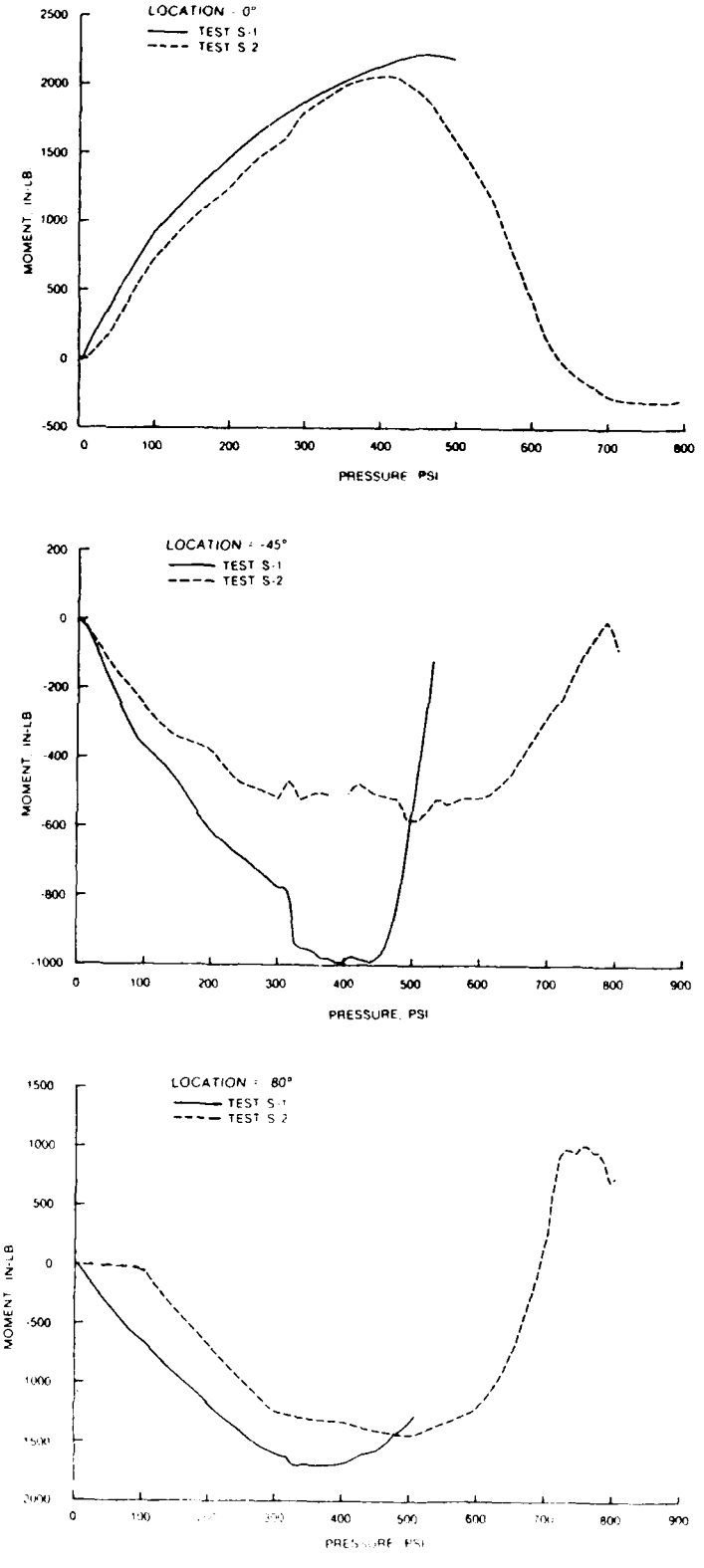

Figure 49. Moment-pressure comparisons between tests.

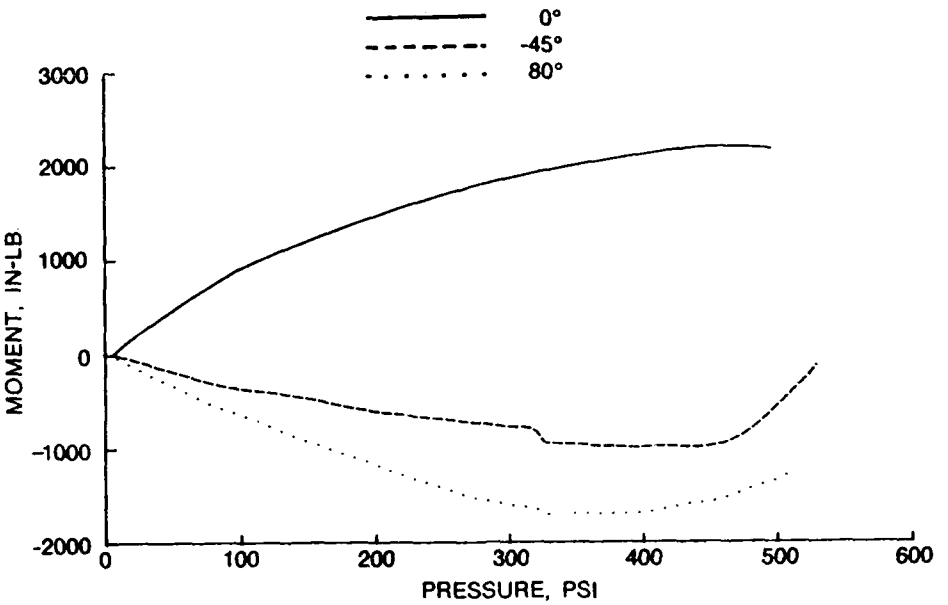

a. Arch S-1.

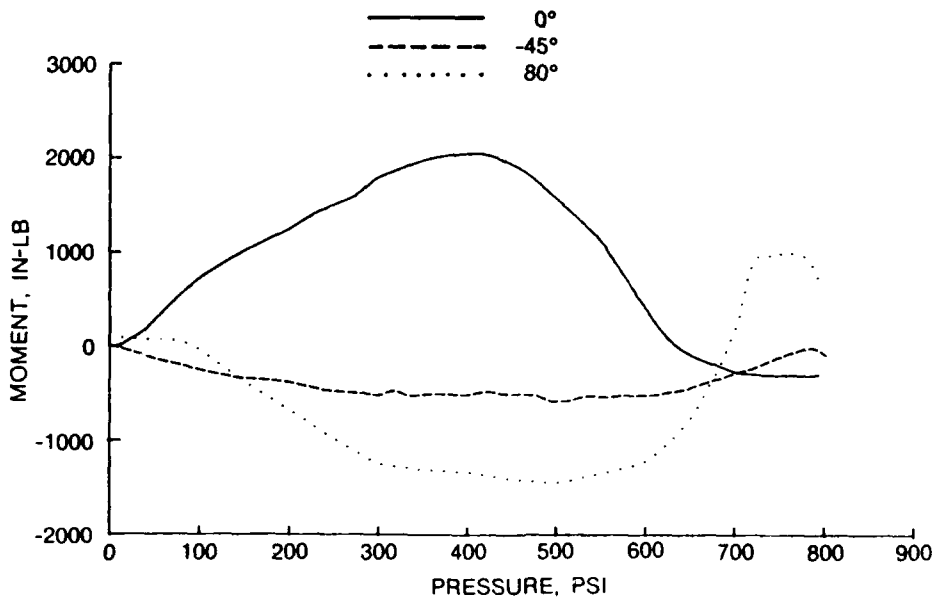

b. Arch S-2.

Figure 50. Moment-pressure comparisons between locations in each test.

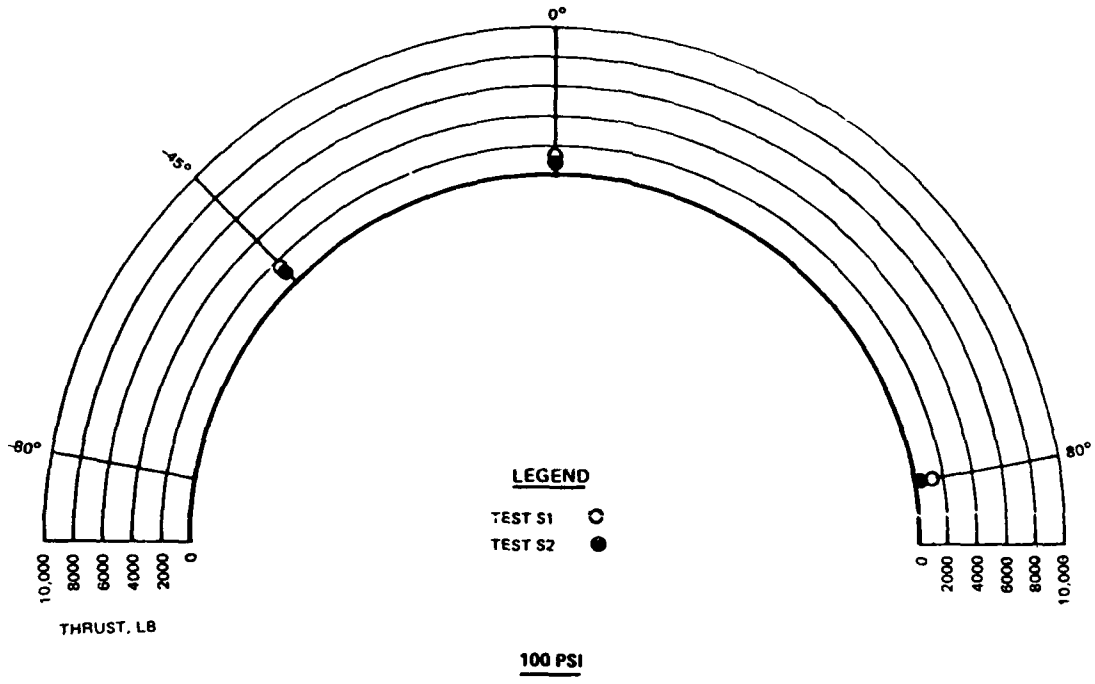

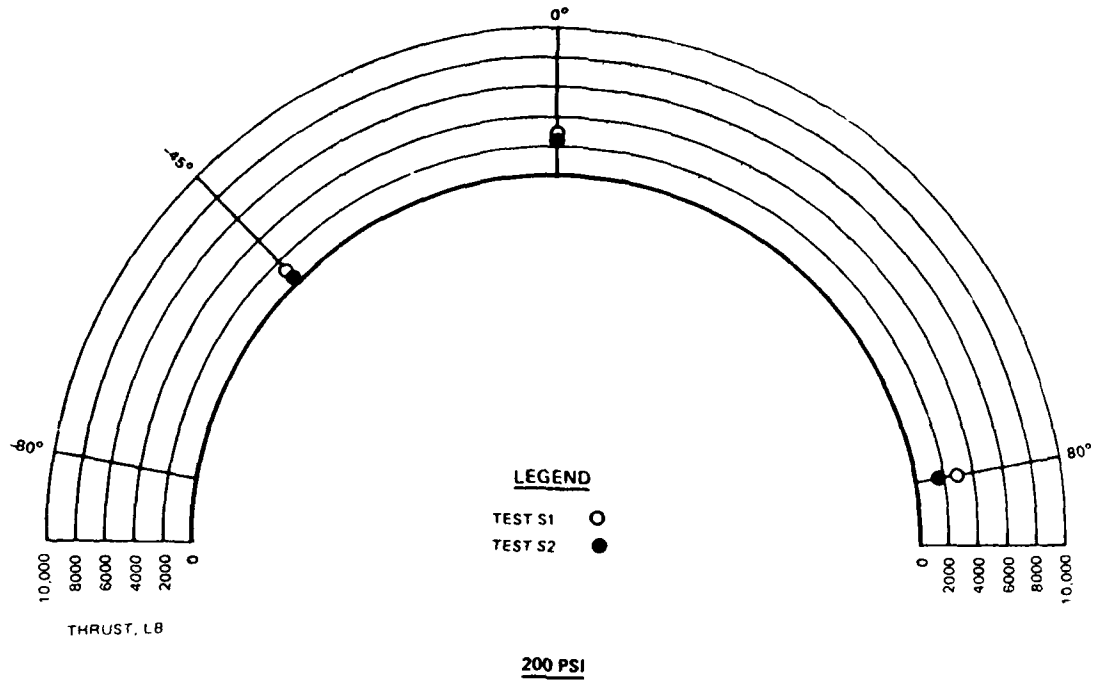

Figure 51. Experimental thrust in arch ring at water pressure (WP) = 100 and 200 psi.

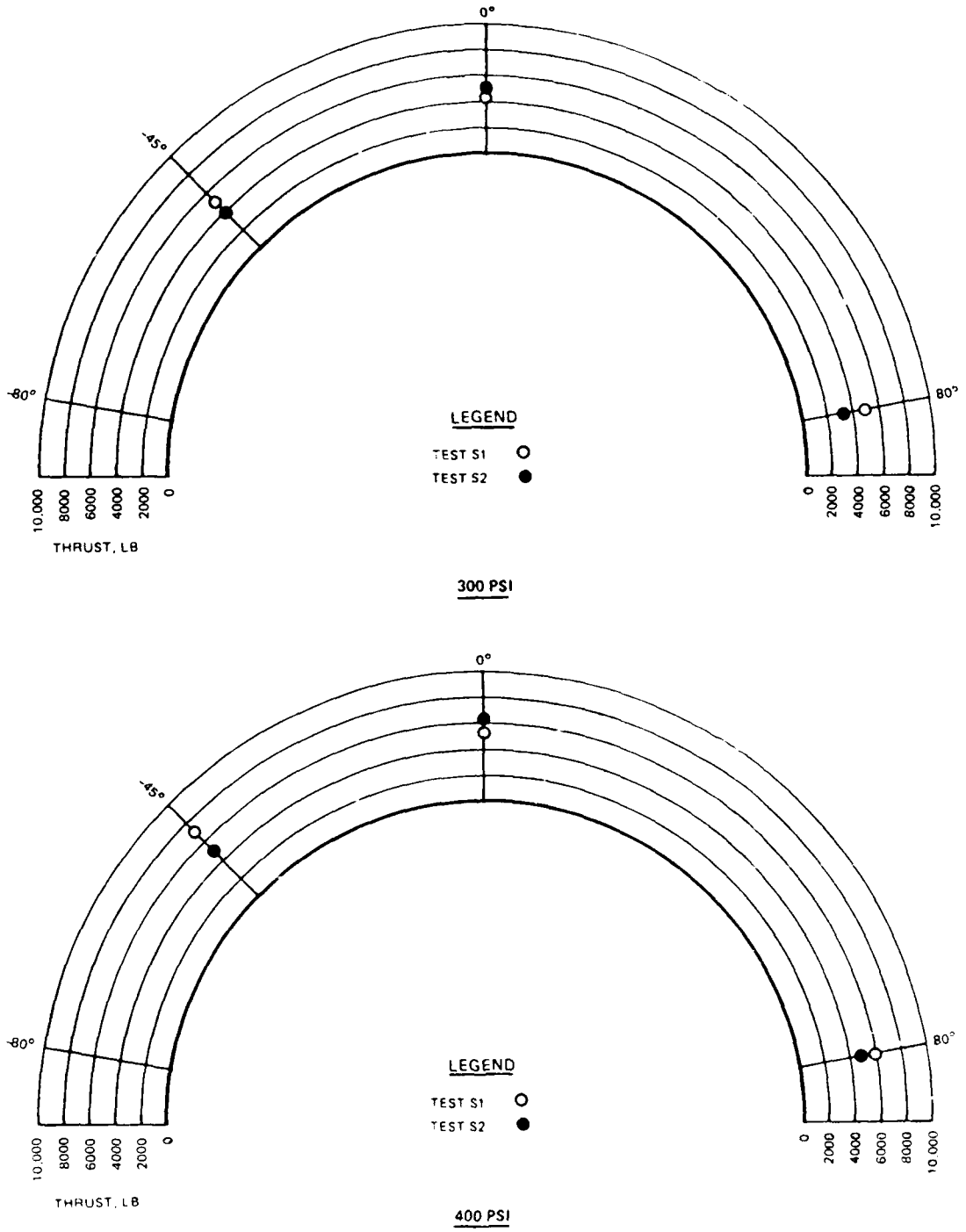

Figure 52. Experimental thrust in arch ring at water pressure (WP) = 300 and 400 psi.

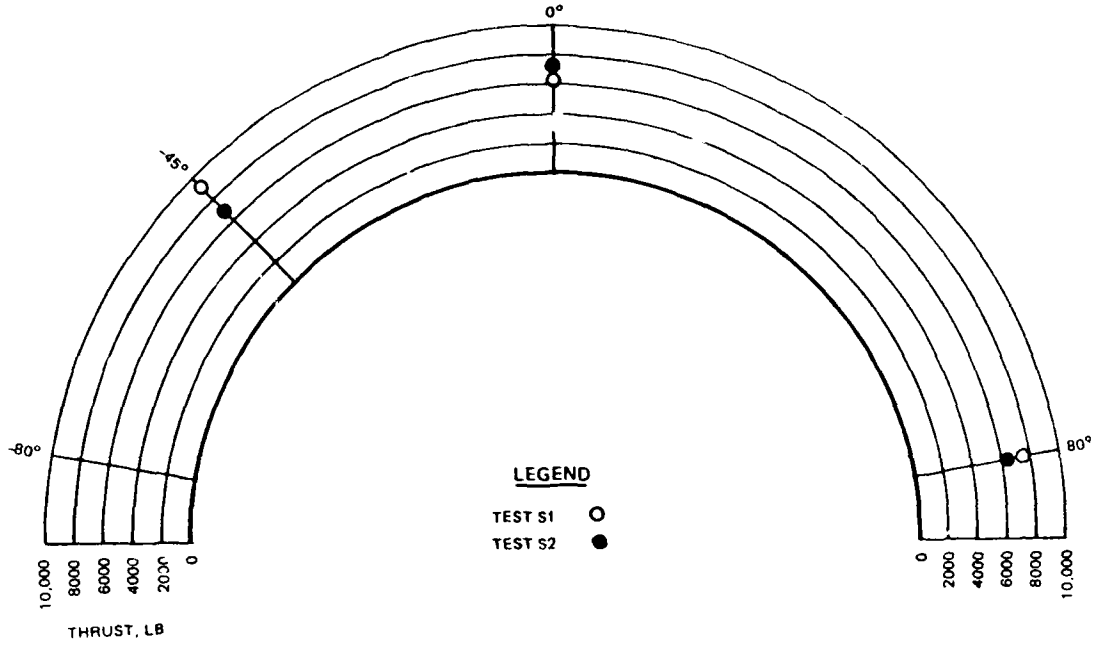

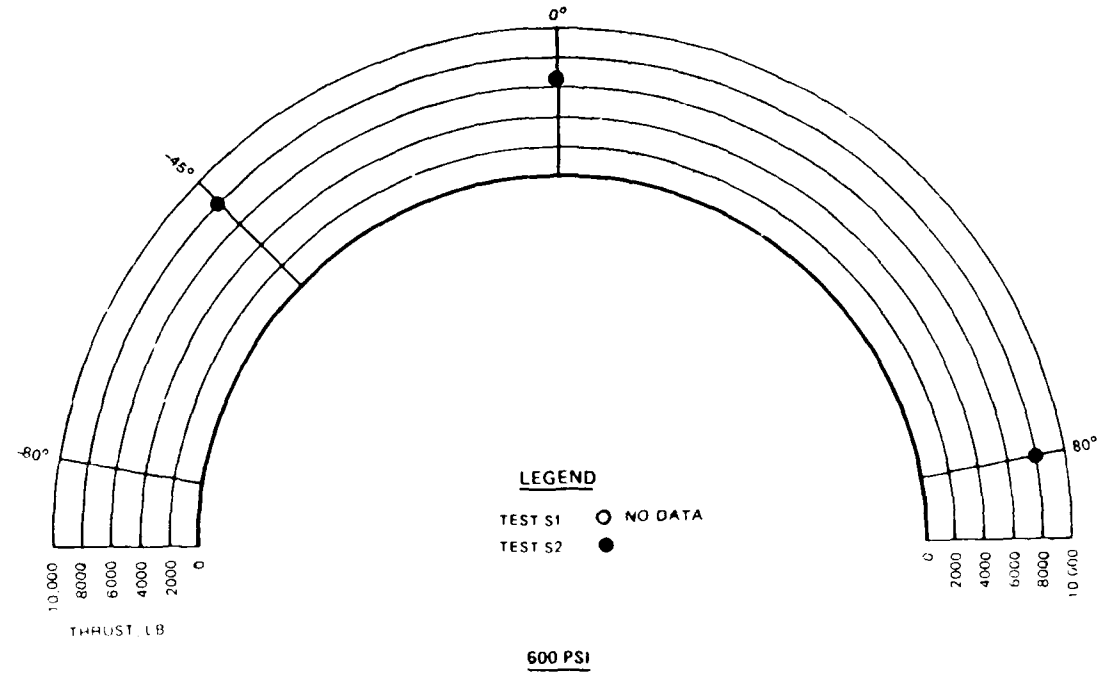

Figure 53. Experimental thrust in arch ring at water pressure (WP) = 500 and 600 psi.

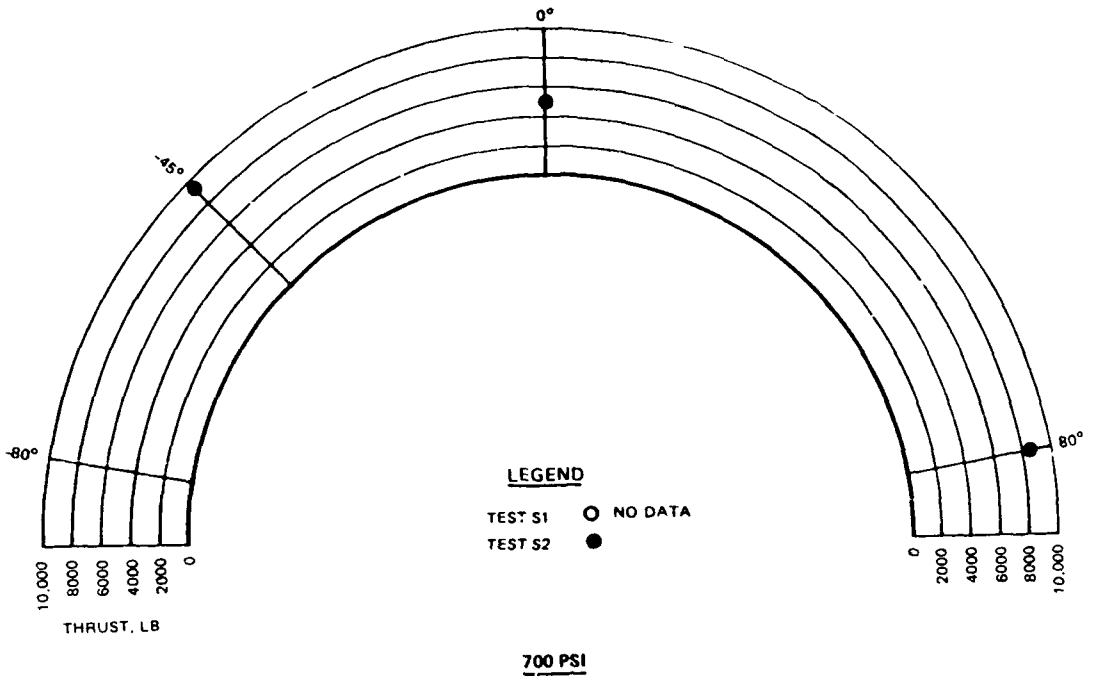

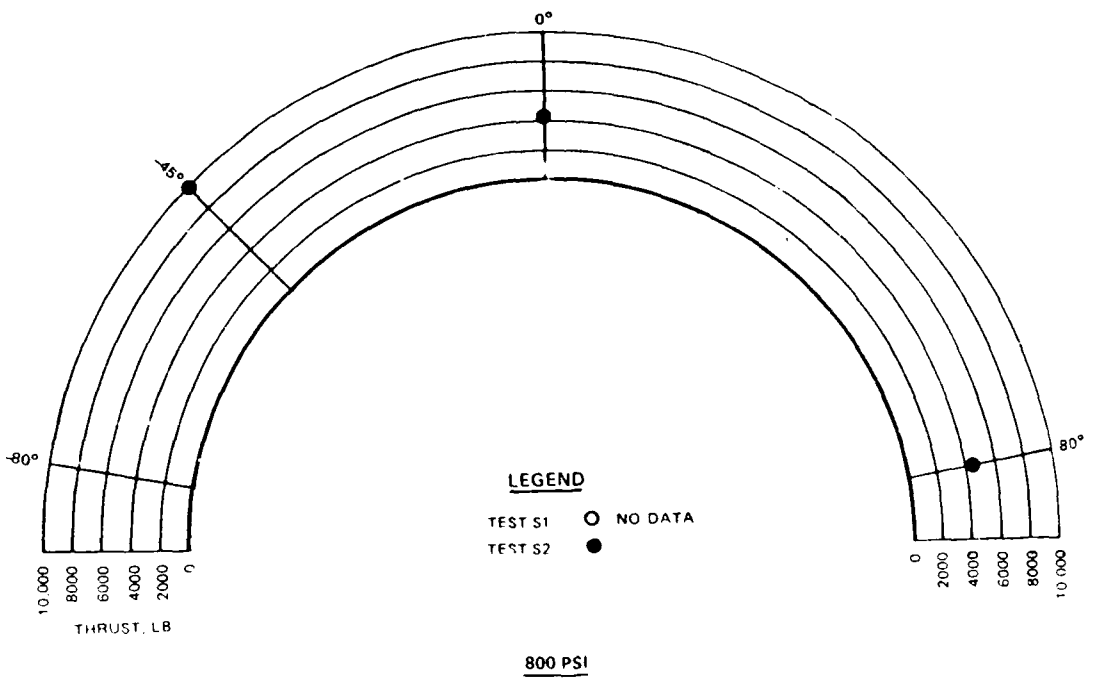

Figure 54. Experimental thrust in arch ring at water pressure (WP) = 700 and 800 psi.

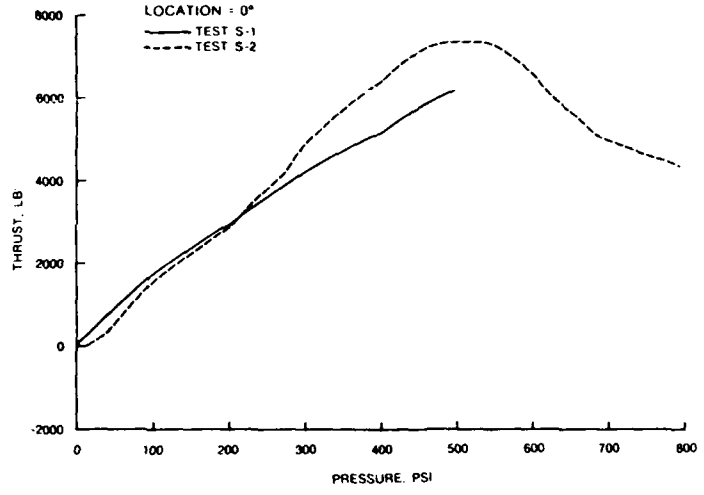

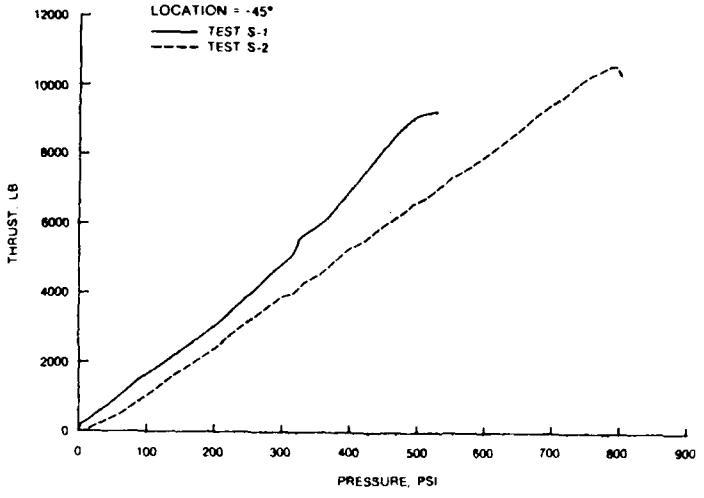

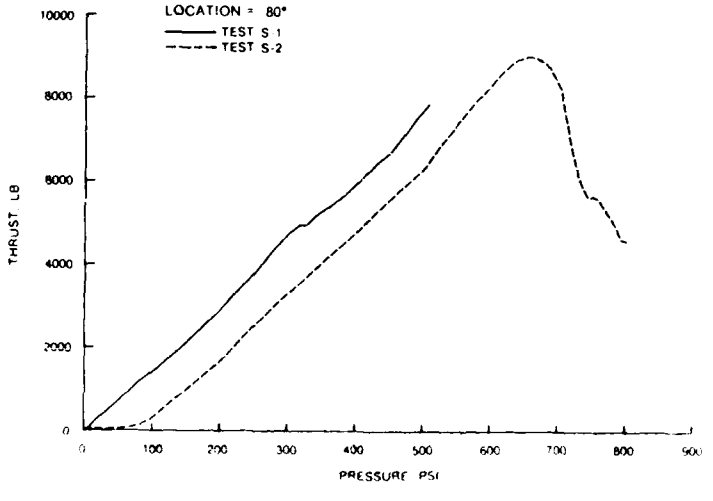

Figure 55. Thrust-pressure comparisons between tests.

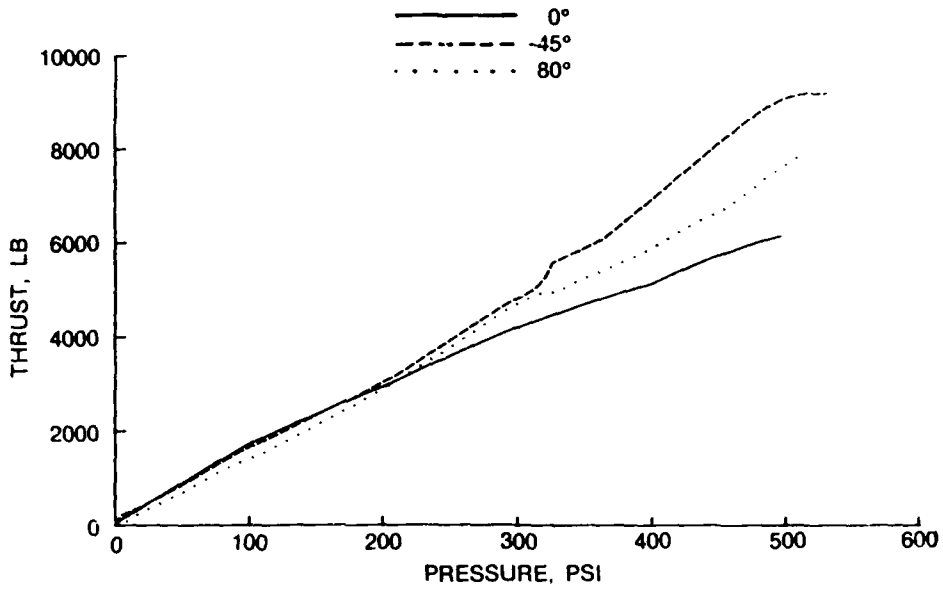

a. Arch S-1.

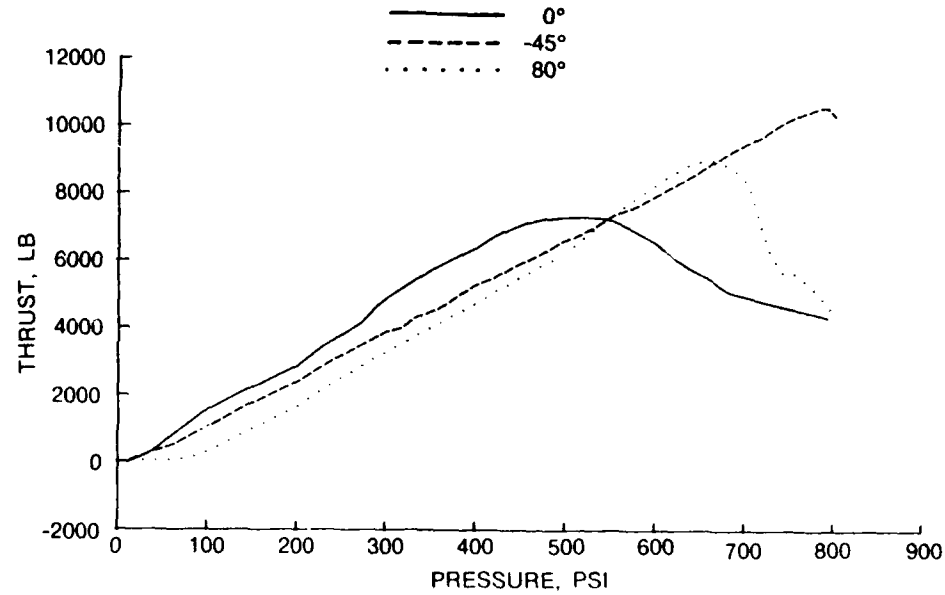

b. Arch S-2.

Figure 56. Thrust-pressure comparisons between locations in each test.

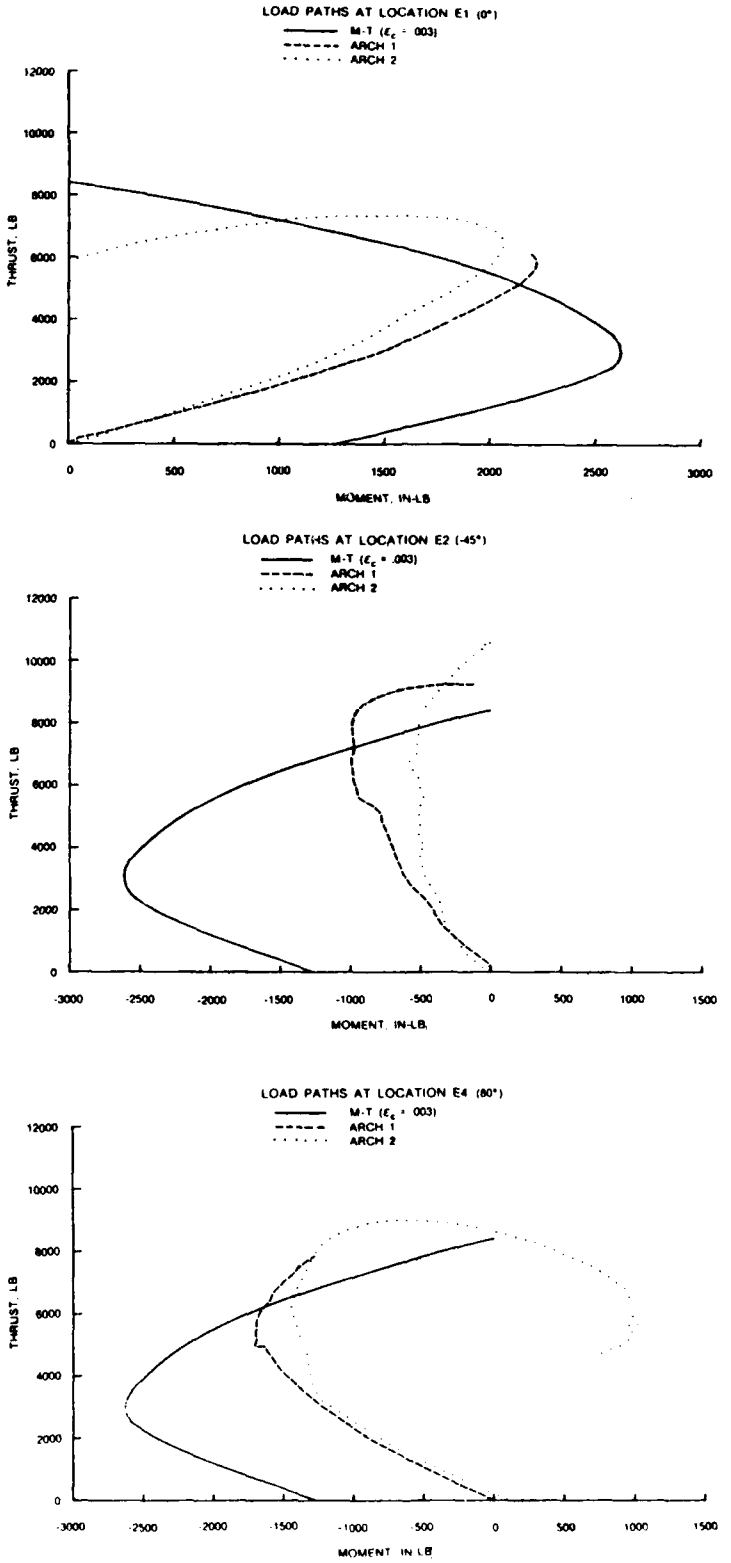

Figure 57. Load-path comparison between tests in each location.

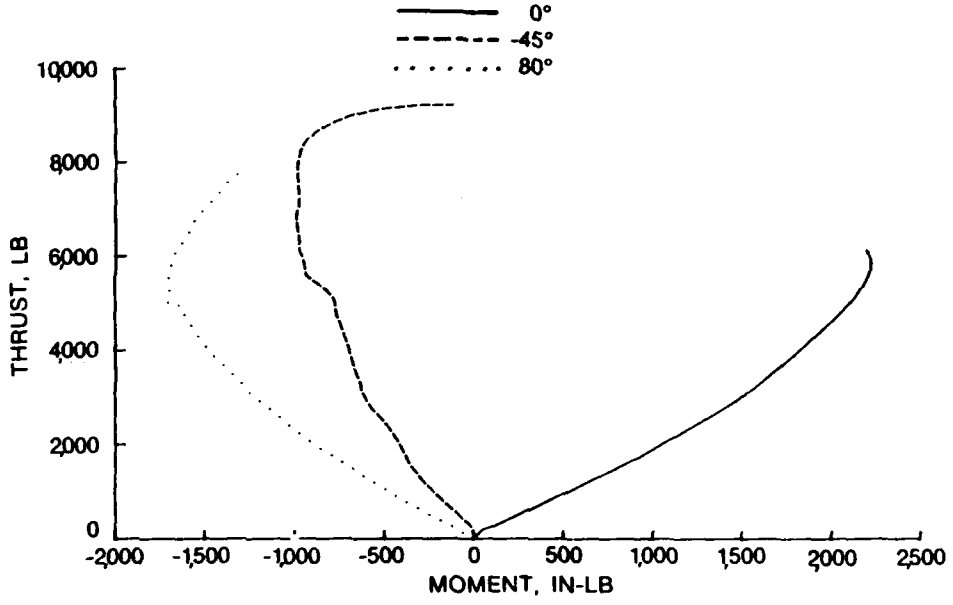

a. Arch S-1.

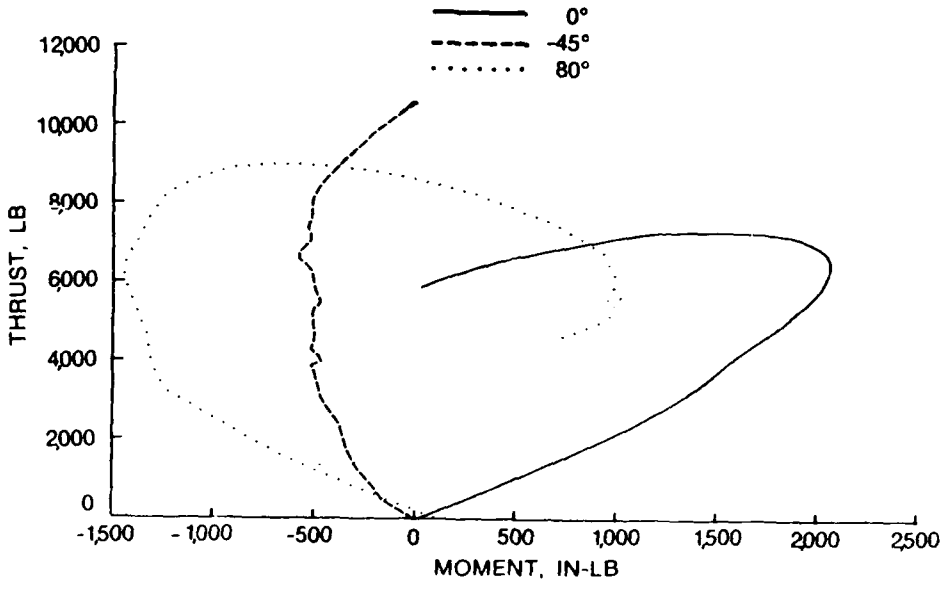

b. Arch S-2.

Figure 58. Load-path comparison between locations in each test.

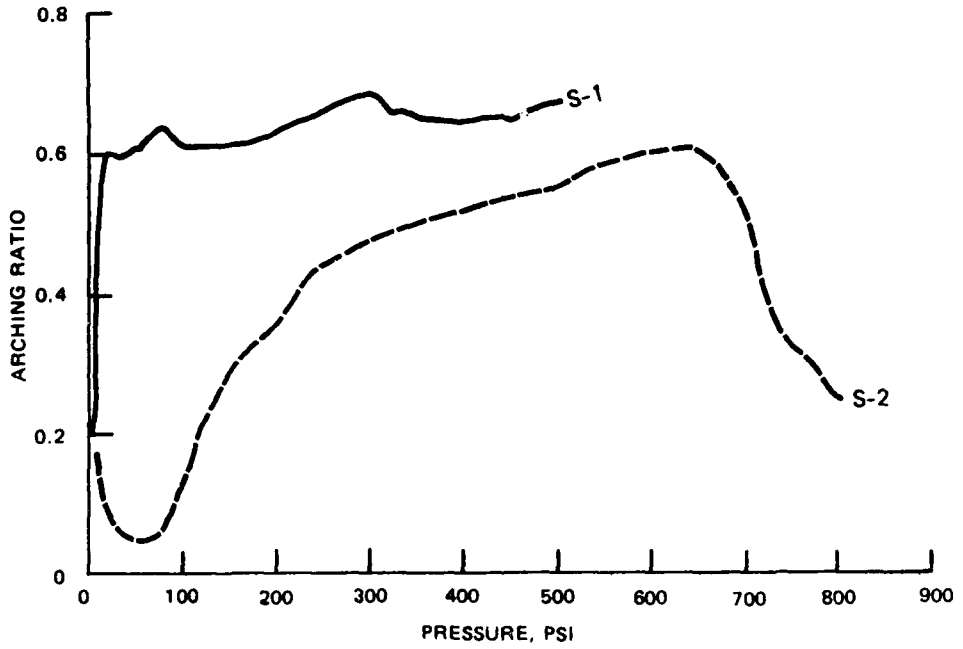

Figure 59. Arching ratio comparison.

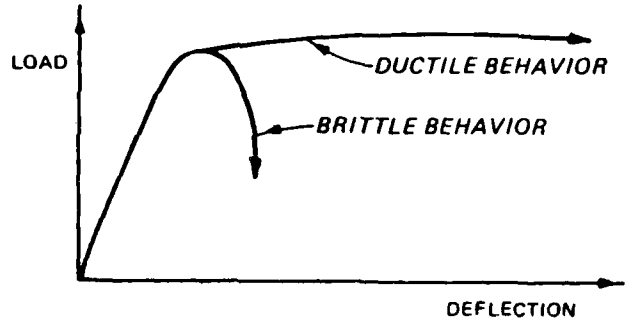

Figure 60. Load-deflection behavior of a flexural member.

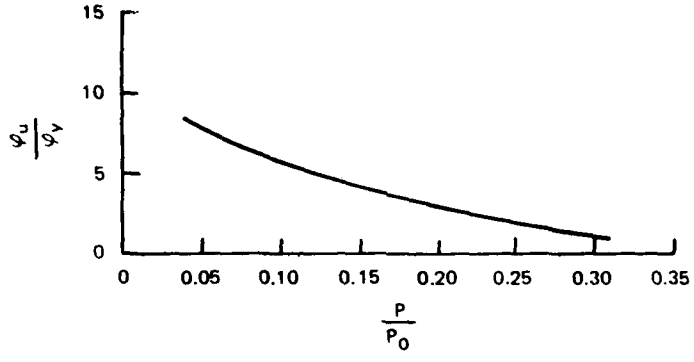

Figure 61. Effect of axial load on curvature ductility.

SECTION 5

CONCLUSIONS AND RECOMMENDATIONS

5.1 CONCLUSIONS

Based on the thrust-moment plots shown in Figure 57, it can be seen that the behavior of both arches was similar; however, the arch with the Teflon interface behaved more in compression than did the other arch. Internal moments were generally lower in the Teflon-covered arch which contradicts FE calculations referred to in Reference 9. In test S-1 (no Teflon) the theoretical ultimate capacity of the concrete section at 0, -45, and 80 degrees was reached at nearly the same overpressure and with moments which were higher than in test S-2. A more gradual slope up to the maximum load in the load-deflection curve for test S-1 resulted from increased deflection due to bending (Figure 39).

In both tests the maximum overpressure reached was much higher than the ultimate resistance computed using the equation in Reference 6. Much of this difference can be attributed to the global soil arching that occurred (Figure 59), which resulted in load being arched away from the structure. Rigid body displacement of the arch could have contributed significantly to the soil-structure interaction effects, especially in test S-1, because the rigid body displacement accounted for a significant percentage of the total deflection at maximum overpressure. This indicates that the width of the footing could play an important role in determining the loading and resulting behavior of a buried arch.

When inspecting the damage to both arches slightly above the springline, it does not appear likely that the arch could have been reloaded significantly. Therefore, a negative or decay slope on the resistance seems more reasonable.

5.2 RECOMMENDATIONS

Nonlinear FE calculations are presently being conducted that take into account the effects of interface skin friction on the behavior of buried arches. The Coulomb friction law will be used at the soil-structure interface. These calculations should provide greater insight into the importance of incorporating friction effects into a simplified analysis procedure.

Other parameters which should be studied include backfill type, footing width, arch radius-to-thickness ratio, and DOB. The effects of these parameters on arch loading and response should be studied both experimentally and analytically so that they can be incorporated into a simplified analysis procedure.

REFERENCES

1. G. D. Meyer, and W. J. Flathau; "Static and Dynamic Laboratory Tests of Unreinforced Concrete Fixed-End Arches Buried in Dry Sand"; Technical Report No. 1-758, February 1967; US Army Engineer Waterways Experiment Station, Vicksburg, MS.

2. J. F. Munn, G. L. Carre, and T. E. Kennedy; "Failure of Footing-Supported Buried Steel Arches Loaded Statistically"; Miscellaneous Paper N-70-2, March 1970; US Army Engineer Waterways Experiment Station, Vicksburg, MS.

3. G. G. Meyerhof; "Some Research on underground Flexible Arches"; Proceedings, Conference on Subway Construction, Budapest, and Proceedings, VI World Highway Conference, September 1970, Montreal, Canada.

4. H. L. Gill, and J. R. Algood; "Static Loading on Small Buried Arches"; Technical Report R-278, January 1964; US Naval Civil Engineering Laboratory, Port Hueneme, CA.

5. C. K. Wiehle; "Review of Soil-Structure Interaction"; Symposium on soil-Structure Interaction held at University of Arizona, June 1964; URS Corporation, Burlingame, CA.

6. [illegible] D. Haltiwanger; "Design of Structures to Resist Nuclear Weapons Effects"; Manual No. 42; Manual Subcommittee of the Committee on Structural Dynamics, Engineering Mechanics Division, American Society of Civil Engineers.

7. W. J. Flathau, L. M. Bryant, and P. F. Mlakar; "Single-Degree-of-Freedom Analysis of Buried Arches Loaded by Conventional Ground Shock"; International Symposium Concerning Conventional Weapons Effects, March 1987, Mannheim, West Germany.

8. R. E. Elling; "The Influence of Interface Friction and Tensile Debonding on Stresses in Buried Cylinders"; Transportation Research Record 1008, "Culverts: Analysis of Soil-Culvert Interaction and Design"; Transportation Research Board, National Research Council, Washington, DC.

9. M. G. Katona and others; "Cande - A Modern Approach for the Structural Design and Analysis of Buried Culverts"; PB-275 807, October 1976; US Naval Civil Engineering Laboratory, Port Hueneme, CA.

10. J. G. Potyondy; "Skin Friction Between Various Soils and Construction Materials"; Geotechnique, Institution of Civil Engineers, Vol 11, No. 4, December 1961.

11. W. F. Brumund, and G. A. Leonards; "Experimental Study of Static and Dynamic Friction Between Sand and Typical Construction Materials"; Journal of Testing and Evaluation, American Society for Testing and Materials, Vol 1, No. 2, March 1973.

12. F. H. Kulhawy, and M. S. Peterson; "Behavior of Sand-Concrete Interfaces"; Sixth Panamerican Conference on Soil Mechanics and Foundation Engineering, Vol 2, December 1979.

13. American Society for Testing and Materials; "Standard Specifications for Deformed and Plain Billet Steel Bars for Concrete Reinforcement"; 1969 Annual Book of ASTM Standards, Part 4, 1969; Philadelphia, PA.

14. US Department of Defense; "Unified Soil Classification System for Roads, Airfields, Embankments, and Foundations"; Military Standard MIL-STD-619B, June 1968; Washionton, DC.

15. K. J. Bathe; "User's Manual for ADINA, A Finite Element Program for Automatic Dynamic Incremental Nonlinear Analysis"; Report AE 84, December 1984; ADINA Engineering, Watertown, MA.

16. R. Park, and T. Paulay; "Reinforced Concrete Structure"; 1975; Wiley, New York.

17. J. A. Blume, N. M. Newmark, and L. H. Corning; "Design of Multistory Reinforced Concrete Buildings for Earthquake Motions"; 1961; Portland Cement Association, Chicago, IL.

18. E. O. Pfrang, C. P. Seiss, and M. A. Sozen; "Load-Moment-Curvature Characteristics of Reinforced Concrete Cross Sections," Journal, American Concrete Institute, Vol 61, No. 7, July 1964.

APPENDIX A: ANALOG DATA PLOTTED VERSUS WATER PRESSURE

SBS ARCH TEST S-1

SBS ARCH TEST S-1
BP-1

MAXIMUM	SIGMA CAL	CAL VAL
530.1949	2.5146	501.9

CHANNEL NO. 1 8697 1
09/18/86 RD905

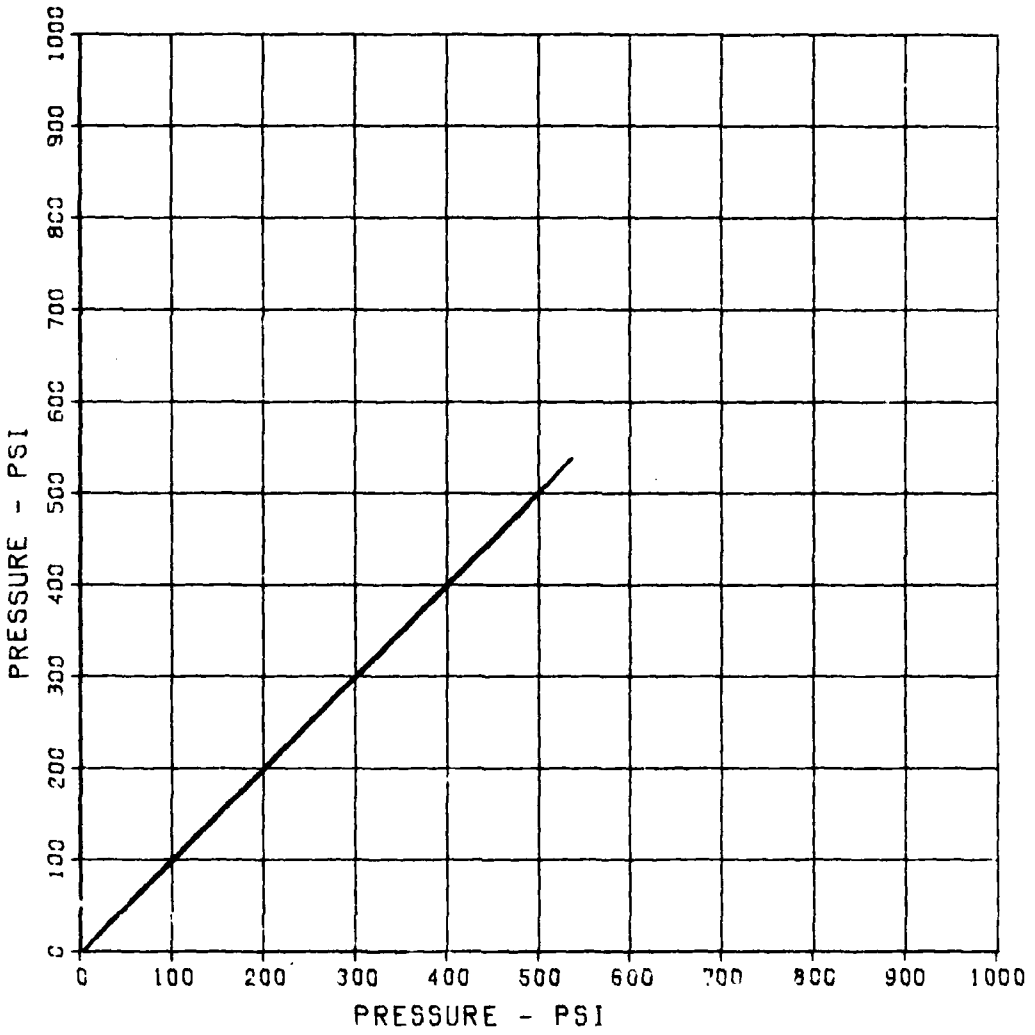

SBS ARCH TEST S-1
BP-2

MAXIMUM	SIGMA CAL	CAL VAL
521.0080	2.4597	562.0

CHANNEL NO. 2 8697 1
09/18/86 R0905

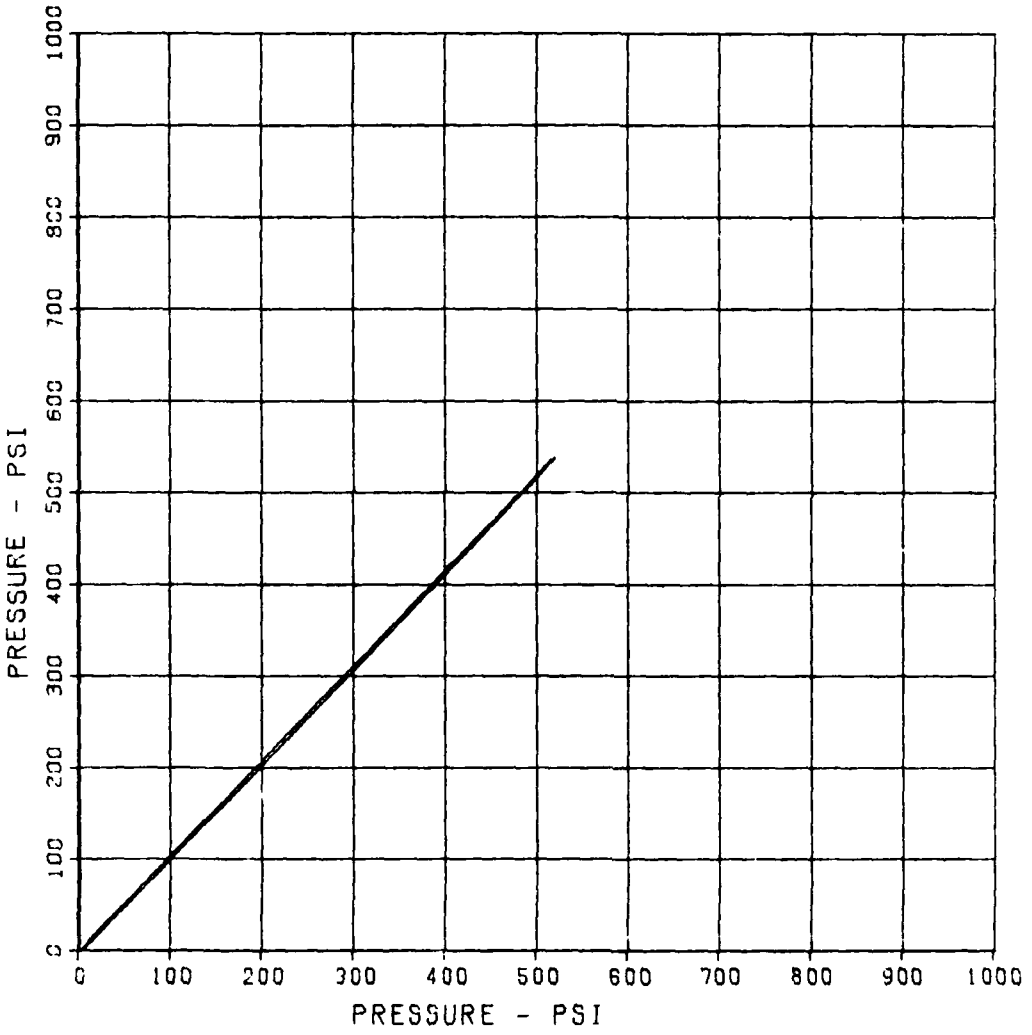

SBS ARCH TEST S-1
IP-1

MAXIMUM	SIGMA CAL	CAL VAL
324.2683	2.6474	566.2

CHANNEL NO. 3 8697 1
09/18/86 R0905

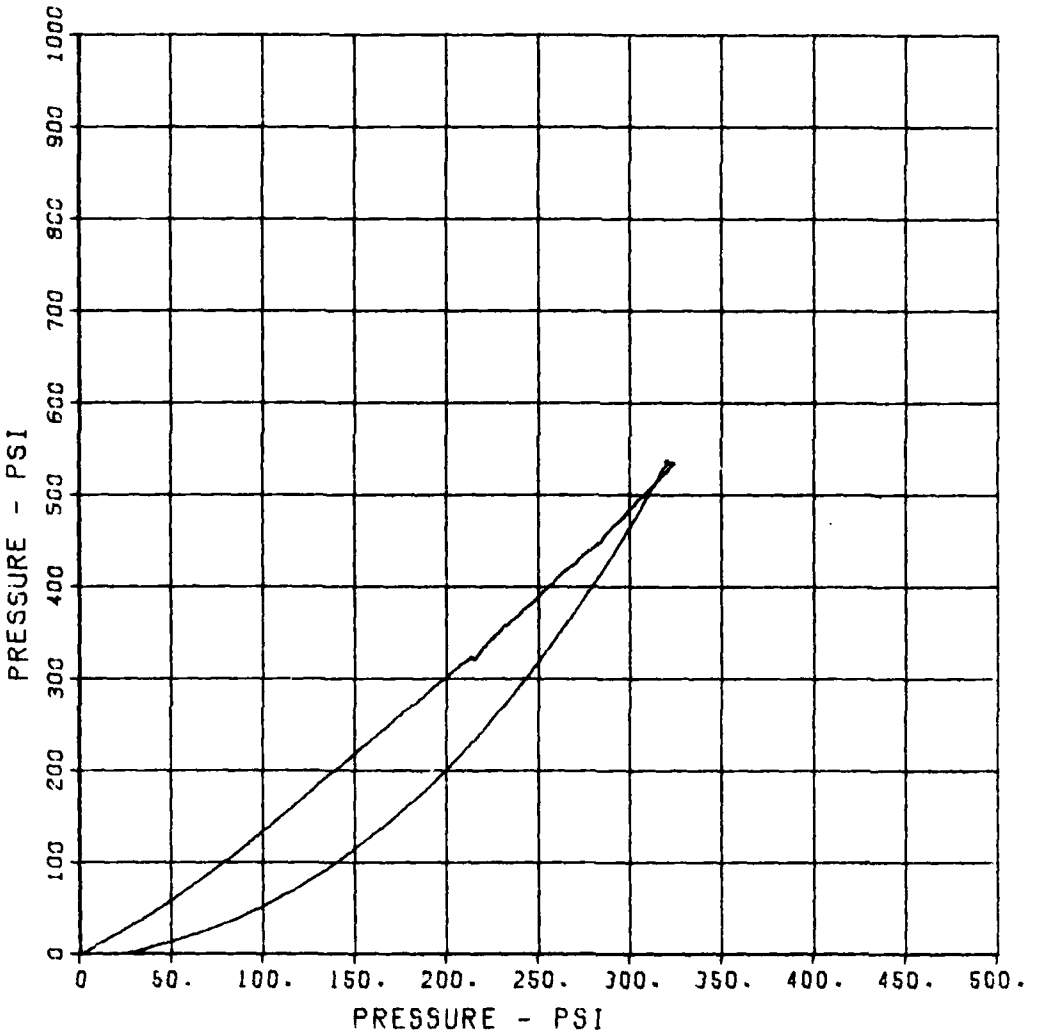

SBS ARCH TEST S-1
IP-2

MAXIMUM	SIGMA CAL	CAL VAL
393.9113	2.7814	618.9

CHANNEL NO. 4 8697 1
09/18/86 R0905

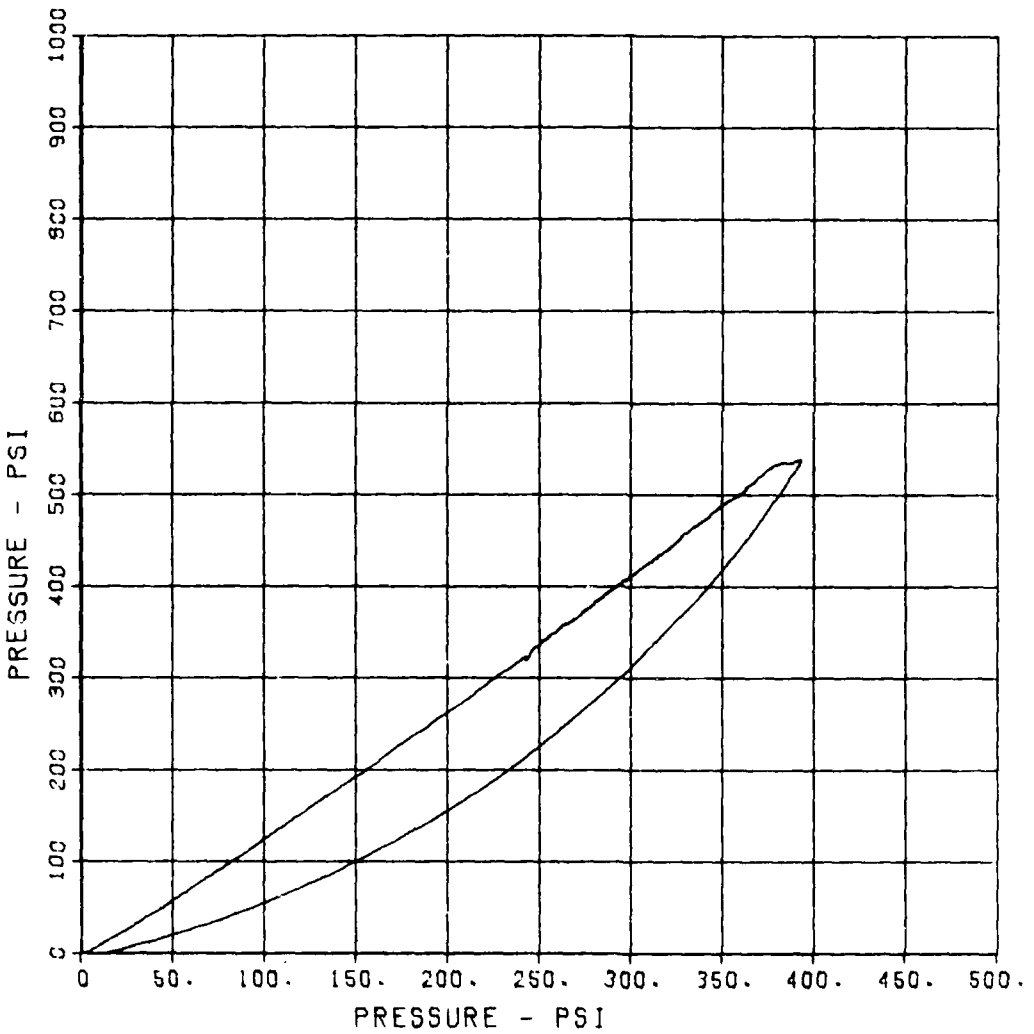

SBS ARCH TEST S-1
IP-3

MAXIMUM	SIGMA CAL	CAL VAL
369.6159	2.7889	633.4

CHANNEL NO. 5 8697 1
09/18/86 R0905

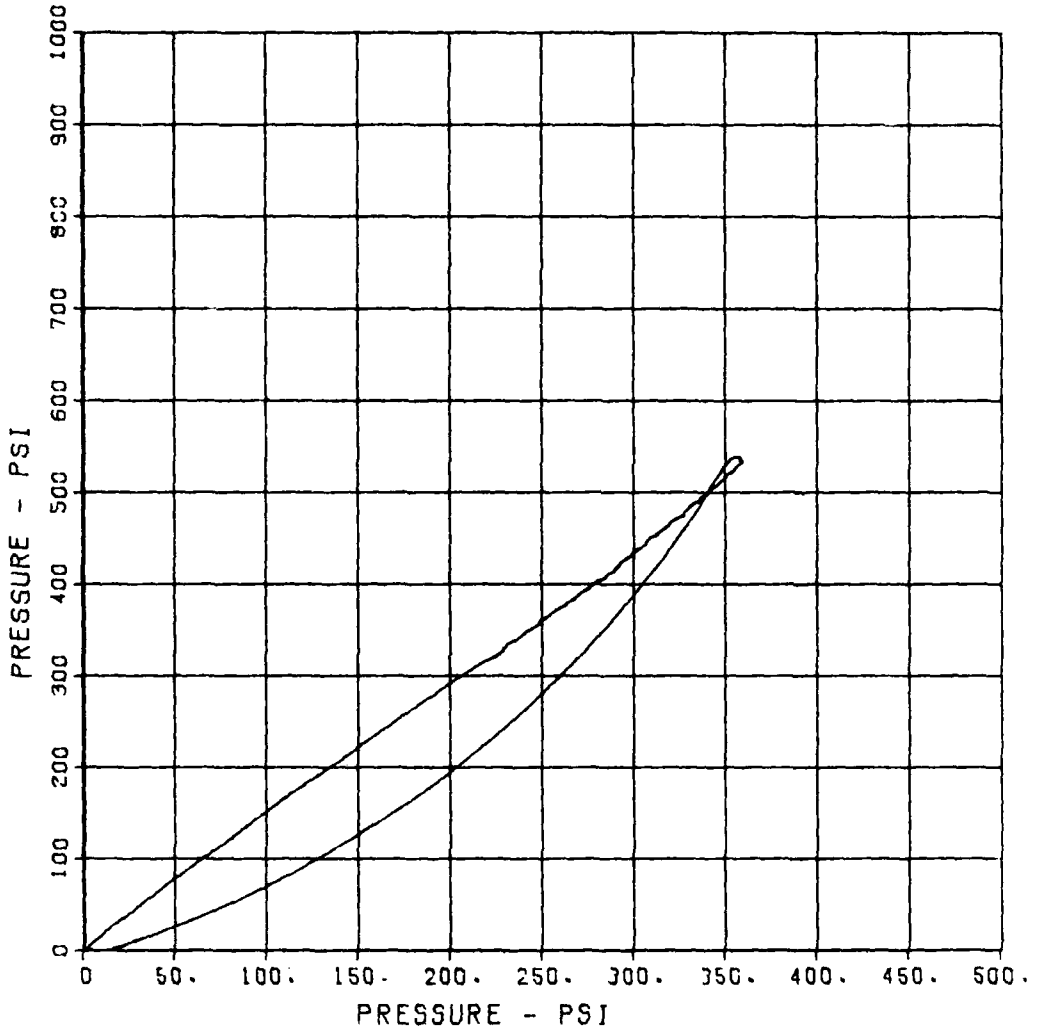

SBS ARCH TEST S-1
IP-4

MAXIMUM	SIGMA CAL	CAL VAL
362.0462	2.8530	551.1

CHANNEL NO. 6 8697 1
09/18/86 R0905

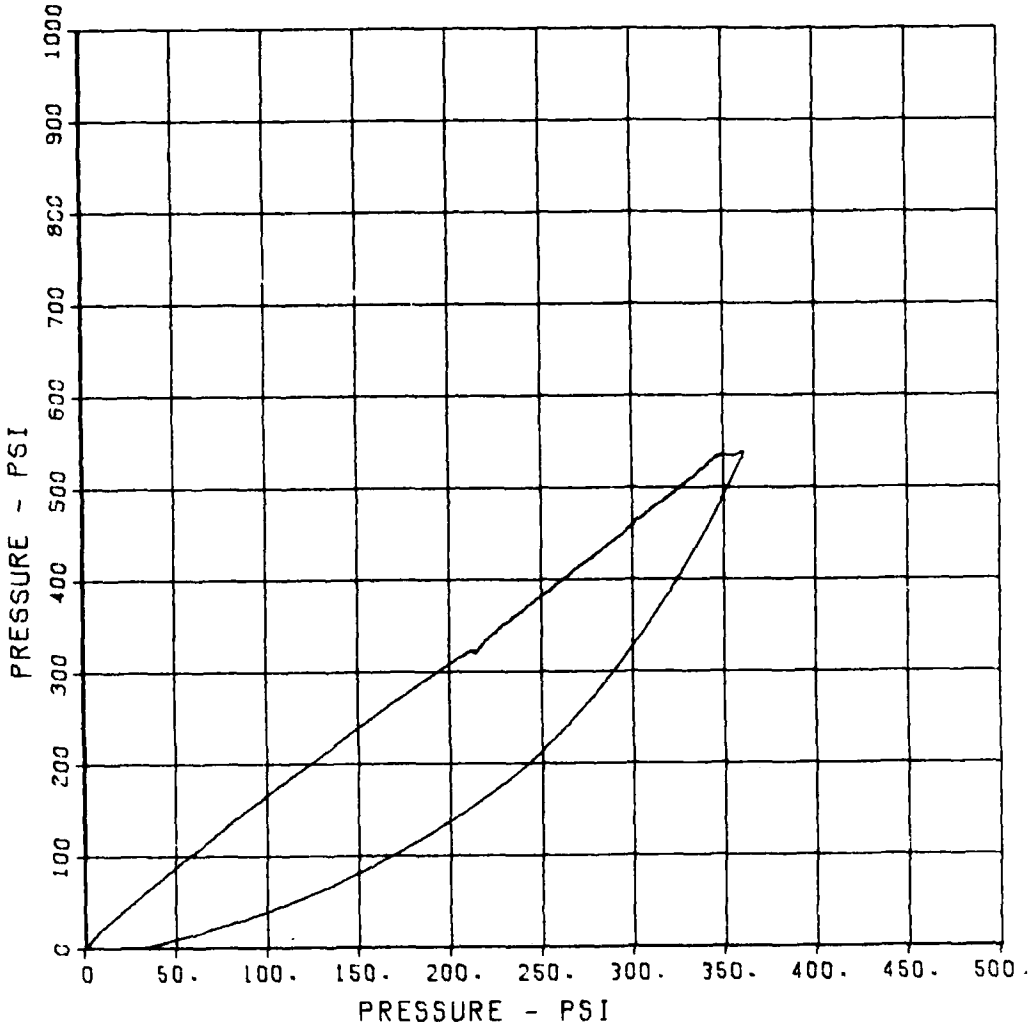

SBS ARCH TEST S-1
IP-5

MAXIMUM	SIGMA CAL	CAL VAL
88.7790	2.4053	361.1

CHANNEL NO. 7 8697 1
09/18/86 R0905

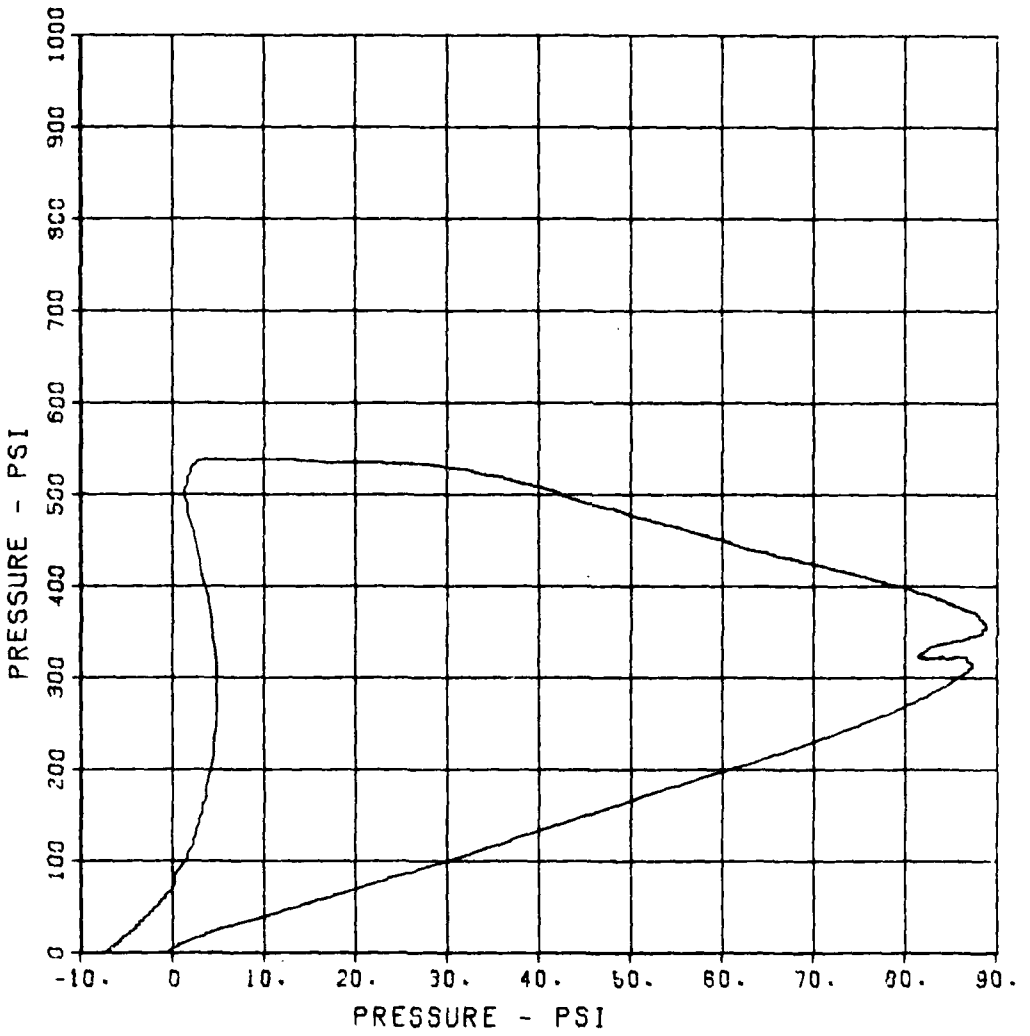

SBS ARCH TEST S-1
IP-6

MAXIMUM	SIGMA CAL	CAL VAL
398.6879	2.5617	602.9

CHANNEL NO. 8 8697 1
09/18/86 R0905

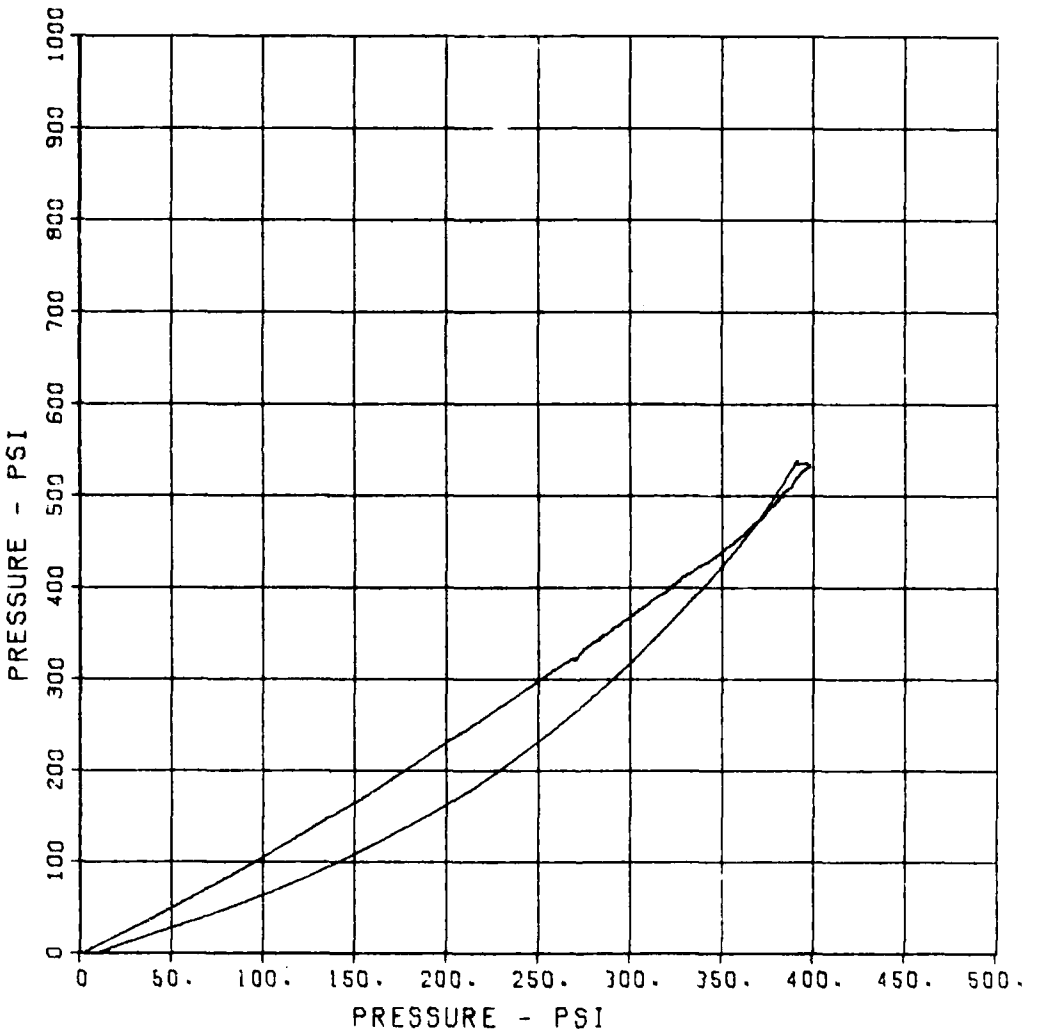

SBS ARCH TEST S-1
IP-7

MAXIMUM	SIGMA CAL	CAL VAL
337.3079	2.6348	591.7

CHANNEL NO. 9 8697
09/18/86 R0905

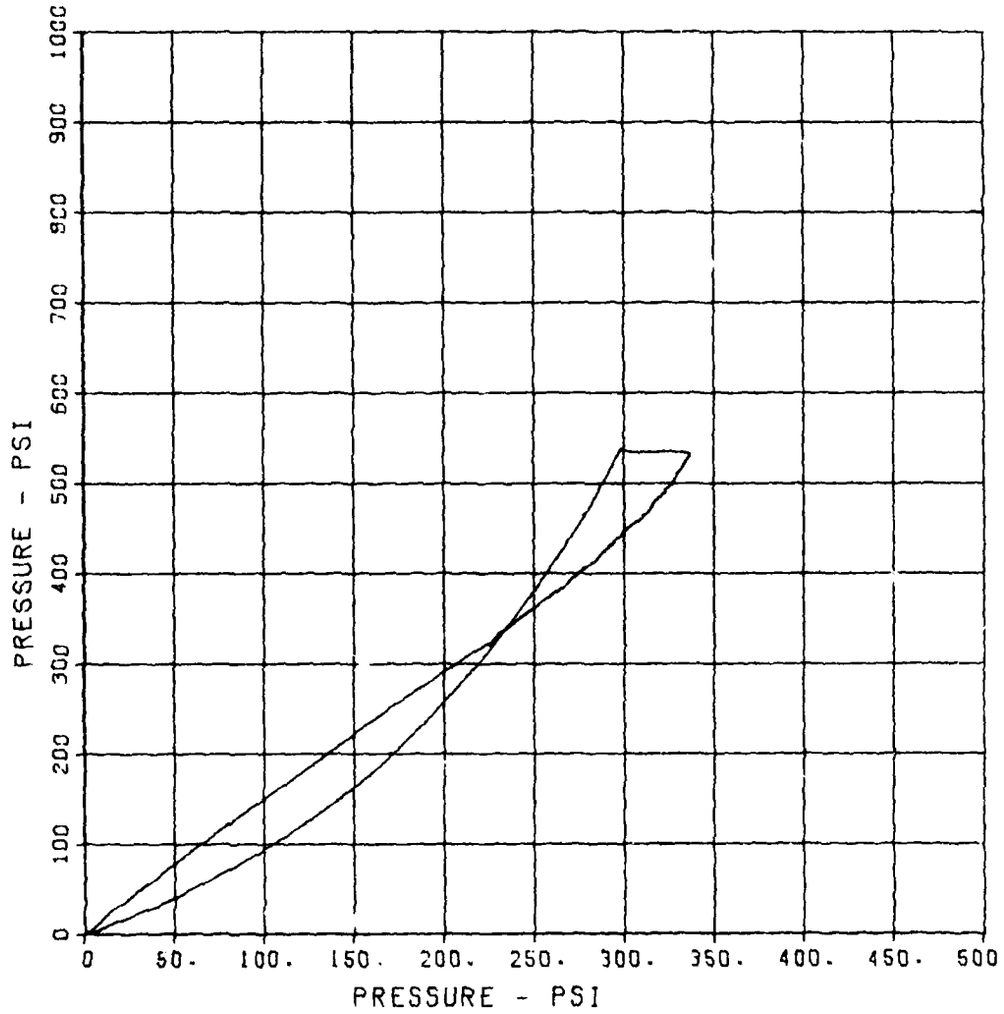

SBS ARCH TEST S-1
IP-8

MAXIMUM	SIGMA CAL	CAL VAL
418.4632	2.3667	397.0

CHANNEL NO. 10 8697 1
09/18/86 R0905

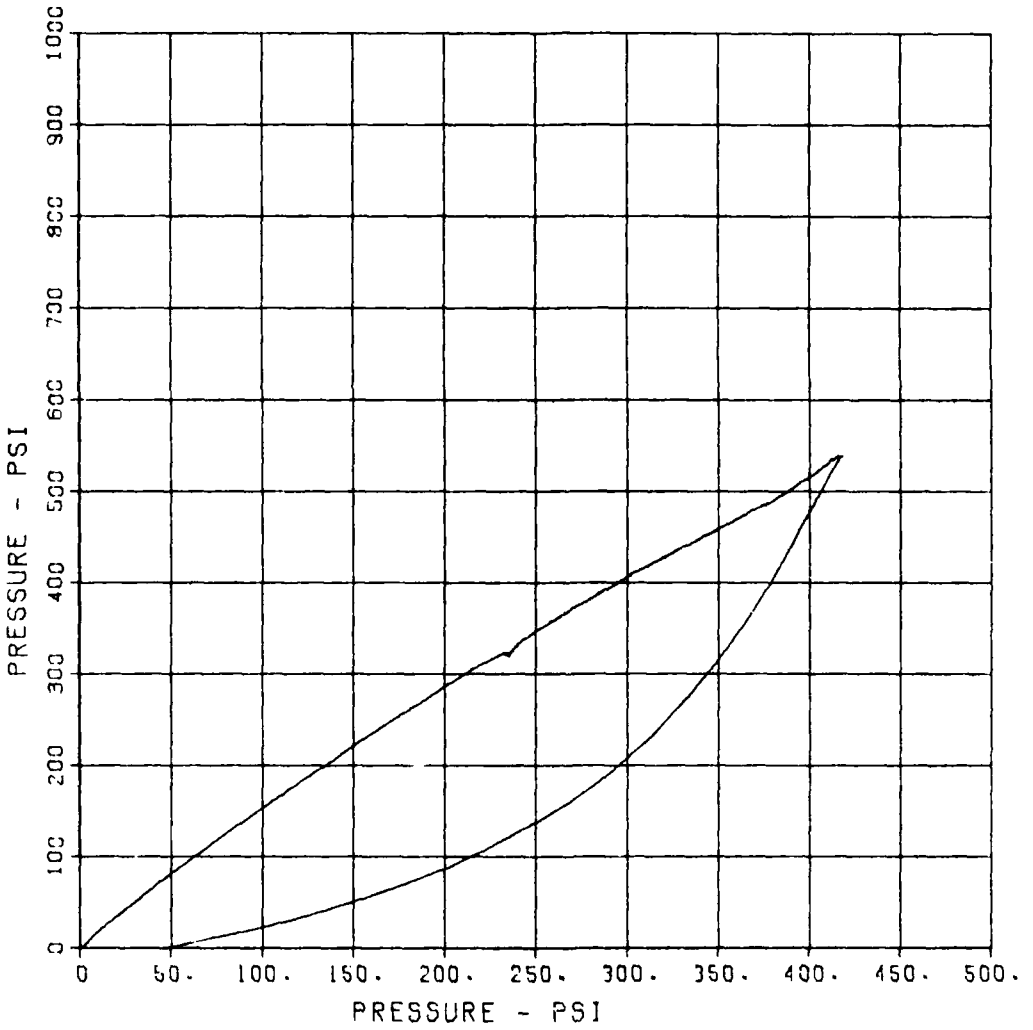

SBS ARCH TEST S-1
IP-9

MAXIMUM	SIGMA CAL	CAL VAL
112.9553	2.3388	370.4

CHANNEL NO. 11 8697 1
09/18/86 R0905

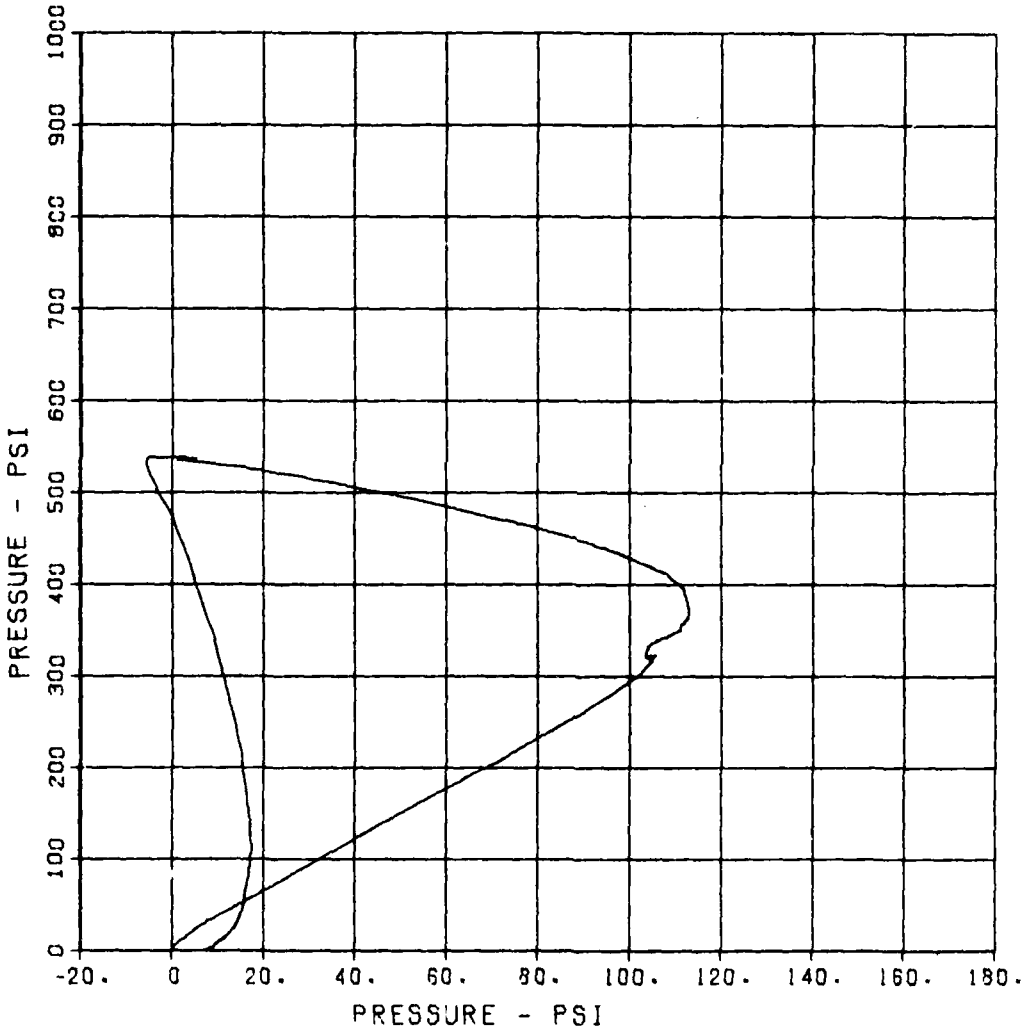

SBS ARCH TEST S-1
SE-1

MAXIMUM	SIGMA CAL	CAL VAL
446.2714	2.5417	690.8

CHANNEL NO. 12 8697 1
09/16/86 R0905

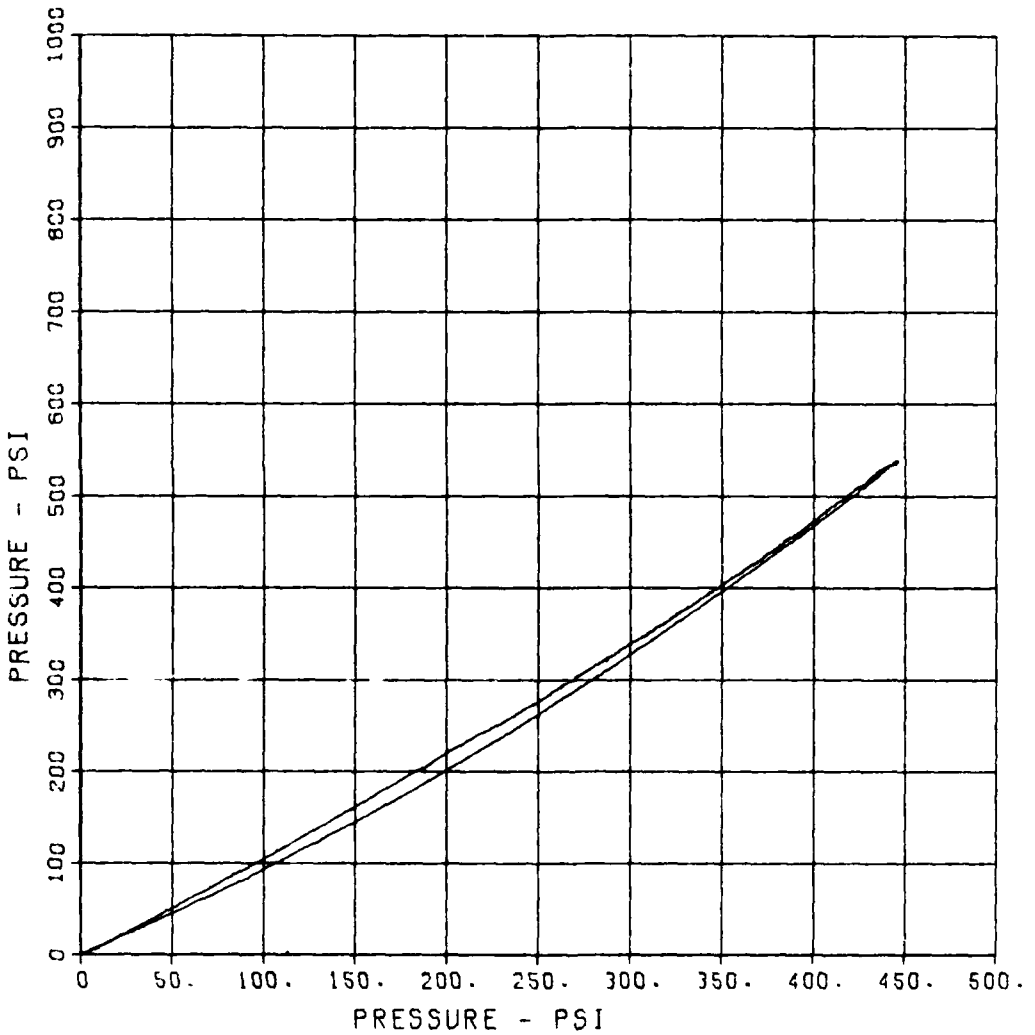

SBS ARCH TEST S-1
SE-2

MAXIMUM	SIGMA CAL	CAL VAL
573.5456	2.7409	496.0

CHANNEL NO. 13 8697
09/18/86 R0905

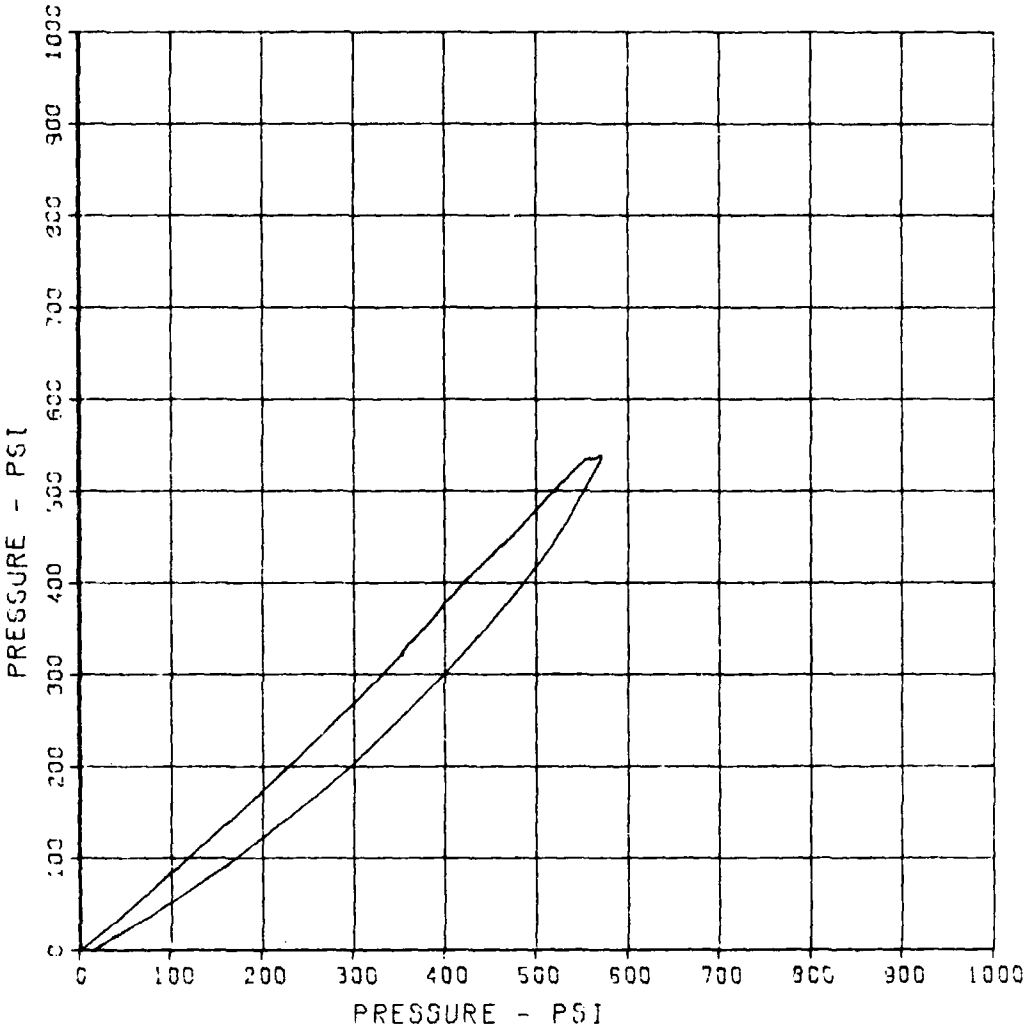

SBS ARCH TEST S-1
SE-3

MAXIMUM	SIGMA CAL	CAL VAL
344.5563	5.0372	512.3

CHANNEL NO. 14 8697 1
09/18/86 R0905

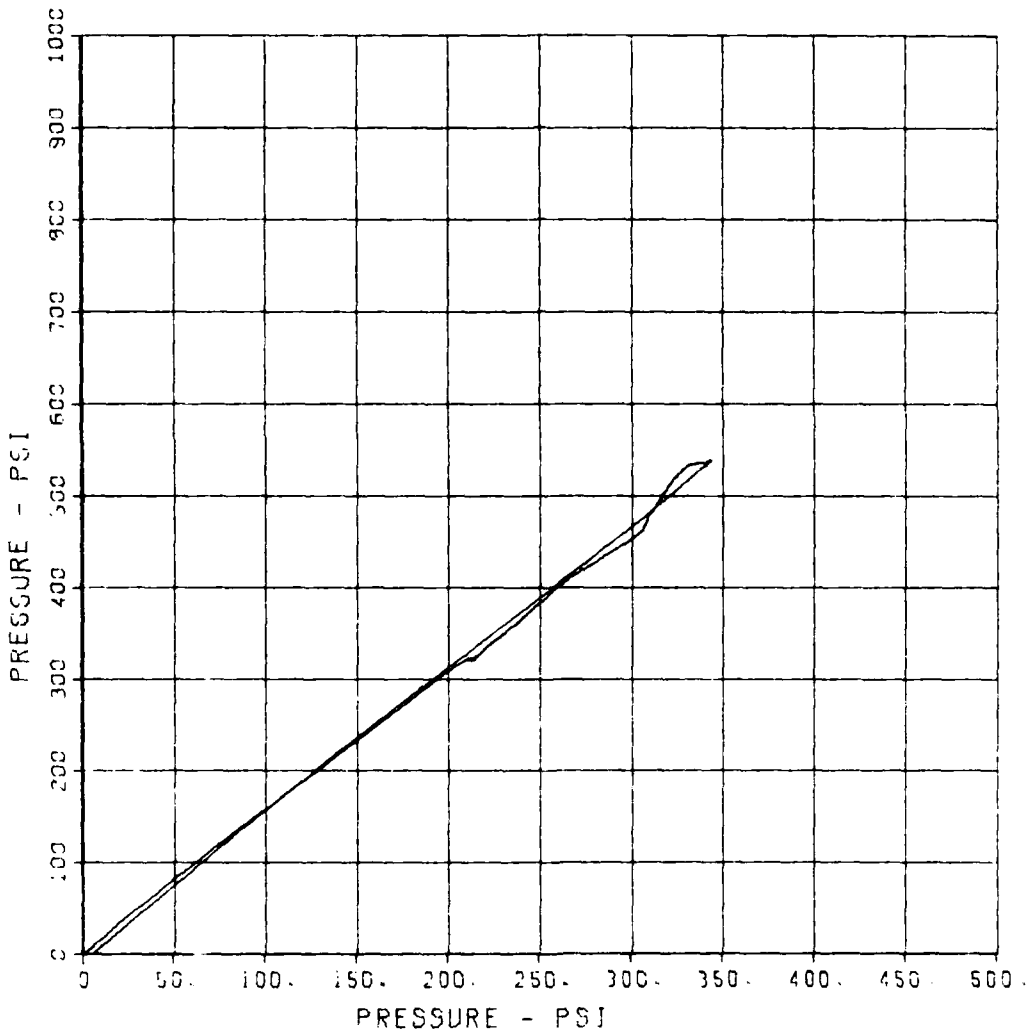

SBS ARCH TEST S-1
SE-4

MAXIMUM	SIGMA CAL	CAL VAL
541.8504	2.4696	497.9

CHANNEL NO. 15 8697 1
09/18/86 R0905

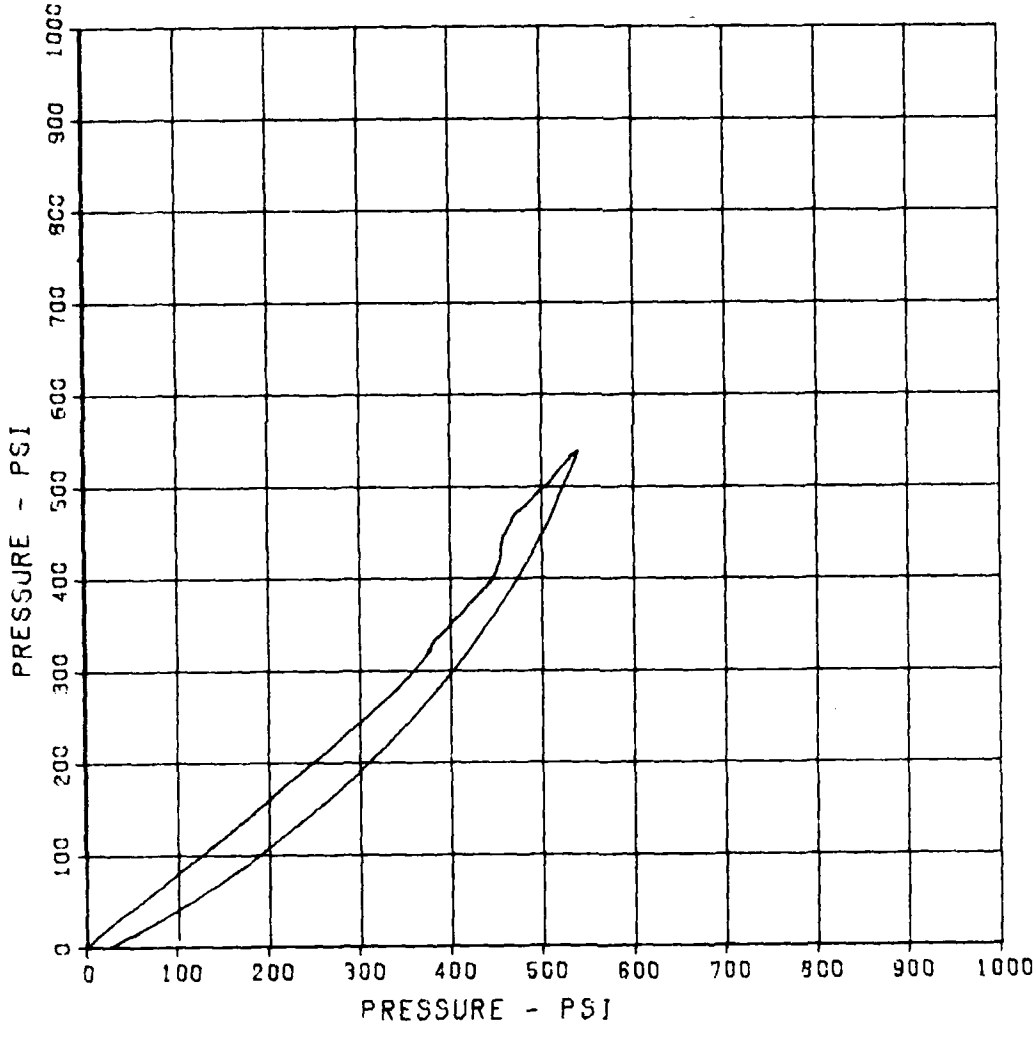

SBS ARCH TEST S-1
SE-5

MAXIMUM	SIGMA CAL	CAL VAL
-984.7613	2.3299	508.7

CHANNEL NO. 16 8697 1
09/10/86 R0905

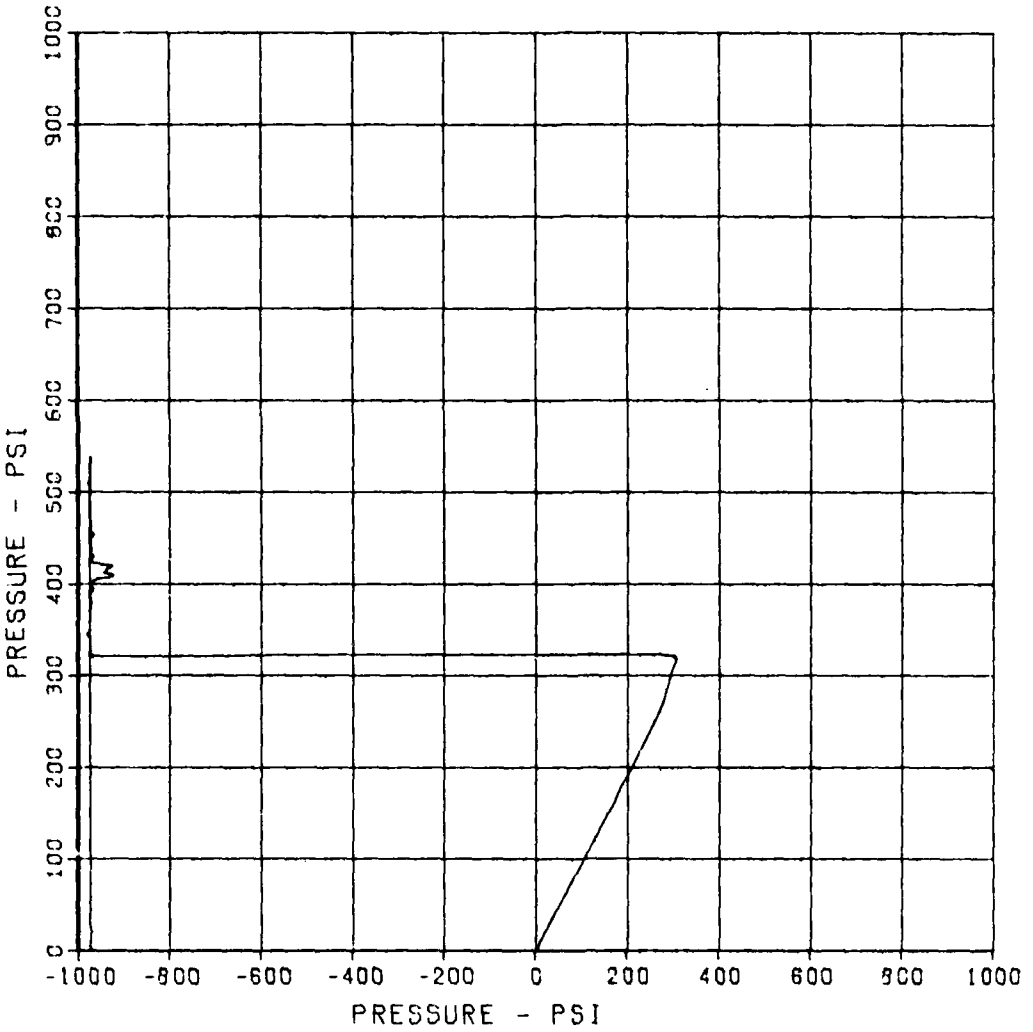

SBS ARCH TEST S-1
SE-6

MAXIMUM	SIGMA CAL	CAL VAL
438.5967	2.9114	535.9

CHANNEL NO. 17 8697 1
09/18/86 R0905

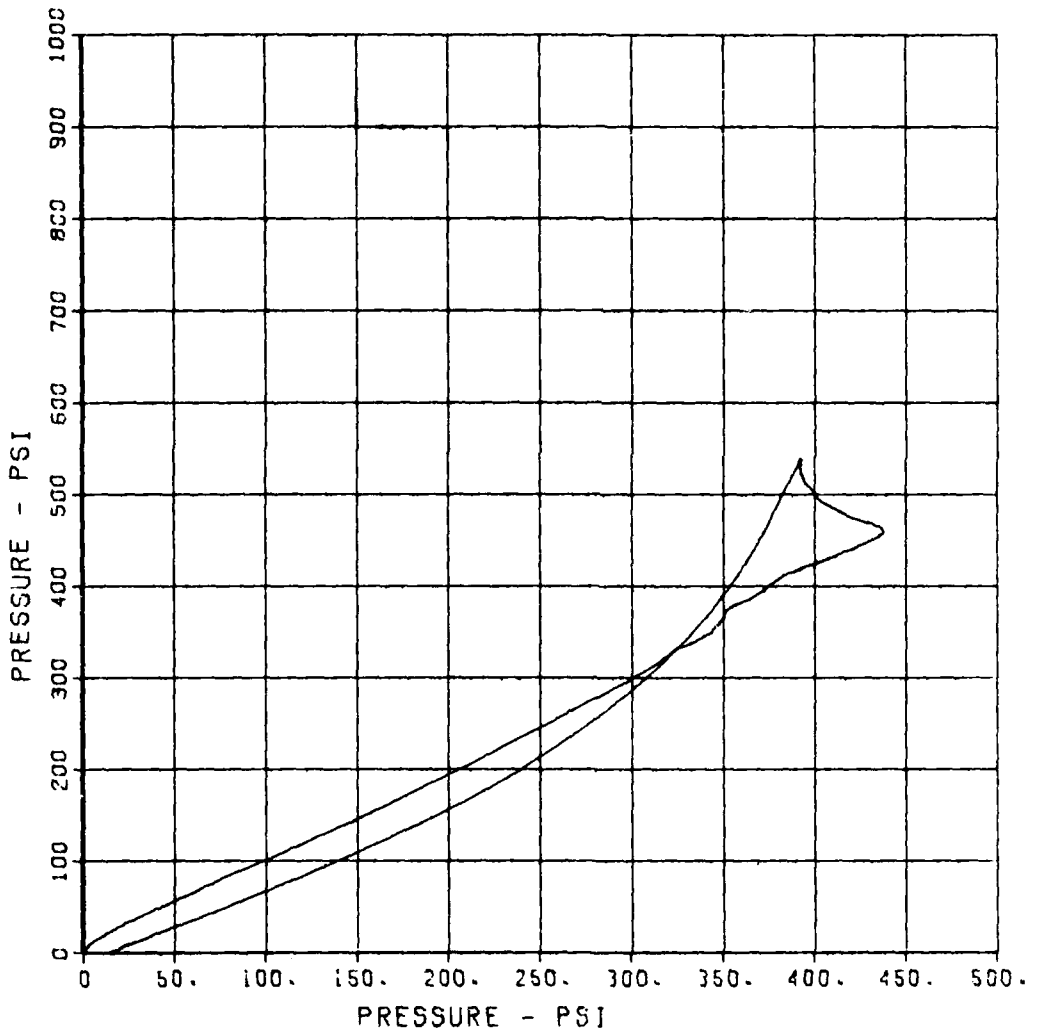

SBS ARCH TEST S-1
SE-7

MAXIMUM	SIGMA CAL	CAL VAL
86.4815	3.1337	594.9

CHANNEL NO. 18 8697 1
09/18/86 R0905

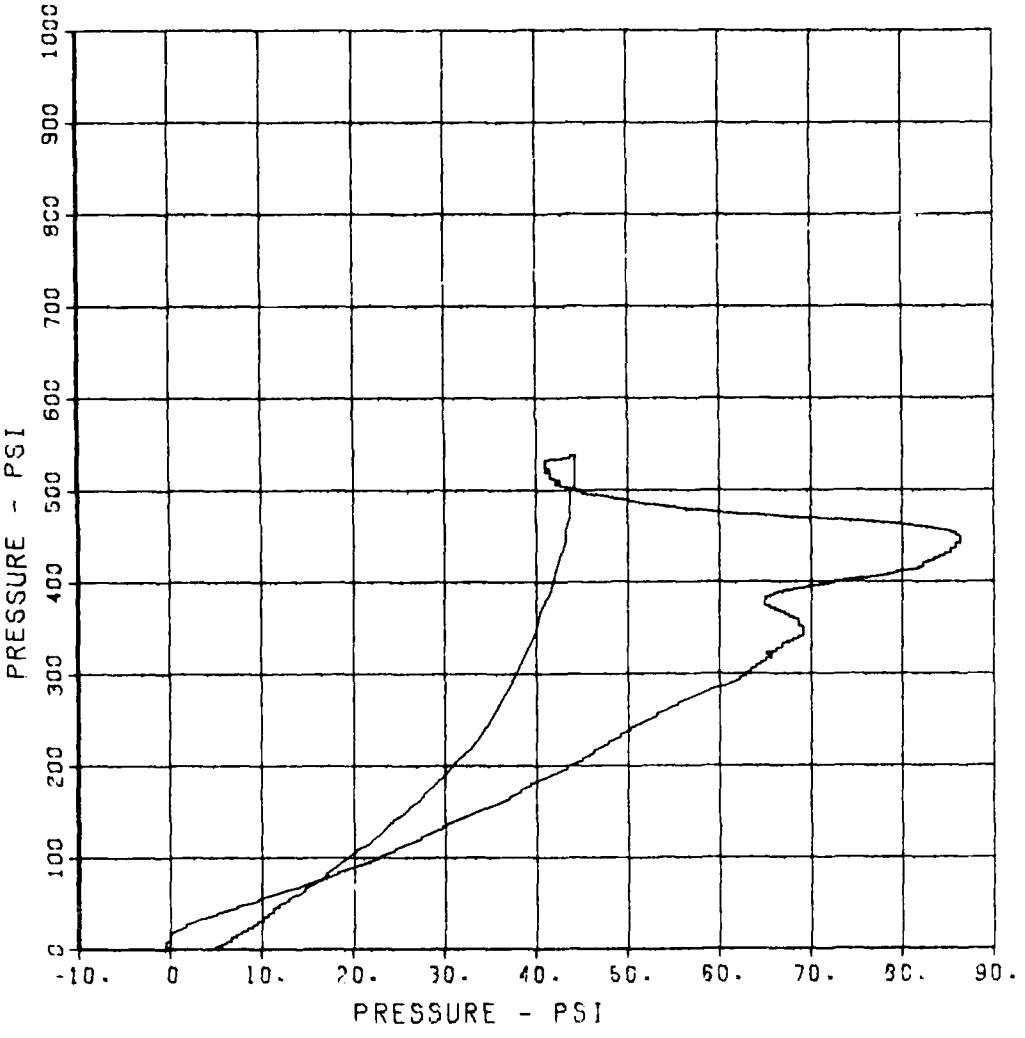

SBS ARCH TEST S-1
SE-8

MAXIMUM	SIGMA CAL	CAL VAL
782.0581	3.4926	484.5

CHANNEL NO. 19 8697 1
09/18/86 R0905

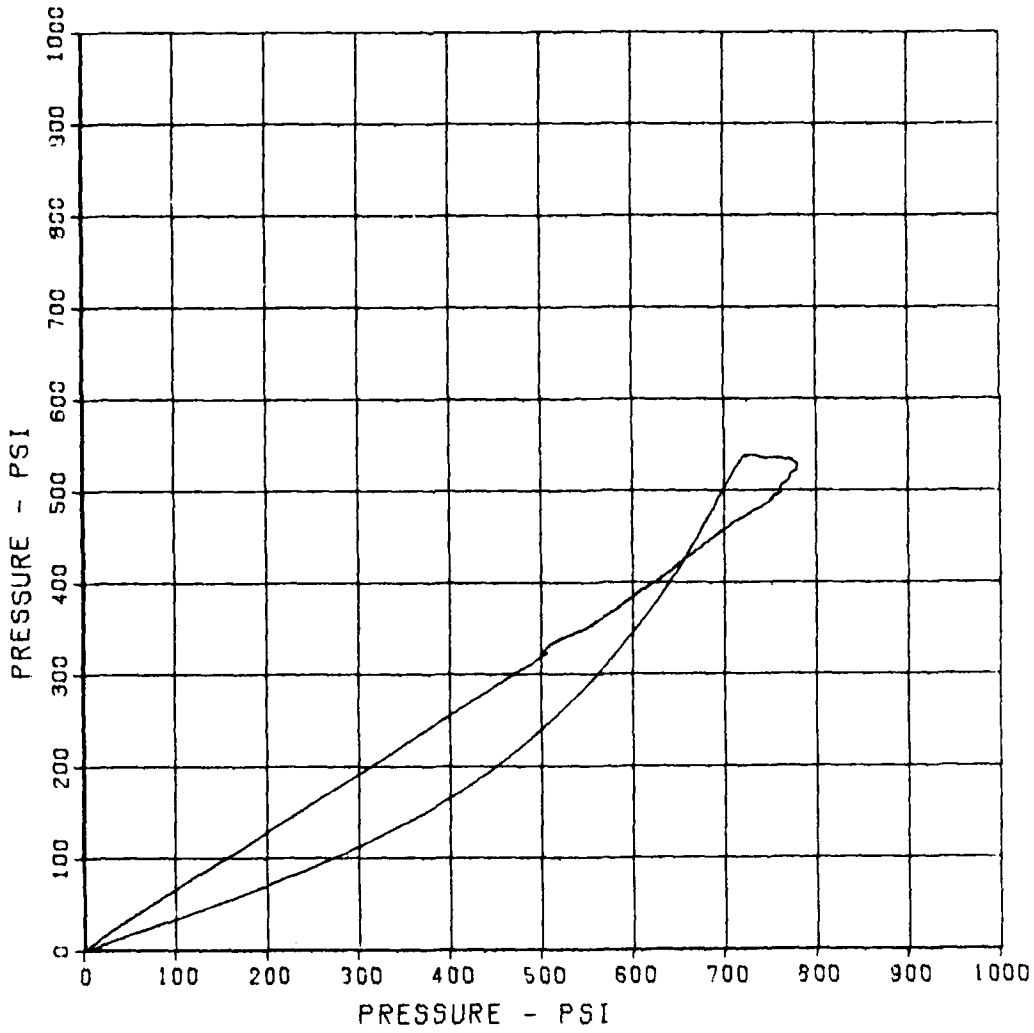

SBS ARCH TEST S-1
SE-9

MAXIMUM	SIGMA CAL	CAL VAL
363.9693	3.0826	609.9

CHANNEL NO. 20 8697 1
09/18/86 R0905

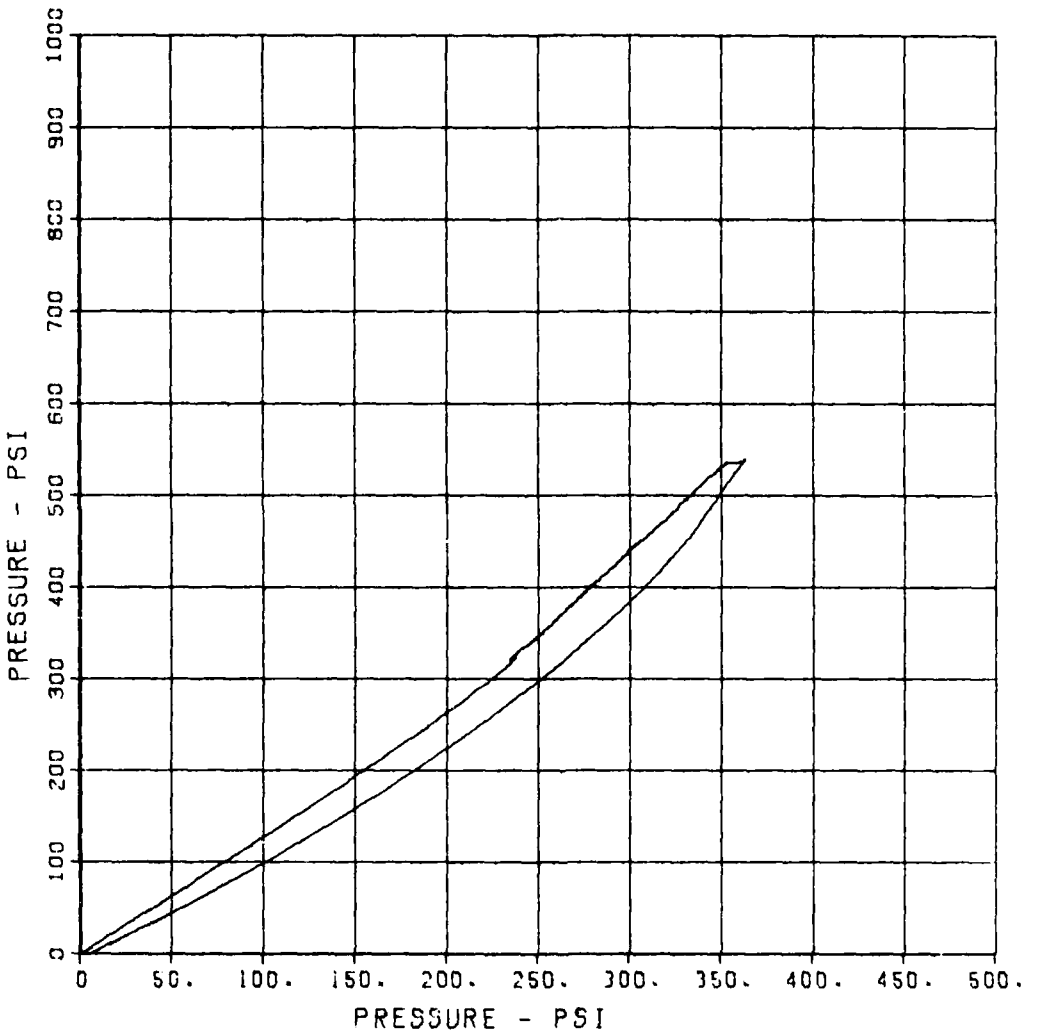

SBS ARCH TEST S-1
EO-1

MAXIMUM	SIGMA CAL	CAL VAL
-2289.7316	2.6269	11400.7

CHANNEL NO. 21 8697 i
09/18/86 R0905

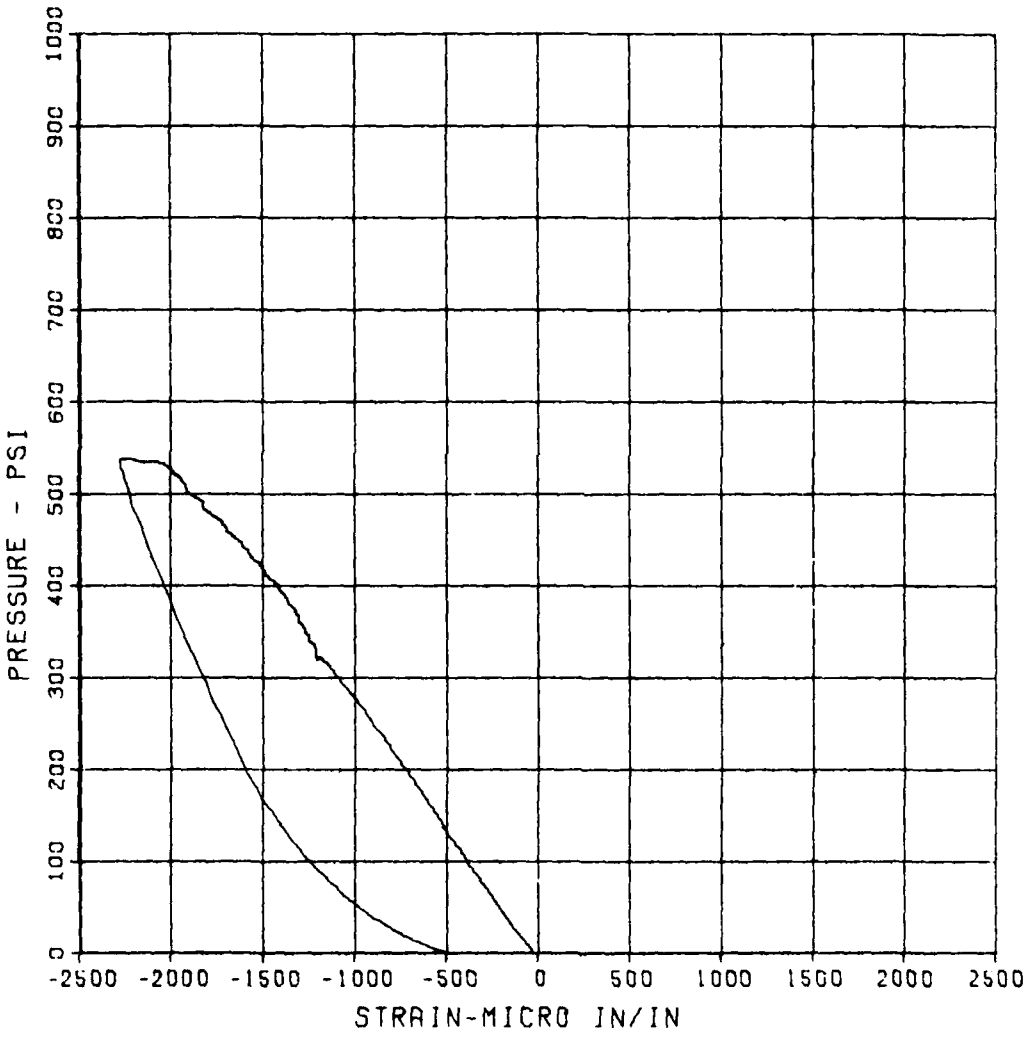

SBS ARCH TEST S-1
EJ-1

MAXIMUM	SIGMA CAL	CAL VAL
290.6422	2.9031	11400.7

CHANNEL NO. 22 8697 1
09/10/86 R0905

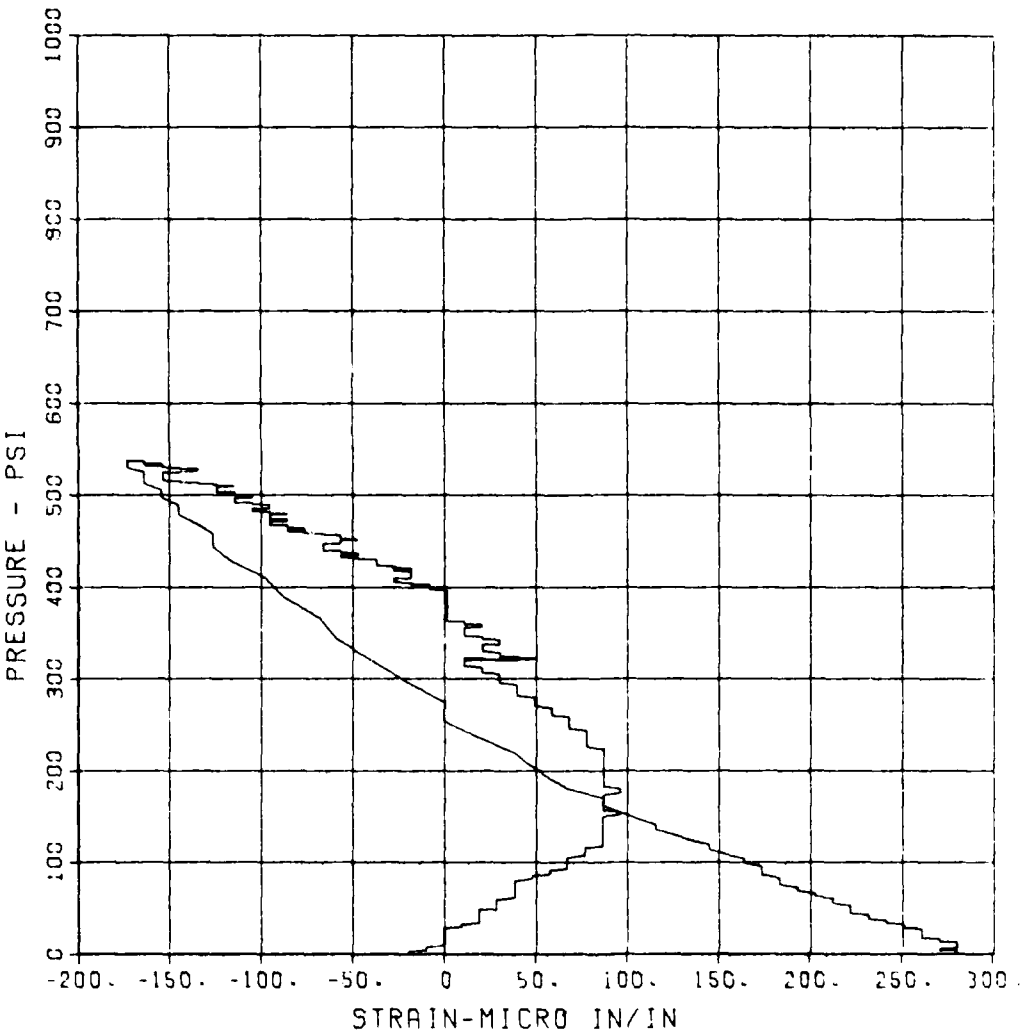

SBS ARCH TEST S-1
E0-2

MAXIMUM	SIGMA CAL	CAL VAL
-1562.1561	2.8990	11400.7

CHANNEL NO. 23 8697 1
09/18/86 R0905

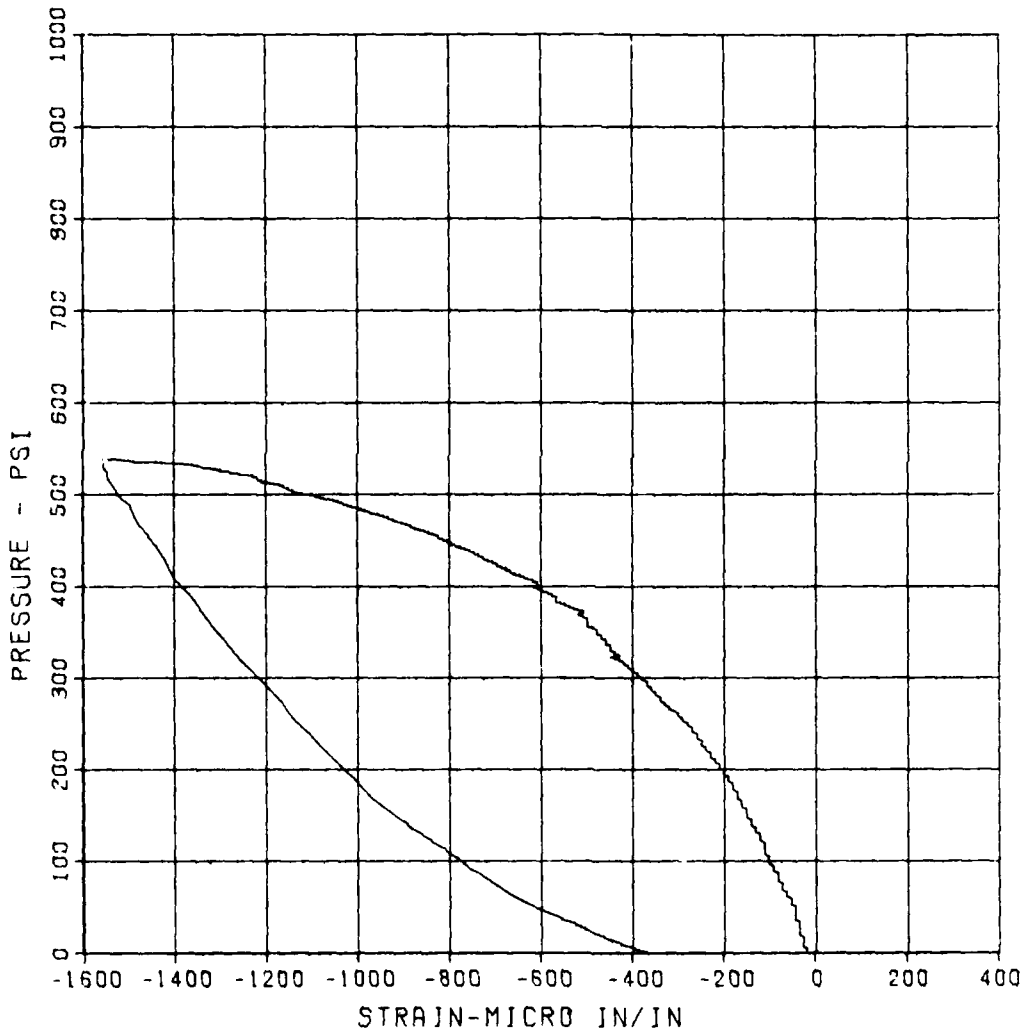

SBS ARCH TEST S-1
EI-2

MAXIMUM	SIGMA CAL	CAL VAL
-2578.5003	2.7153	11400.7

CHANNEL NO. 24 8697 L
09/18/86 R0905

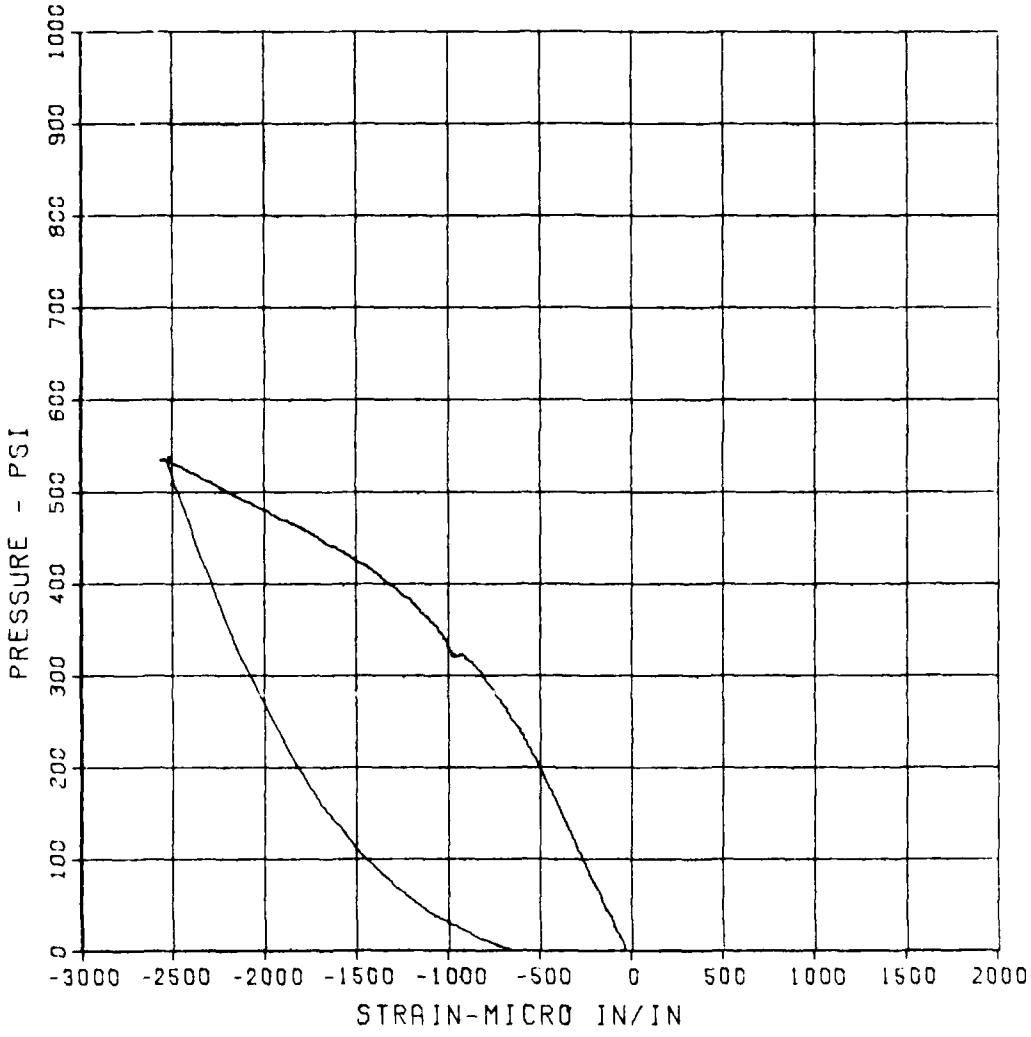

SBS ARCH TEST S-1
E0-3

MAXIMUM	SIGMA CAL	CAL VAL
-17305.0537	2.5571	11400.7

CHANNEL NO. 25 8697 1
09/18/86 R0905

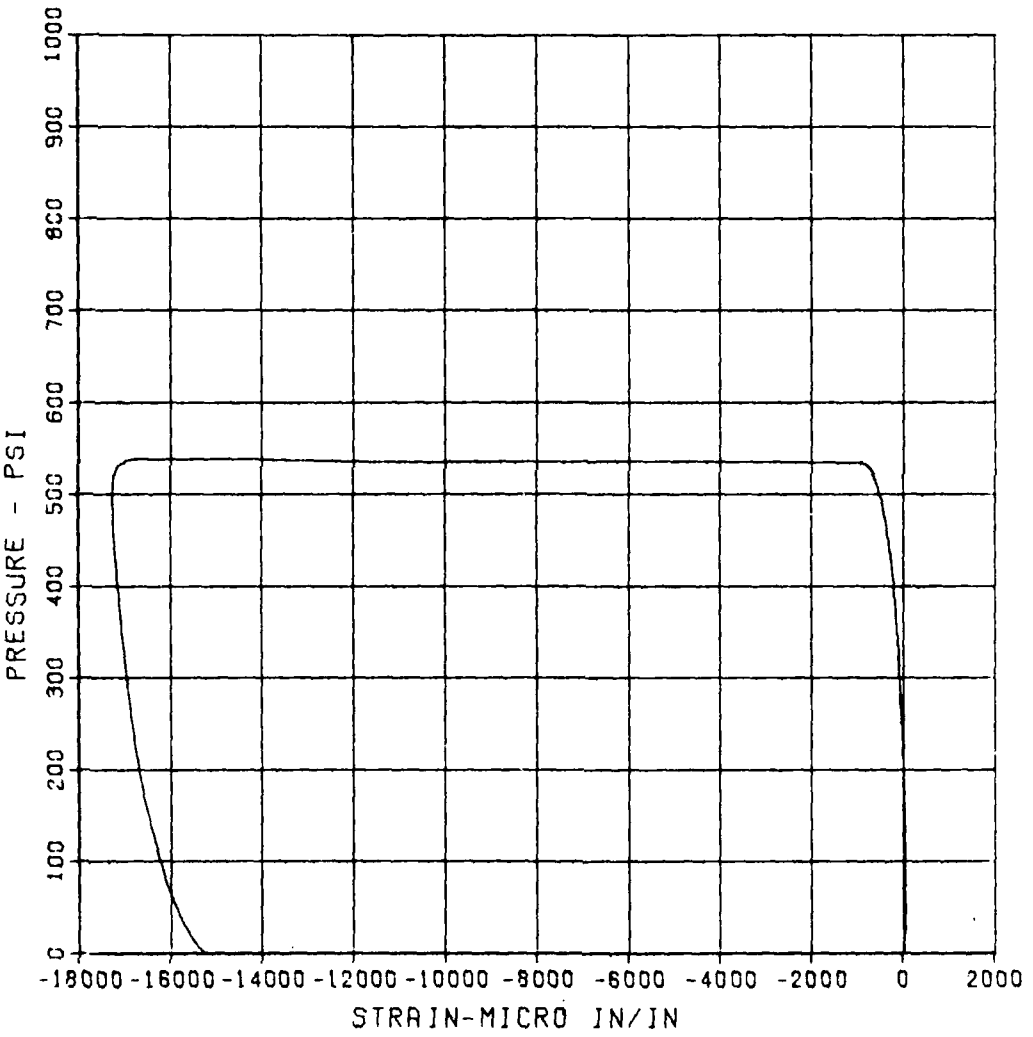

SBS ARCH TEST S-1
EI-3

MAXIMUM	SIGMA CAL	CAL VAL
-19690.7130	2.8823	11400.7

CHANNEL NO. 26 8697 1
09/18/86 R0905

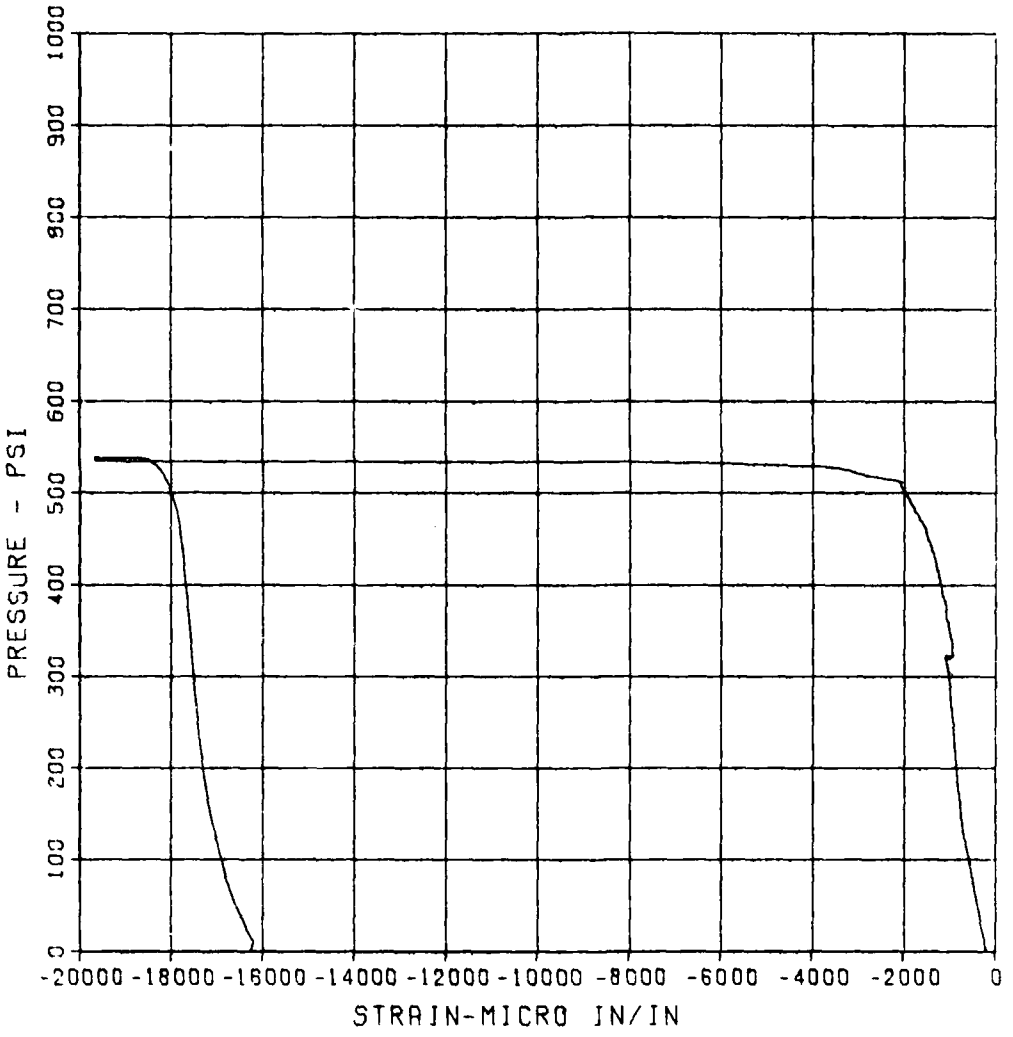

SBS ARCH TEST S-1
EO-4

MAXIMUM	SIGMA CAL	CAL VAL
-1127.3371	0.9172	11400.7

CHANNEL NO. 27 859' 1
09/18/86 R0905

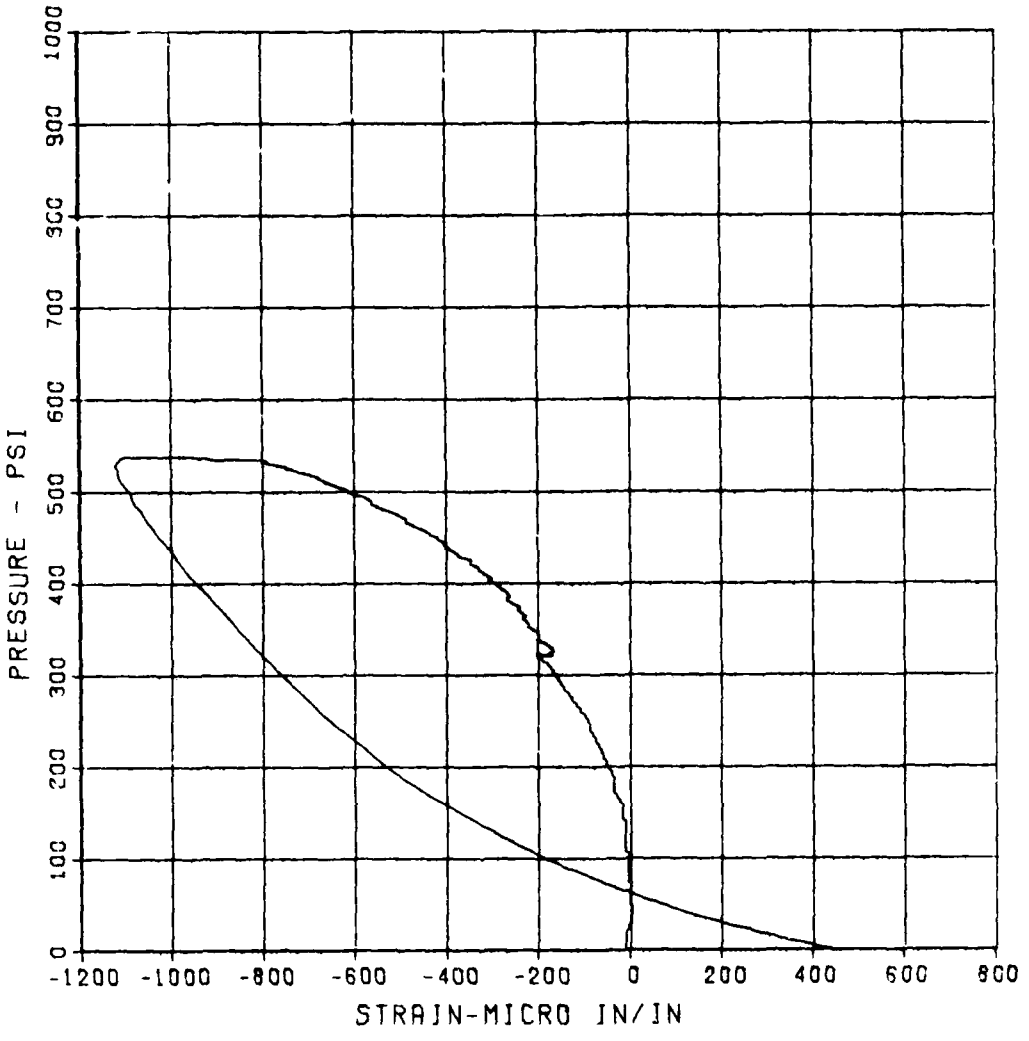

SBS ARCH TEST S-1
EI-4A

MAXIMUM	SIGMA CAL	CAL VAL
-2968.0519	2.3750	11400.7

CHANNEL NO. 28 8697 1
09/18/86 R0905

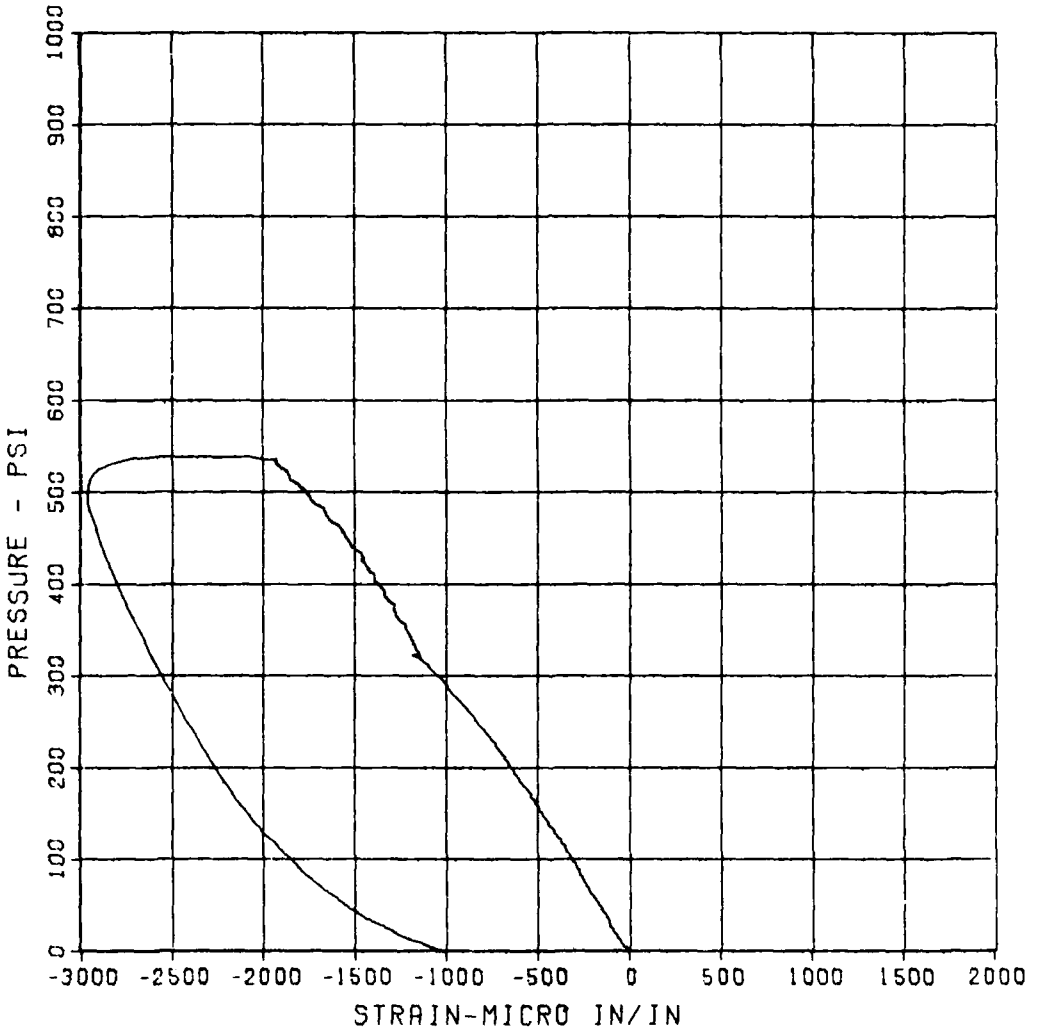

SBS ARCH TEST S-1
D-1

MAXIMUM	SIGMA CAL	CAL VAL
0.3598	2.2900	10.0

CHANNEL NO. 29 8697 1
09/18/86 R0905

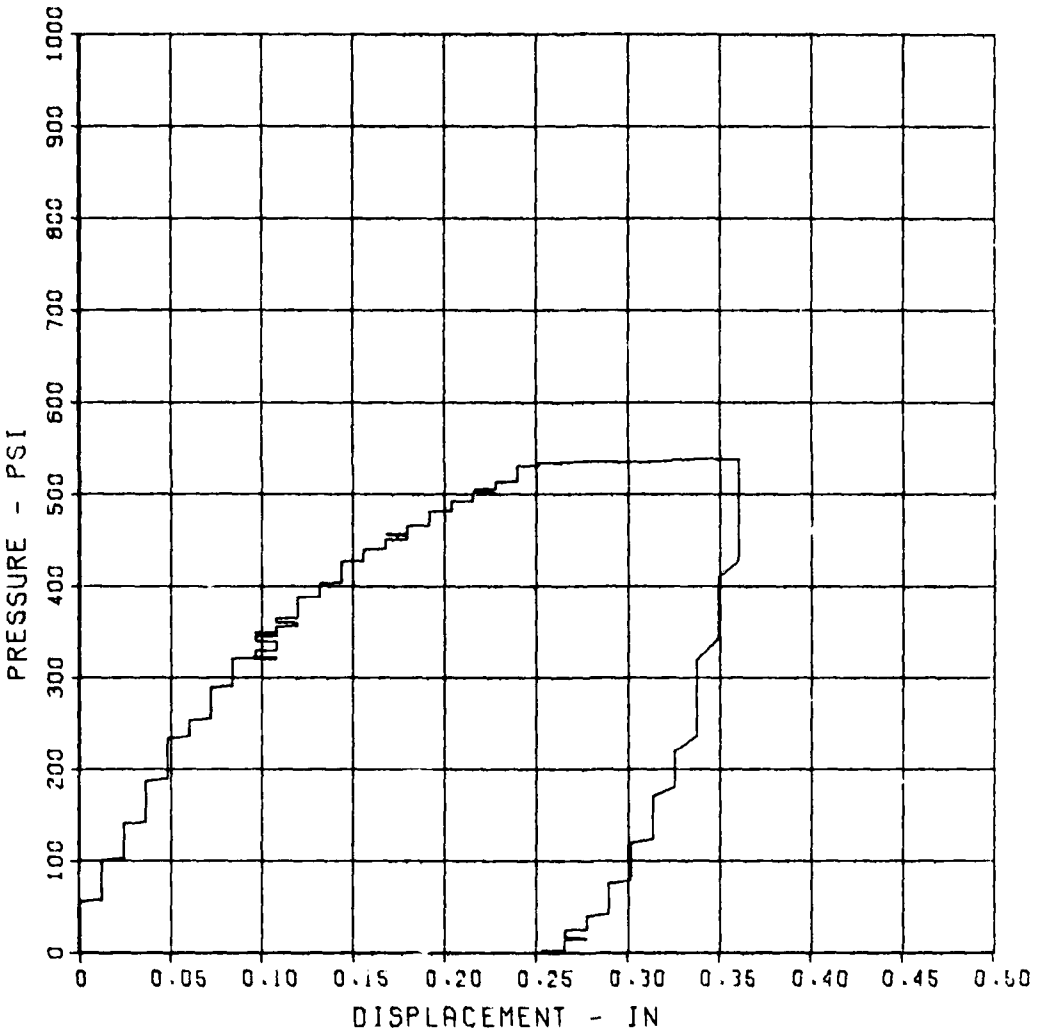

SBS ARCH TEST S-1
D-2

MAXIMUM	SIGMA CAL	CAL VAL
0.1098	3.1718	2.1

CHANNEL NO. 30 8697 1
09/18/86 R0905

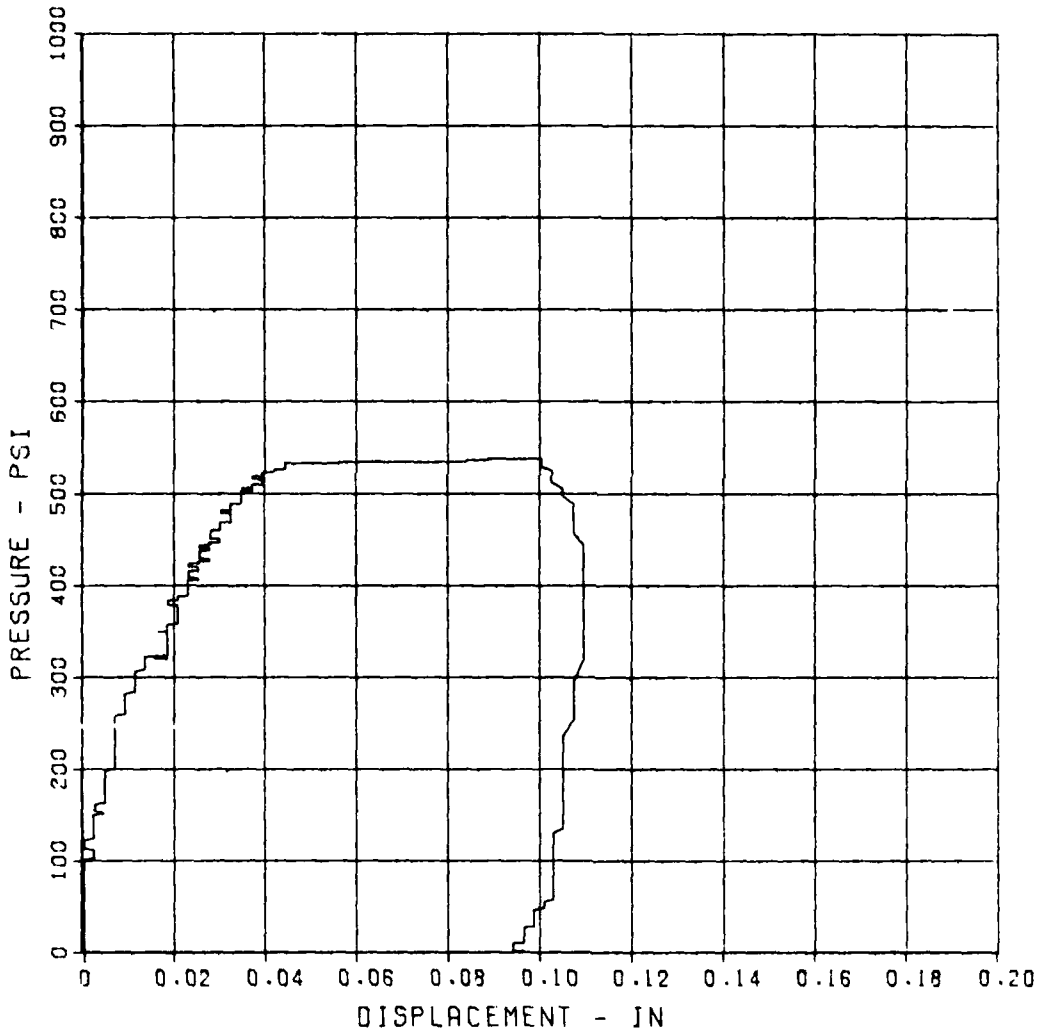

SBS ARCH TEST S-1A

SBS ARCH TEST S-1A
BP-1

MAXIMUM	SIGMA CAL	CAL VAL
830.0130	2.4118	1149.5

CHANNEL NO. 1 8935 1
09/19/86 R0906

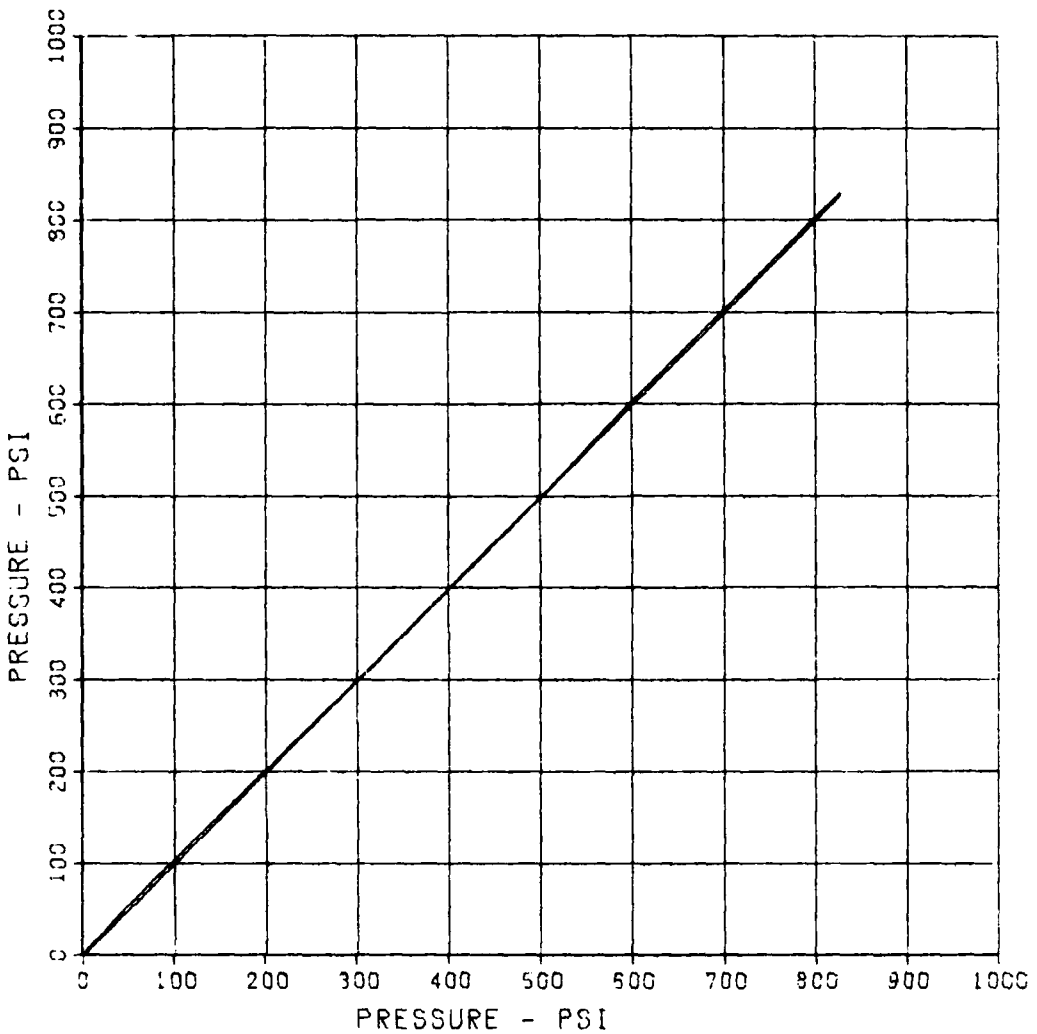

SBS ARCH TEST S-1A
BP-2

MAXIMUM	SIGMA CAL	CAL VAL
807.9816	2.7312	1110.3

CHANNEL NO. 2 8835 1
09/19/86 R0906

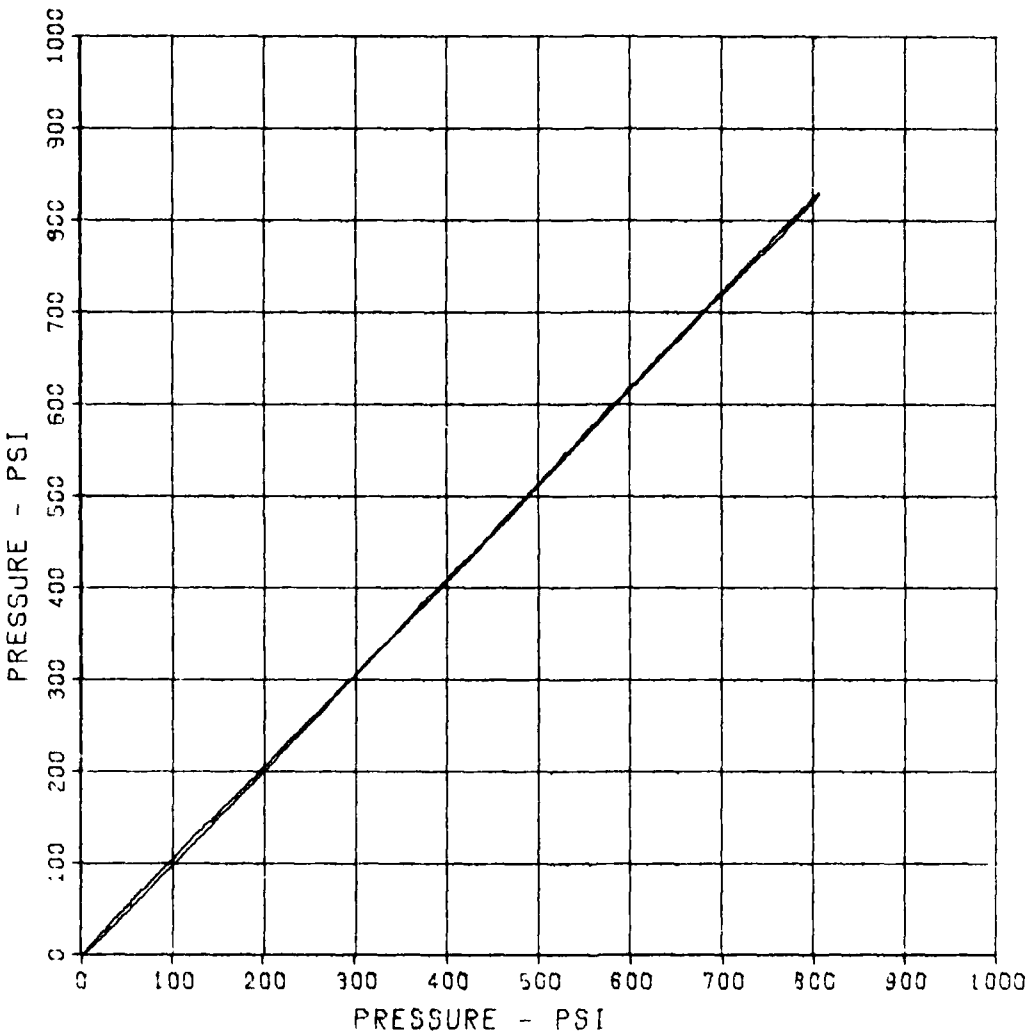

SBS ARCH TEST S-1A
IP-1

MAXIMUM	SIGMA CAL	CAL VAL
387.7284	3.0665	566.2

CHANNEL NO. 3 8835 1
09/19/86 R0906

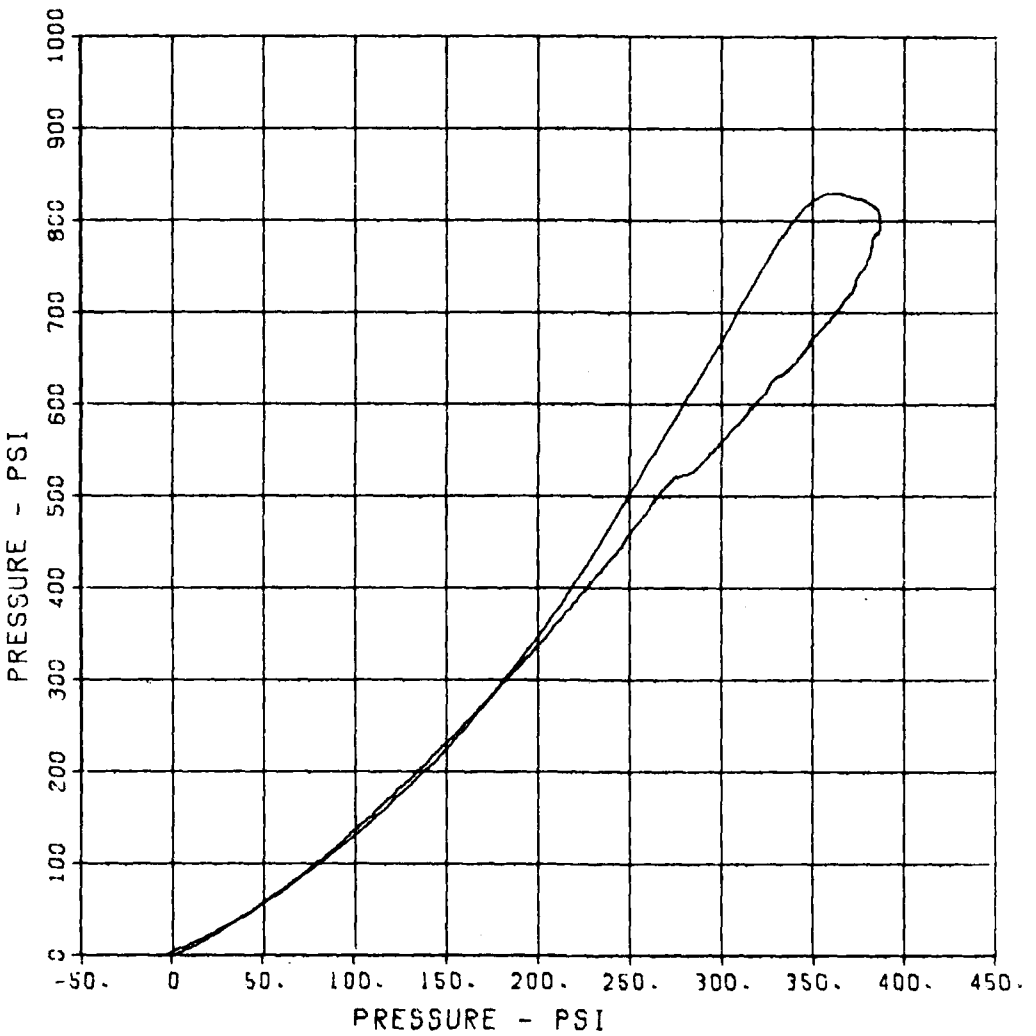

SBS ARCH TEST S-1A
IP-2

MAXIMUM	SIGMA CAL	CAL VAL
452.0706	3.3397	618.9

CHANNEL NO. 4 8835 1
09/19/86 R0906

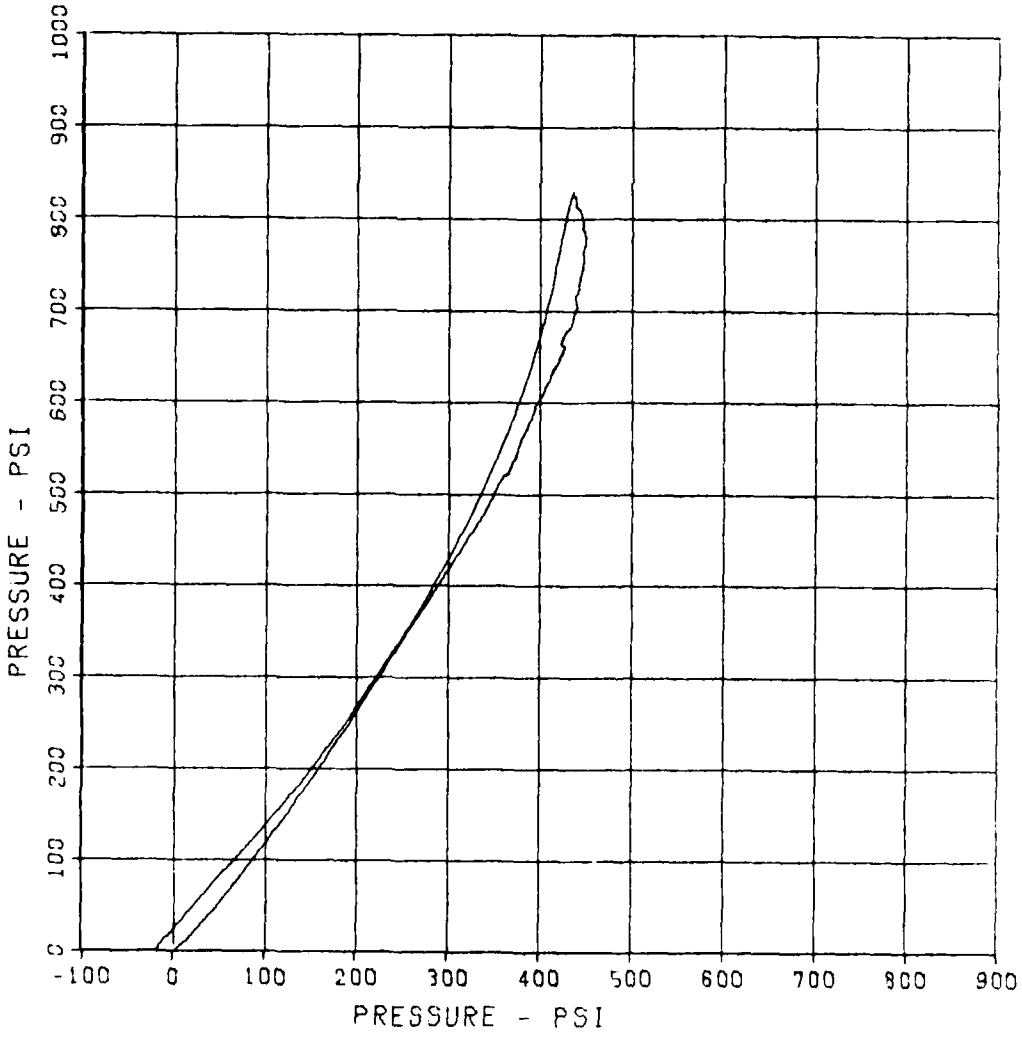

SBS ARCH TEST S-1A
IP-3

MAXIMUM	SIGMA CAL	CAL VAL
300.2569	2.8488	633.4

CHANNEL NO. 5 8835 1
09/19/86 RD906

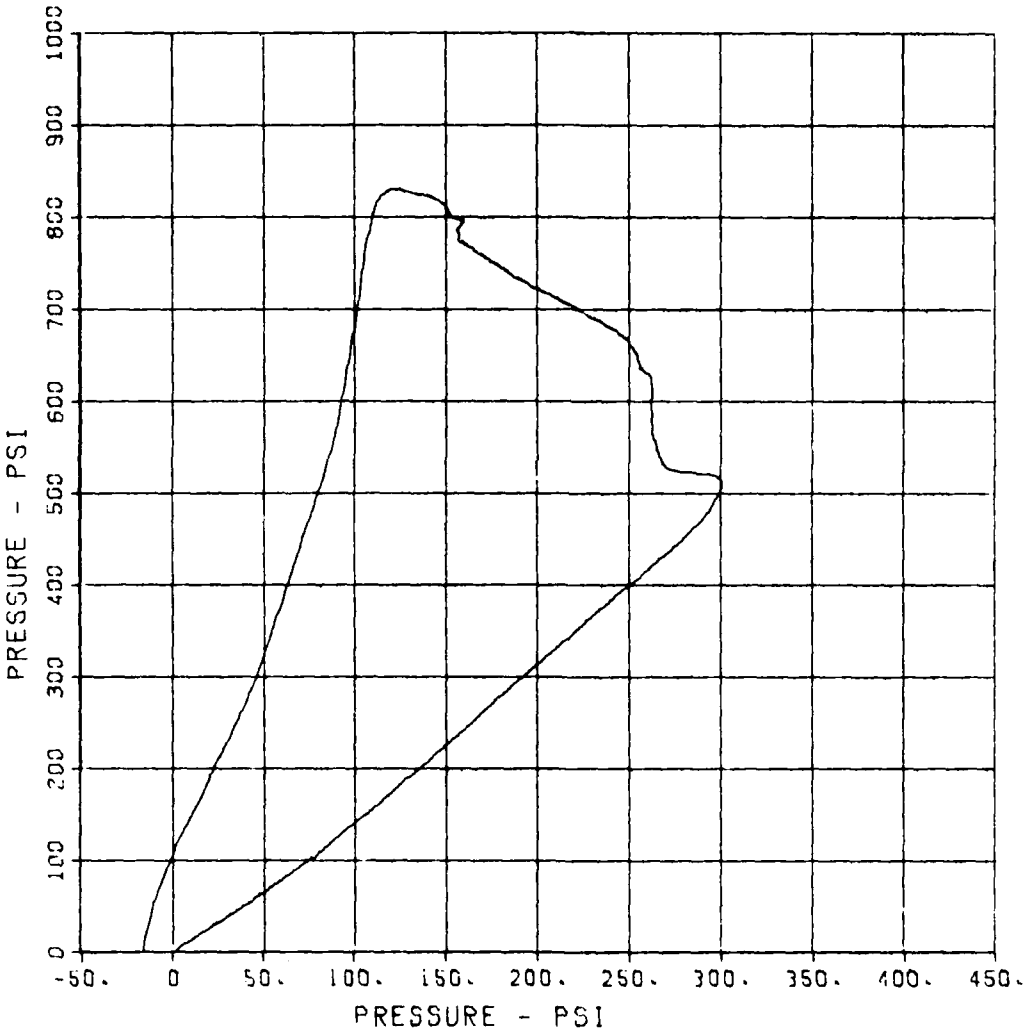

SBS ARCH TEST S-1A
IP-4

MAXIMUM	SIGMA CAL	CAL VAL
386.4806	3.2169	551.1

CHANNEL NO. 6 8835 1
09/19/86 R0906

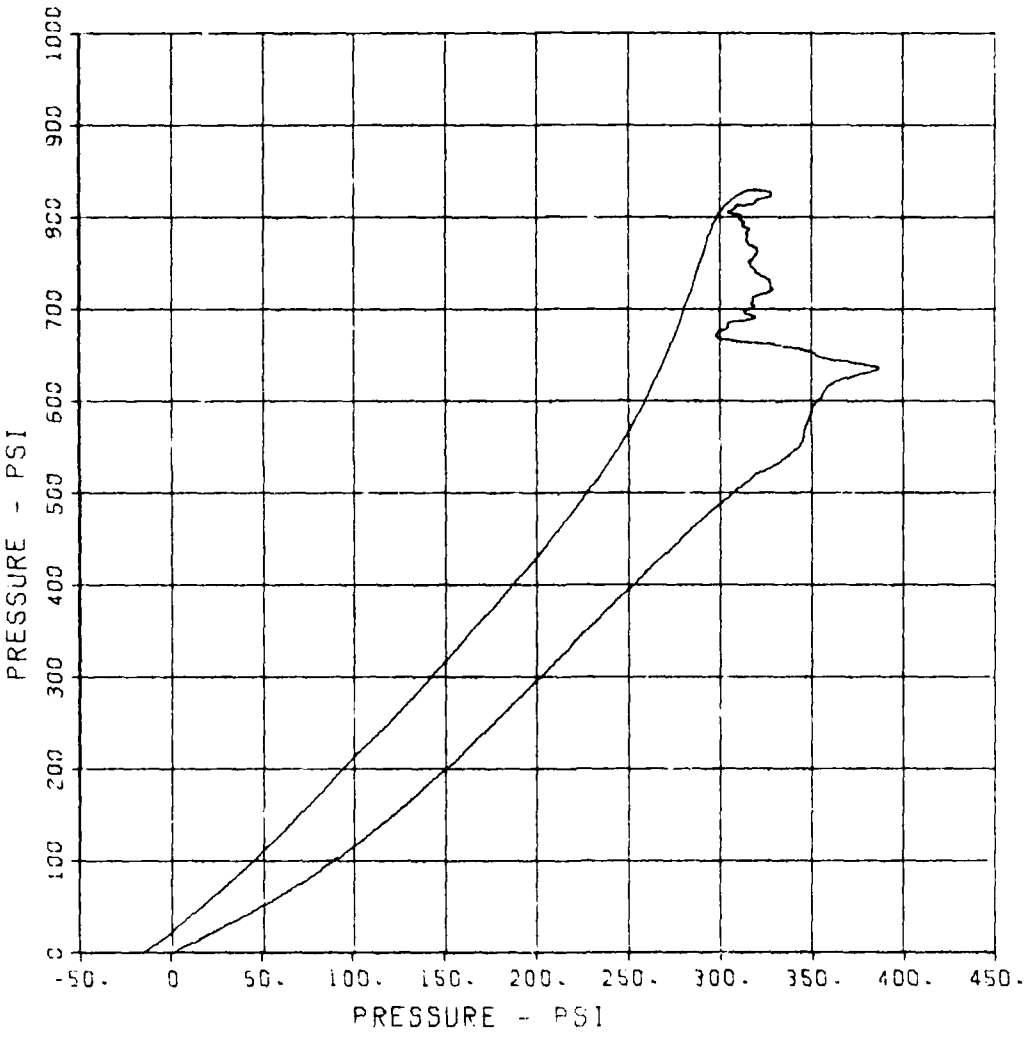

SBS ARCH TEST S-1A
IP-5

MAXIMUM	SIGMA CAL	CAL VAL
-150.0951	2.5175	361.1

CHANNEL NO. 7 8835 1
09/19/86 R0906

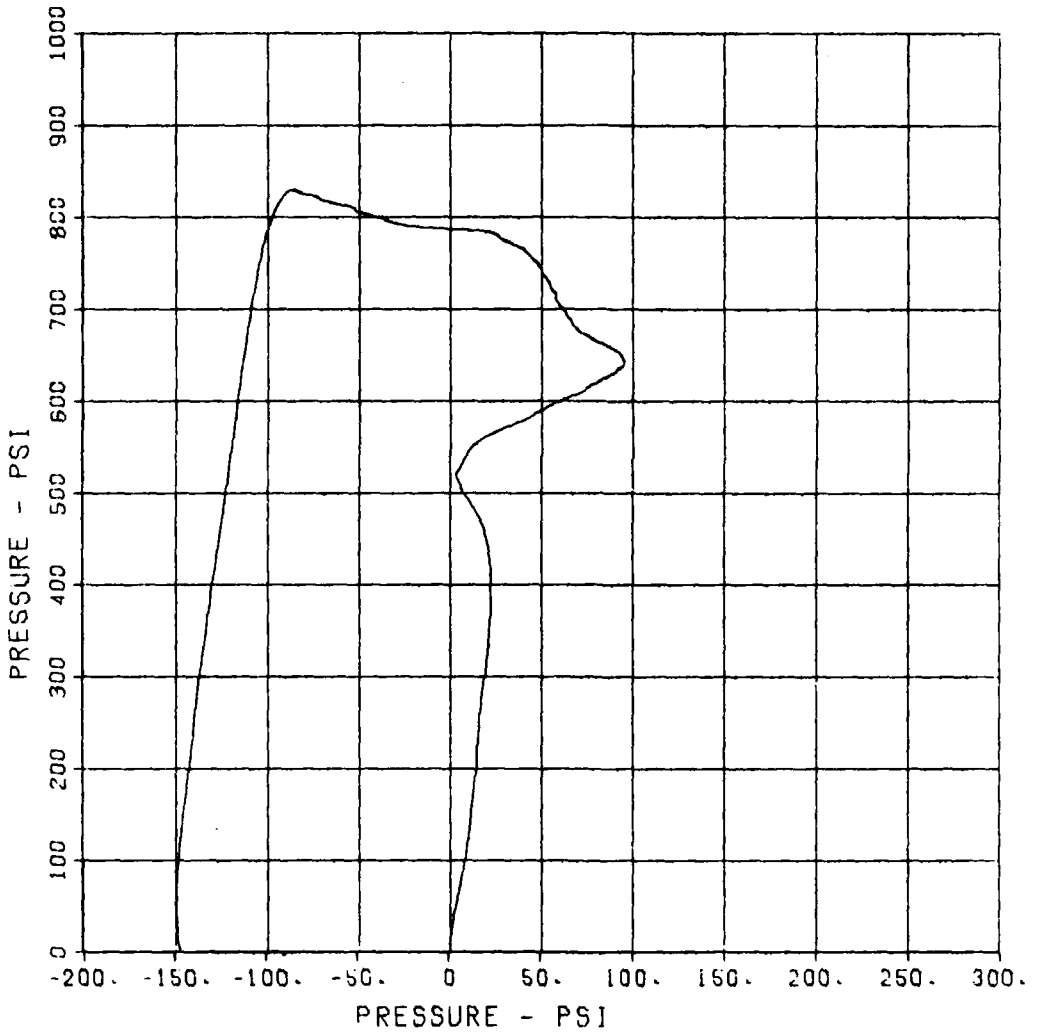

SBS ARCH TEST S-1A
IP-6

MAXIMUM	SIGMA CAL	CAL VAL
416.3818	2.7473	602.9

CHANNEL NO. 8 8835 1
09/19/86 R0906

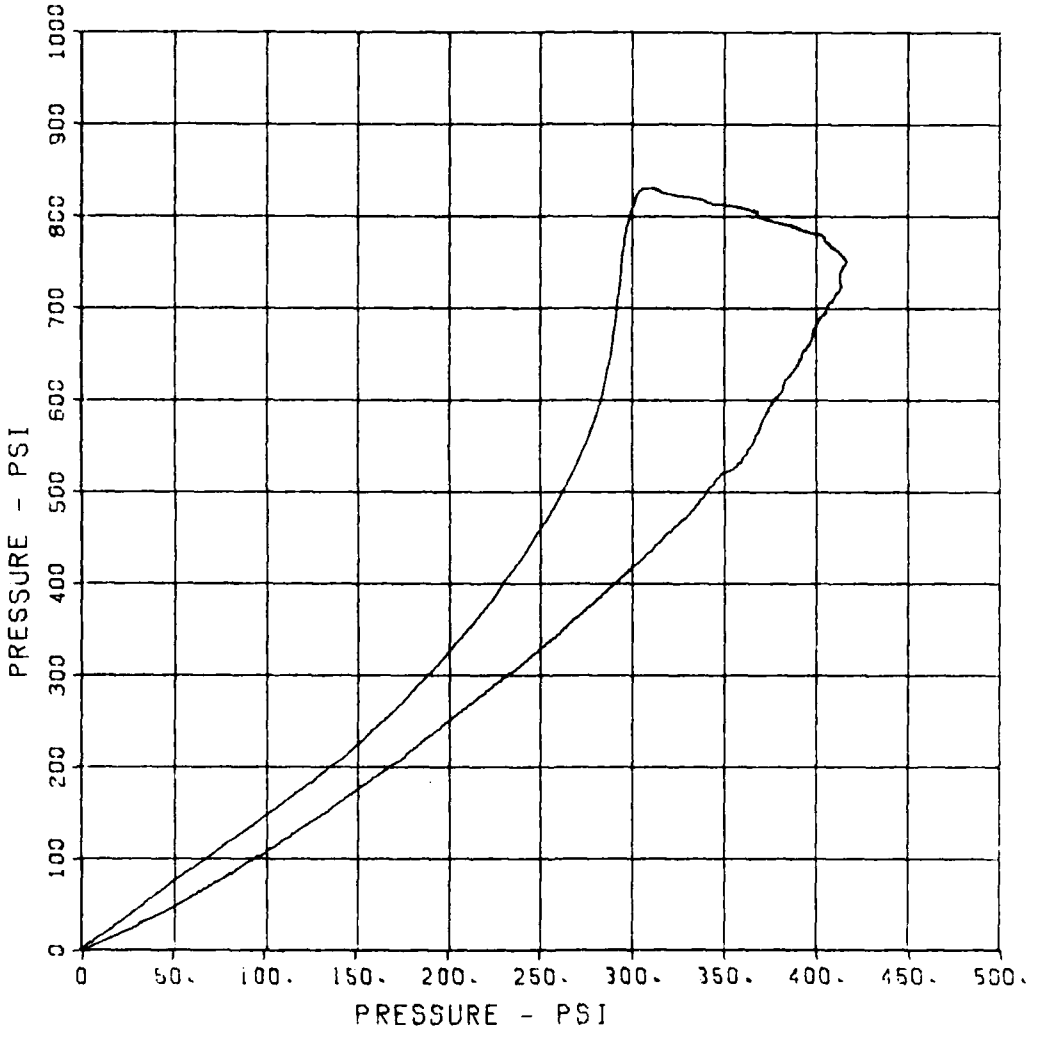

SBS ARCH TEST S-1A
IP-7

MAXIMUM	SIGMA CAL	CAL VAL
324.1860	2.6457	591.7

CHANNEL NO. 9 8835 1
09/19/86 R0906

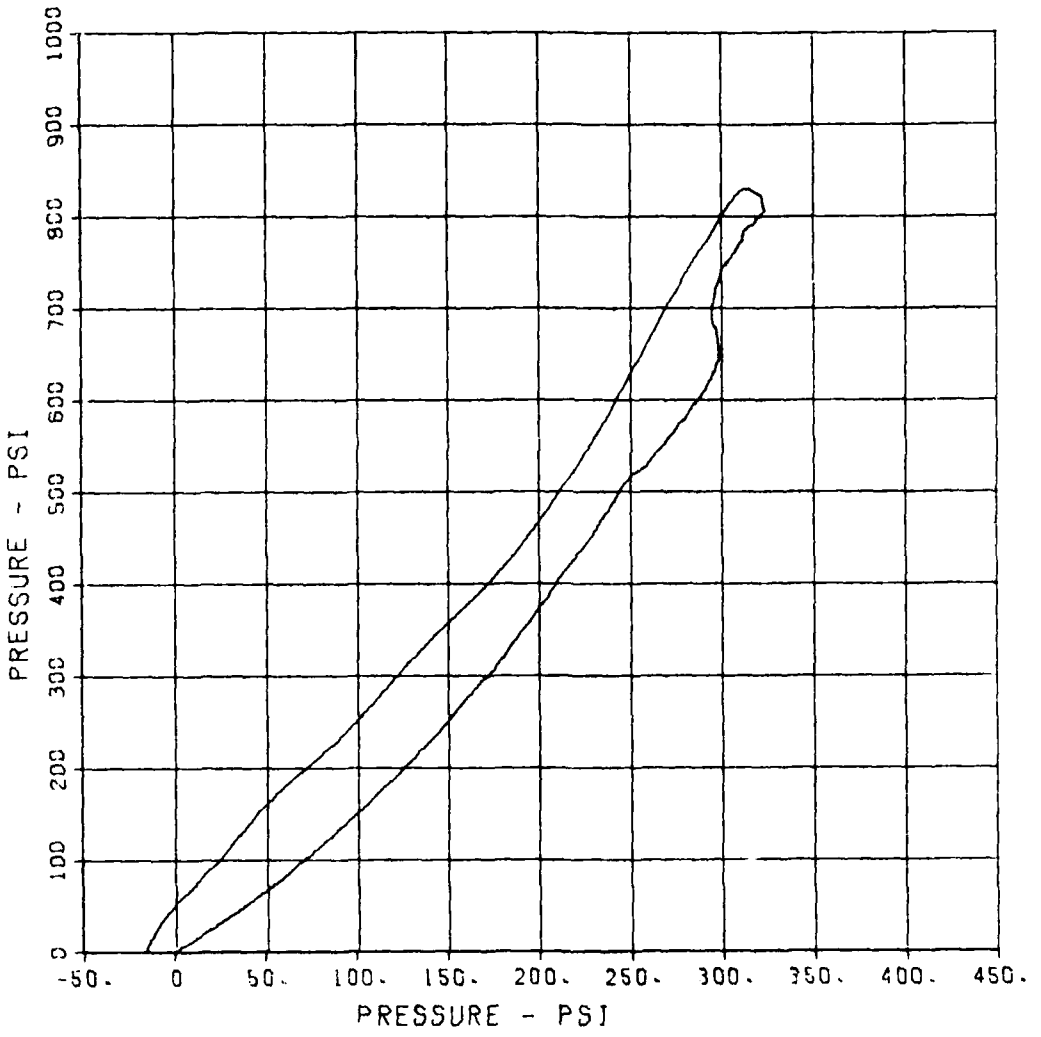

SBS ARCH TEST S-1A
IP-8

MAXIMUM	SIGMA CAL	CAL VAL
298.4051	2.7865	397.0

CHANNEL NO. 10 8835 1
09/19/86 R0906

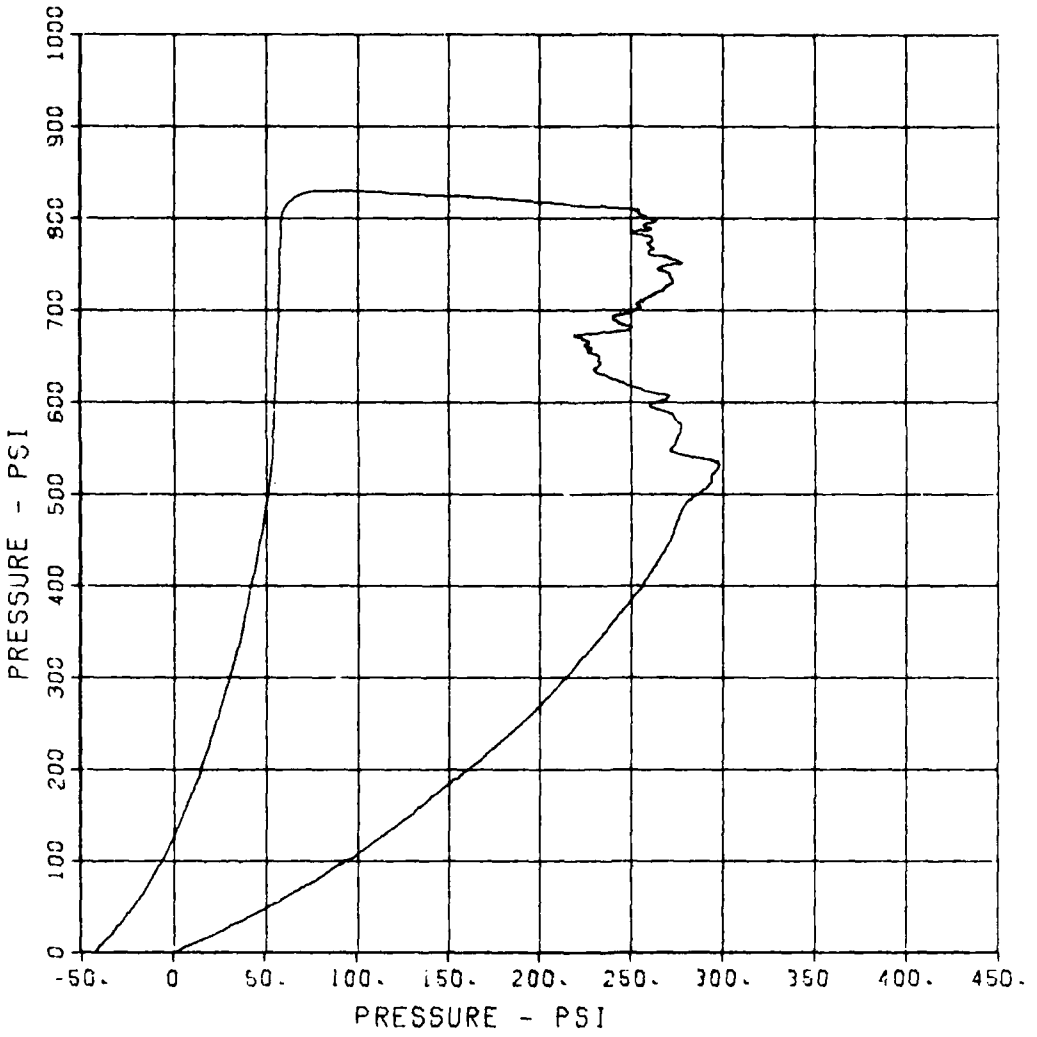

SBS ARCH TEST S-1A
IP-9

MAXIMUM	SIGMA CAL	CAL VAL
185.0904	2.4862	370.4

CHANNEL NO. 11 8835 1
09/19/86 R0906

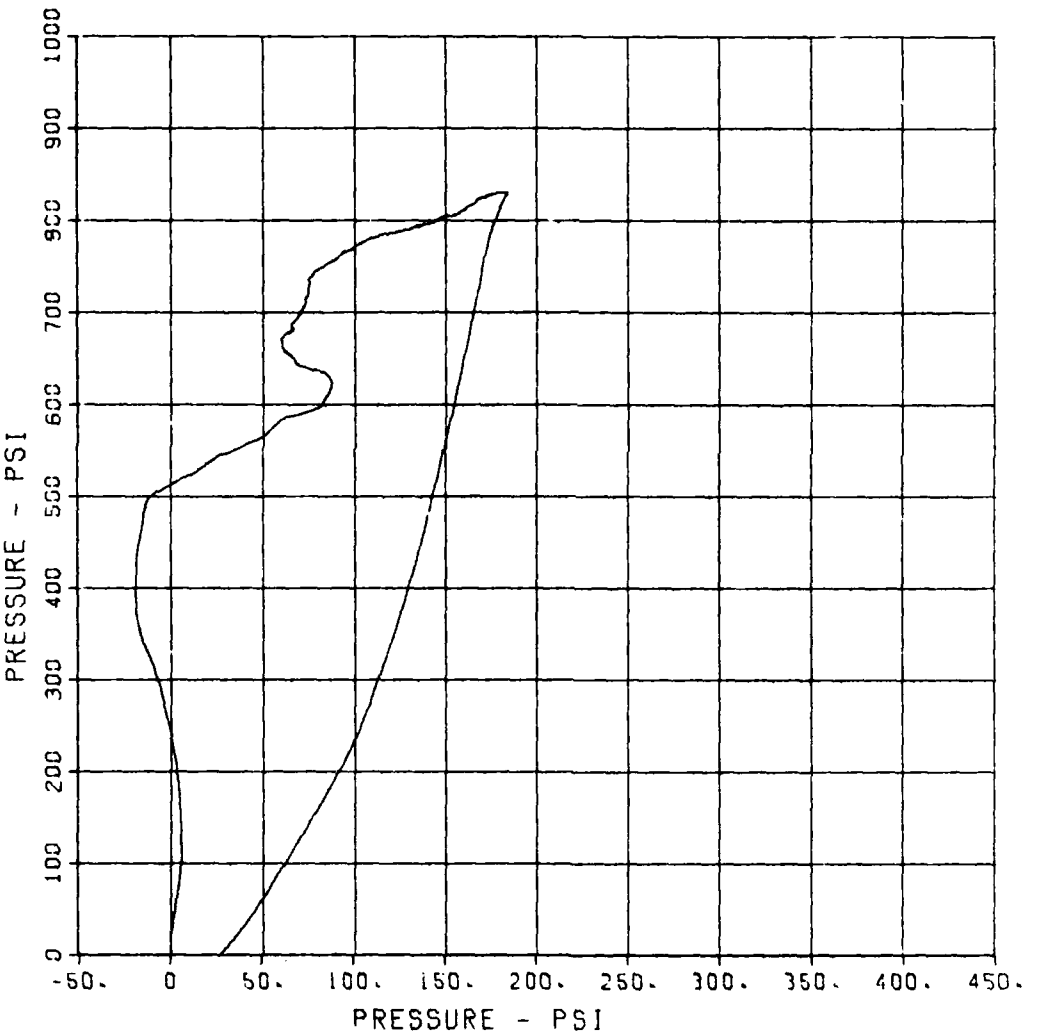

SBS ARCH TEST S-1A
SE-1

MAXIMUM	SIGMA CAL	CAL VAL
658.8568	2.9790	690.8

CHANNEL NO. 12 8835 1
09/19/86 R0906

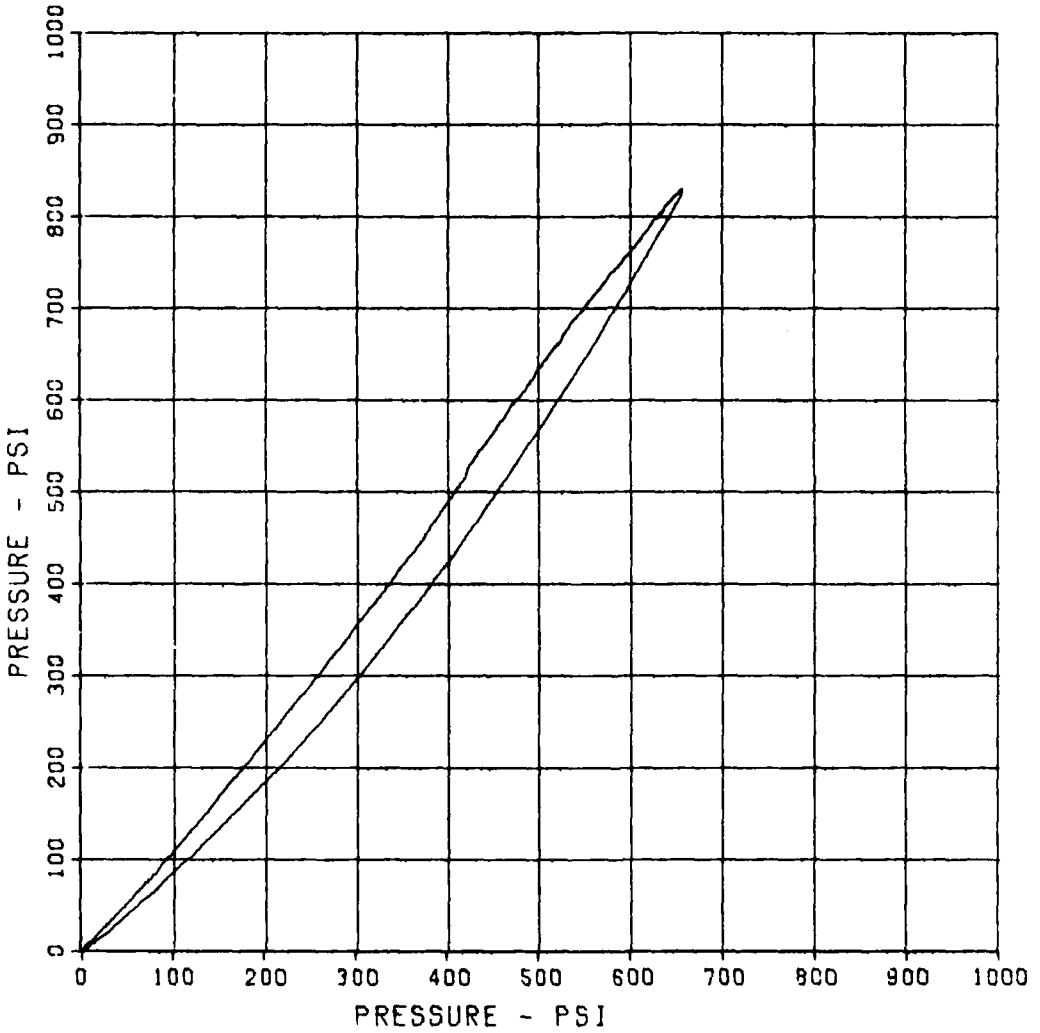

SBS ARCH TEST S-1A
SE-2

MAXIMUM	SIGMA CAL	CAL VAL
886.8161	2.9744	486.5

CHANNEL NO. 13 8835 1
09/19/86 R0906

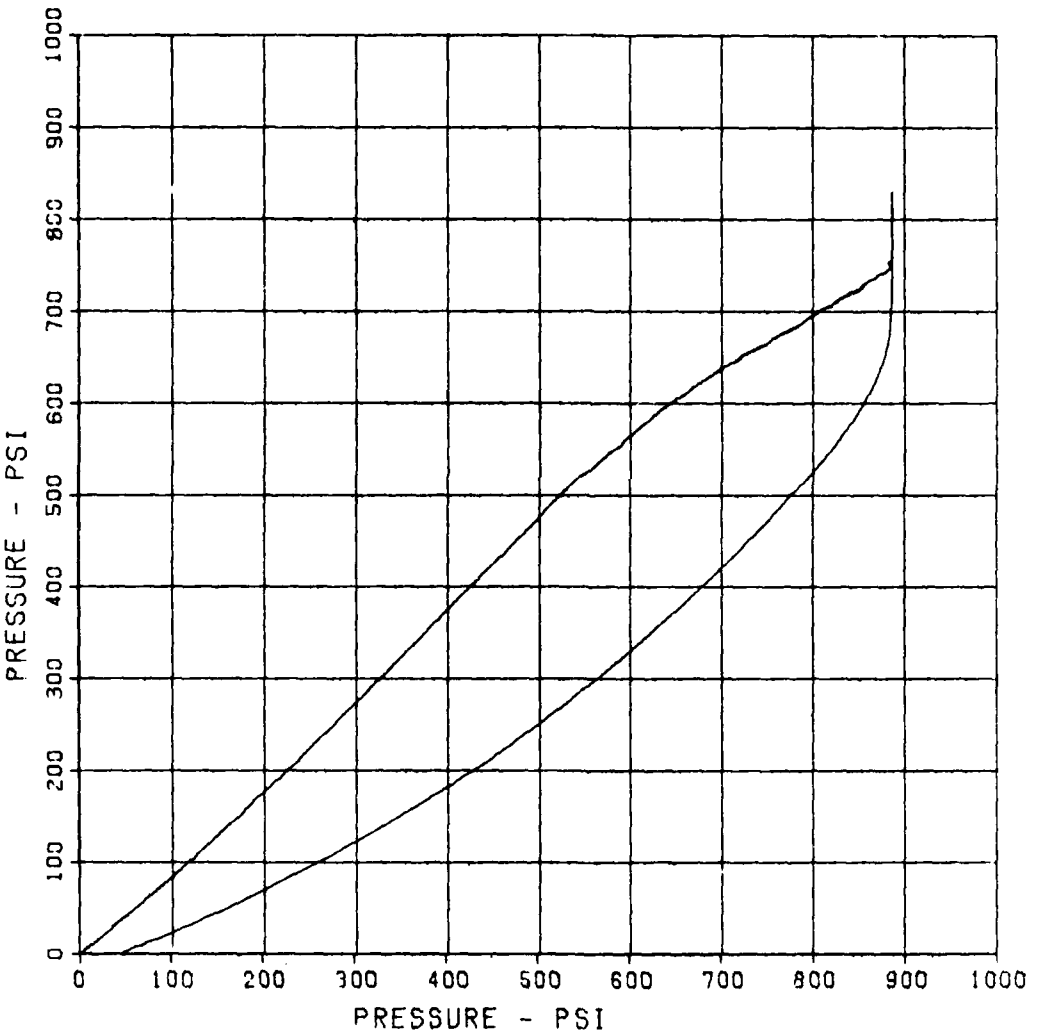

SBS ARCH TEST S-1A
SE-3

MAXIMUM	SIGMA CAL	CAL VAL
810.3023	3.4724	512.3

CHANNEL NO. 14 8835 1
09/19/86 R0906

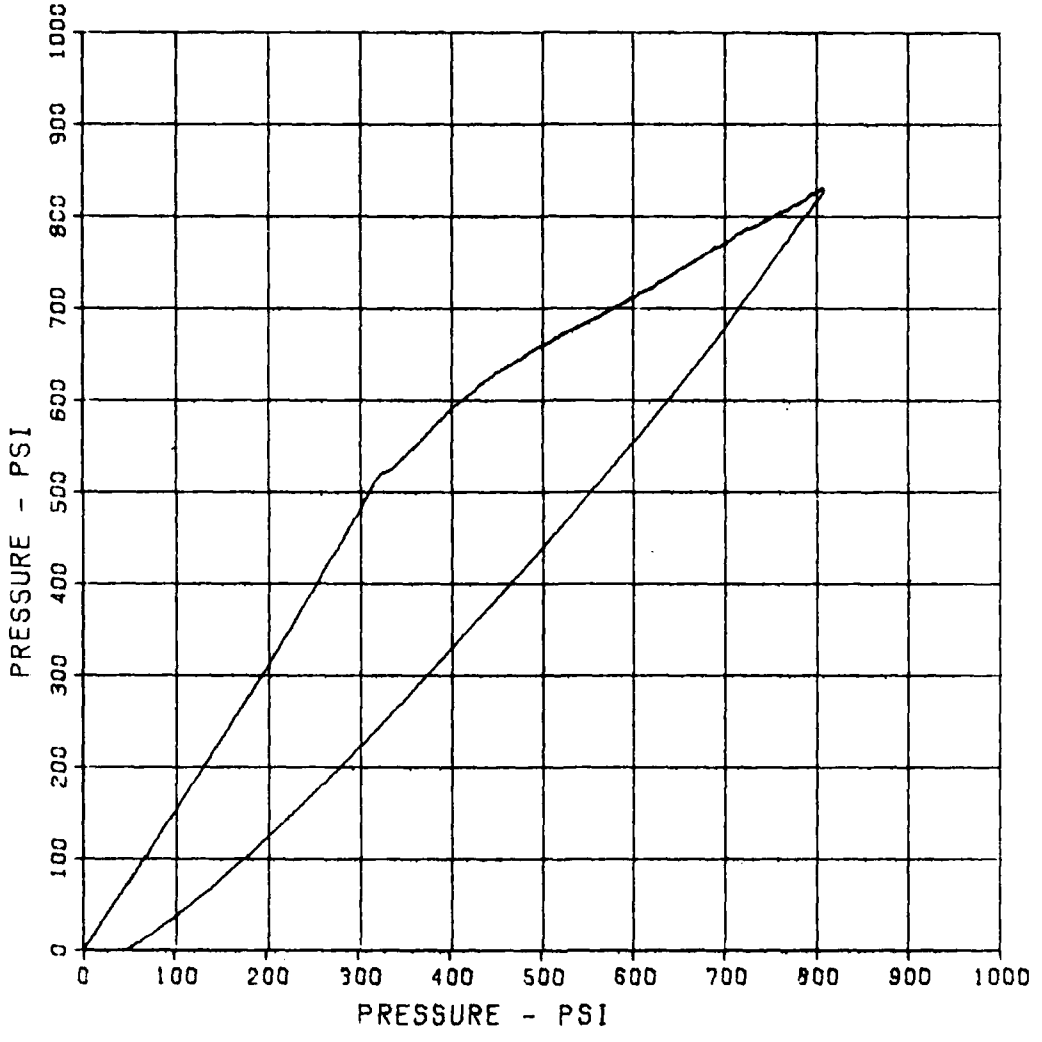

SBS ARCH TEST S-1A
SE-4

MAXIMUM	SIGMA CAL	CAL VAL
856.3481	3.6514	497.9

CHANNEL NO. 15 8835 1
09/19/86 R0906

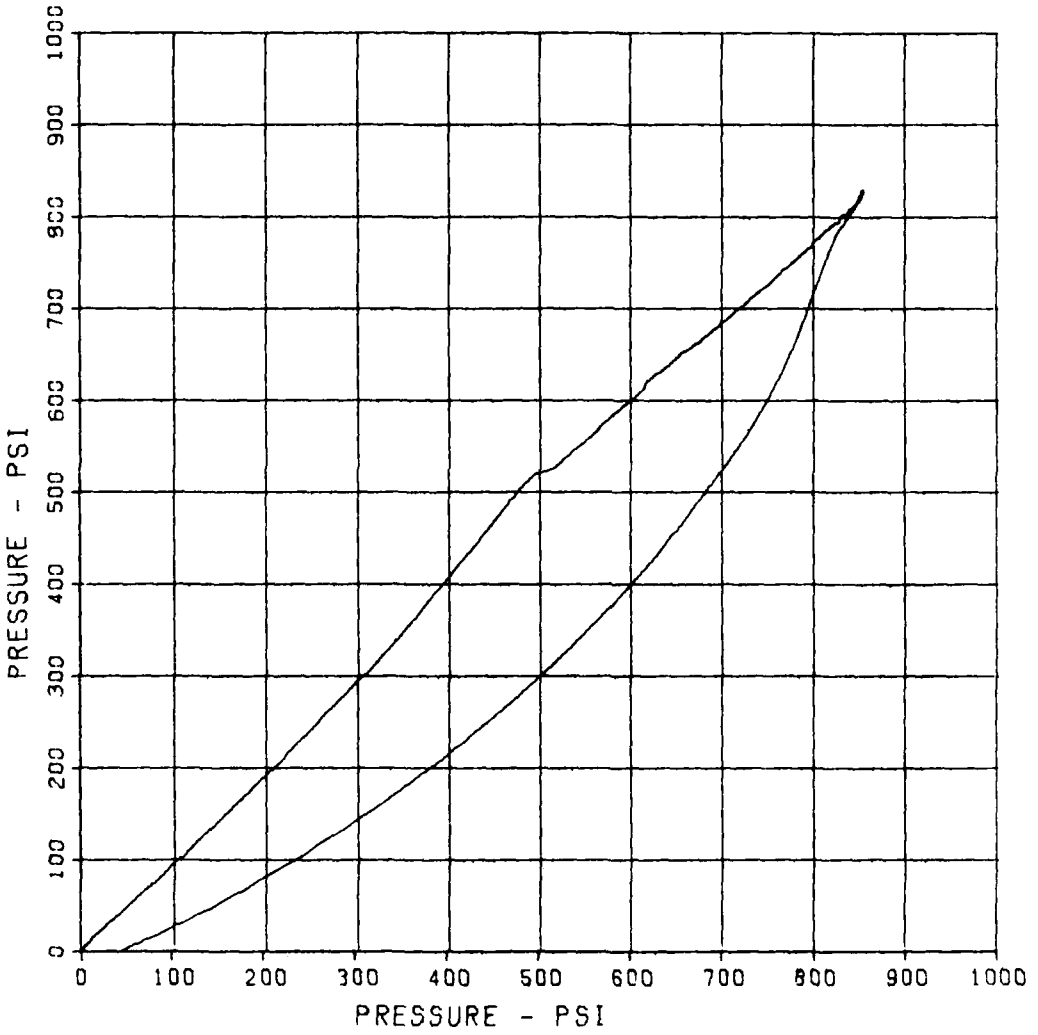

SBS ARCH TEST S-1A
SE-6

MAXIMUM	SIGMA CAL	CAL VAL
523.9047	3.0668	535.9

CHANNEL NO. 17 8835 L
09/19/86 R0906

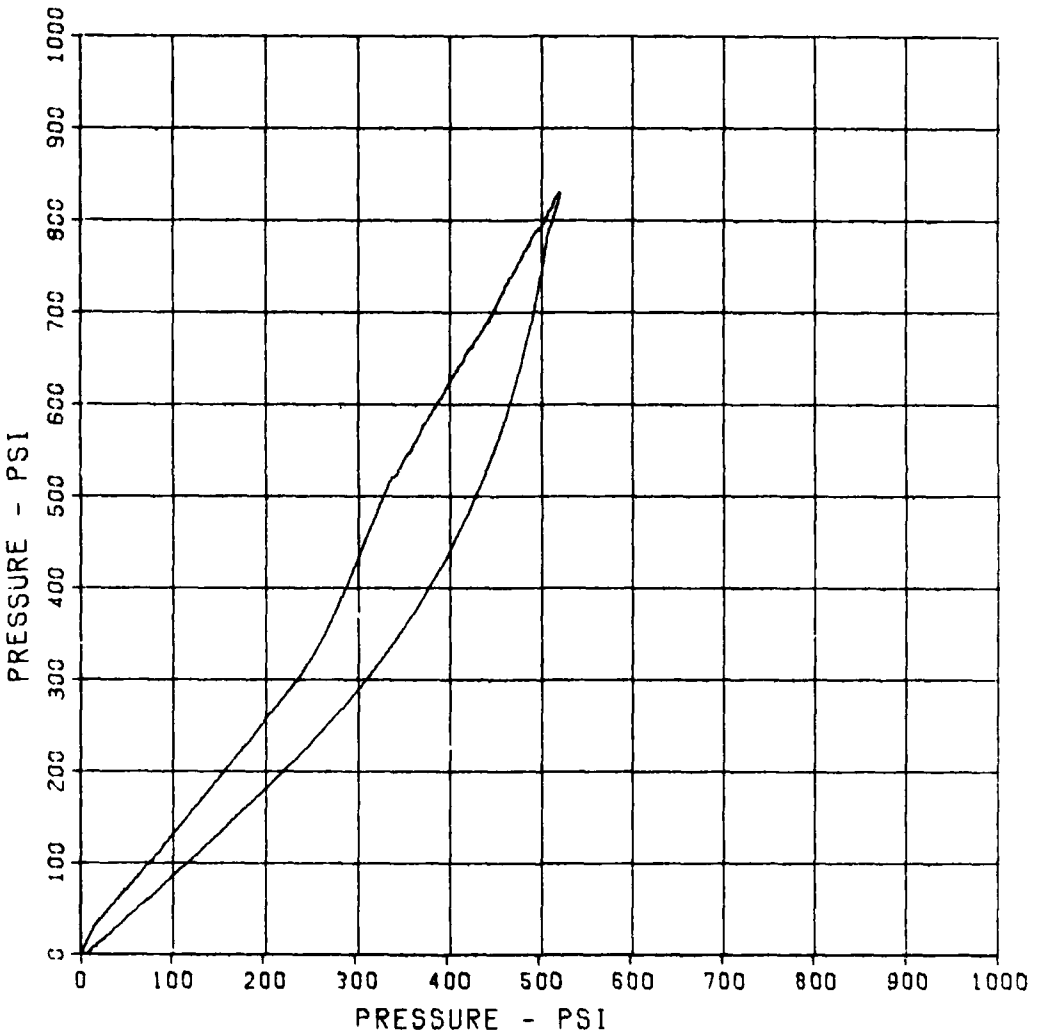

SBS ARCH TEST S-1A
SE-7

MAXIMUM	SIGMA CAL	CAL VAL
63.1710	3.1013	594.9

CHANNEL NO. 18 8835 1
09/19/86 R0906

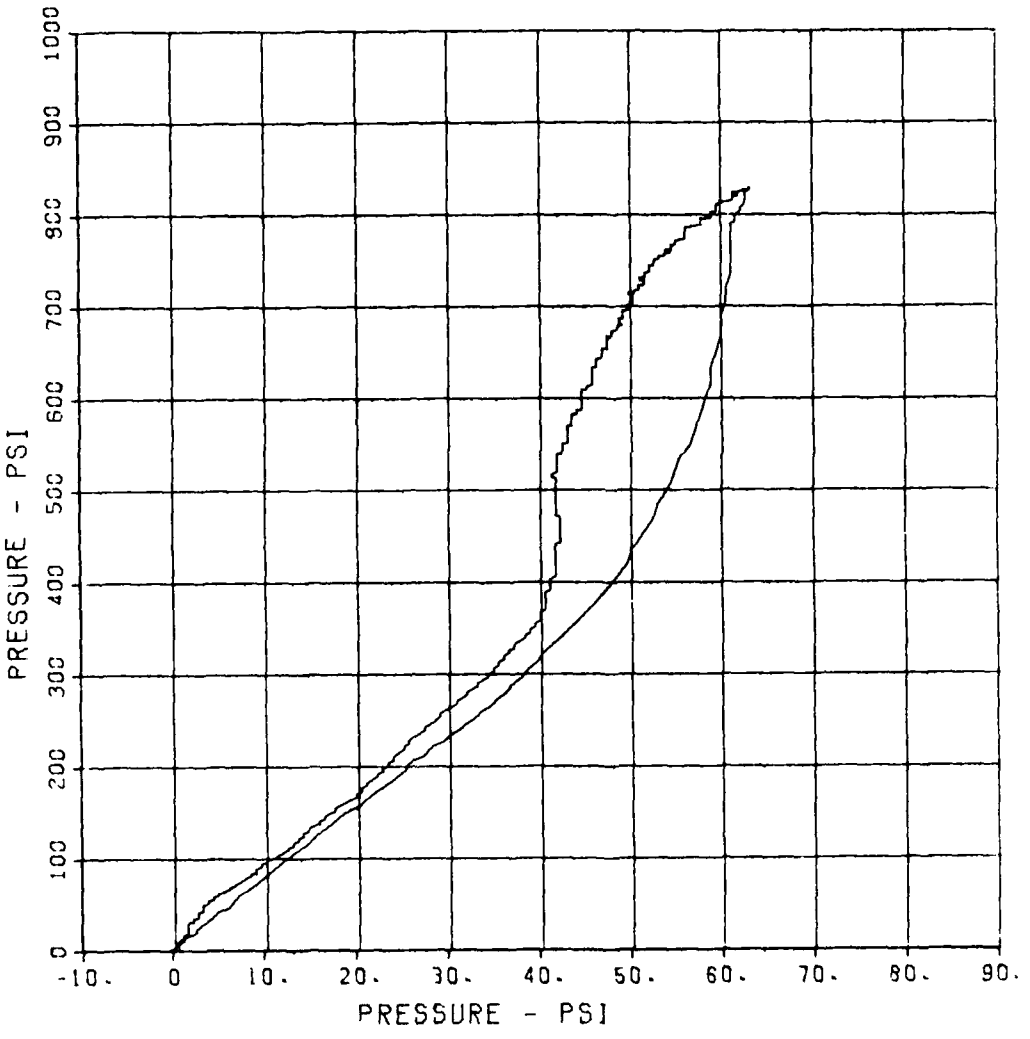

SBS ARCH TEST S-1A
SE-8

MAXIMUM	SIGMA CAL	CAL VAL
796.7005	3.3188	484.5

CHANNEL NO. 19 8835 1
09/19/86 R0906

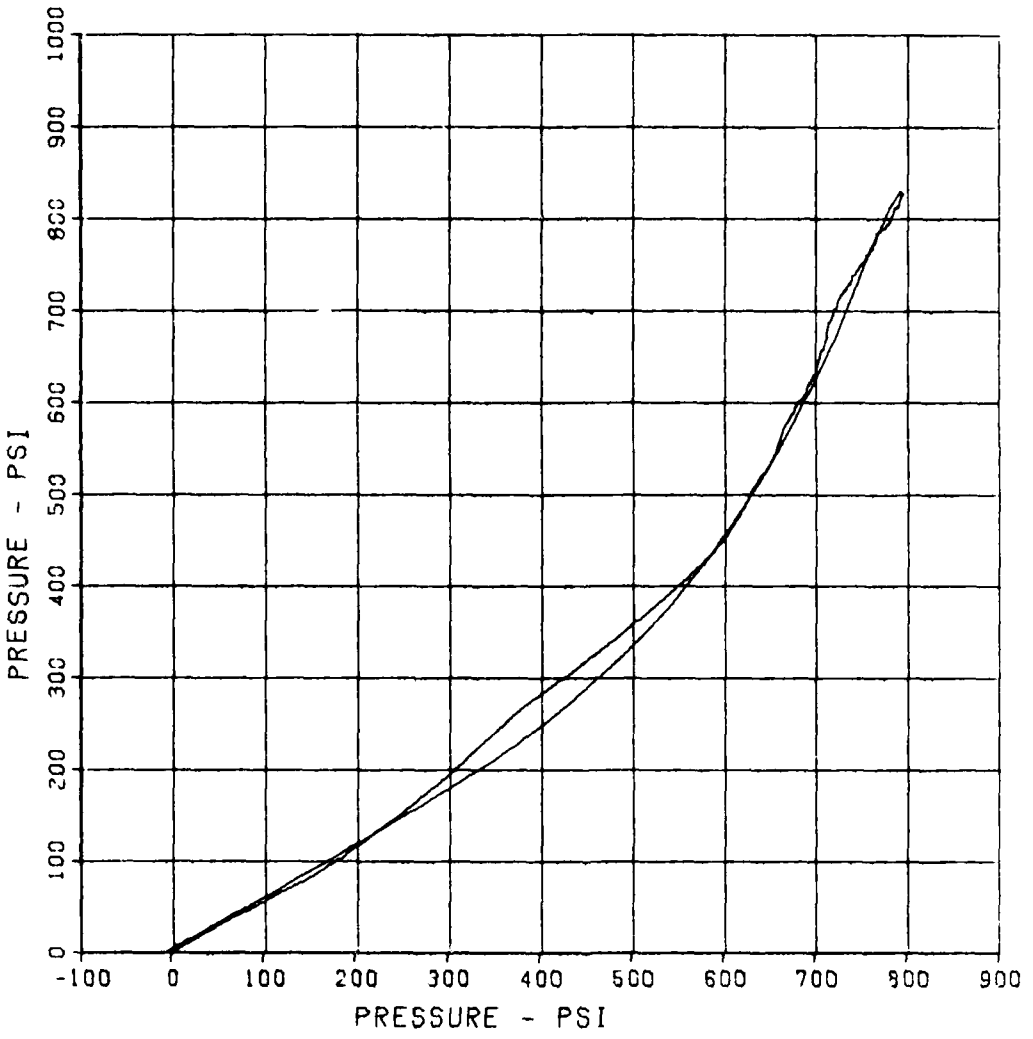

SBS ARCH TEST S-1A
SE-9

MAXIMUM	SIGMA CAL	CAL VAL
529.9216	3.2114	609.9

CHANNEL NO. 20 8835 1
09/19/86 R0906

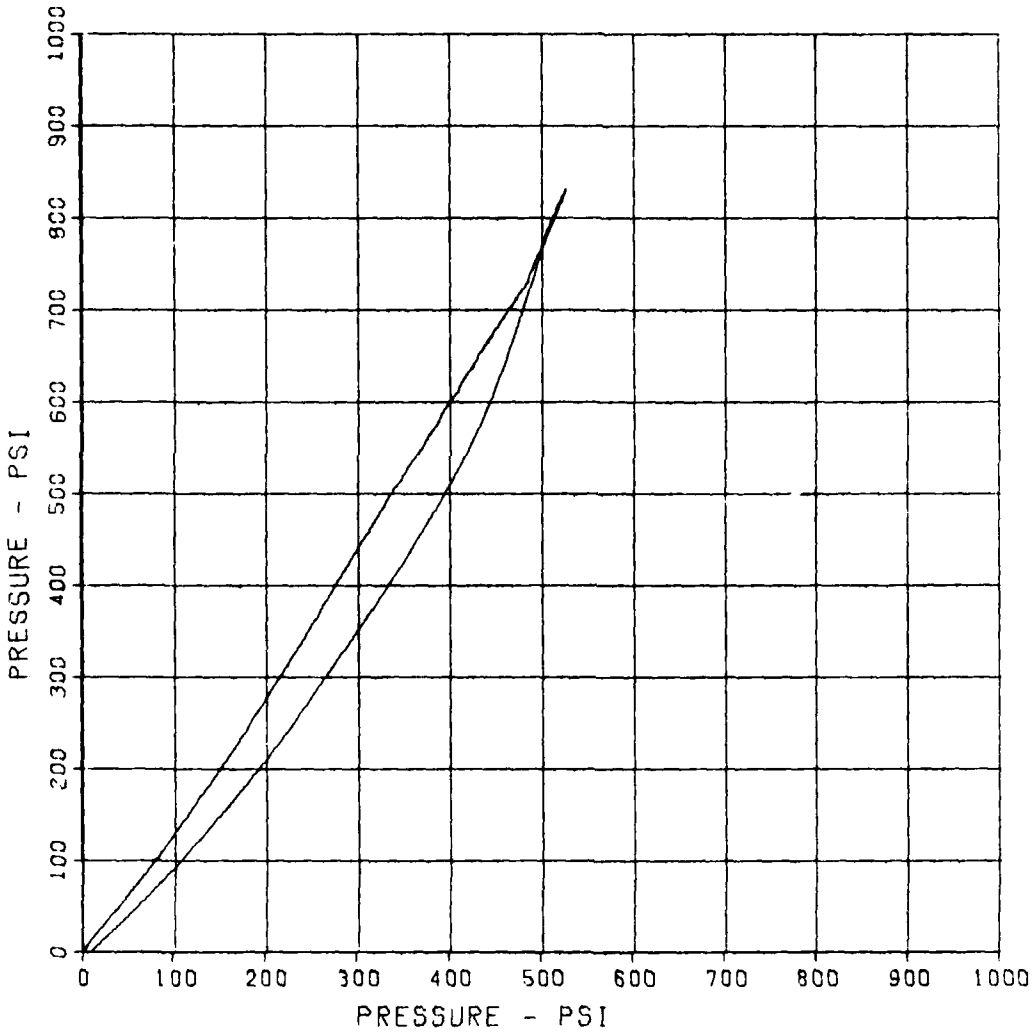

SBS ARCH TEST S-1A
E0-1

MAXIMUM	SIGMA CAL	CAL VAL
-11137.3719	2.5873	11400.7

CHANNEL NO. 21 8835 1
09/19/86 R0906

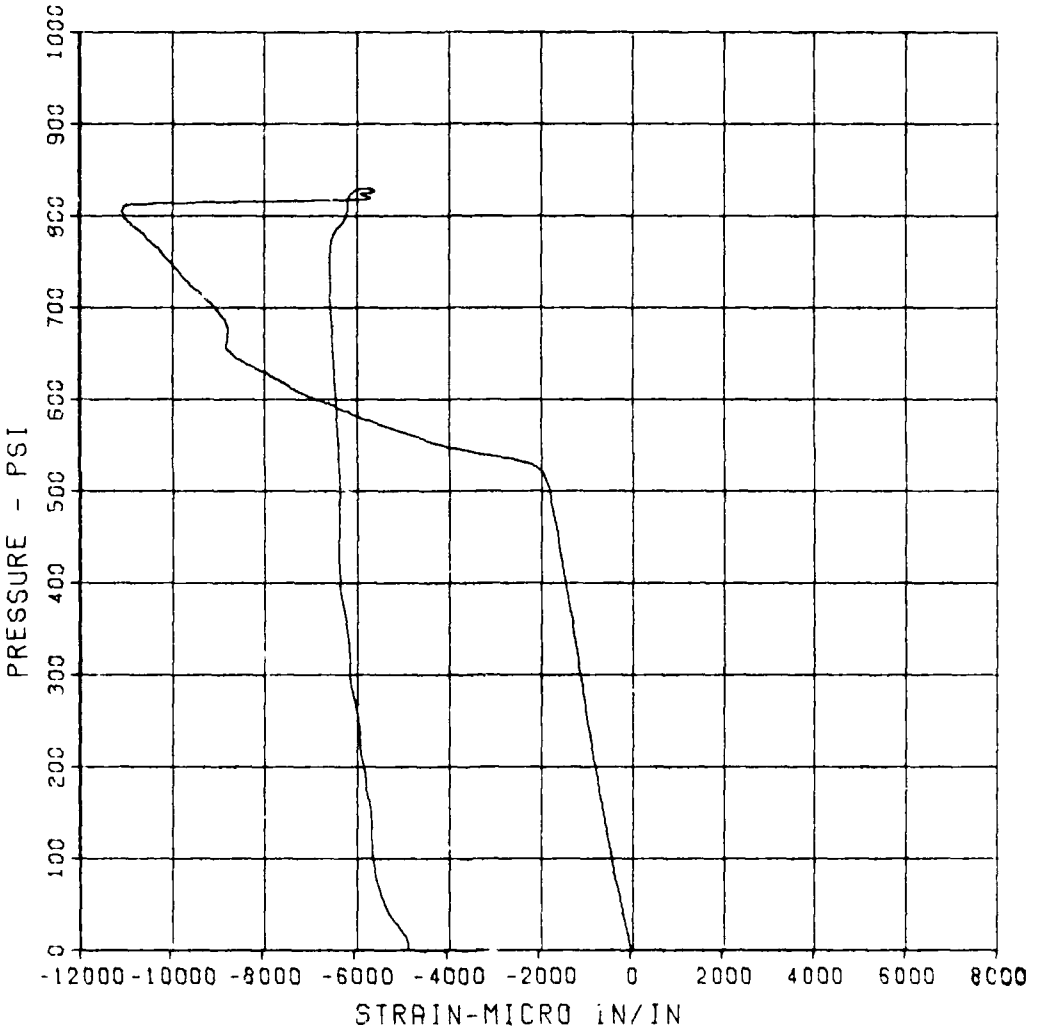

SBS ARCH TEST S-1A
EI-1

MAXIMUM	SIGMA CAL	CAL VAL
-532.7605	2.7338	11400.7

CHANNEL NO. 22 8835 1
09/19/86 R0906

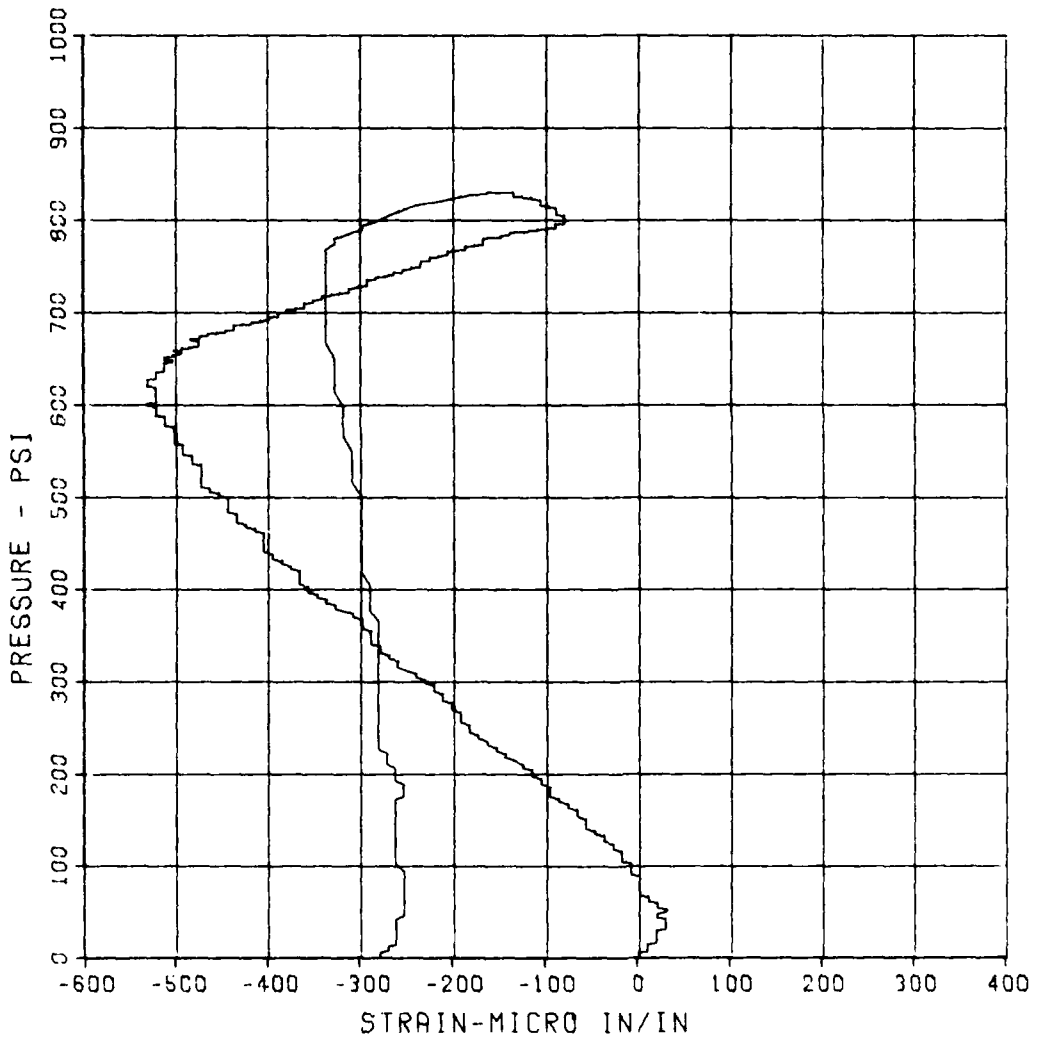

SBS ARCH TEST S-1A
E0-2

MAXIMUM	SIGMA CAL	CAL VAL
-10531.3216	3.2470	11400.7

CHANNEL NO. 23 8835 1
09/19/86 R0906

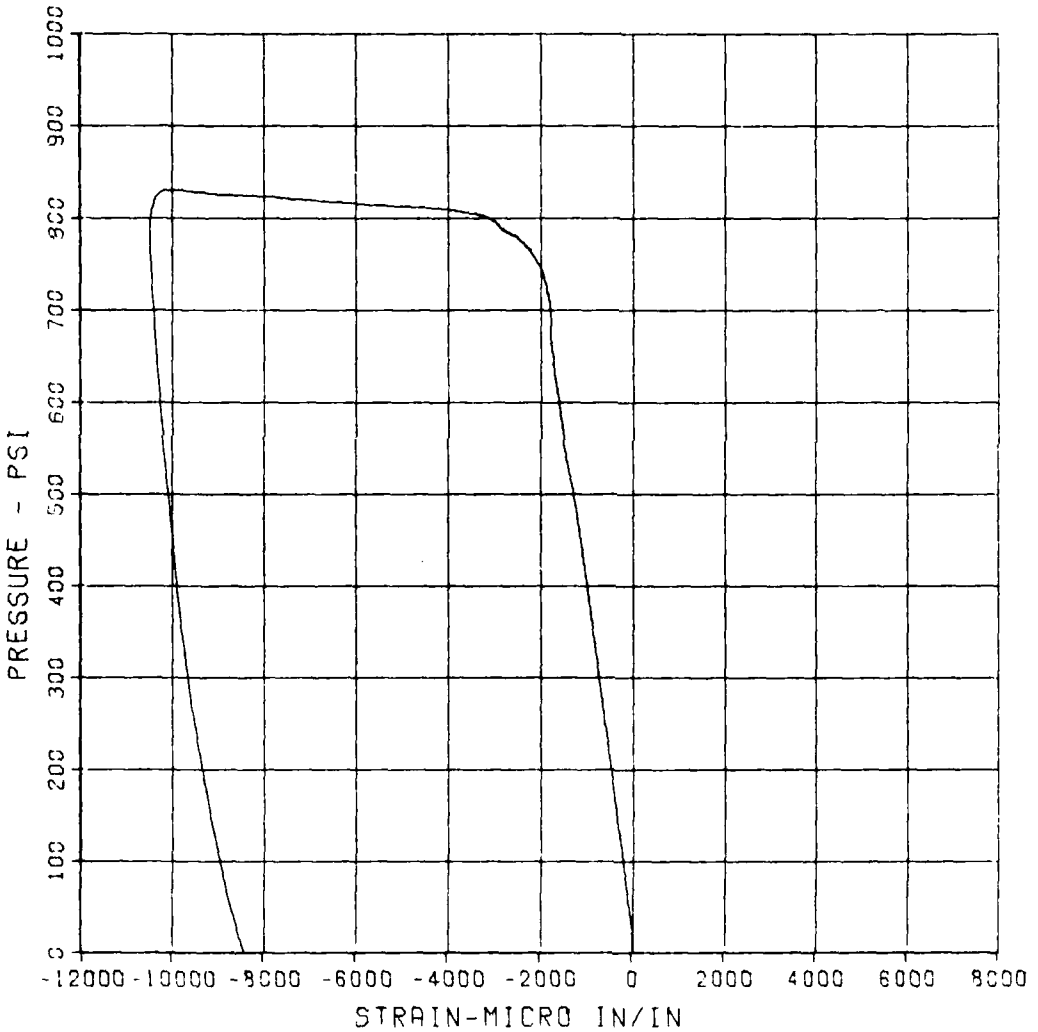

SBS ARCH TEST S-1A
EI-2

MAXIMUM	SIGMA CAL	CAL VAL
-14256.1248	2.9849	11400.7

CHANNEL NO. 24 9835 1
09/19/86 R0906

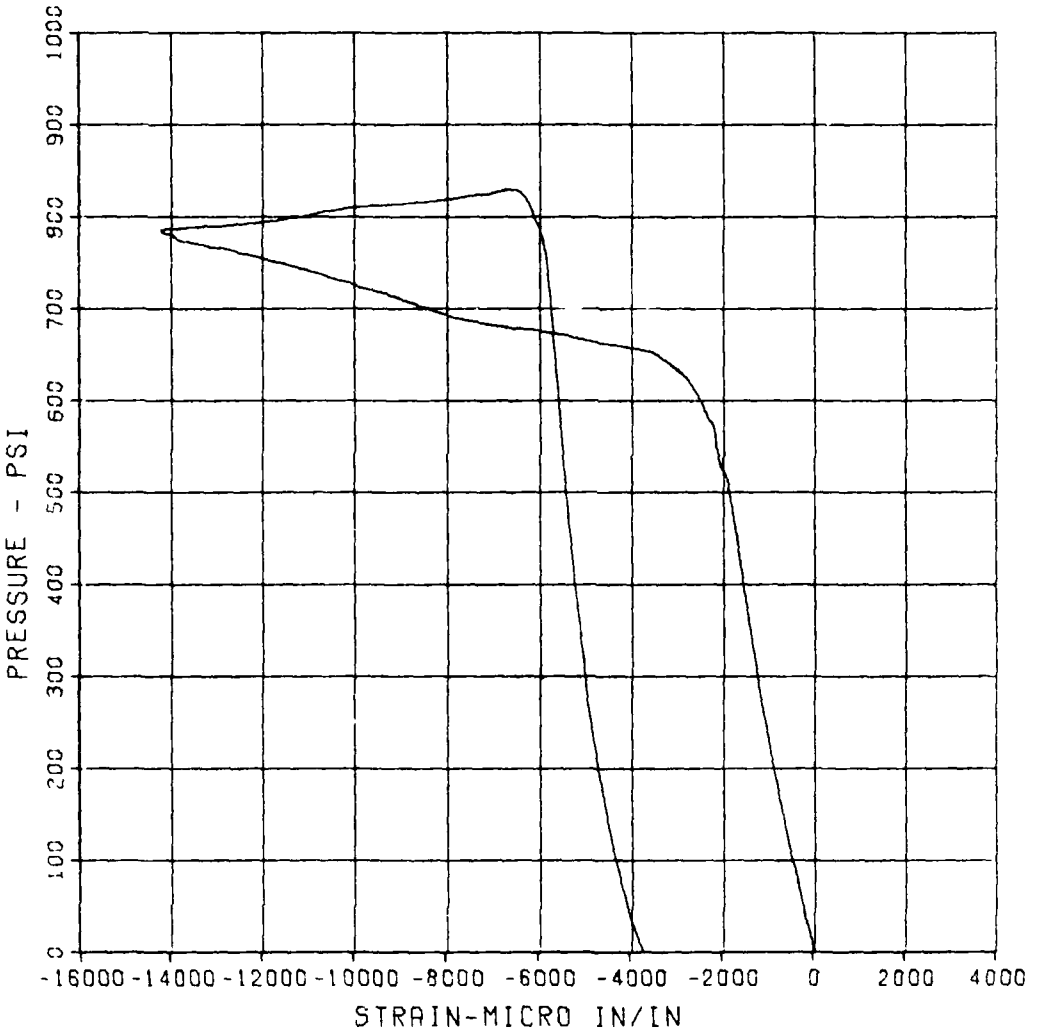

SBS ARCH TEST S-1A
E0-3

MAXIMUM	SIGMA CAL	CAL VAL
-7855.2741	2.3303	11400.7

CHANNEL NO. 25 8835 1
09/19/86 R0906

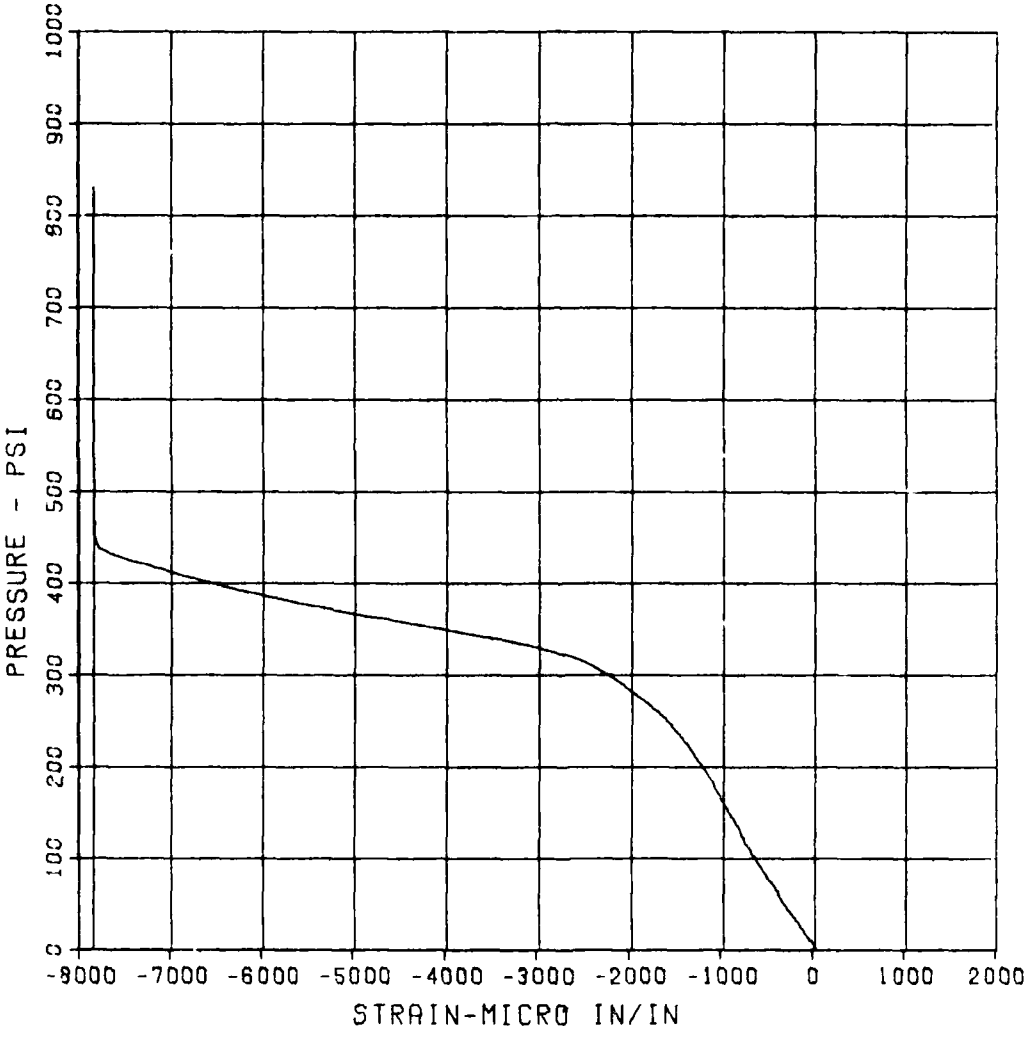

SBS ARCH TEST S-1A
EI-3

MAXIMUM	SIGMA CAL	CAL VAL
34089.4721	5.4392	11400.7

CHANNEL NO. 26 8835 1
09/19/86 R0906

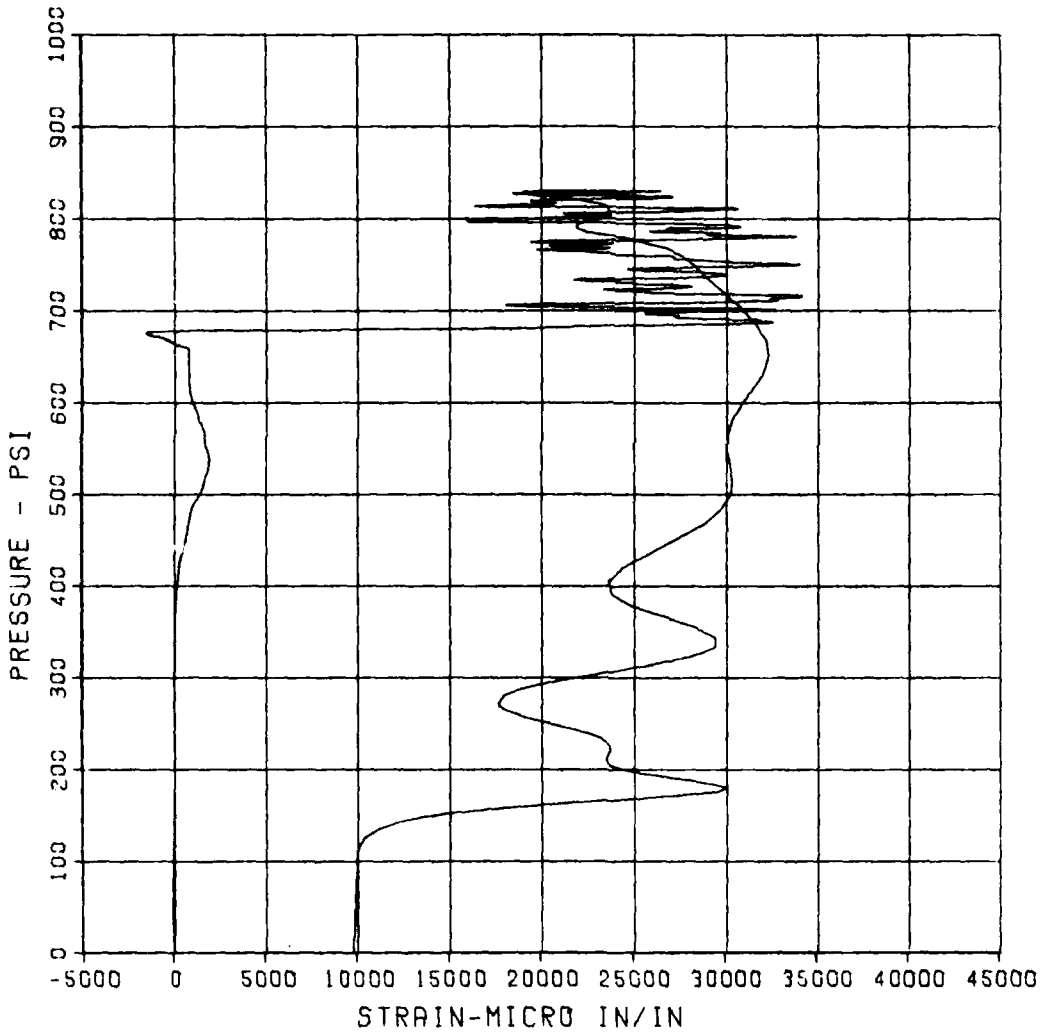

SBS ARCH TEST S-1A
EO-4

MAXIMUM	SIGMA CAL	CAL VAL
-13812.8342	0.9172	11400.7

CHANNEL NO. 27 8835 1
09/19/86 R0906

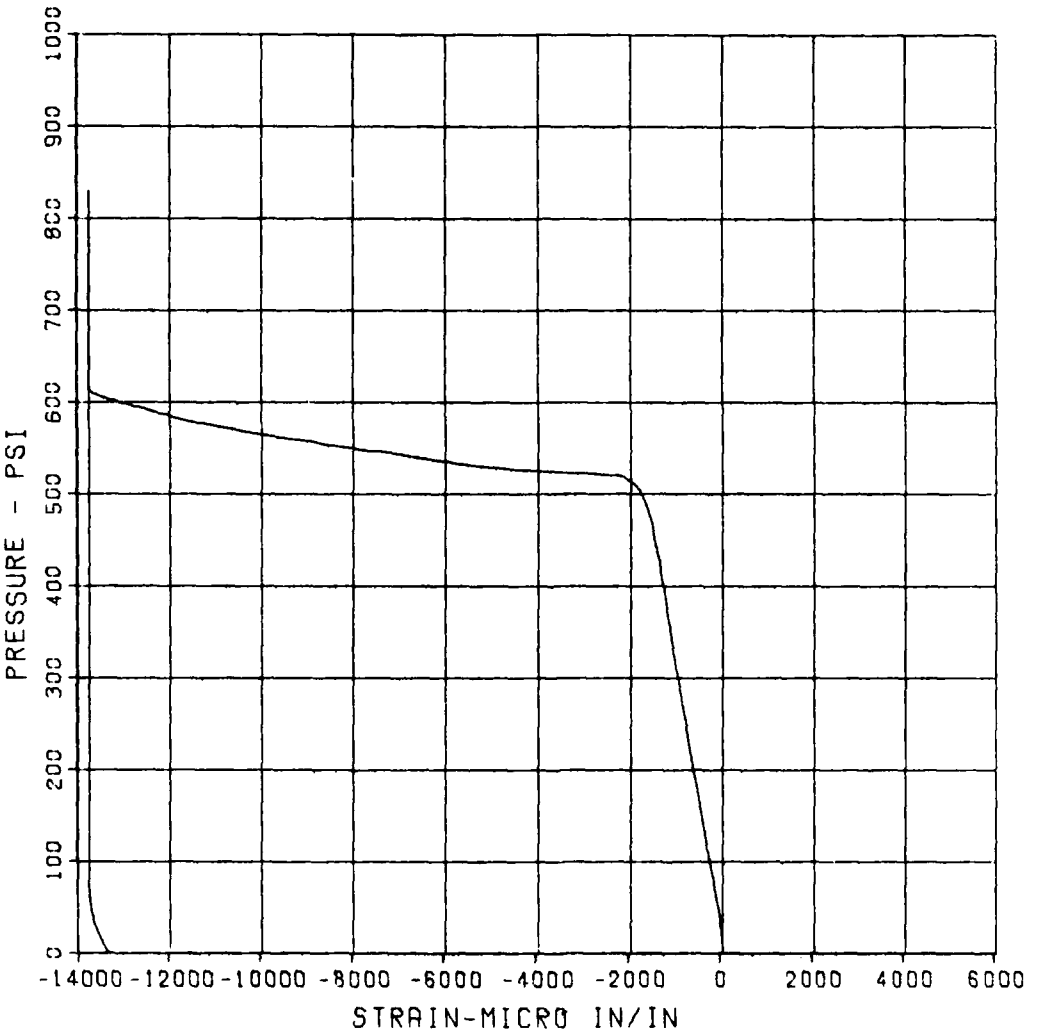

SBS ARCH TEST S-1A
EI-4A

MAXIMUM	SIGMA CAL	CAL VAL
-5206.2810	2.3969	11400.7

CHANNEL NO. 28 8835 1
09/19/86 R0906

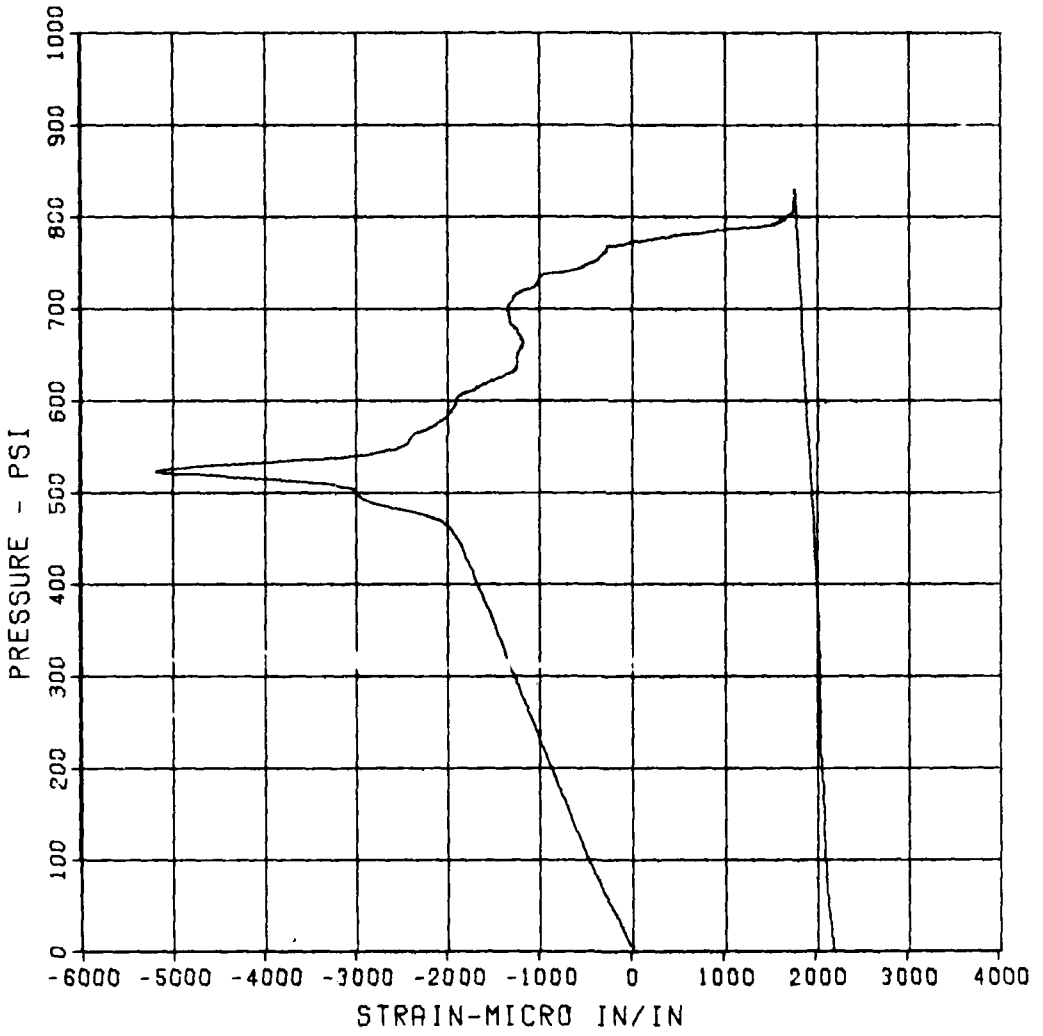

SBS ARCH TEST S-1A
D-1

MAXIMUM	SIGMA CAL	CAL VAL
2.0899	2.3266	10.8

CHANNEL NO. 29 8835 !
09/19/86 R0906

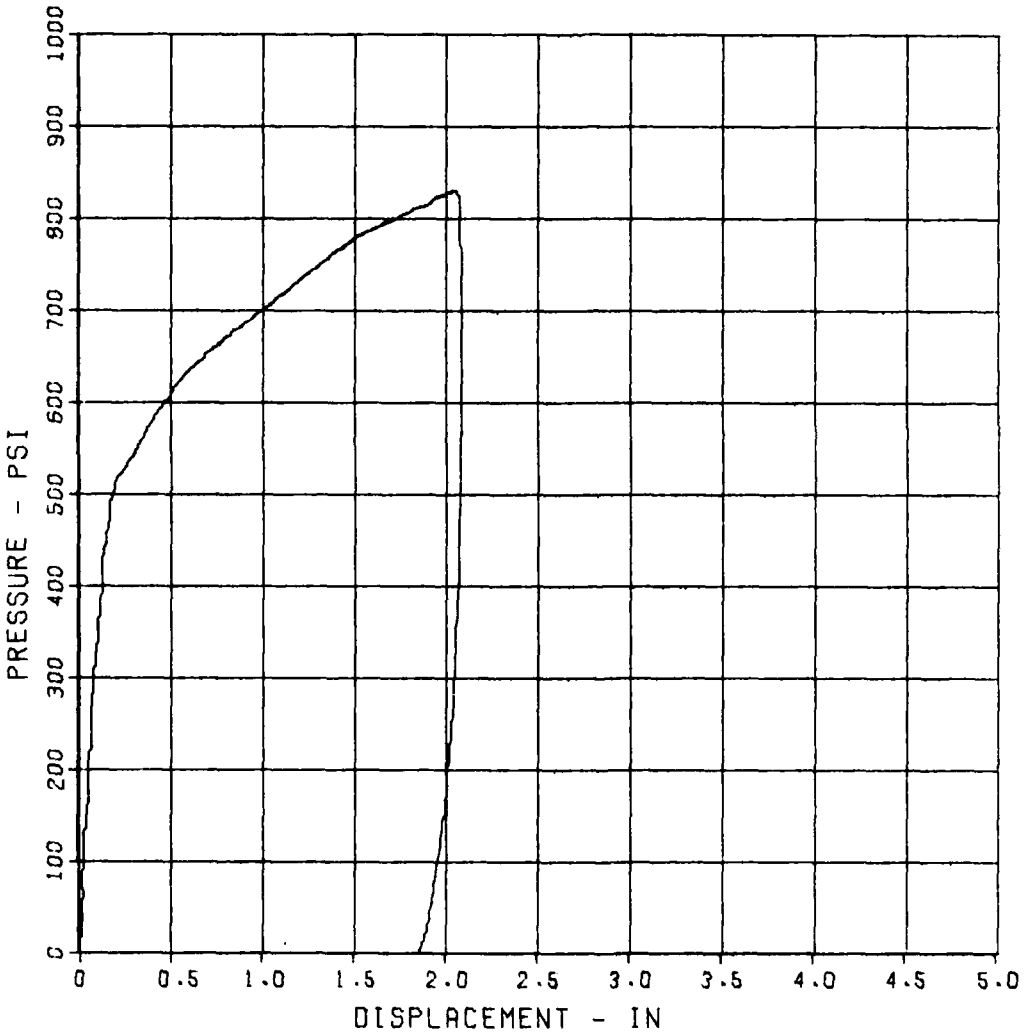

SBS ARCH TEST S-1A
D-2

MAXIMUM	SIGMA CAL	CAL VAL
0.7290	3.1770	2.1

CHANNEL NO. 30 8835 1
09/19/86 R0906

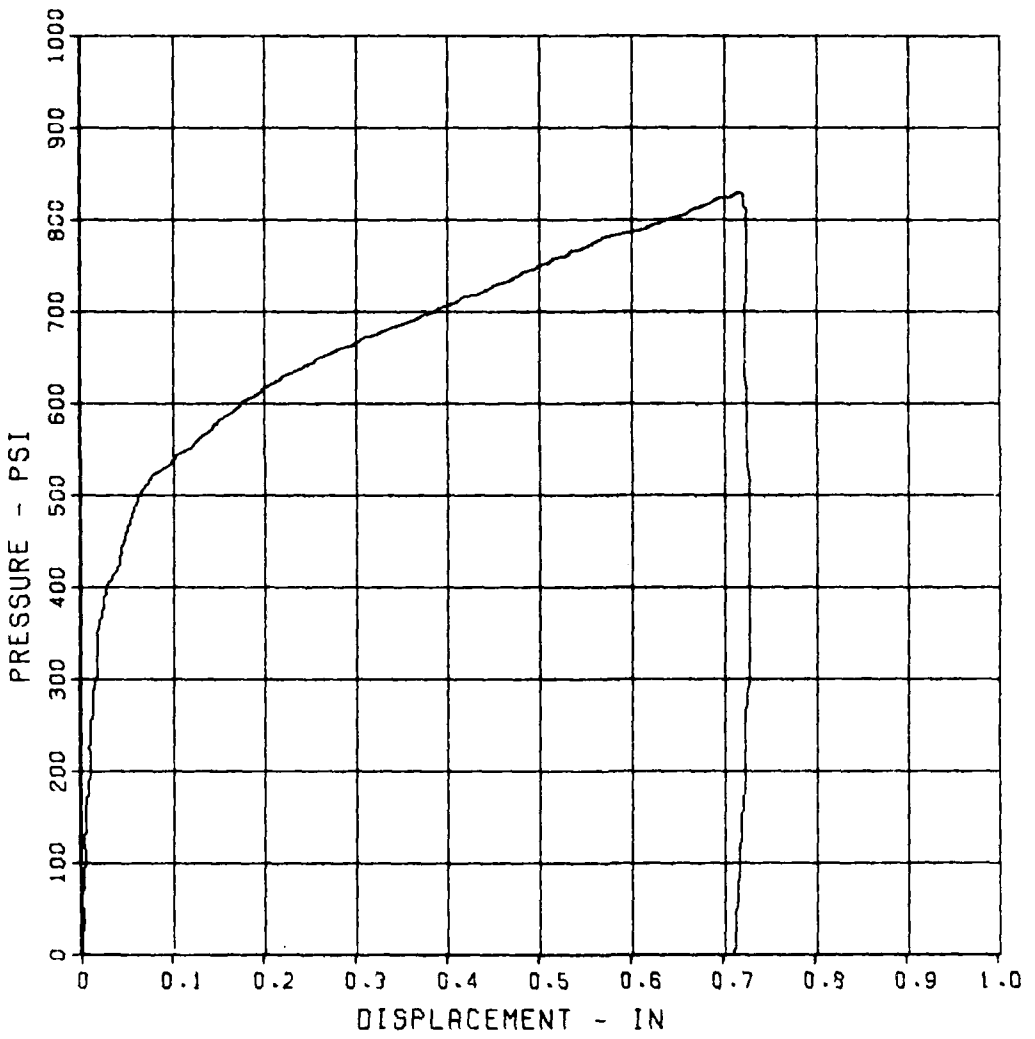

SBS ARCH TEST S-1B

SBS ARCH TEST S-1B
BP--1

MAXIMUM	SIGMA CAL	CAL VAL
707.2166	2.4118	1149.6

CHANNEL NO. 1 9806 1
09/19/86 R0911

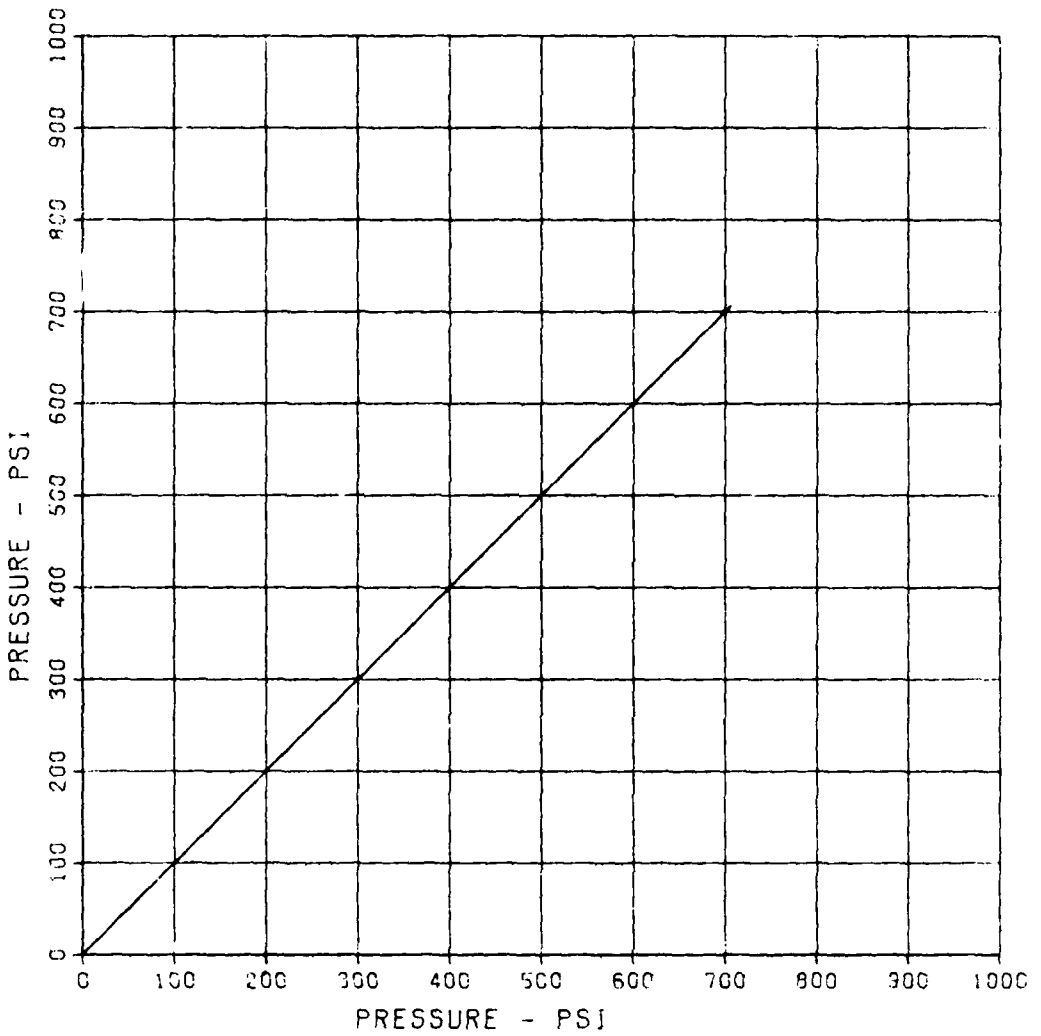

SBS ARCH TEST S-1B
BP-2

MAXIMUM	SIGMA CAL	CAL VAL
683.8442	2.7312	1110.3

CHANNEL NO. 2 9806 1
09/19/86 R0911

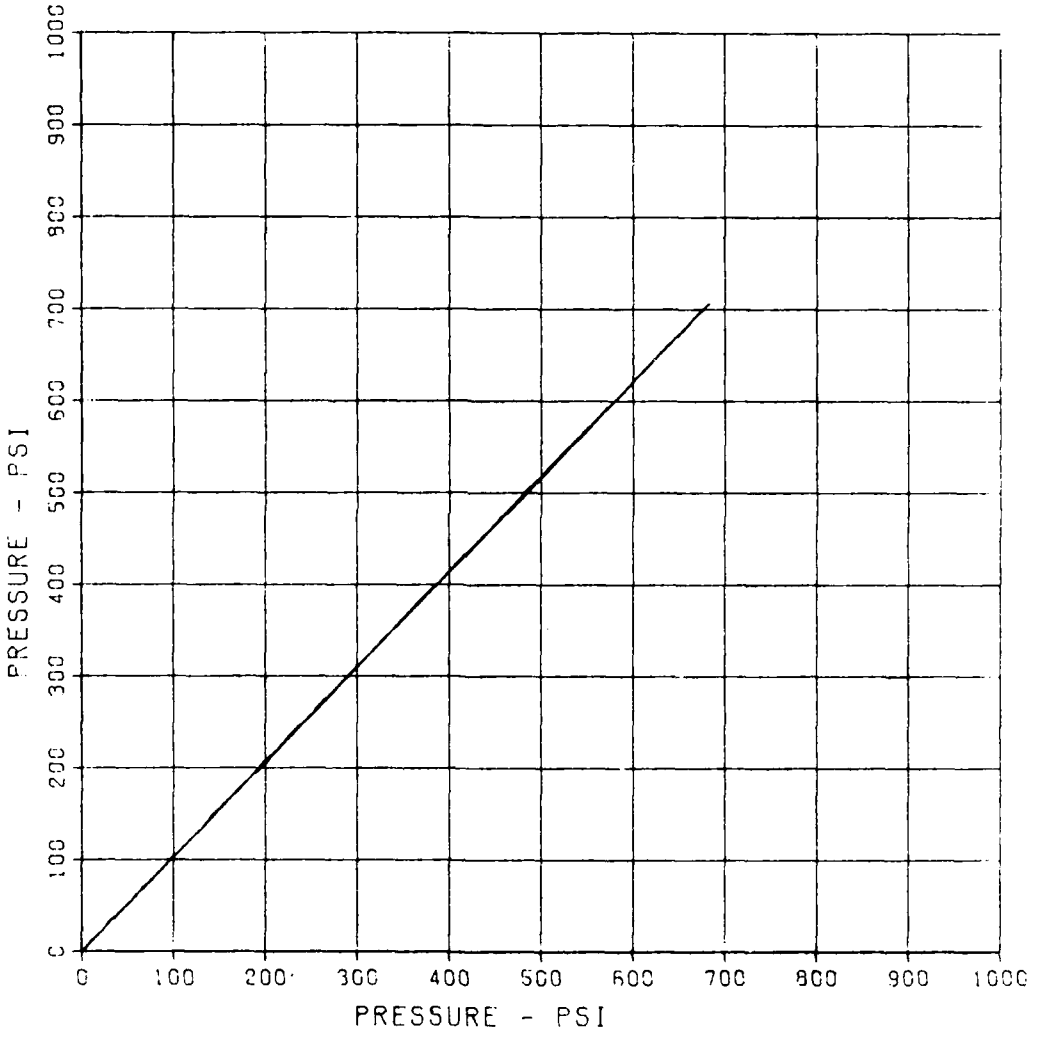

SBS ARCH TEST S-1B
IP-1

MAXIMUM	SIGMA CAL	CAL VAL
257.7481	3.0665	556.2

CHANNEL NO. 3 9806 1
09/19/86 R0911

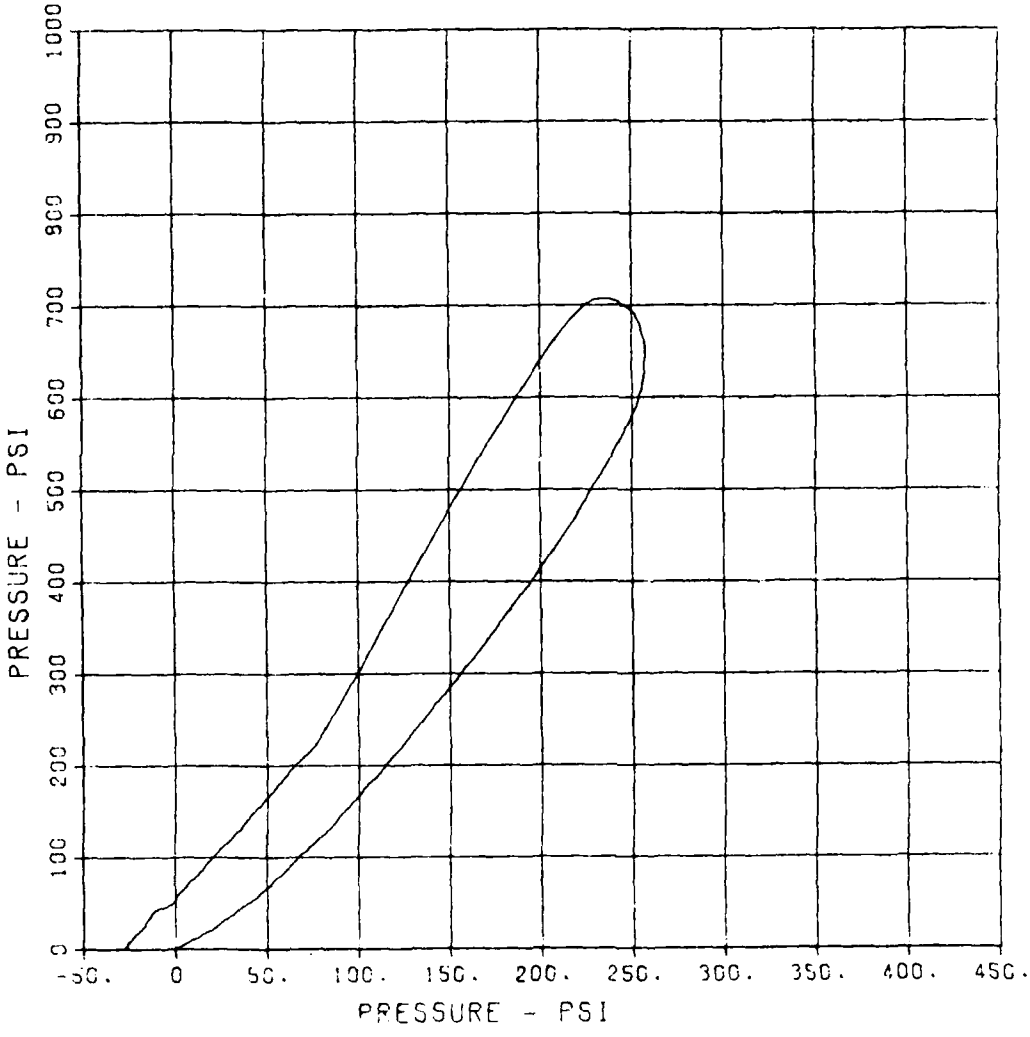

SBS ARCH TEST S-1B
IP-2

MAXIMUM	SIGMA CAL	CAL VAL
391.9967	3.3897	618.9

CHANNEL NO. 4 9806 1
09/19/86 R0911

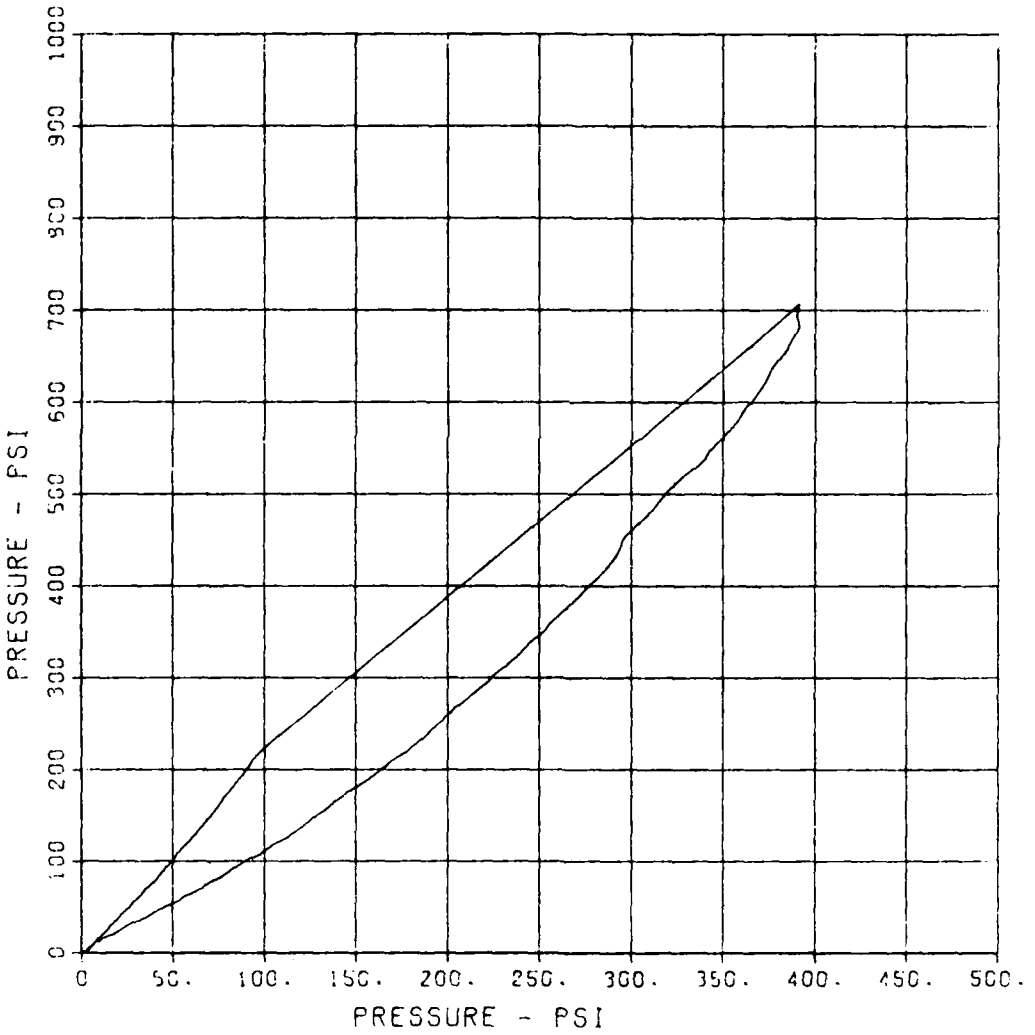

SBS ARCH TEST S-1B
IP-3

MAXIMUM	SIGMA CAL	CAL VAL
172.8930	2.8486	633.4

CHANNEL NO. 5 9806 1
09/19/86 R0911

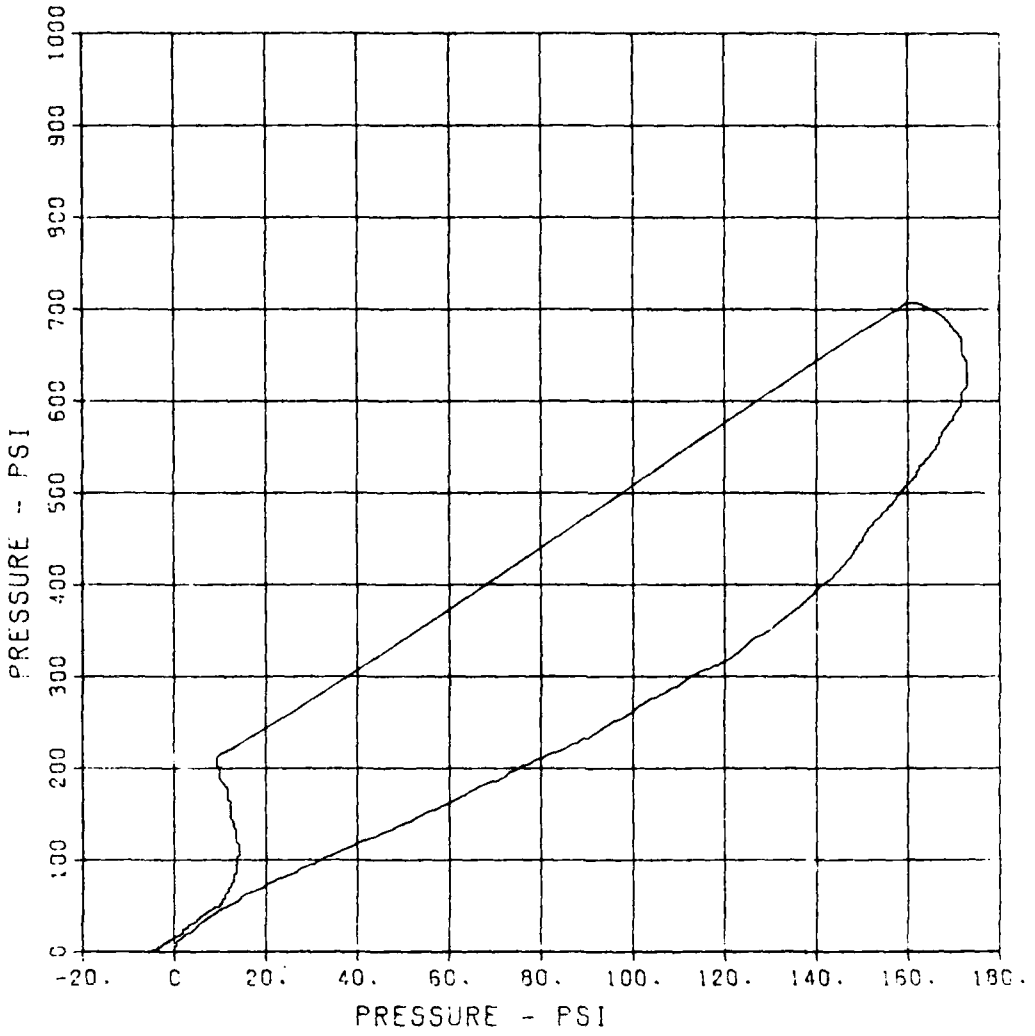

SBS ARCH TEST S-1B
IP-4

MAXIMUM	SIGMA CAL	CAL VAL
278.7640	3.2169	551.1

CHANNEL NO. 6 9806 1
09/19/86 RD911

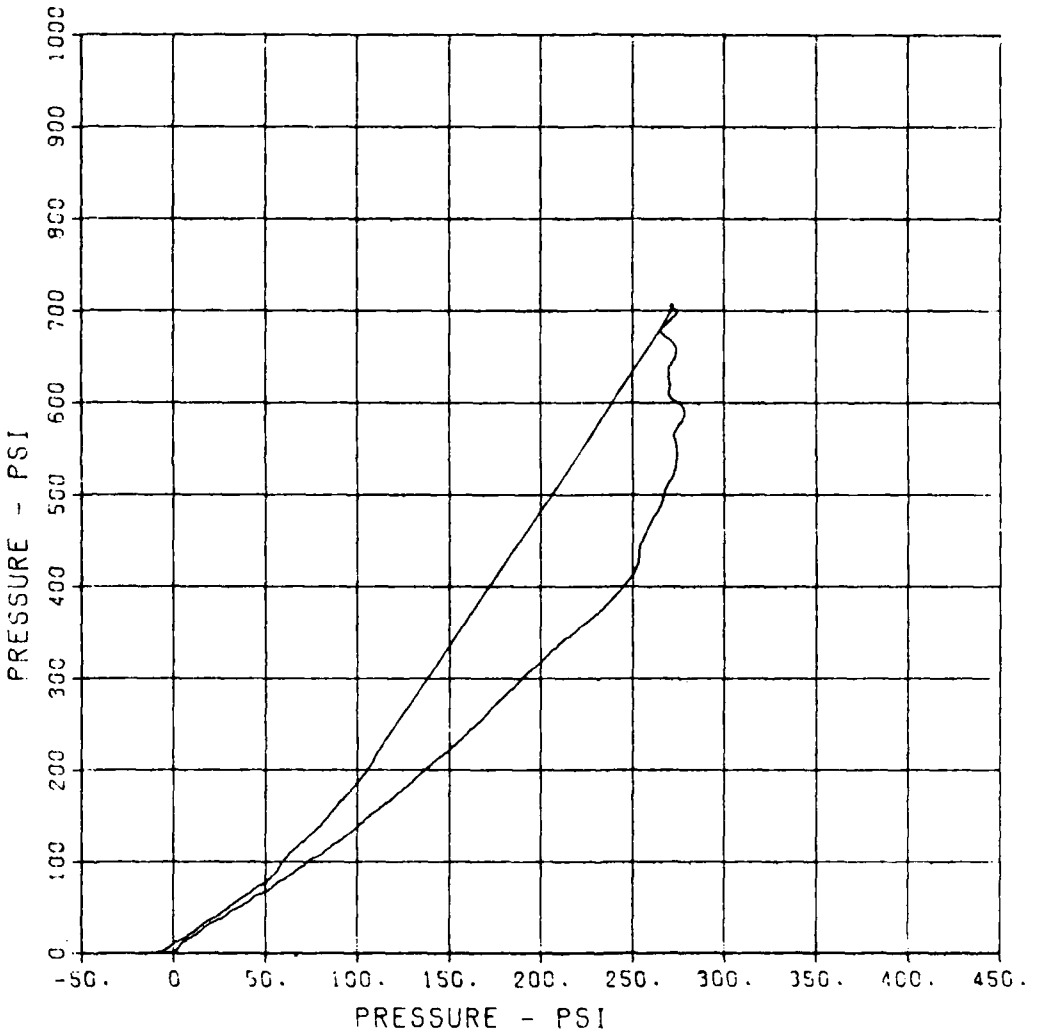

SBS ARCH TEST S-1B
IP-5

MAXIMUM	SIGMA CAL	CAL VAL
135.7837	2.5175	36.1

CHANNEL NO. 7 9806 1
09/19/86 RC911

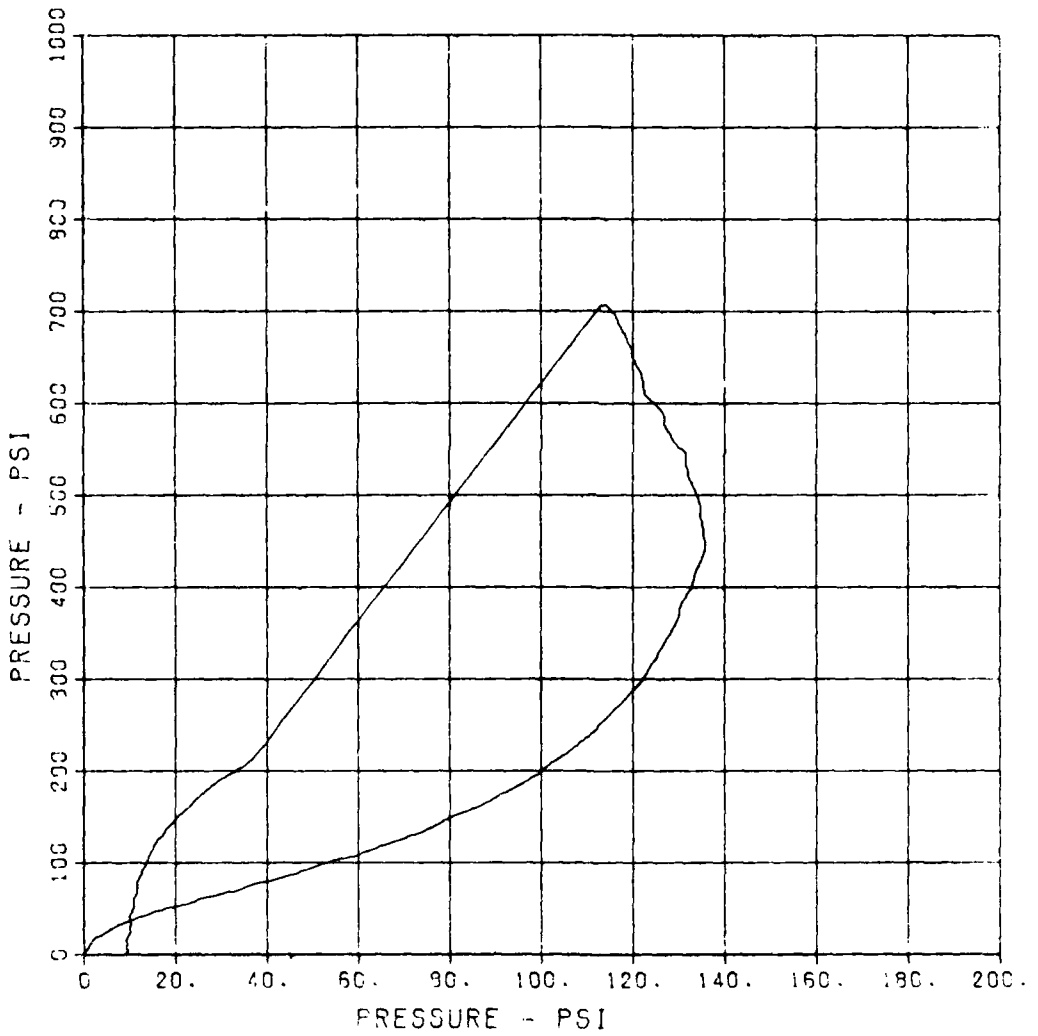

SBS ARCH TEST S-1B
IP--7

MAXIMUM	SIGMA CAL	CAL VAL
287.5289	2.6457	591.7

CHANNEL NO. 9 9806 1
09/19/86 R0911

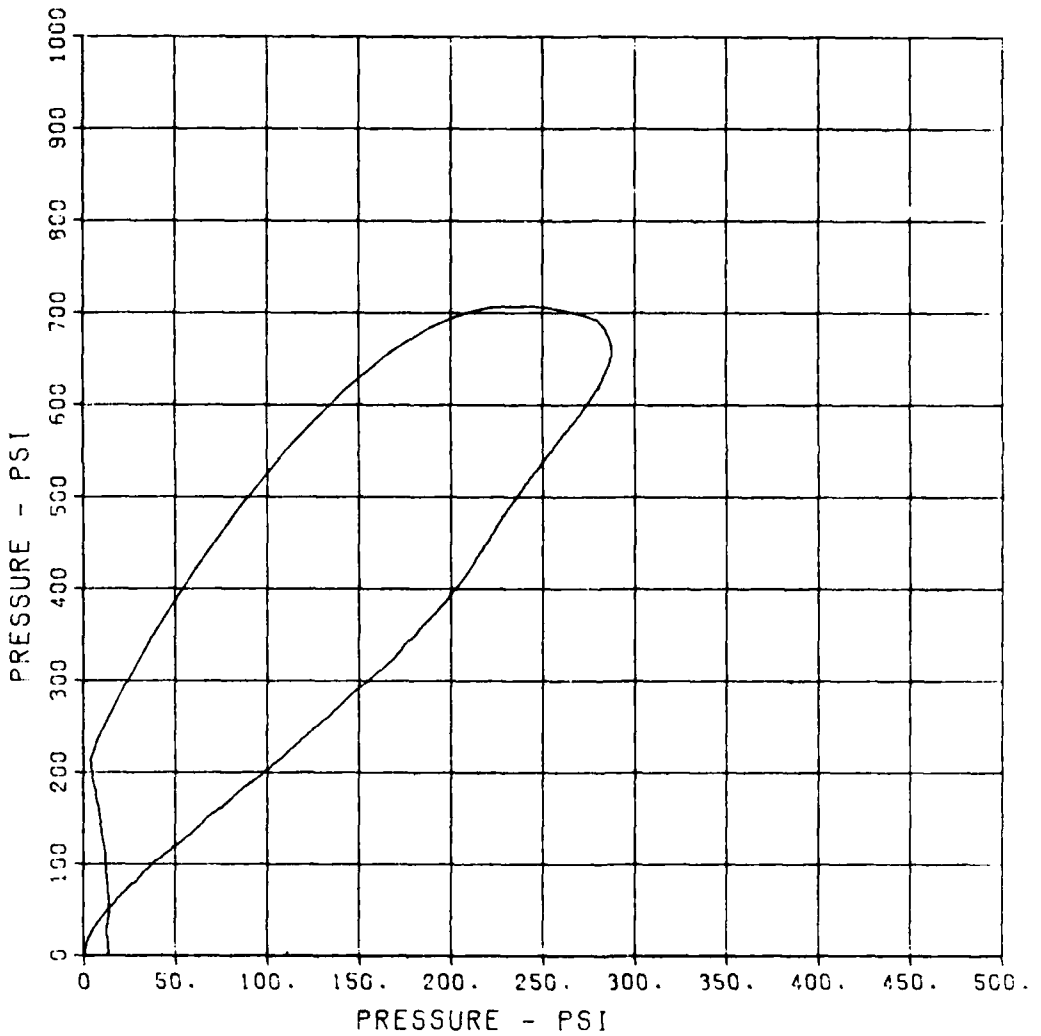

SBS ARCH TEST S-18
IP-8

MAXIMUM	SIGMA CAL	CAL VAL
96.3478	2.7865	397.0

CHANNEL NO. 10 9806 1
09/19/86 R0911

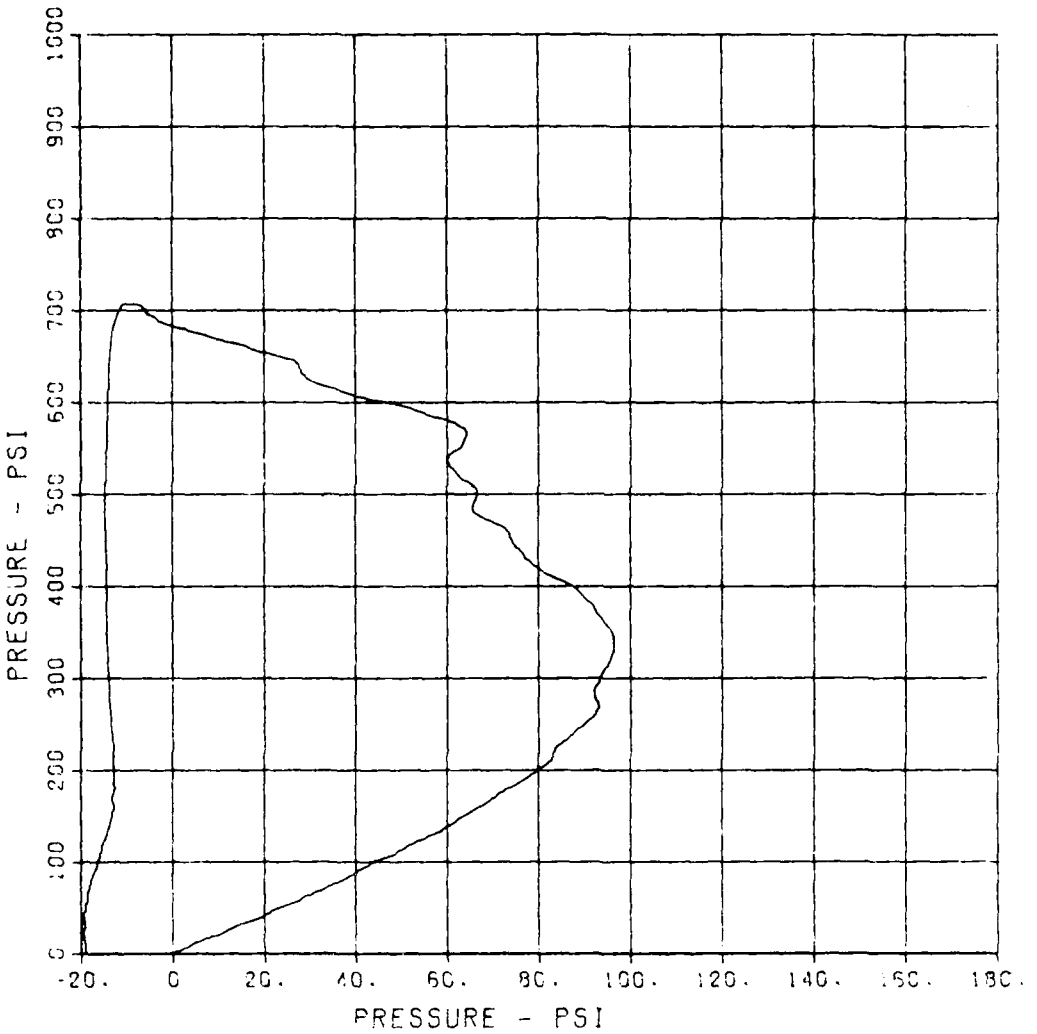

SBS ARCH TEST S-1B
IP-9

MAXIMUM	SIGMA CAL	CAL VAL
109.1744	2.4862	370.4

CHANNEL NO. 11 9806 1
09/19/86 R0911

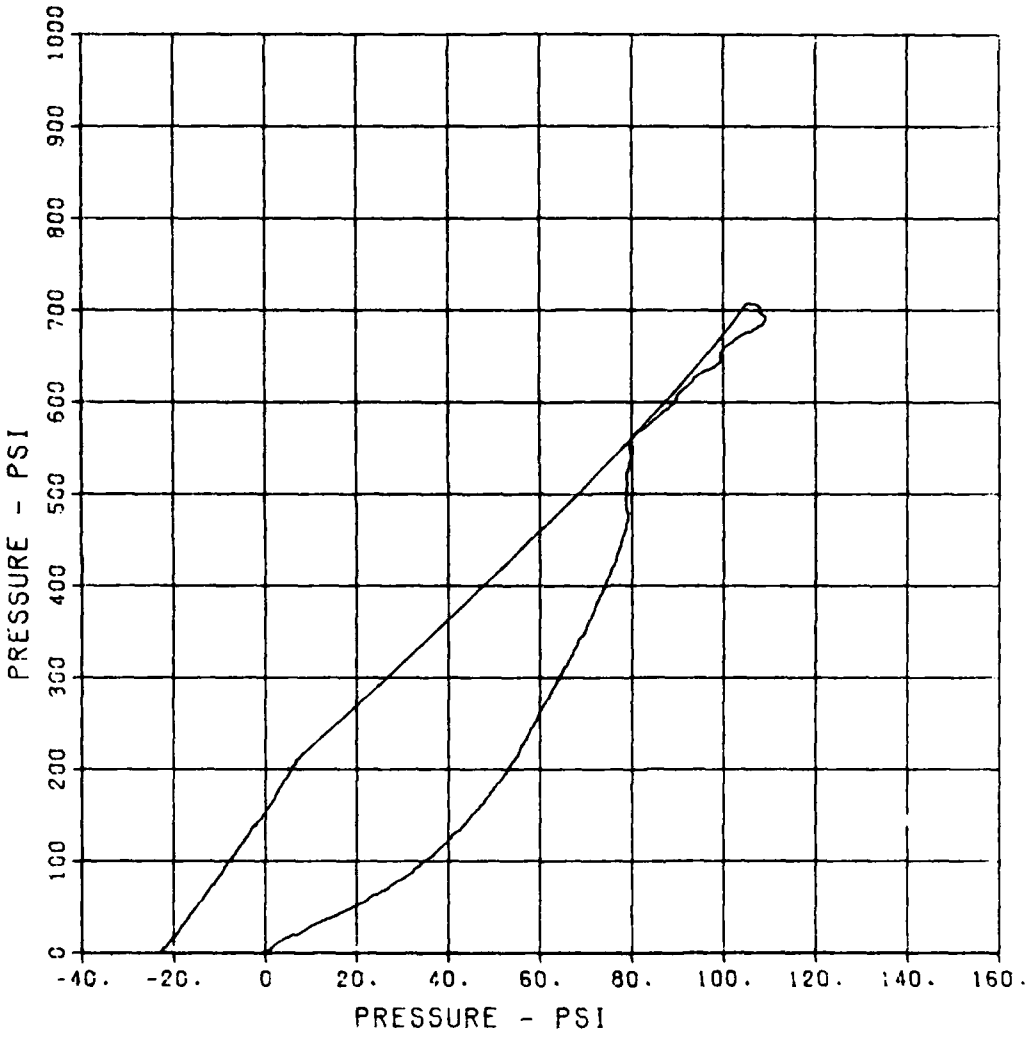

SBS ARCH TEST S-1B
SE-1

MAXIMUM	SIGMA CAL	CAL VAL
571.4983	2.8790	690.8

CHANNEL NO. 12 9806 1
09/19/86 R0911

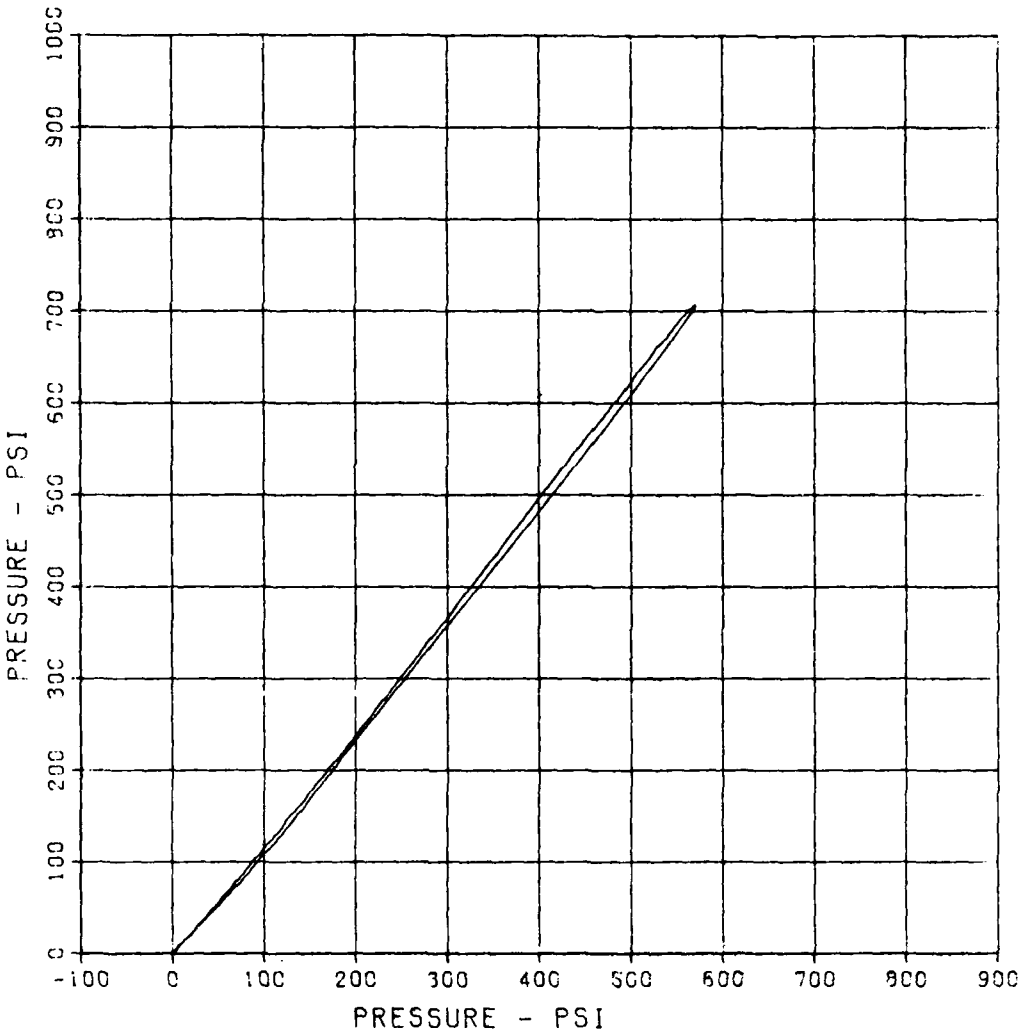

SBS ARCH TEST S-1B
SE-2

MAXIMUM	SIGMA CAL	CAL VAL
791.5150	2.9744	486.5

CHANNEL NO. 13 9806 1
09/19/86 R0911

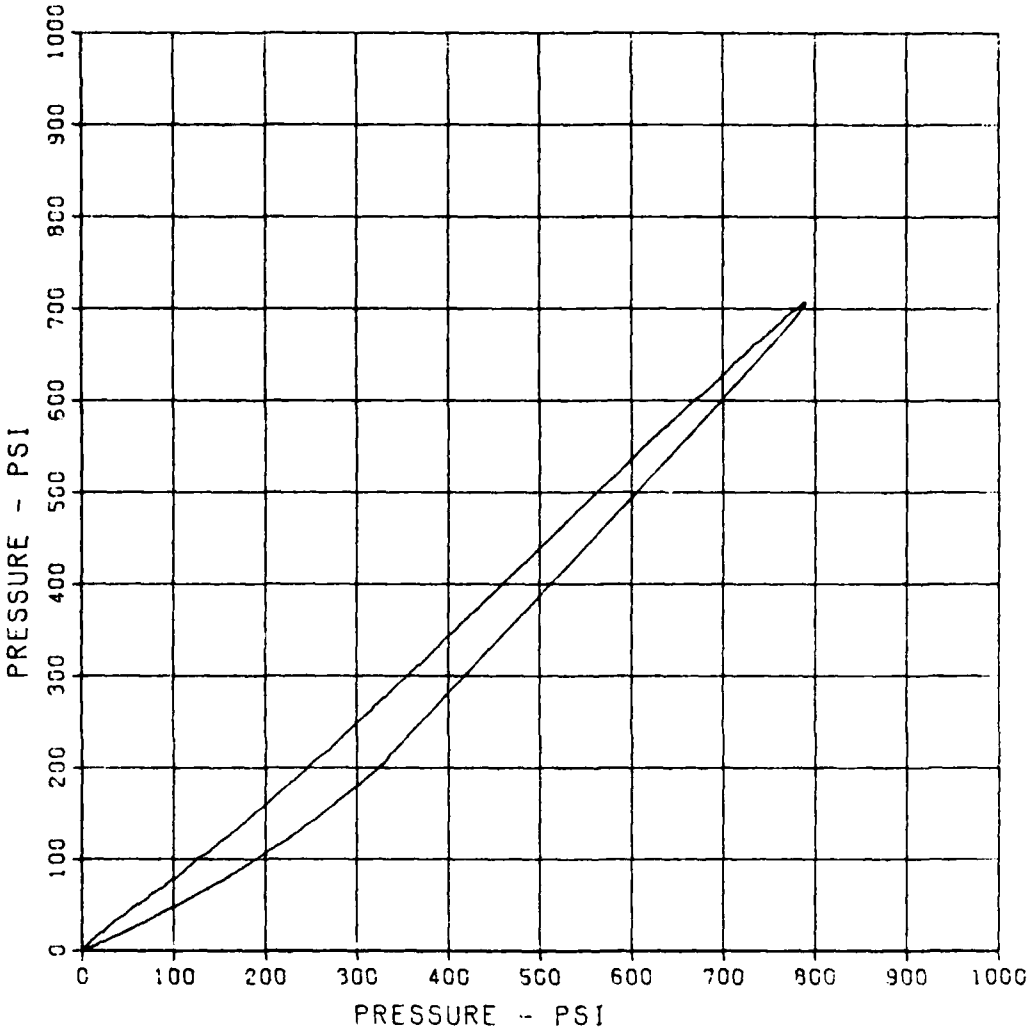

SBS ARCH TEST S-1B
SE-3

MAXIMUM	SIGMA CAL	CAL VAL
663.3381	3.4724	512.3

CHANNEL NO. 14 9806 1
09/19/86 R0911

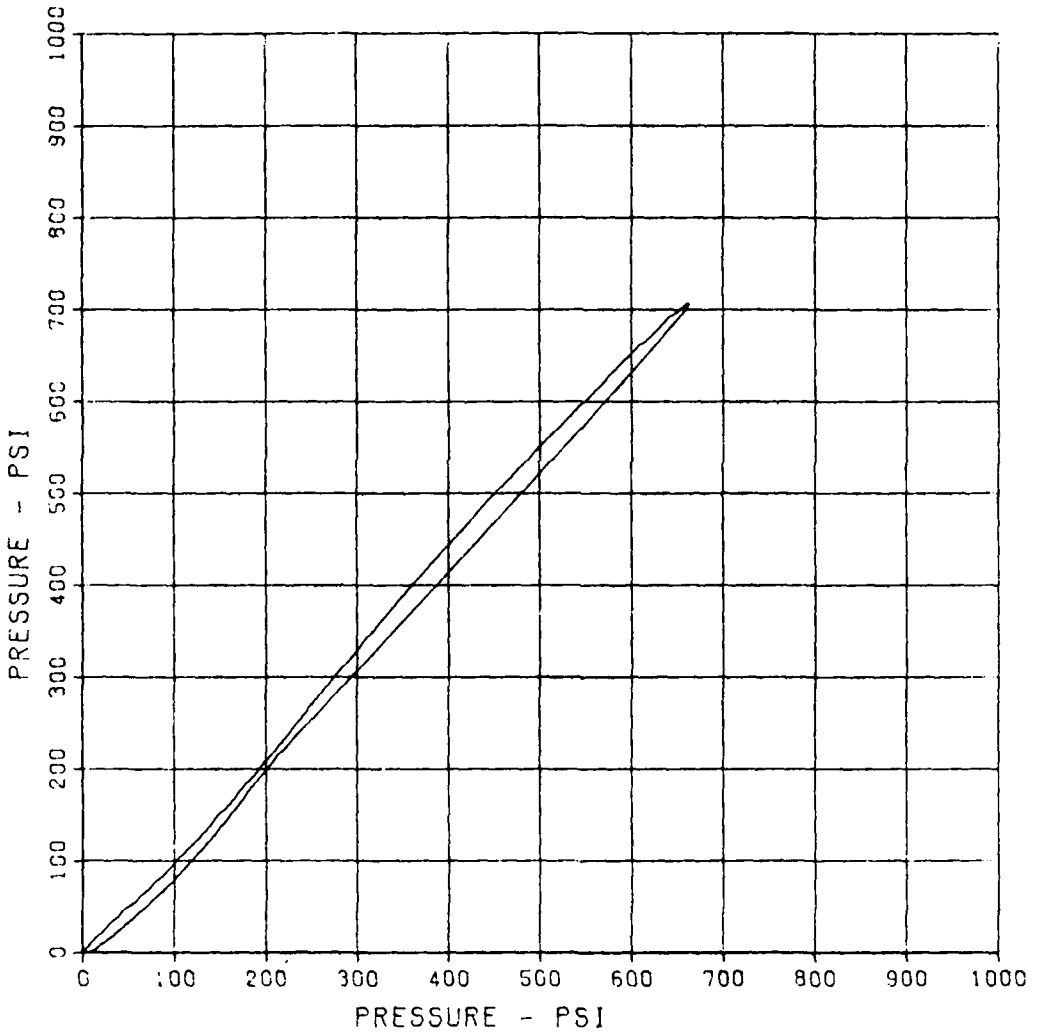

SBS ARCH TEST S-1B
SE-4

MAXIMUM	SIGMA CAL	CAL VAL
710.9305	3.6514	497.9

CHANNEL NO. 15 9806 1
09/19/86 R0911

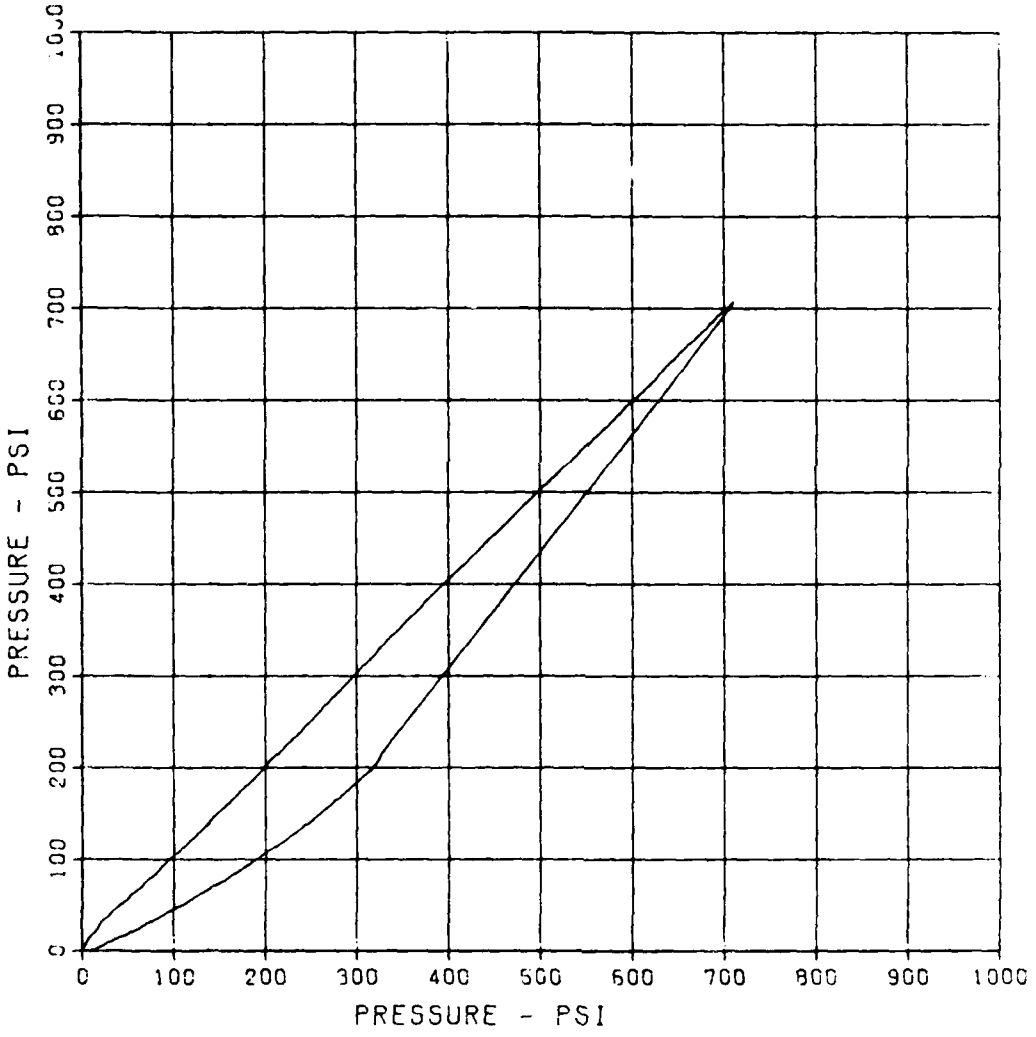

SBS ARCH TEST S-1B
SE-6

MAXIMUM	SIGMA CAL	CAL VAL
486.6146	3.0668	535.9

CHANNEL NO. 17 3806 1
09/19/86 R0911

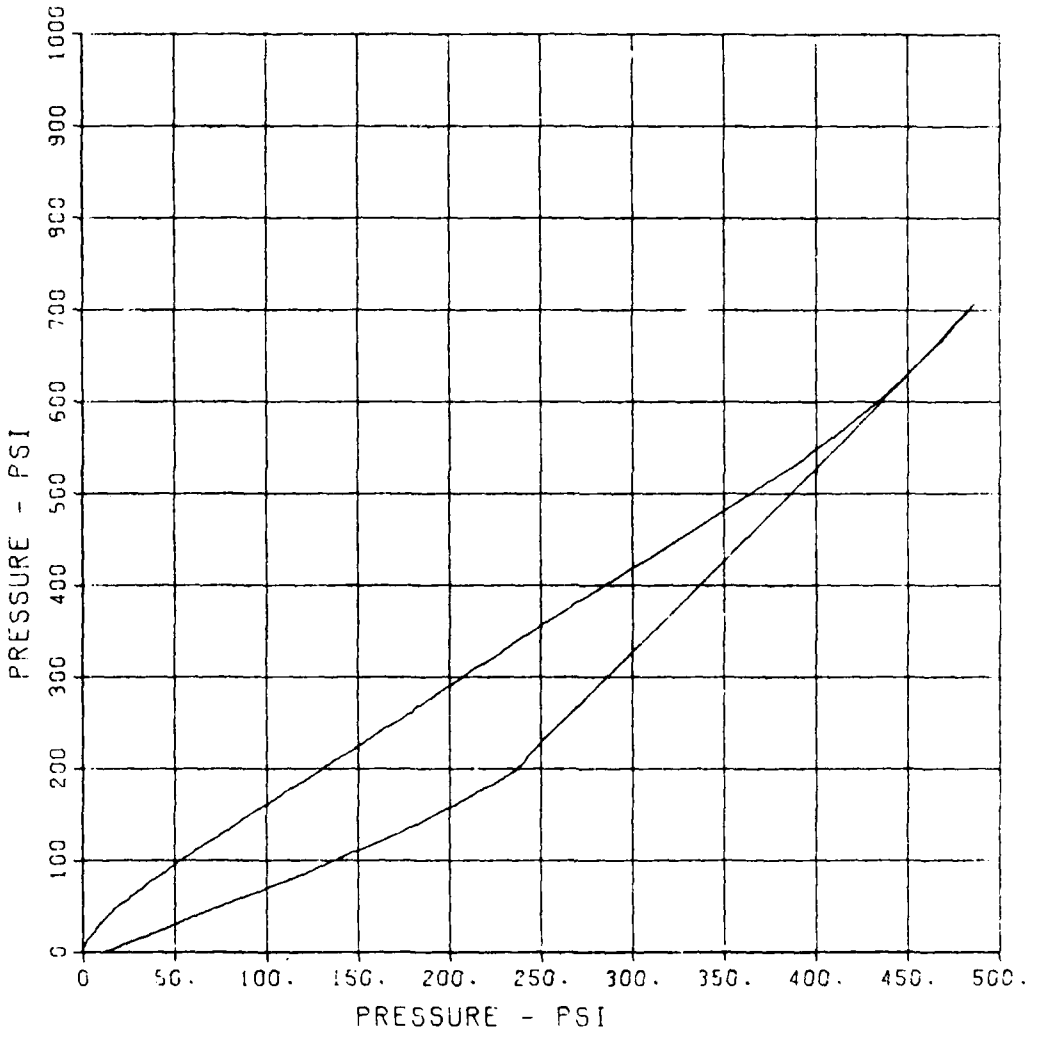

SBS ARCH TEST S-1B
SE-7

MAXIMUM	SIGMA CAL	CAL VAL
76.9537	3.1013	594.9

CHANNEL NO. 18 9806 1
09/19/86 R0911

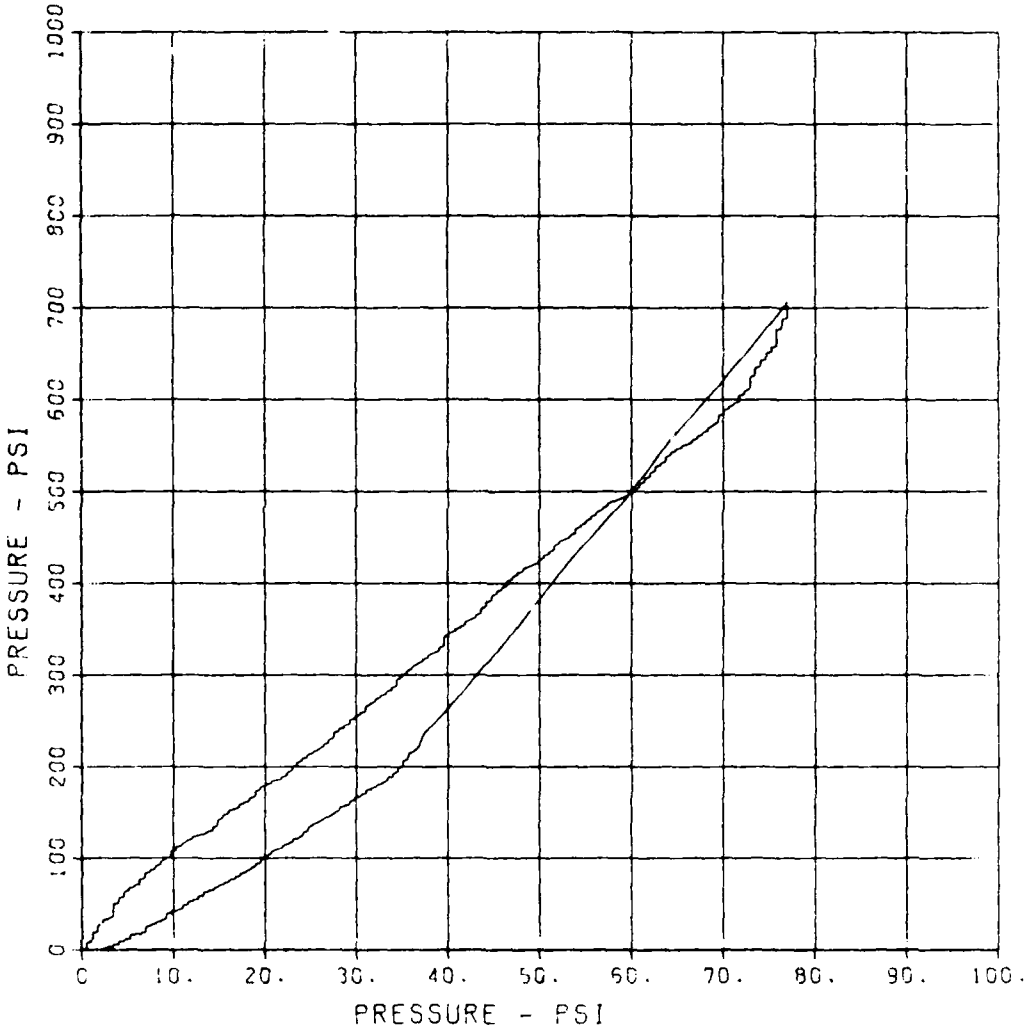

SBS ARCH TEST S-1B
SE-8

MAXIMUM	SIGMA CAL	CAL VAL
714.8446	3.3188	484.5

CHANNEL NO. 19 9806 1
09/19/86 R0911

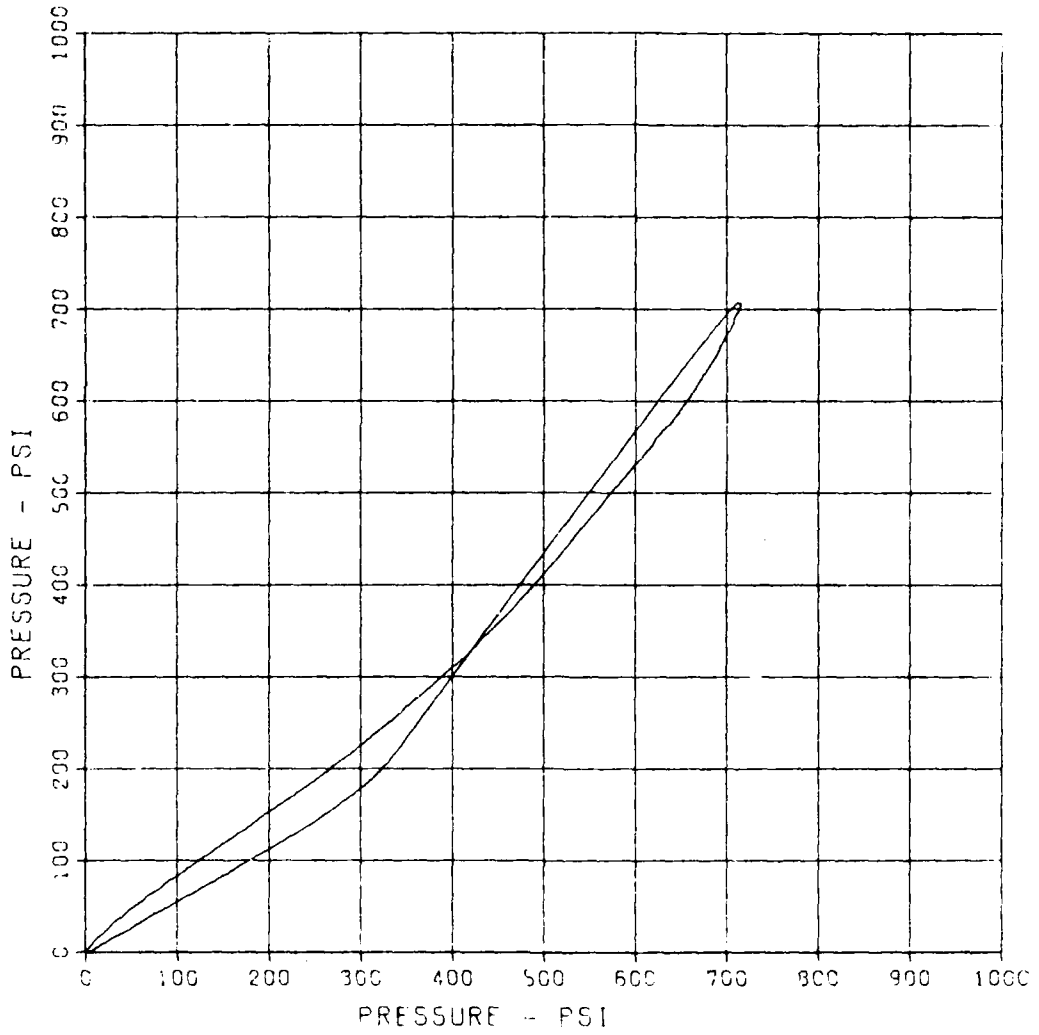

SBS ARCH TEST S-1B
SE-9

MAXIMUM	SIGMA CAL	CAL VAL
469.7971	3.2114	609.9

CHANNEL NO. 20 9806 1
09/19/86 R0911

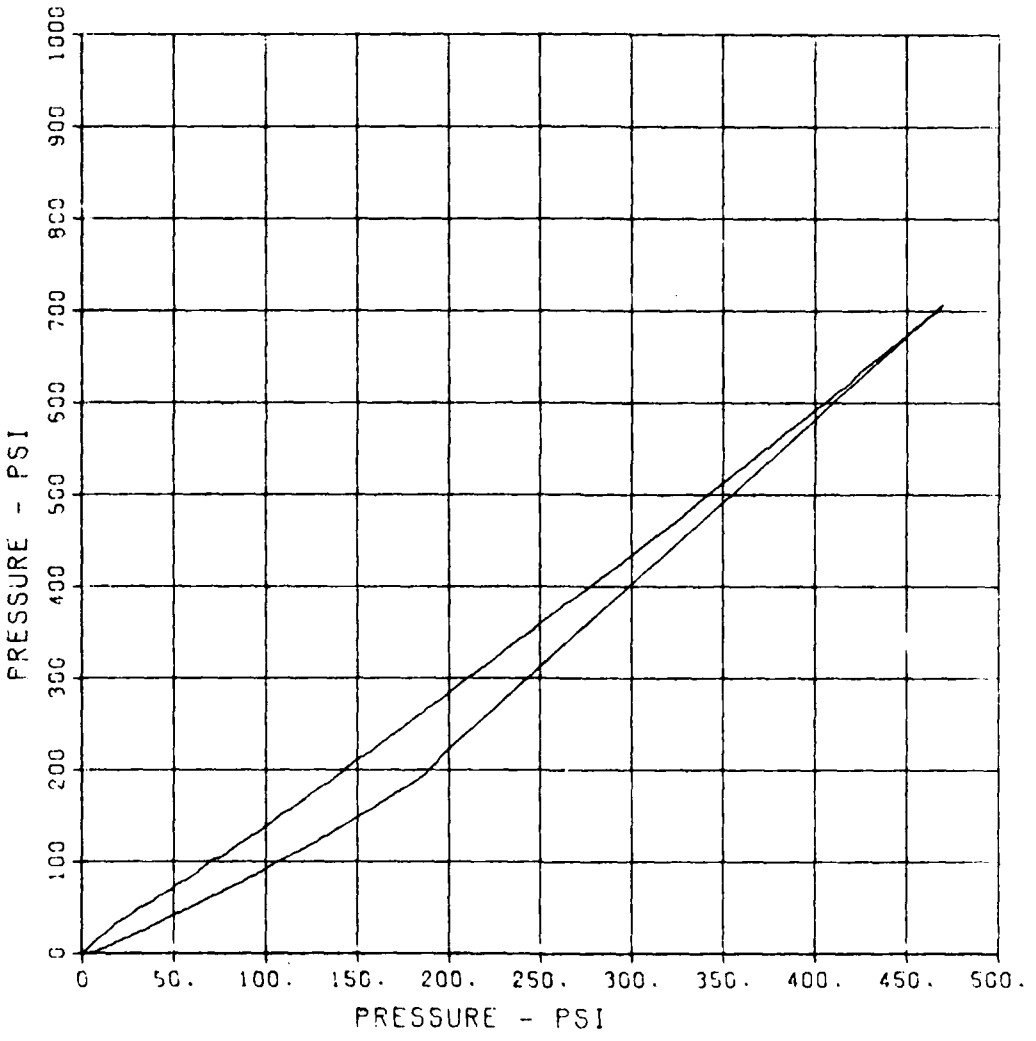

SBS ARCH TEST S-1B
E0-1

MAXIMUM	SIGMA CAL	CAL VAL
-2725.7813	2.5873	11400.7

CHANNEL NO. 21 9906 1
09/19/86 R0911

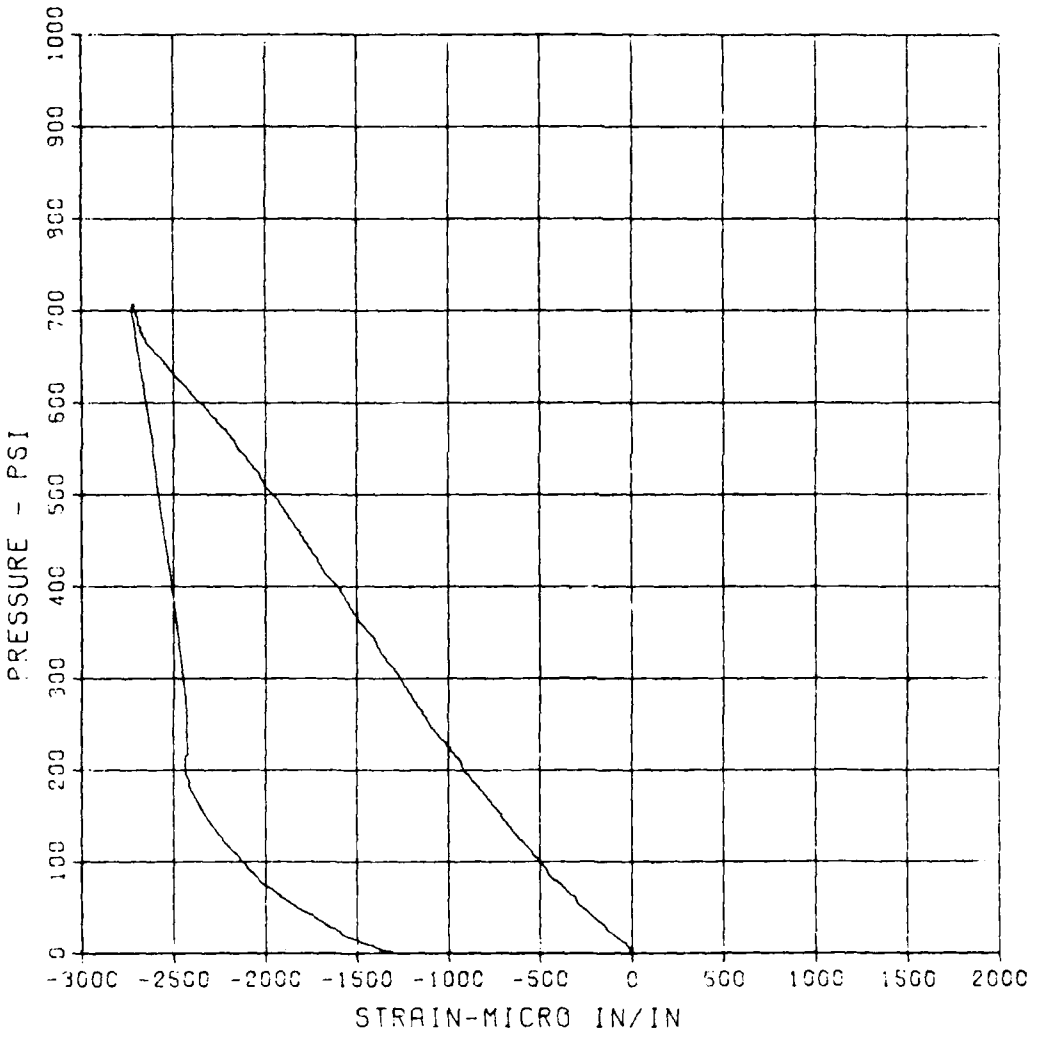

SBS ARCH TEST S-1B
EI-1

MAXIMUM	SIGMA CAL	CAL VAL
1394.8637	2.7338	11400.7

CHANNEL NO. 22 9806 1
09/19/86 R0911

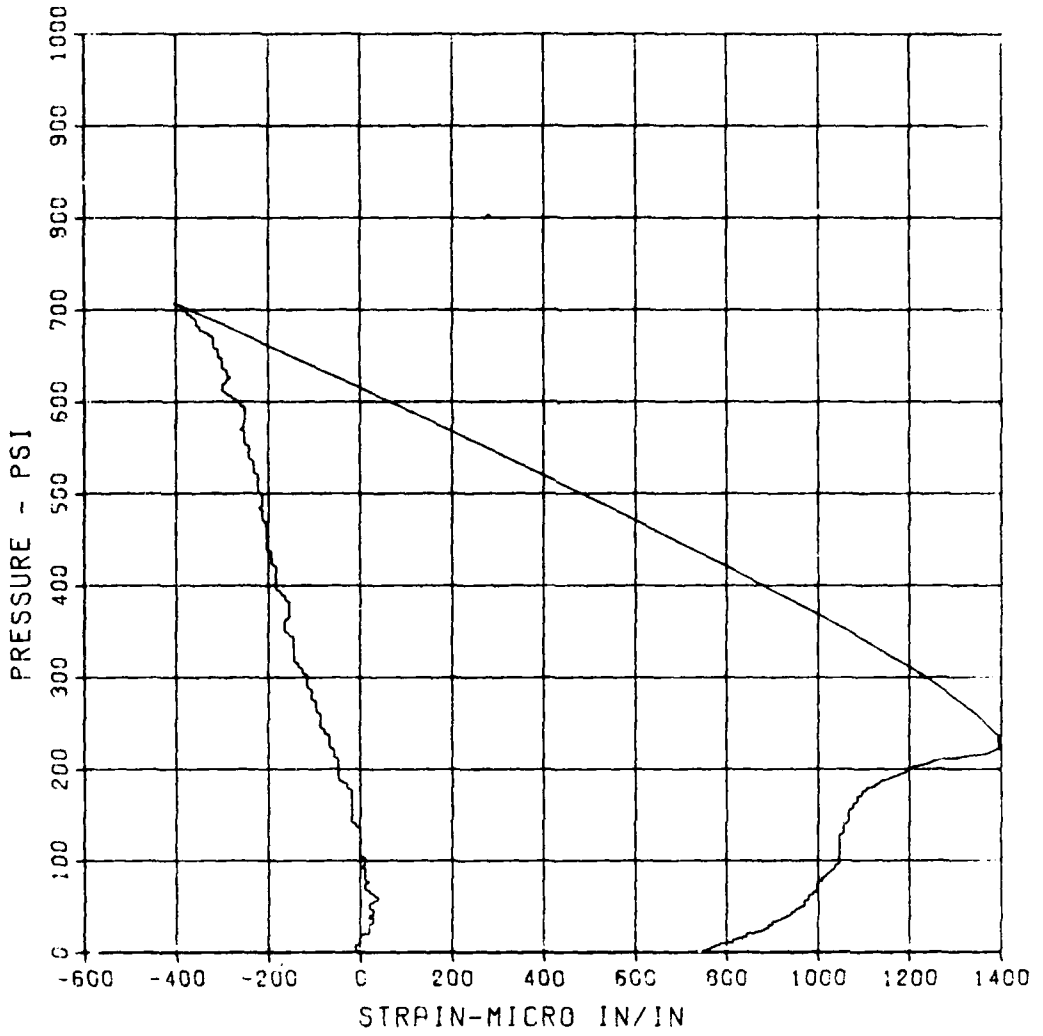

SBS ARCH TEST S-1B
E0-2

MAXIMUM	SIGMA CAL	CAL VAL
-7188.9867	3.2470	11400.7

CHANNEL NO. 23 9806 1
09/19/86 R0911

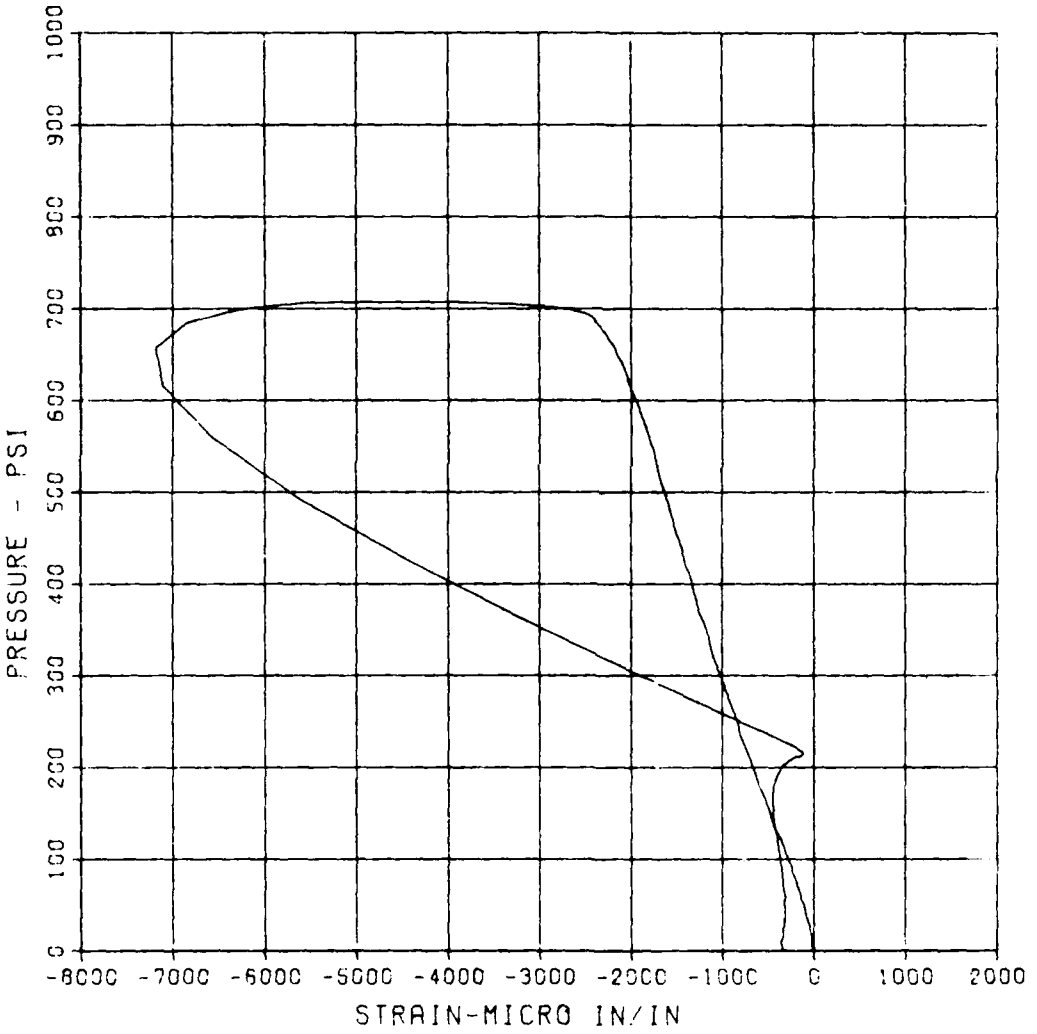

SBS ARCH TEST S-1B
EI-2

MAXIMUM	SIGMA CAL	CAL VAL
780.0327	2.9849	11400.7

CHANNEL NO. 24 9806 1
09/19/86 R0911

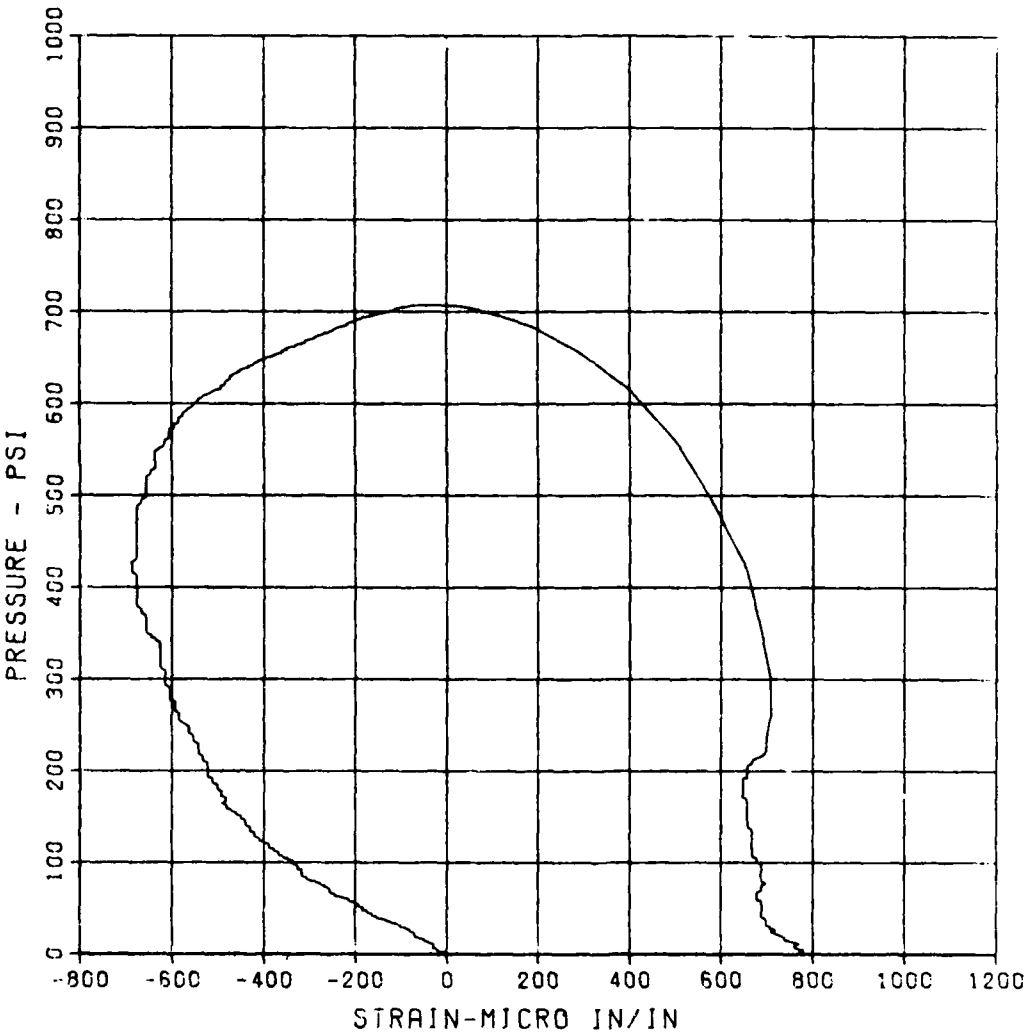

SBS ARCH TEST S-1B
E0-3

MAXIMUM	SIGMA CAL	CAL VAL
26050.6535	2.3303	11400.7

CHANNEL NO. 25 9806 1
09/19/86 R0911

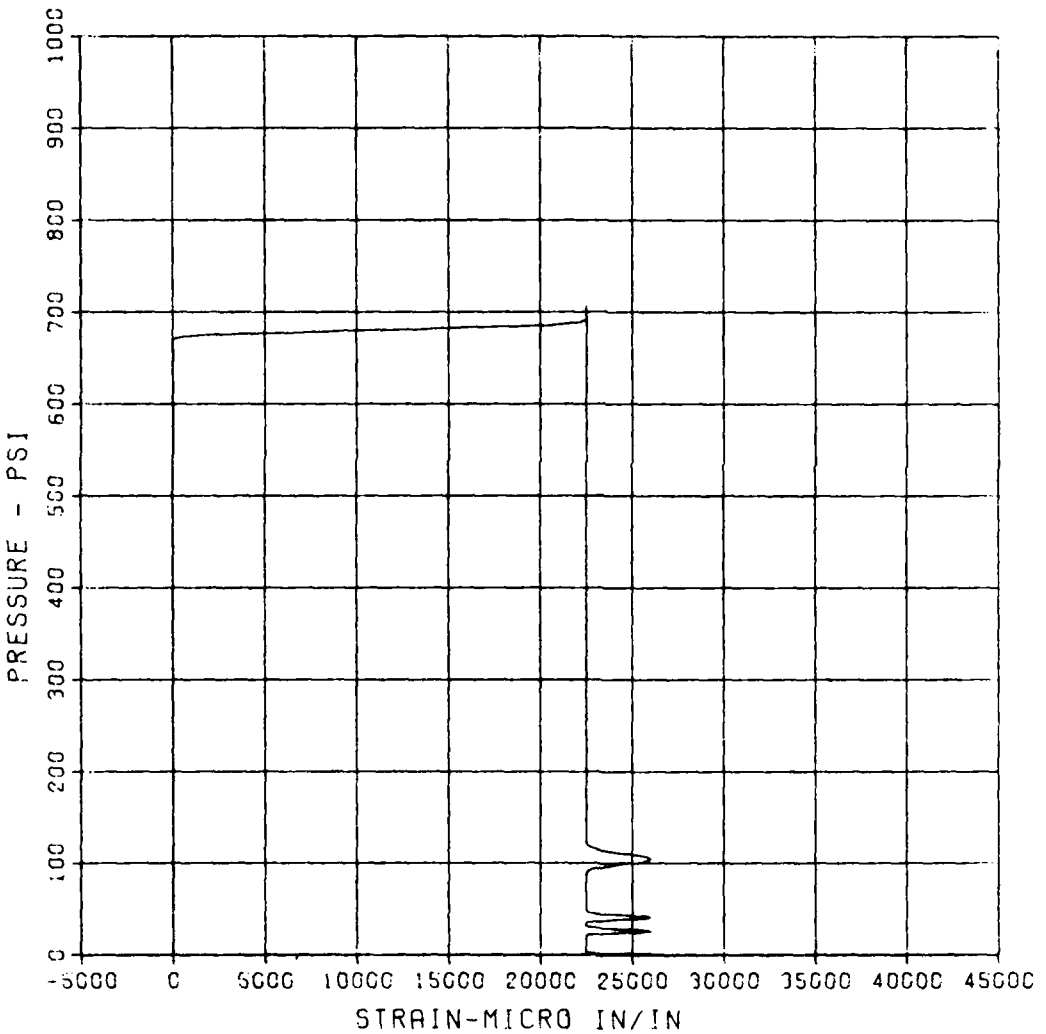

SBS ARCH TEST S-1B
EI-3

MAXIMUM	SIGMA CAL	CAL VAL
-10191.5939	5.4392	11400.7

CHANNEL NO. 26 9806 1
09/19/86 R0911

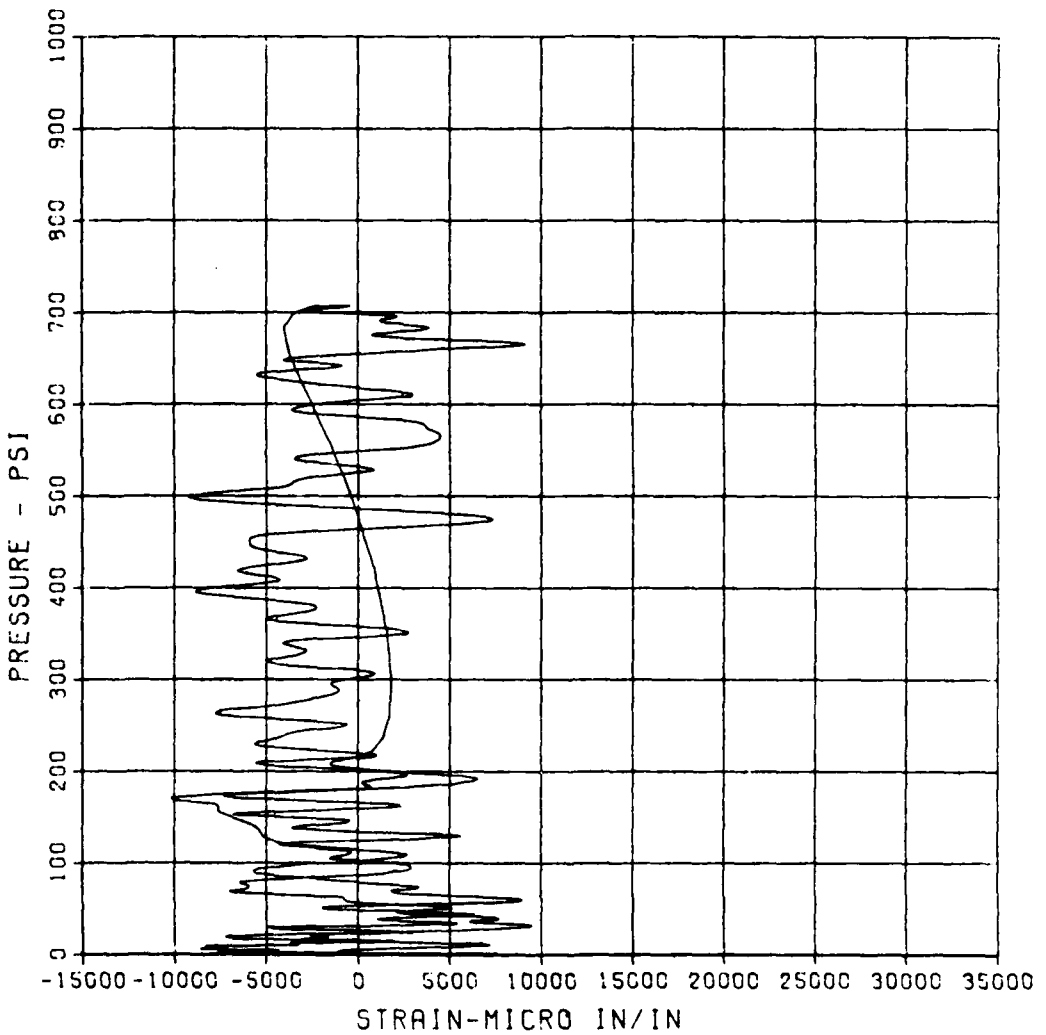

SBS ARCH TEST S-1B
E0-4

MAXIMUM	SIGMA CAL	CAL VAL
-945.4595	0.9172	11400.7

CHANNEL NO. 27 9806 1
09/19/86 R0911

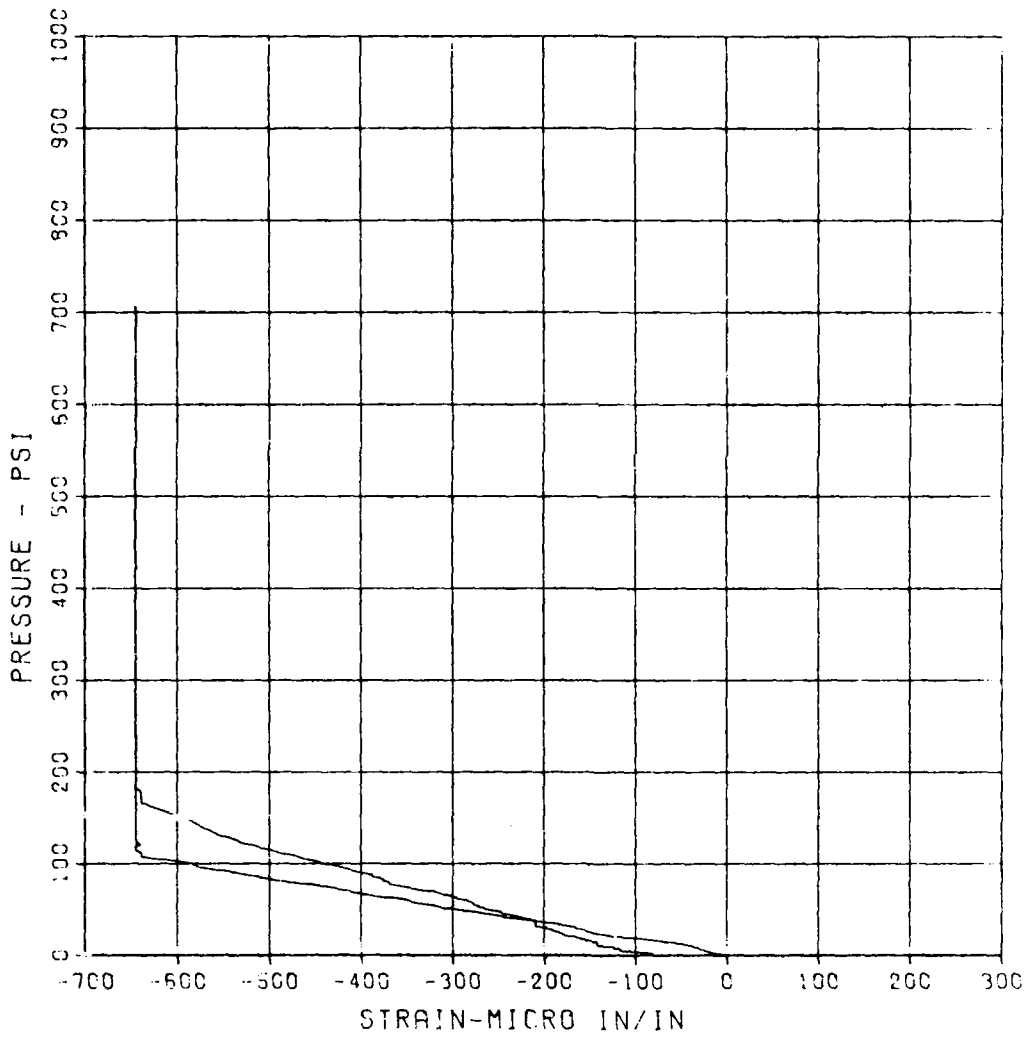

SBS ARCH TEST S-1B
EI-4A

MAXIMUM	SIGMA CAL	CAL VAL
-580.7803	2.3969	11400.7

CHANNEL NO. 28 9806 1
09/19/86 R0911

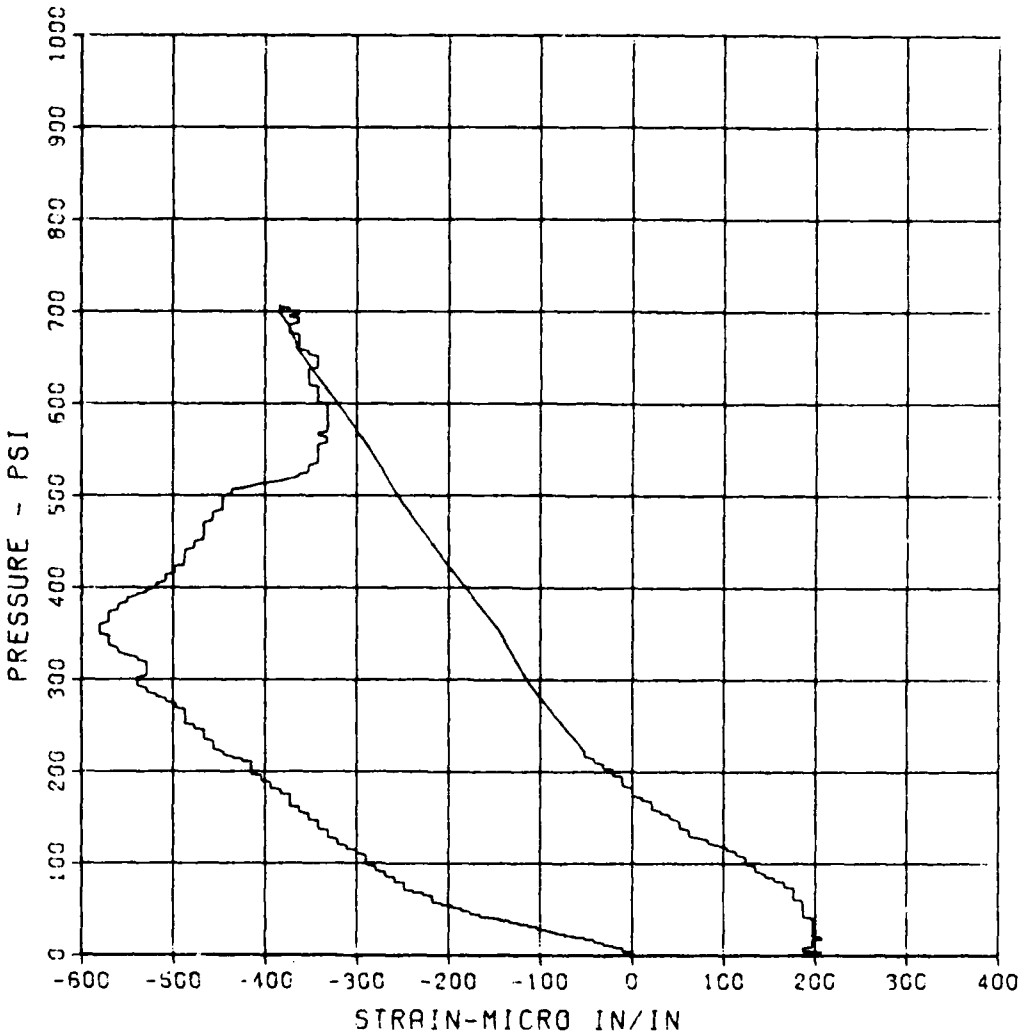

SBS ARCH TEST S-1B
C-1

MAXIMUM	SIGMA CAL	CAL VAL
1.8483	2.3256	10.9

CHANNEL NO. 29 9806 1
09/19/86 R0911

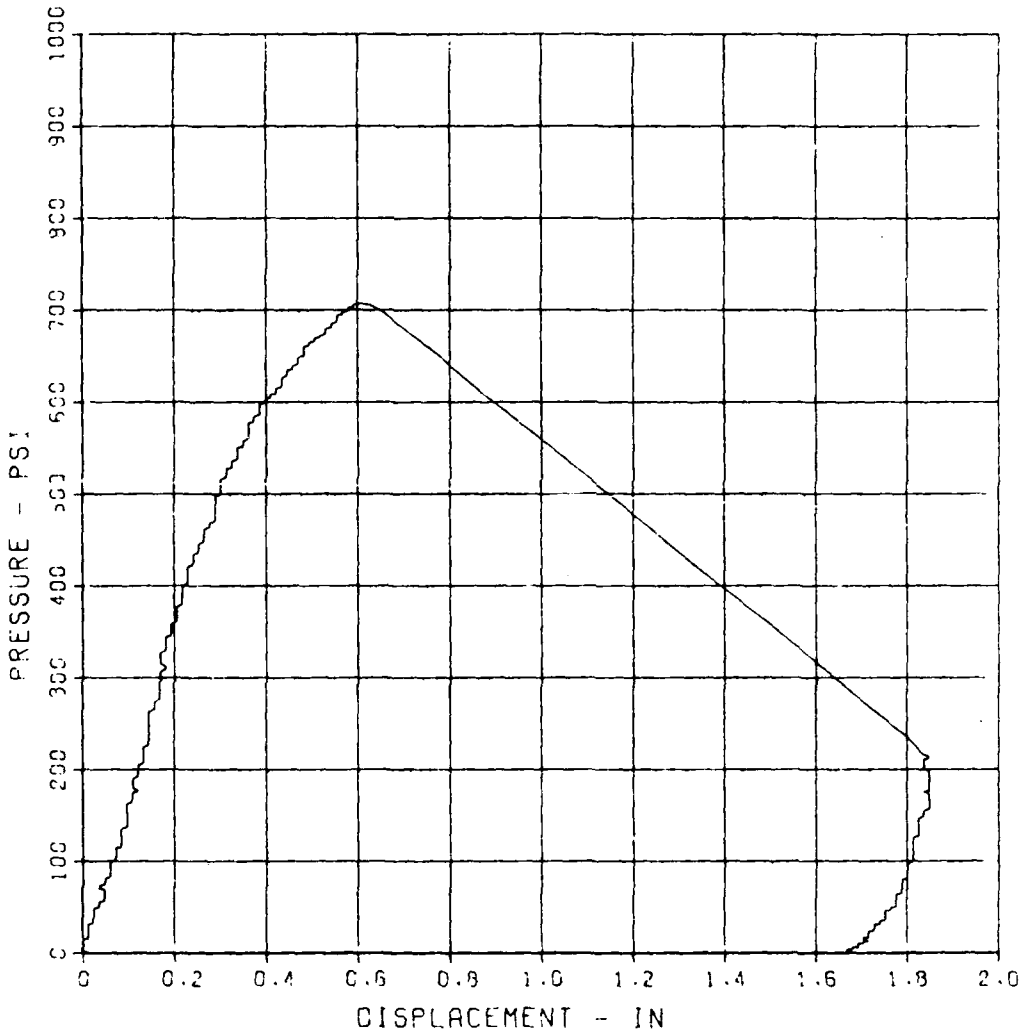

SBS ARCH TEST S-1B
D-2

MAXIMUM	SIGMA CAL	CAL VAL
0.1336	3.1770	2.1

CHANNEL NO. 30 9806 1
09/19/86 R0911

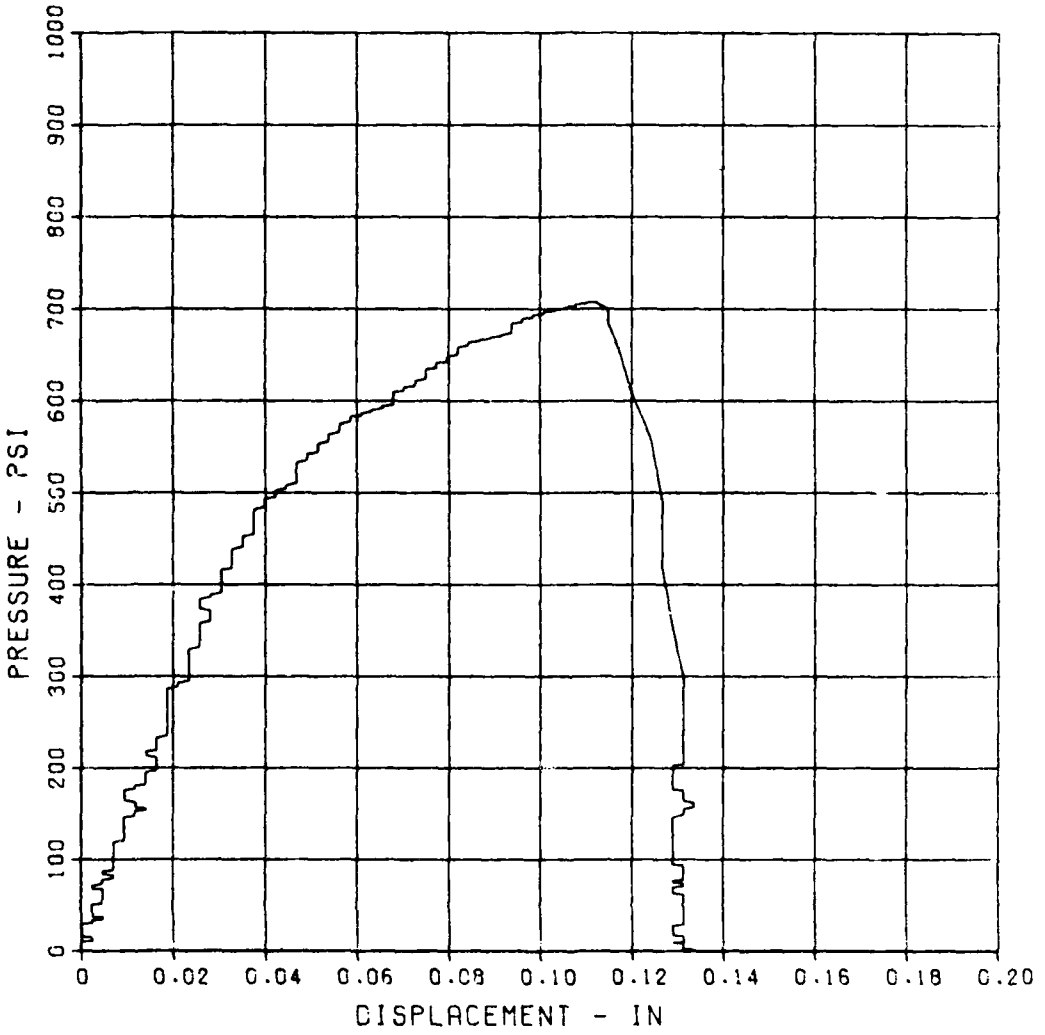

SBS ARCH TEST S-2

SBS ARCH TEST S-2
BP-1

MAXIMUM	SIGMA CAL	CAL VAL
810.0240	2.4636	1149.6

CHANNEL NO. 1 19602 1
09/19/86 R0900

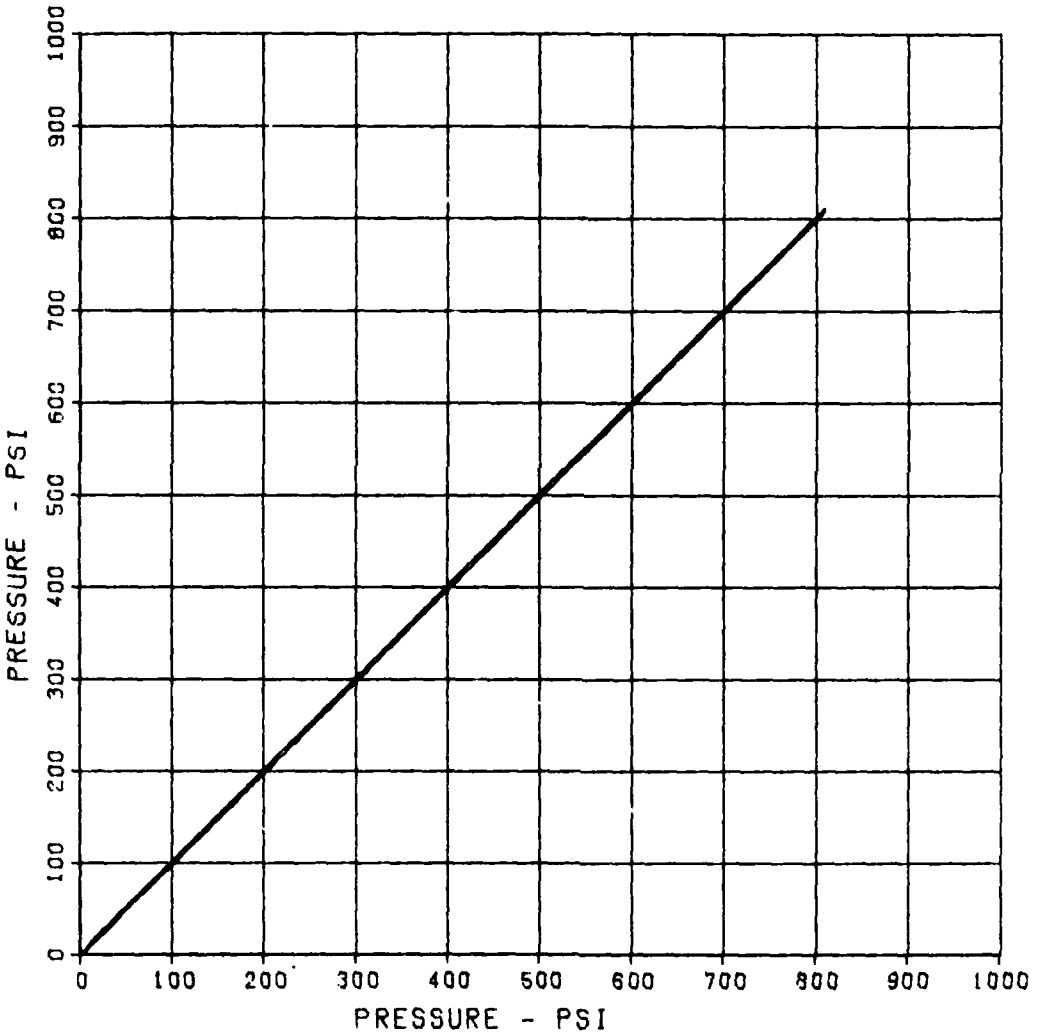

SBS ARCH TEST S-2
BP-2

MAXIMUM	SIGMA CAL	CAL VAL
640.4924	2.7021	1110.3

CHANNEL NO. 2 19602 1
09/19/86 R0908

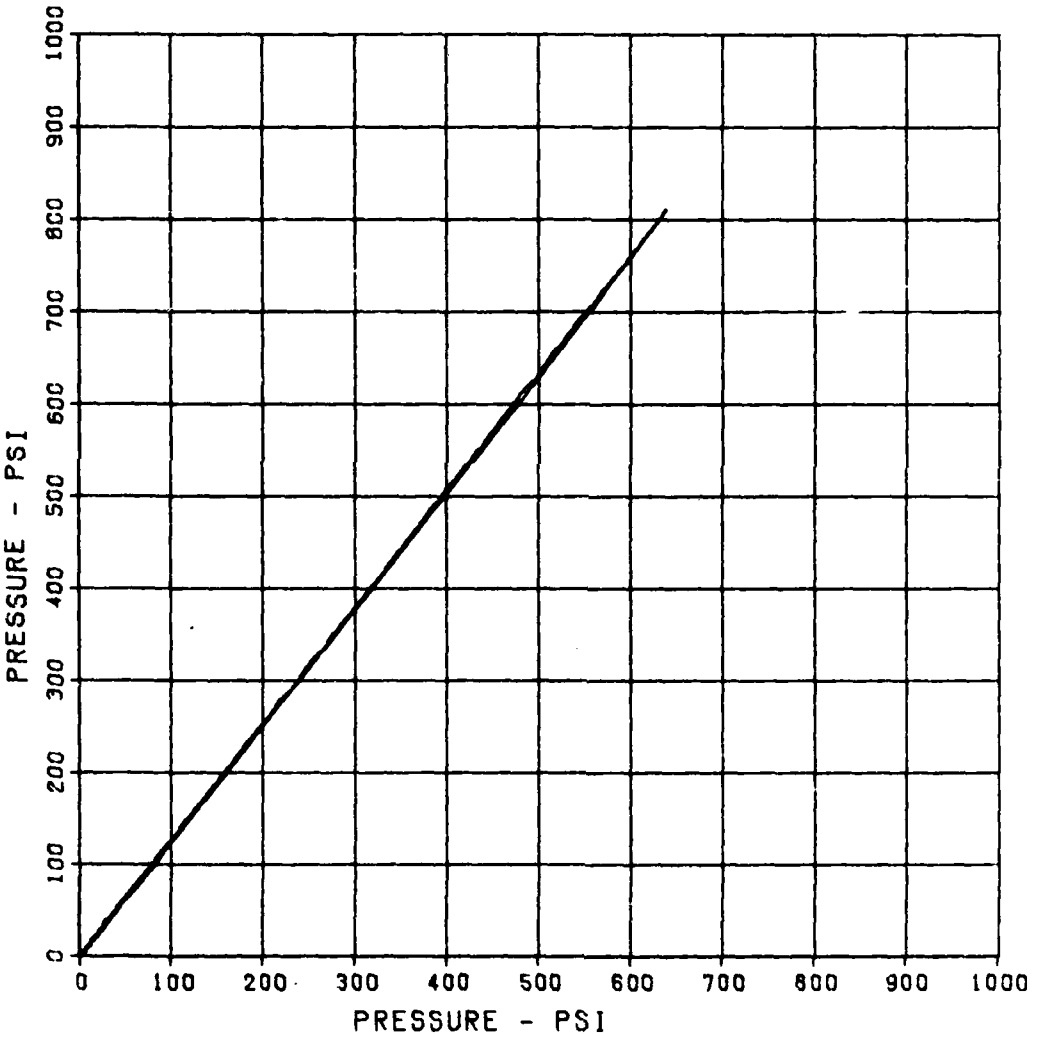

SBS ARCH TEST S-2
IP-1

MAXIMUM	SIGMA CAL	CAL VAL
790.2588	2.9646	1104.8

CHANNEL NO. 3 19602 1
09/19/86 R0908

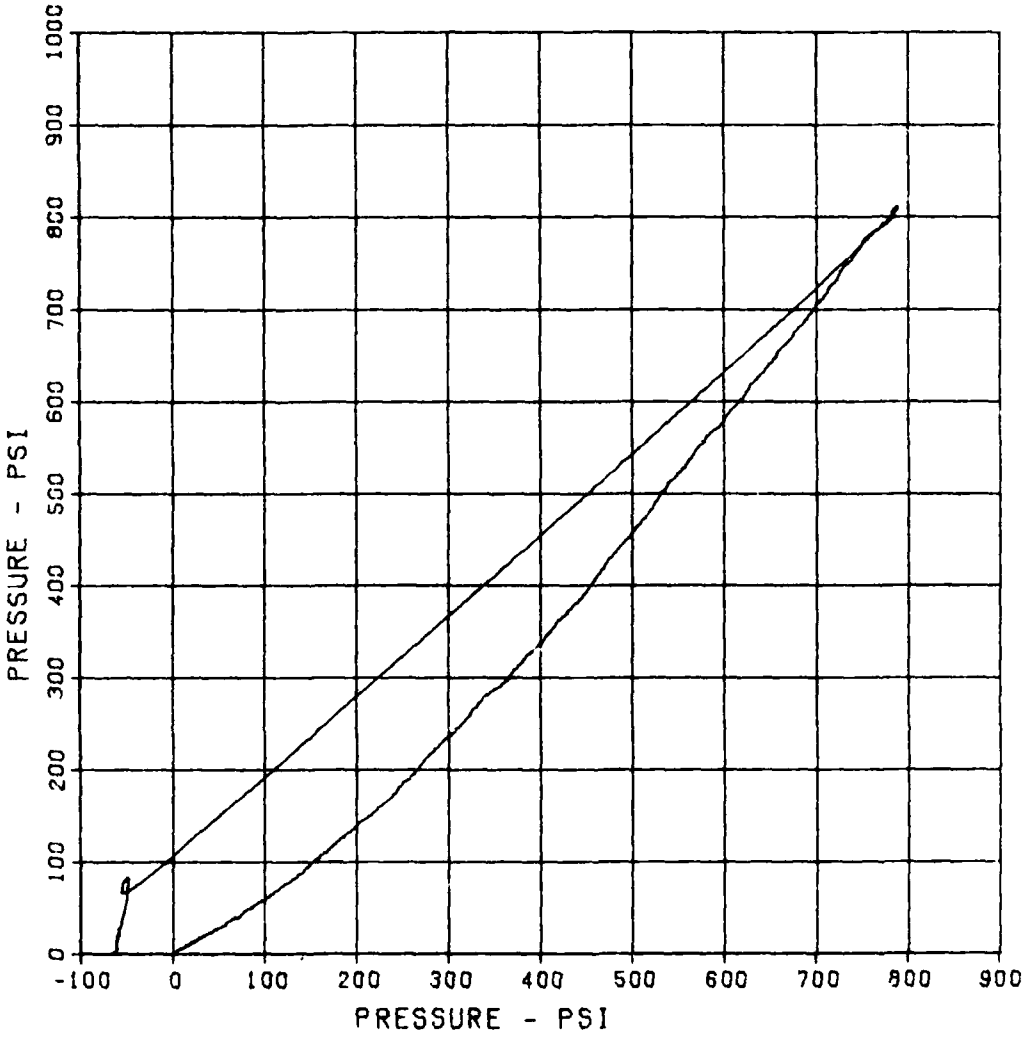

SBS ARCH TEST S-2
IP-2

MAXIMUM	SIGMA CAL	CAL VAL
851.9600	3.1633	1207.0

CHANNEL NO. 4 19602 1
09/19/86 R0908

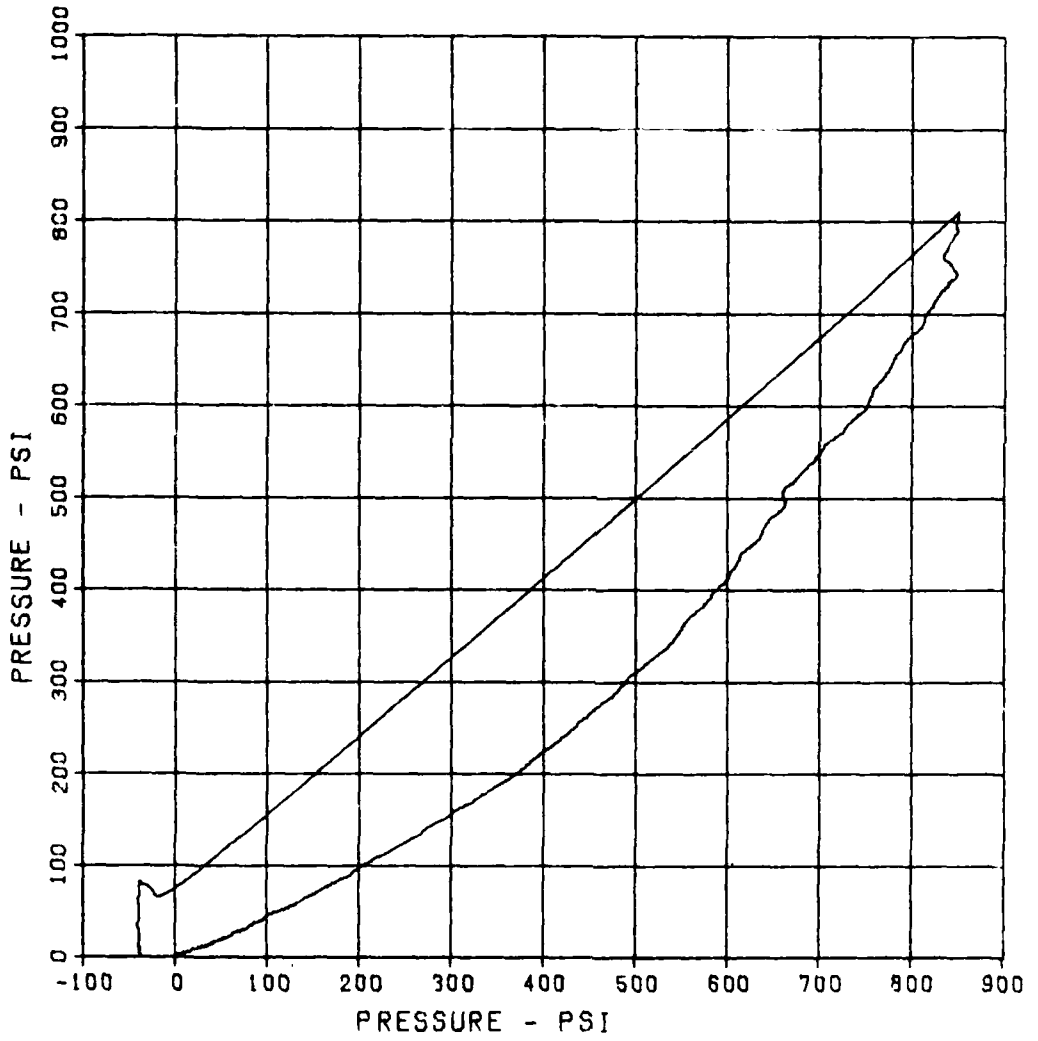

SBS ARCH TEST S-2
IP-3

MAXIMUM	SIGMA CAL	CAL VAL
475.3345	2.6038	1236.1

CHANNEL NO. 5 19602 1
09/19/86 R0908

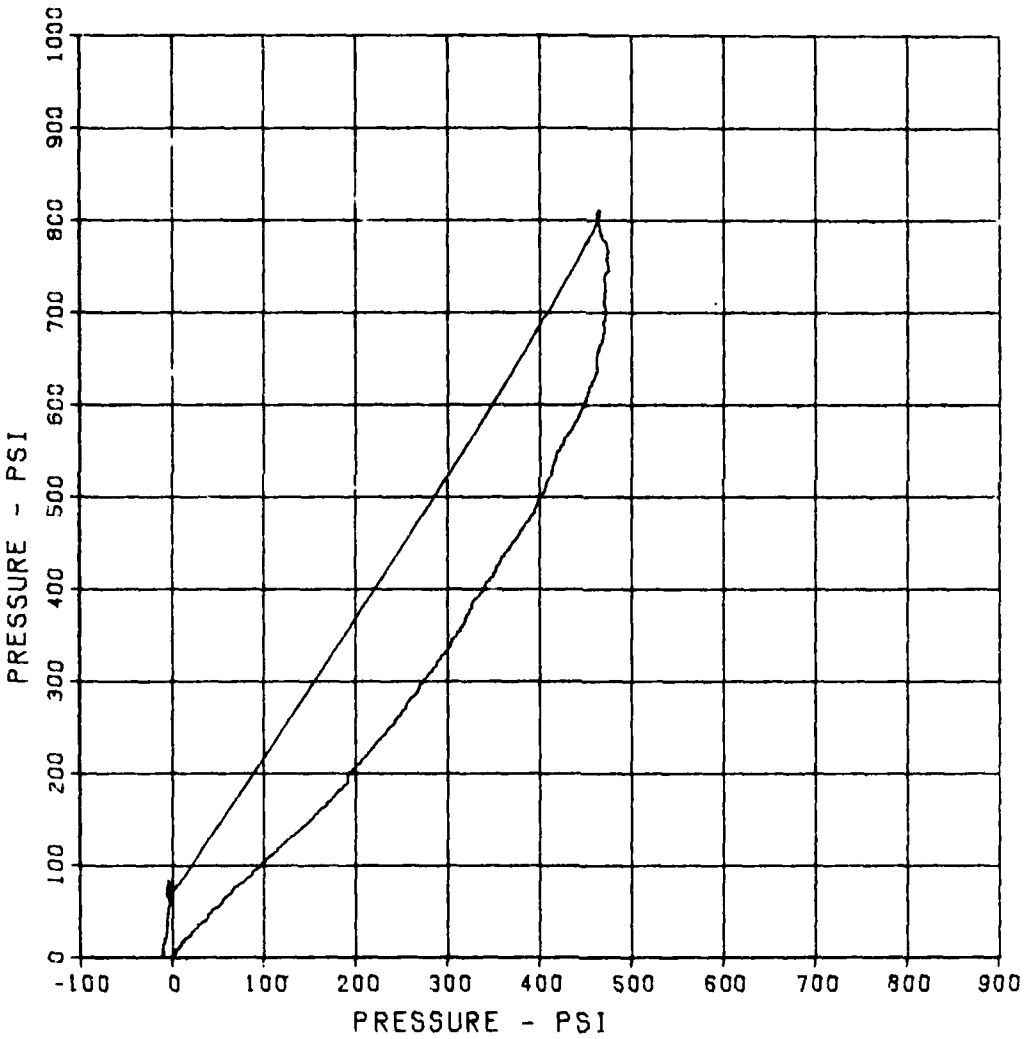

SBS ARCH TEST S-2
IP-4

MAXIMUM	SIGMA CAL	CAL VAL
581.1610	2.9661	728.8

CHANNEL NO. 6 19602 1
09/19/86 R0908

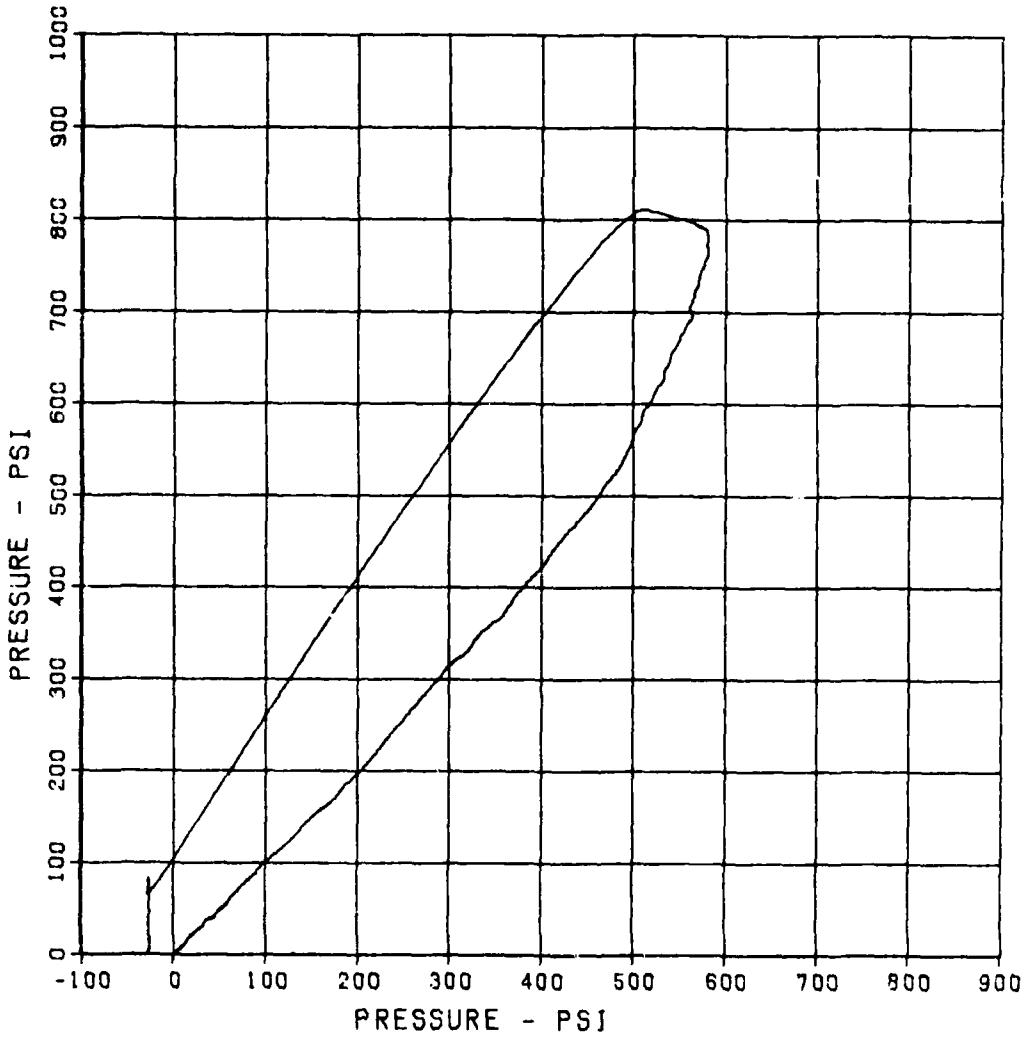

SBS ARCH TEST S-2
IP-5

MAXIMUM	SIGMA CAL	CAL VAL
345.8003	2.5209	658.0

CHANNEL NO. 7 19602 1
09/19/86 R0908

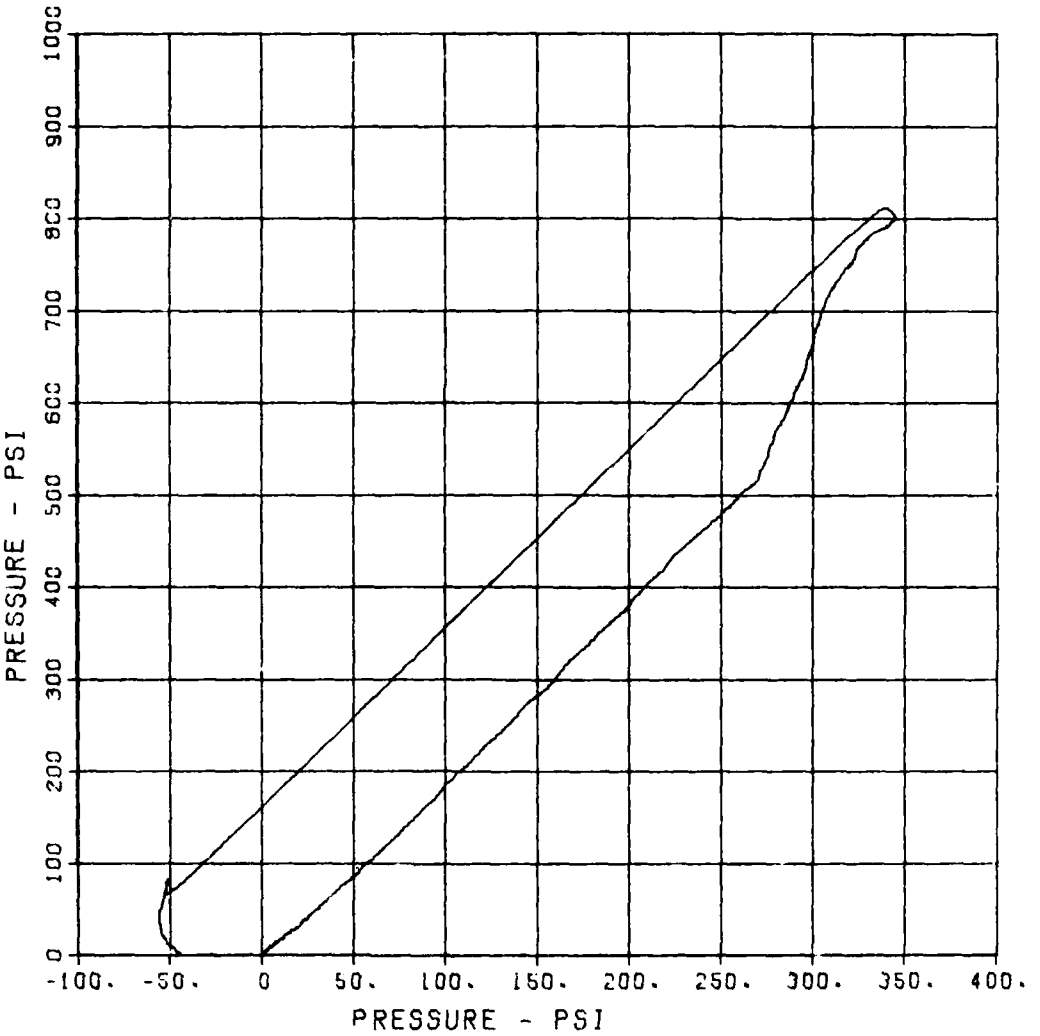

SBS ARCH TEST S-2
IP-6

MAXIMUM	SIGMA CAL	CAL VAL
458.6652	2.4711	1176.5

CHANNEL NO. 8 19602 1
09/19/86 R0908

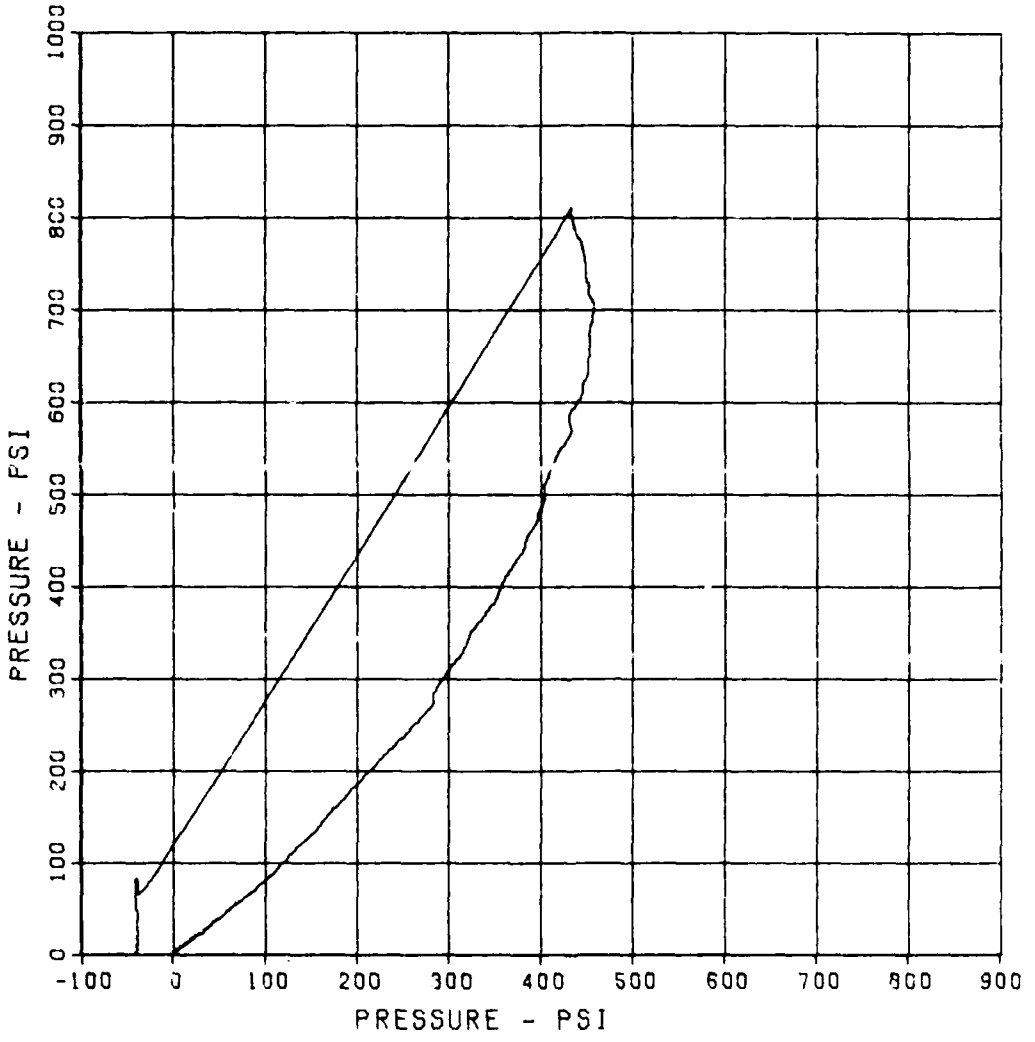

SBS ARCH TEST S-2
IP-7

MAXIMUM	SIGMA CAL	CAL VAL
684.3277	2.2889	1139.5

CHANNEL NO. 9 19602 1
09/19/86 R0908

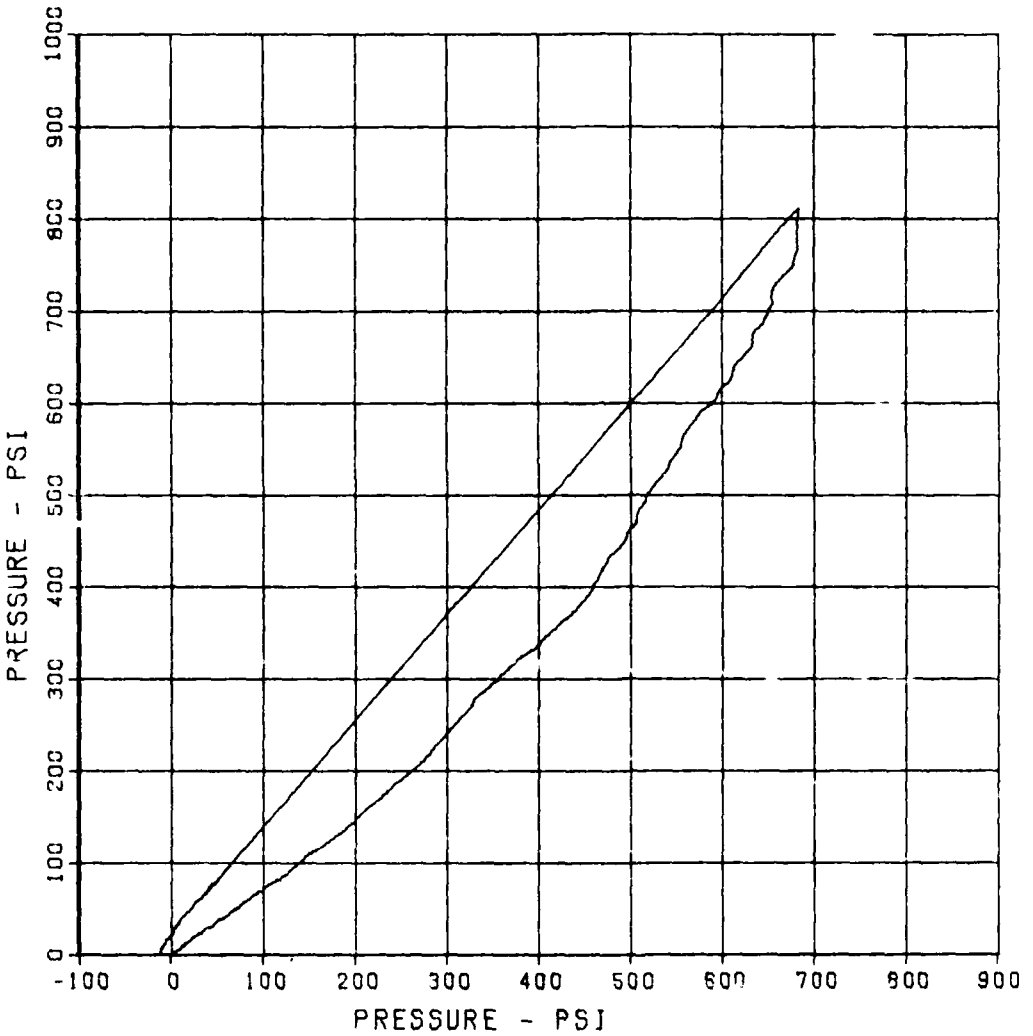

SBS ARCH TEST S-2
IP-8

MAXIMUM	SIGMA CAL	CAL VAL
587.6054	2.5273	749.5

CHANNEL NO. 10 19602 1
09/19/86 R0908

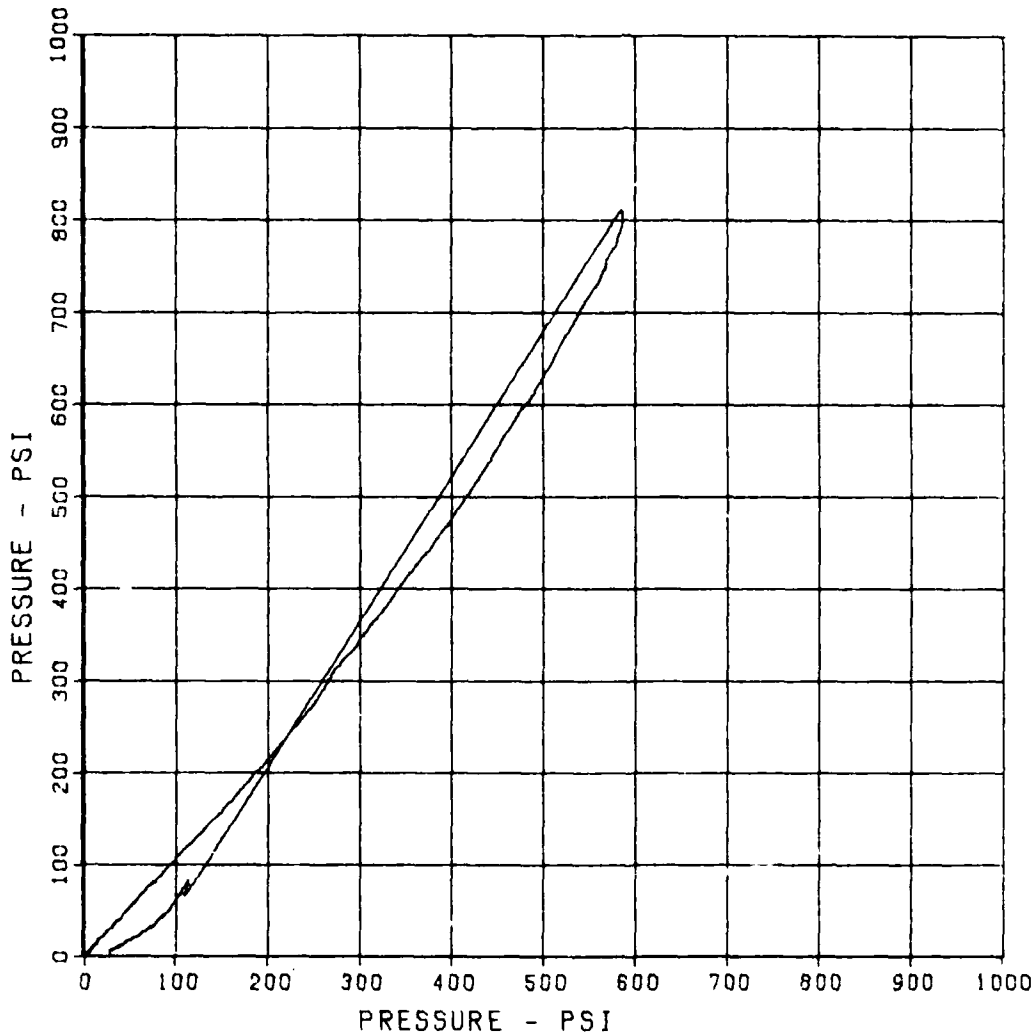

SBS ARCH TEST S-2
IP-9

MAXIMUM	SIGMA CAL	CAL VAL
393.4746	2.1398	738.8

CHANNEL NO. 11 19602 1
09/19/86 R0908

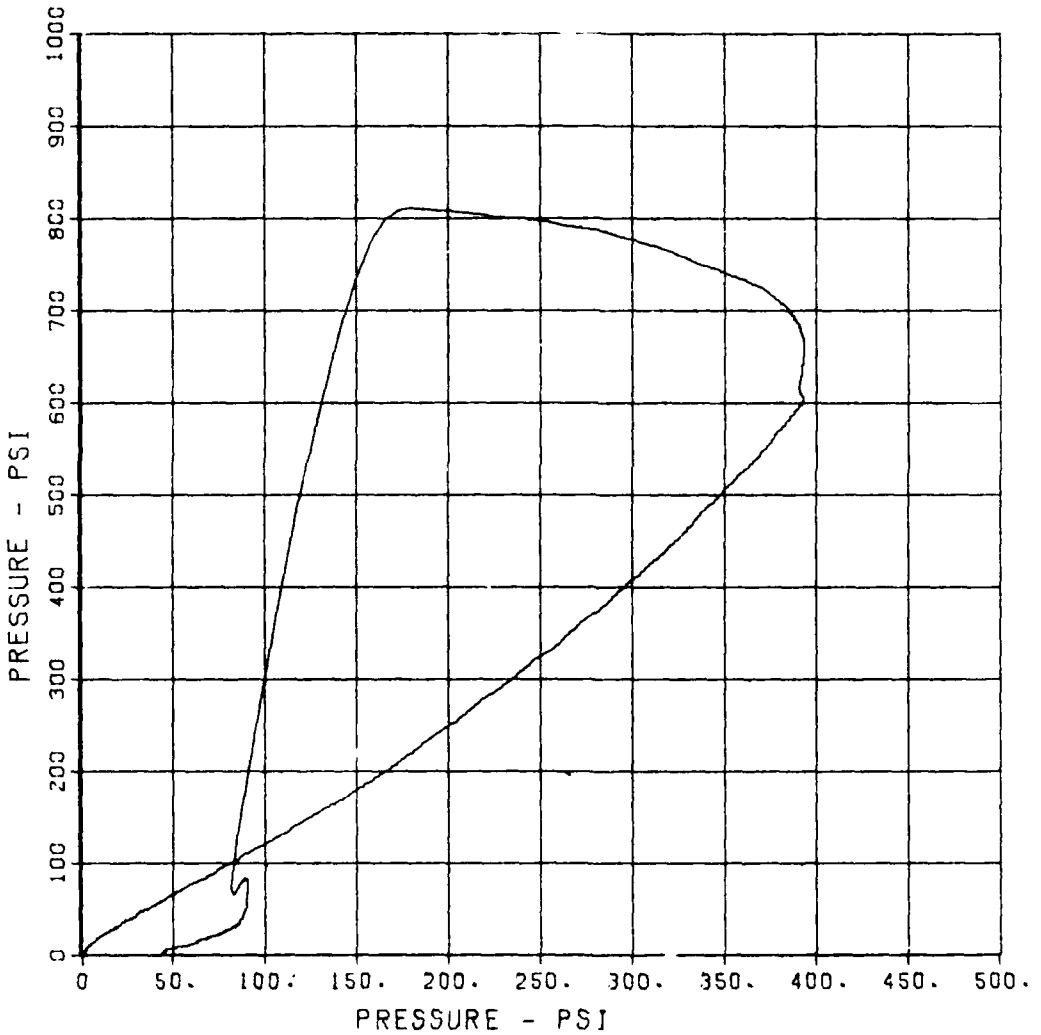

SBS ARCH TEST S-2
SE-1

MAXIMUM	SIGMA CAL	CAL VAL
590.3500	2.1164	1148.1

CHANNEL NO. 12 19602 1
09/19/86 R0908

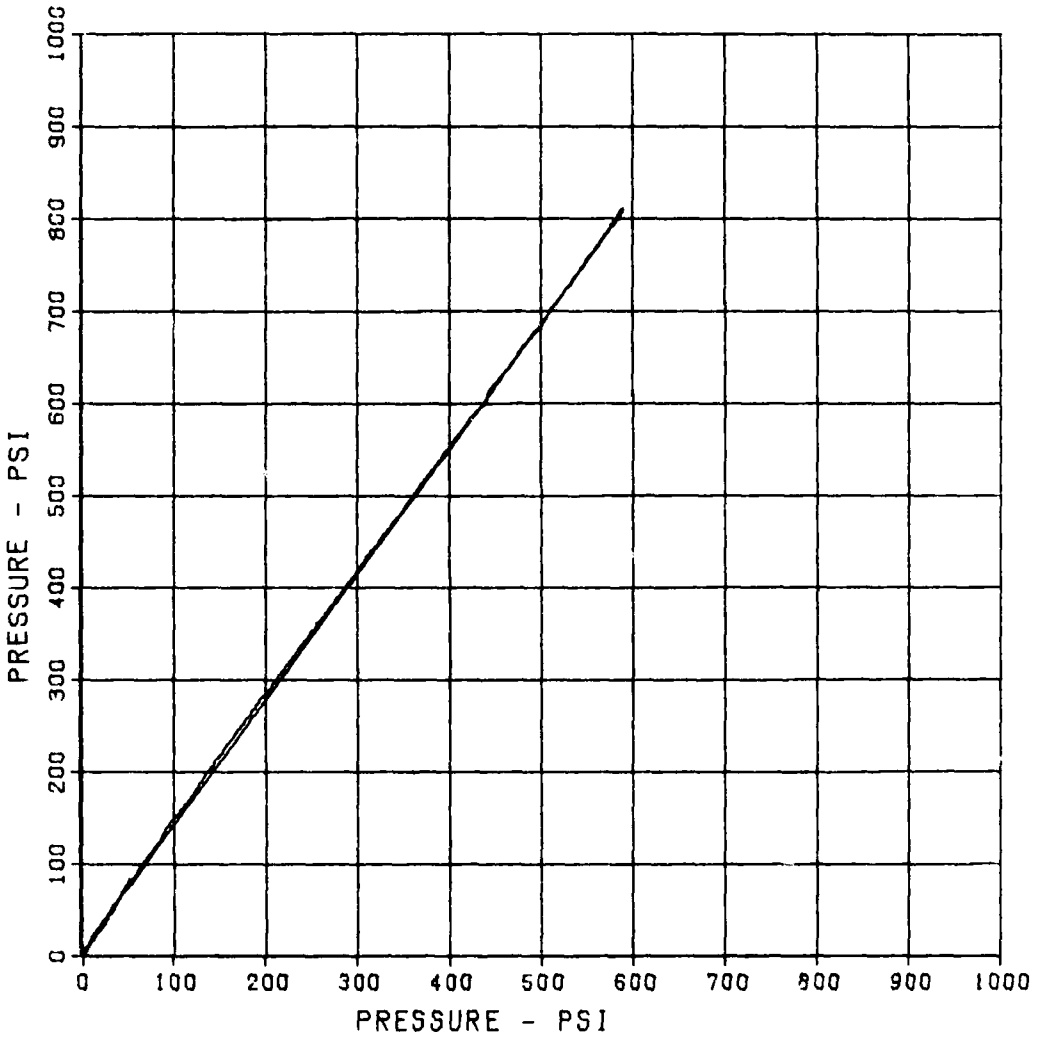

SBS ARCH TEST S-2
SE-2

MAXIMUM	SIGMA CAL	CAL VAL
503.7702	2.4018	1113.6

CHANNEL NO. 13 19602 1
09/19/86 R0908

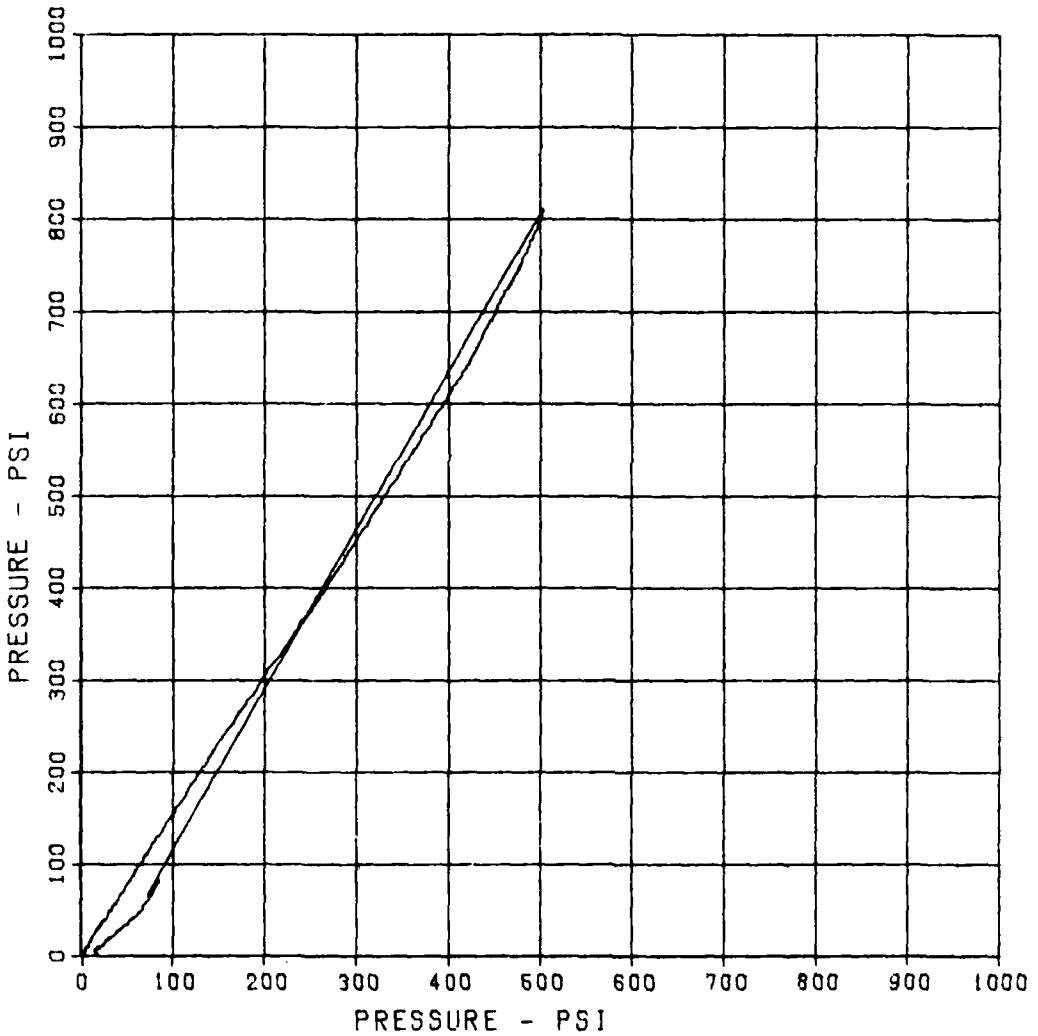

SBS ARCH TEST S-2
SE-3

MAXIMUM	SIGMA CAL	CAL VAL
365.5923	2.6047	1237.2

CHANNEL NO. 14 19602 1
09/19/86 R0908

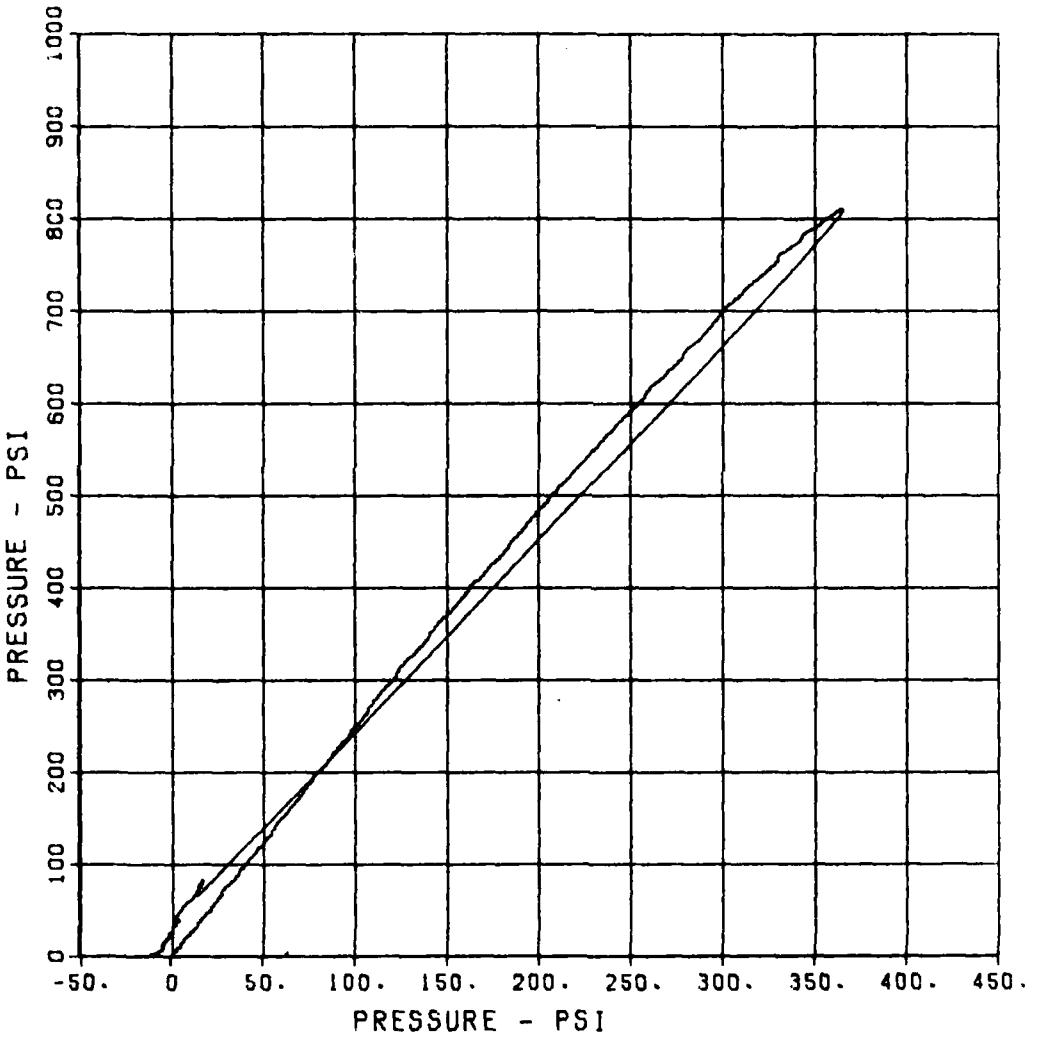

SBS ARCH TEST S-2
SE-4

MAXIMUM	SIGMA CAL	CAL VAL
234.4829	2.4194	1139.6

CHANNEL NO. 15 19602 1
09/19/86 R0908

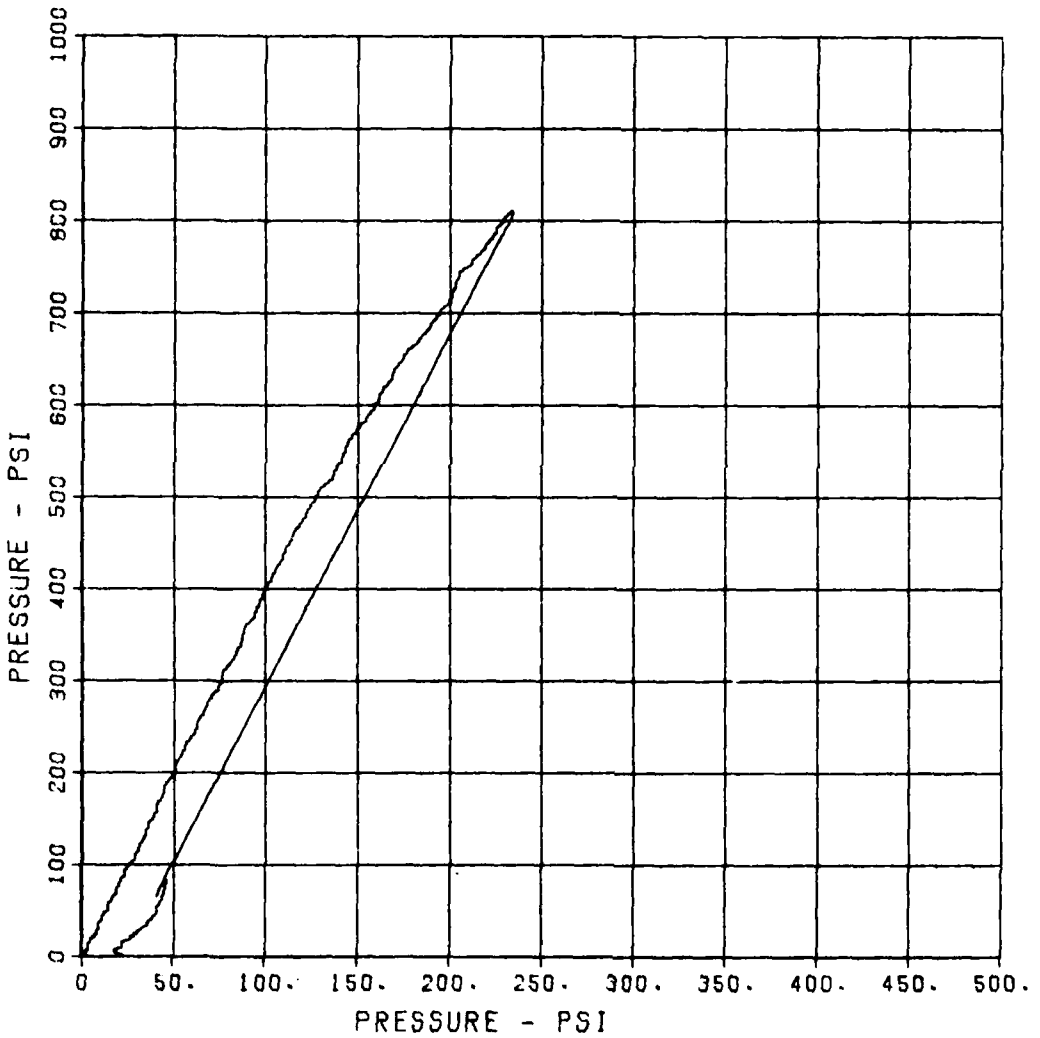

SBS ARCH TEST S-2
SE-6

MAXIMUM	SIGMA CAL	CAL VAL
407.0020	3.2660	890.6

CHANNEL NO. 17 19602 1
09/19/86 R0908

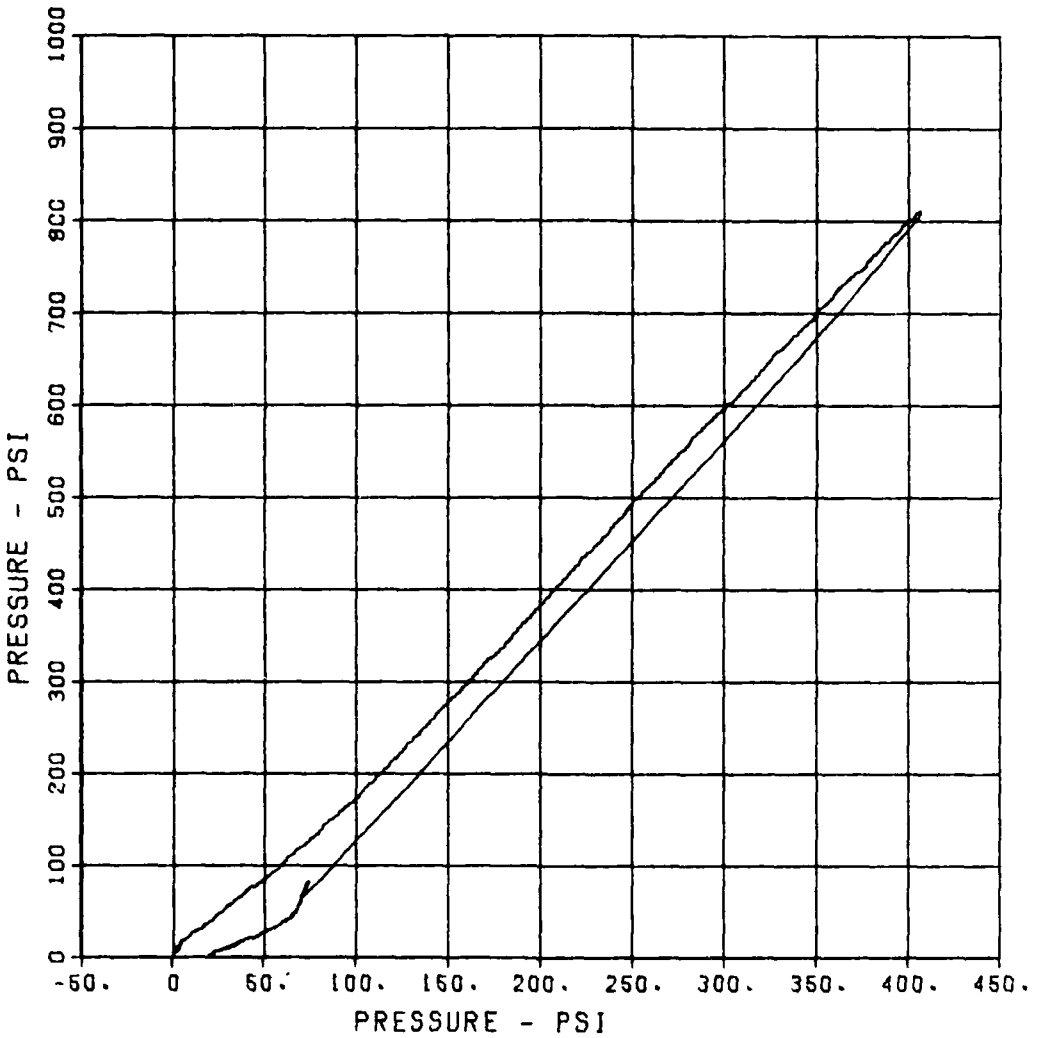

SBS ARCH TEST S-2
SE-7

MAXIMUM	SIGMA CAL	CAL VAL
155.5470	3.2075	988.7

CHANNEL NO. 18 19602 1
09/19/86 R0908

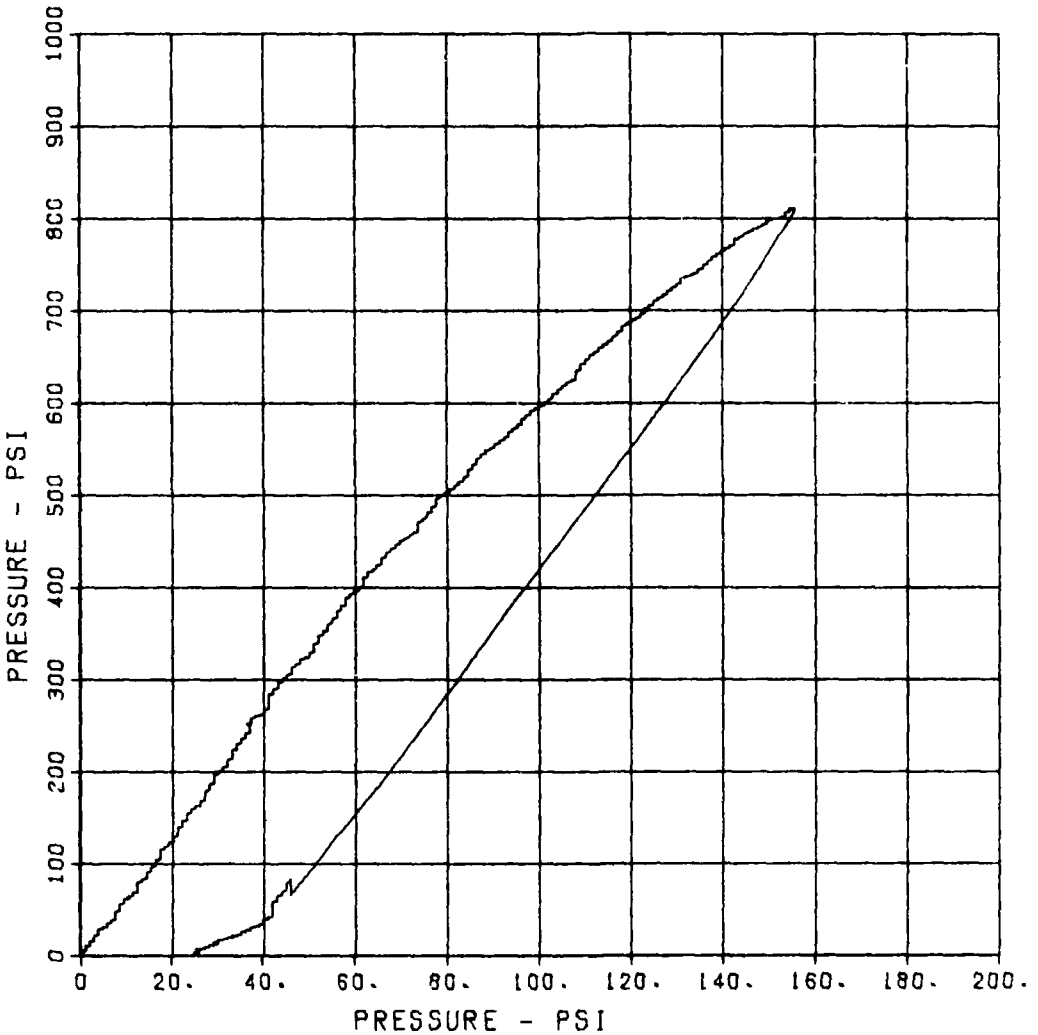

SBS ARCH TEST S-2
SE-8

MAXIMUM	SIGMA CAL	CAL VAL
712.9219	4.0726	1109.0

CHANNEL NO. 19 19602 1
09/19/86 R0908

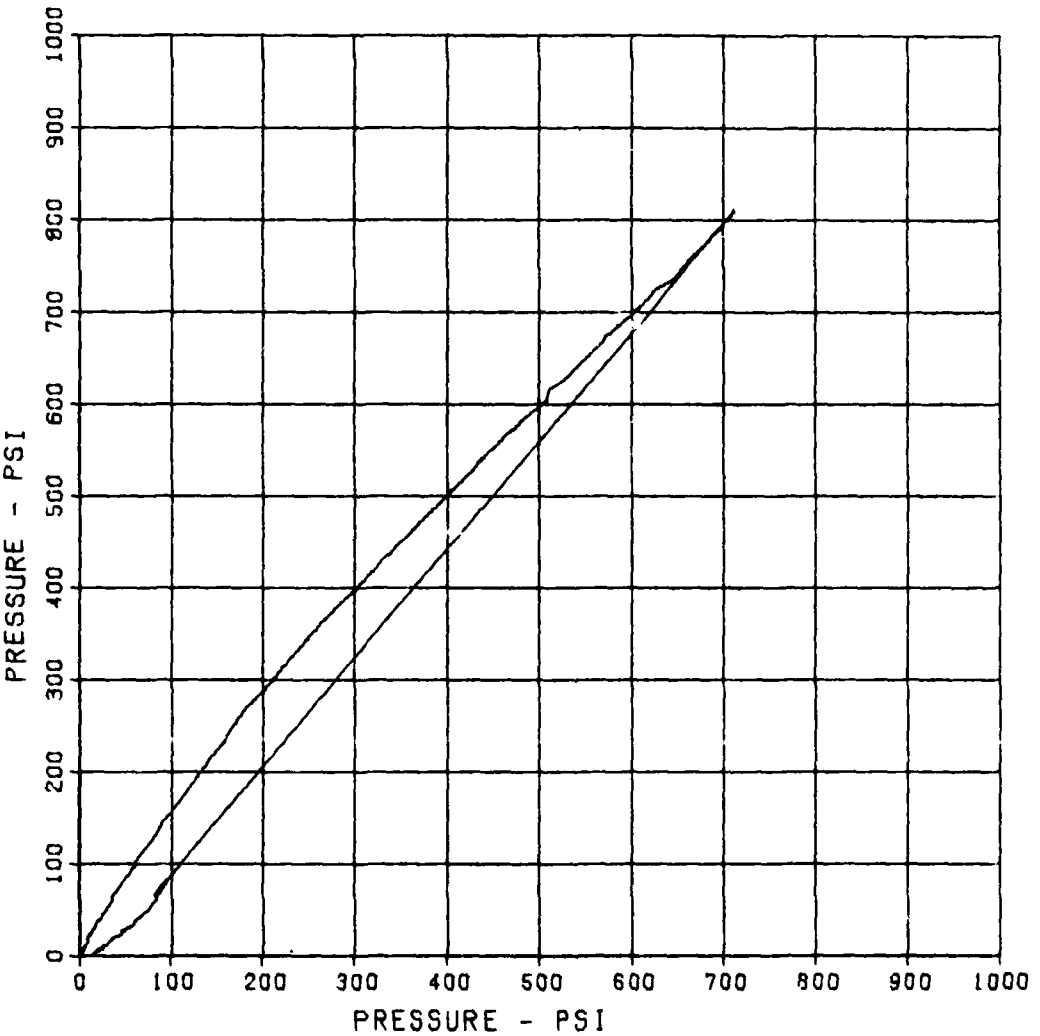

SBS ARCH TEST S-2
SE-9

MAXIMUM	SIGMA CAL	CAL VAL
431.5467	2.9735	1013.5

CHANNEL NO. 20 19602 1
09/19/86 R0908

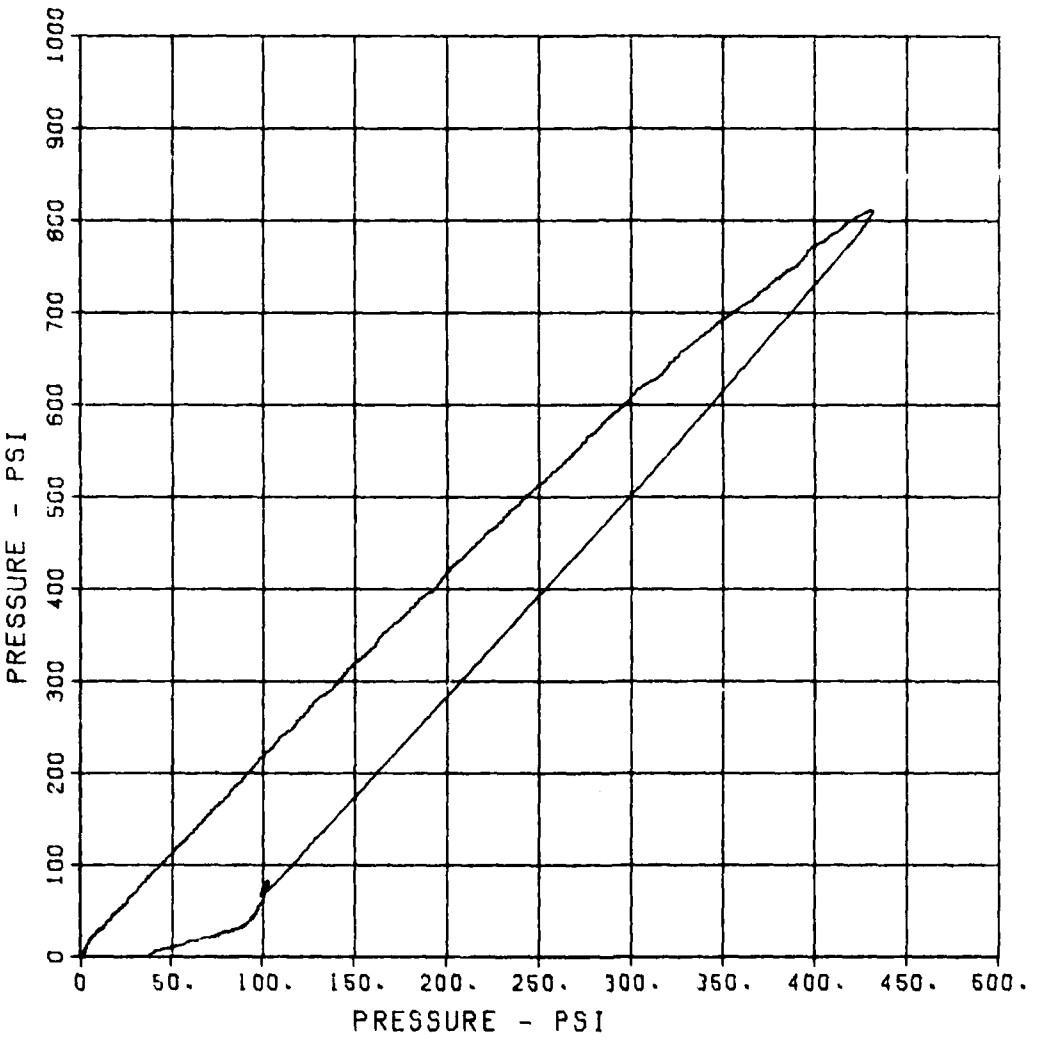

SBS ARCH TEST S-2
EO-1

MAXIMUM	SIGMA CAL	CAL VAL
-9467.1669	2.4585	11400.6

CHANNEL NO. 21 19602 1
09/19/86 R090A

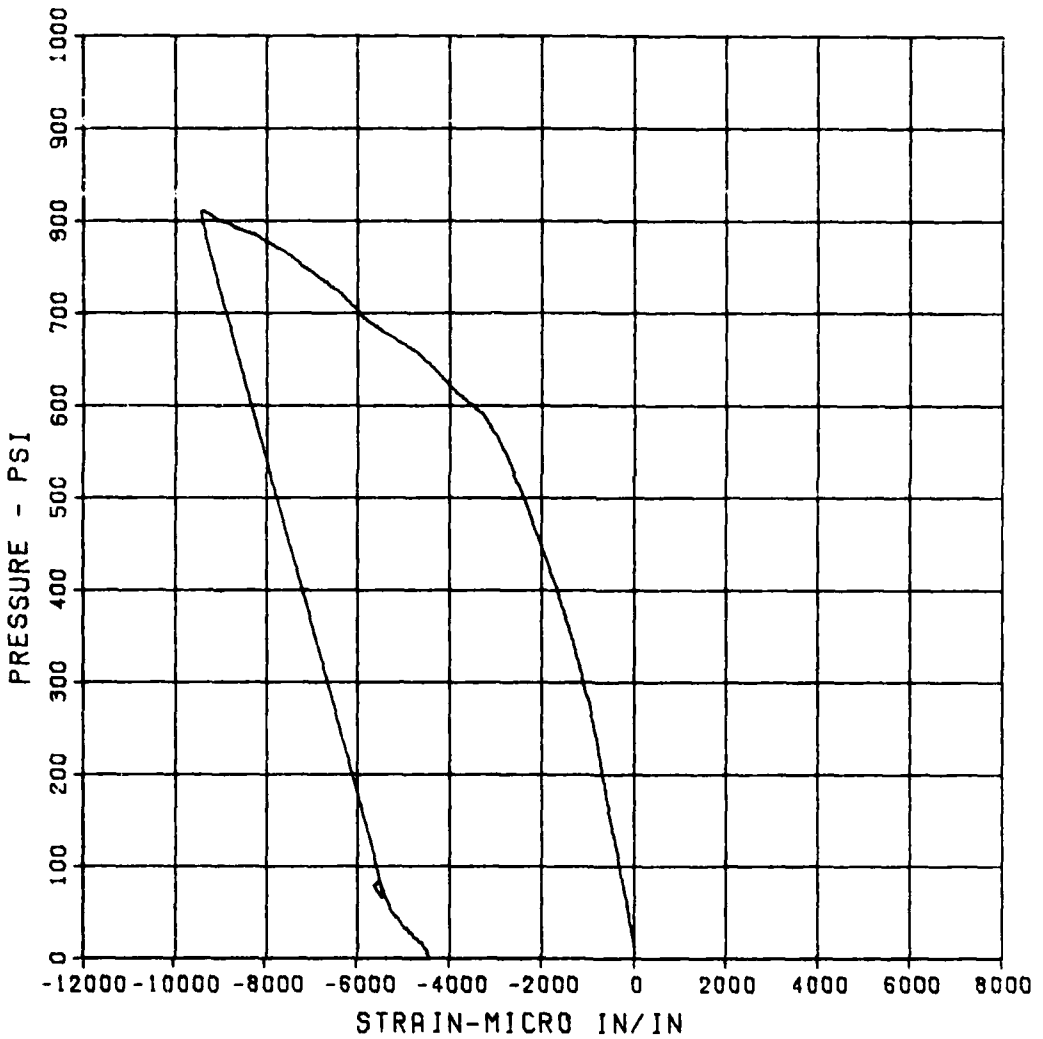

SBS ARCH TEST S-2
EI-1

MAXIMUM	SIGMA CAL	CAL VAL
4424.7548	2.2305	11400.6

CHANNEL NO. 22 19602 1
09/19/86 R0908

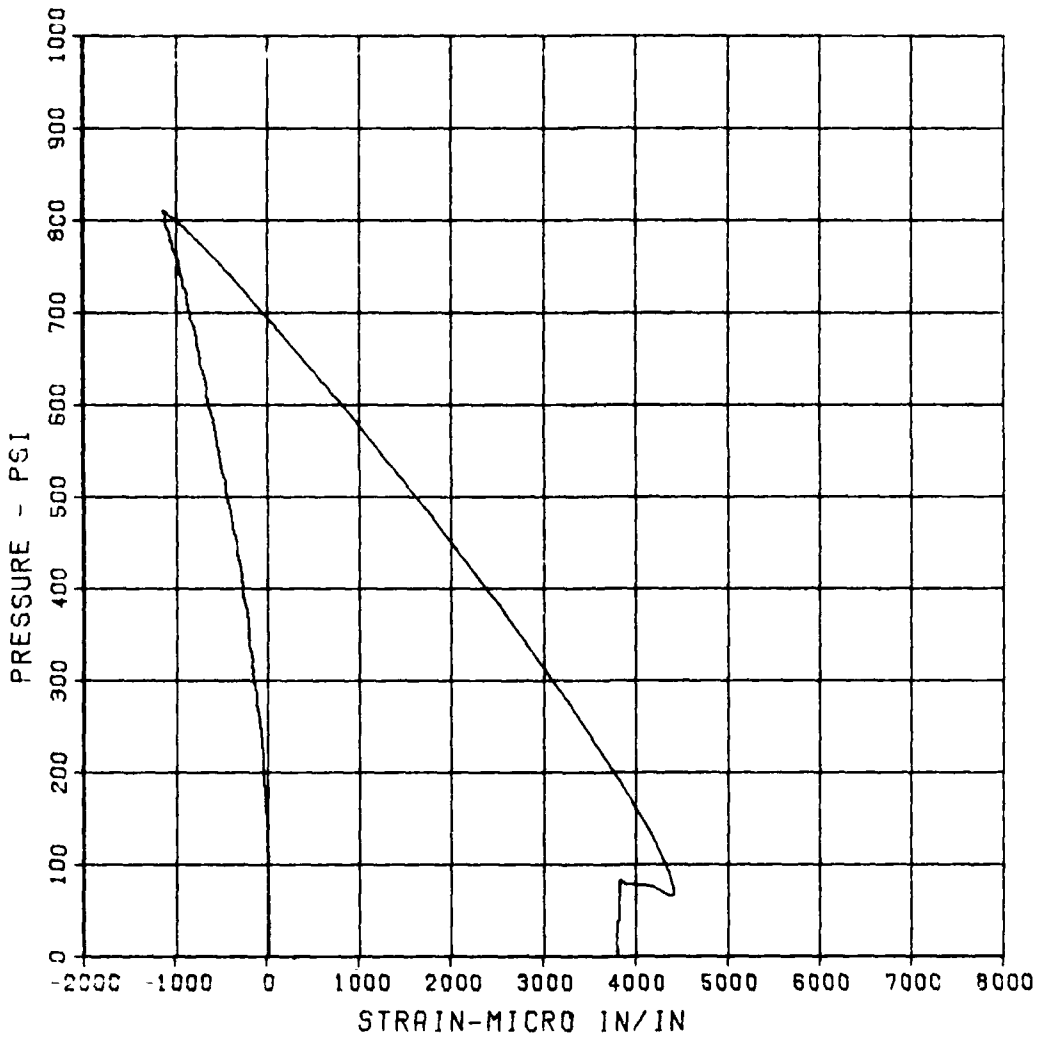

SBS ARCH TEST S-2
E0-2

MAXIMUM	SIGMA CAL	CAL VAL
-2367.7865	2.3812	11400.6

CHANNEL NO. 23 19602 1
09/19/86 R0908

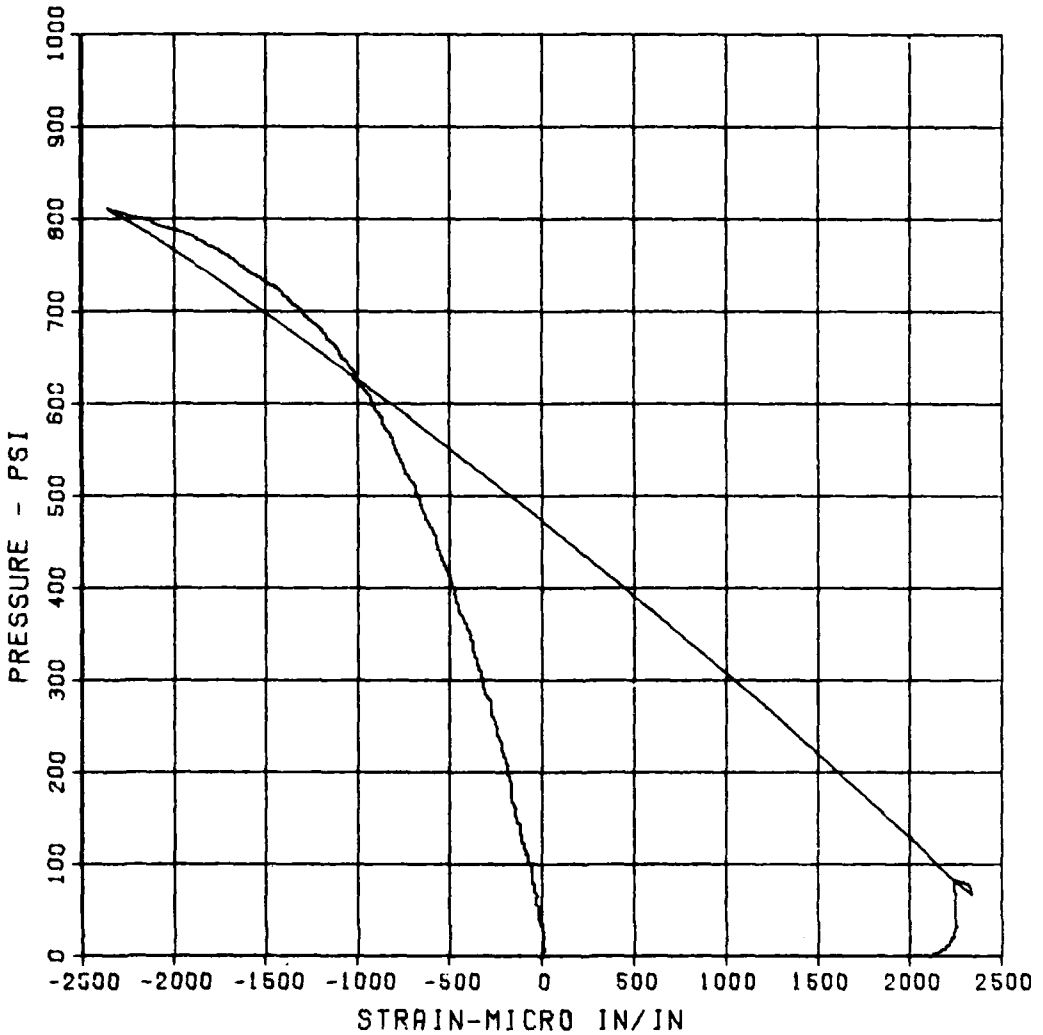

SBS ARCH TEST S-2
EI-2

MAXIMUM	SIGMA CAL	CAL VAL
-2265.7846	2.4745	11400.6

CHANNEL NO. 24 19602 1
09/19/86 R0908

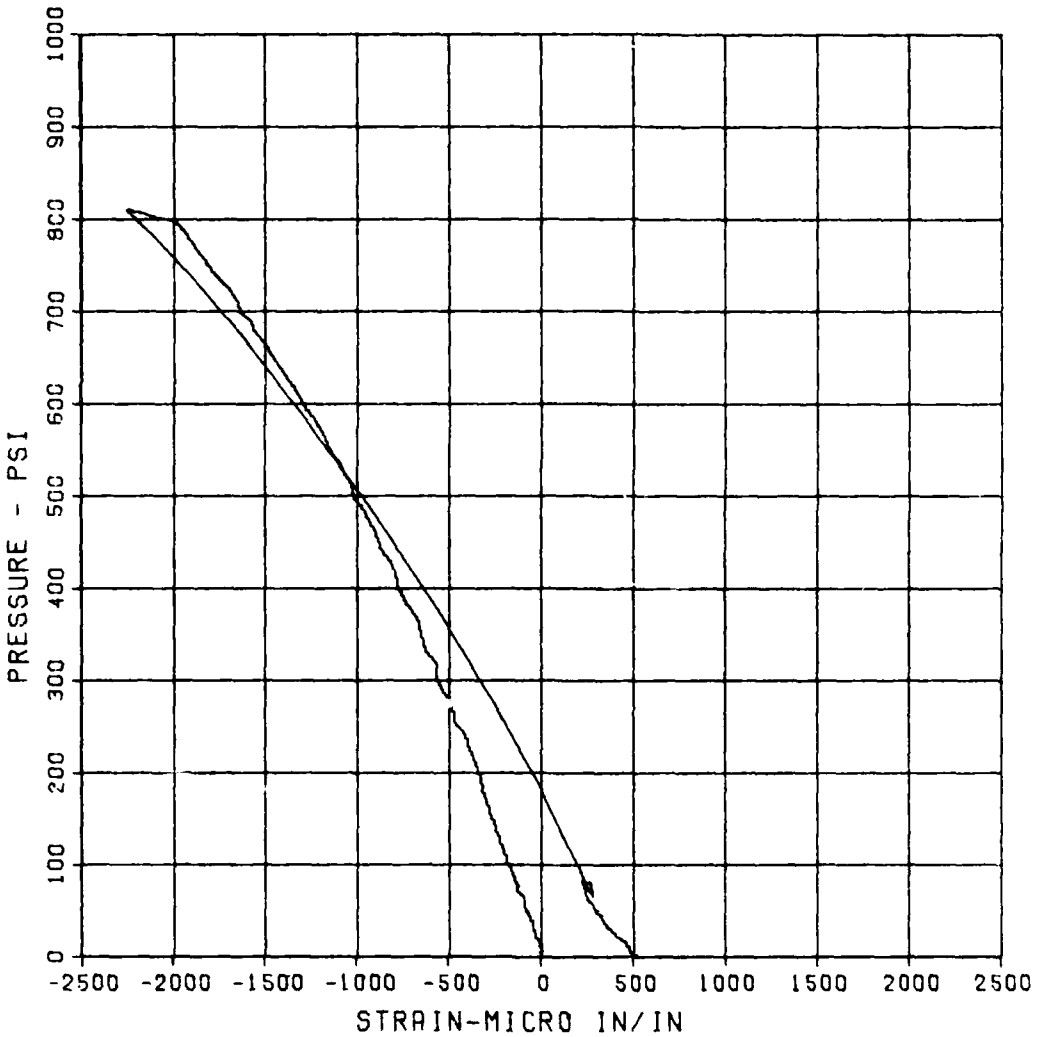

SBS ARCH TEST S-2
EO-3

MAXIMUM	SIGMA CAL	CAL VAL
-2094.7327	2.3958	11400.6

CHANNEL NO. 25 19602 1
09/19/86 R0908

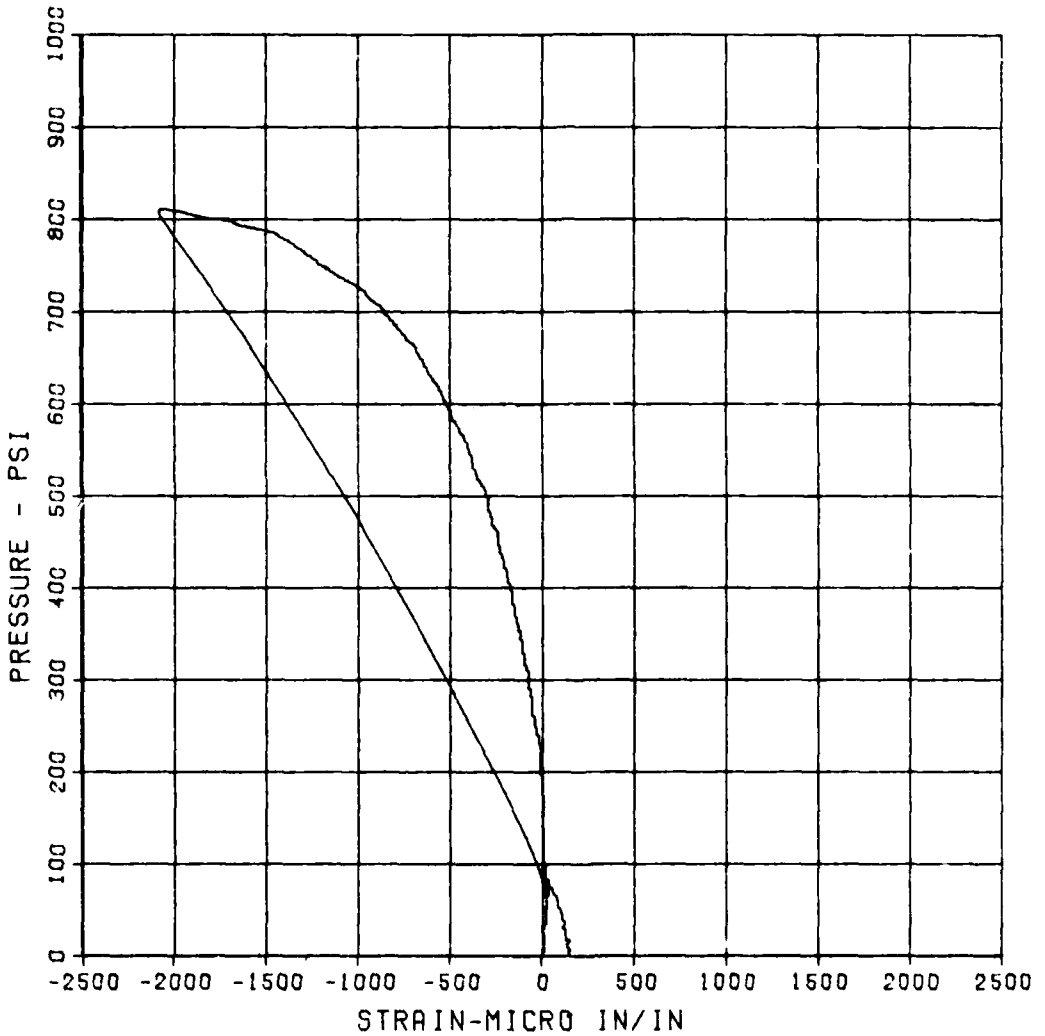

SBS ARCH TEST S-2
EI-3

SIGMA CAL 2.5856 CAL VAL 11400.6

CHANNEL NO. 26 19602 1
09/19/86 R0908

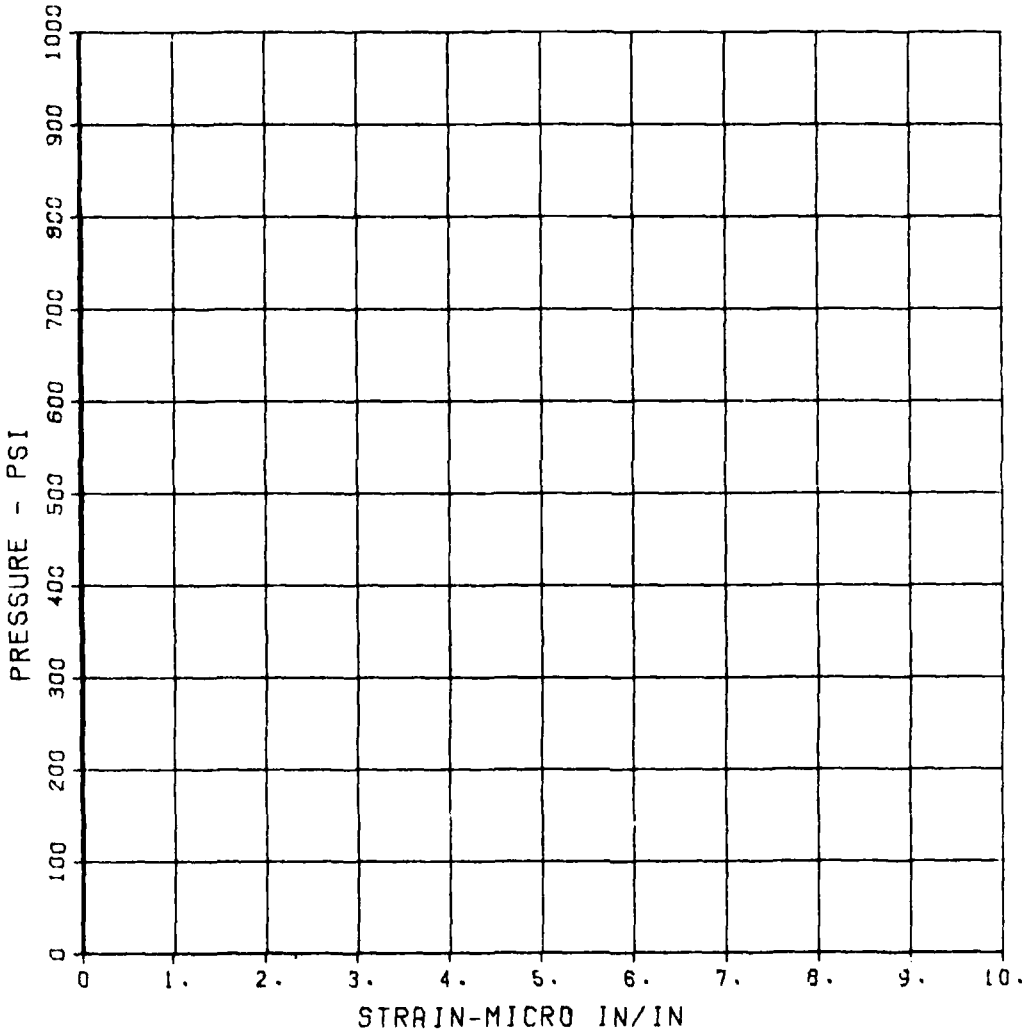

SBS ARCH TEST S-2
EO-4

MAXIMUM	SIGMA CAL	CAL VAL
24203.5788	2.5694	11400.6

CHANNEL NO. 27 19602 1
09/19/86 R0908

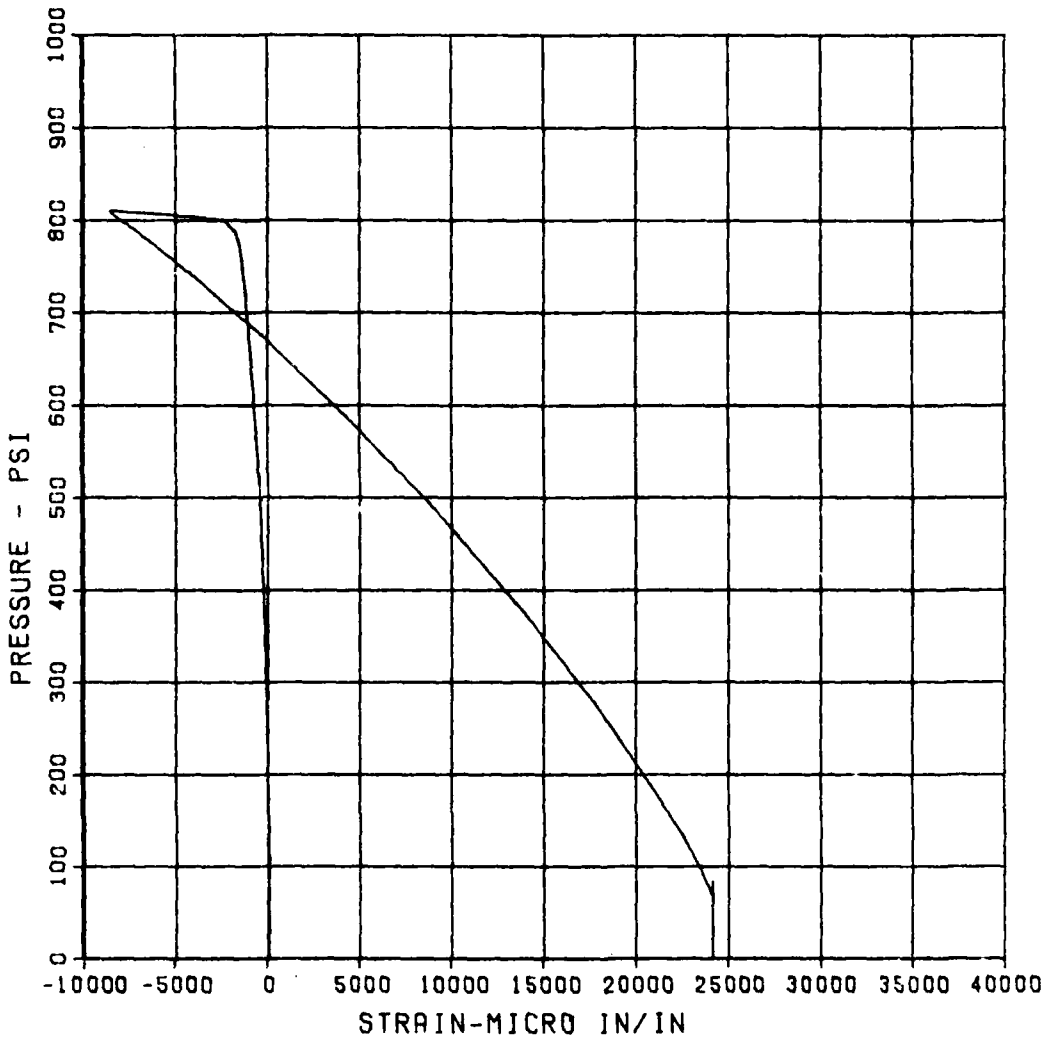

SBS ARCH TEST S-2
EI-4

MAXIMUM	SIGMA CAL	CAL VAL
-14505.0302	2.2535	11400.6

CHANNEL NO. 28 19602 1
09/19/86 R0908

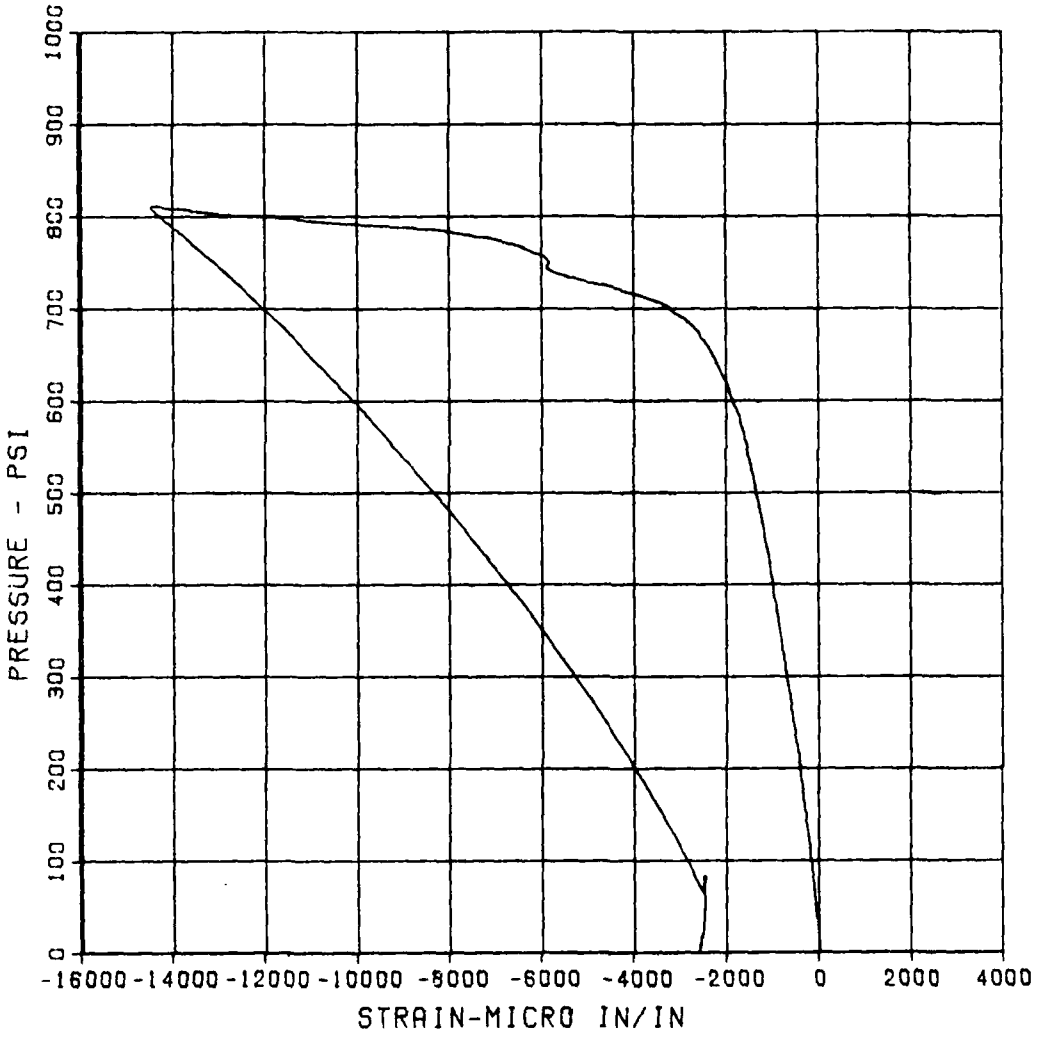

SBS ARCH TEST S-2
D-1

MAXIMUM	SIGNA CAL	CAL VAL
4.7085	2.8811	10.0

CHANNEL NO. 29 19602 1
09/19/86 R0908

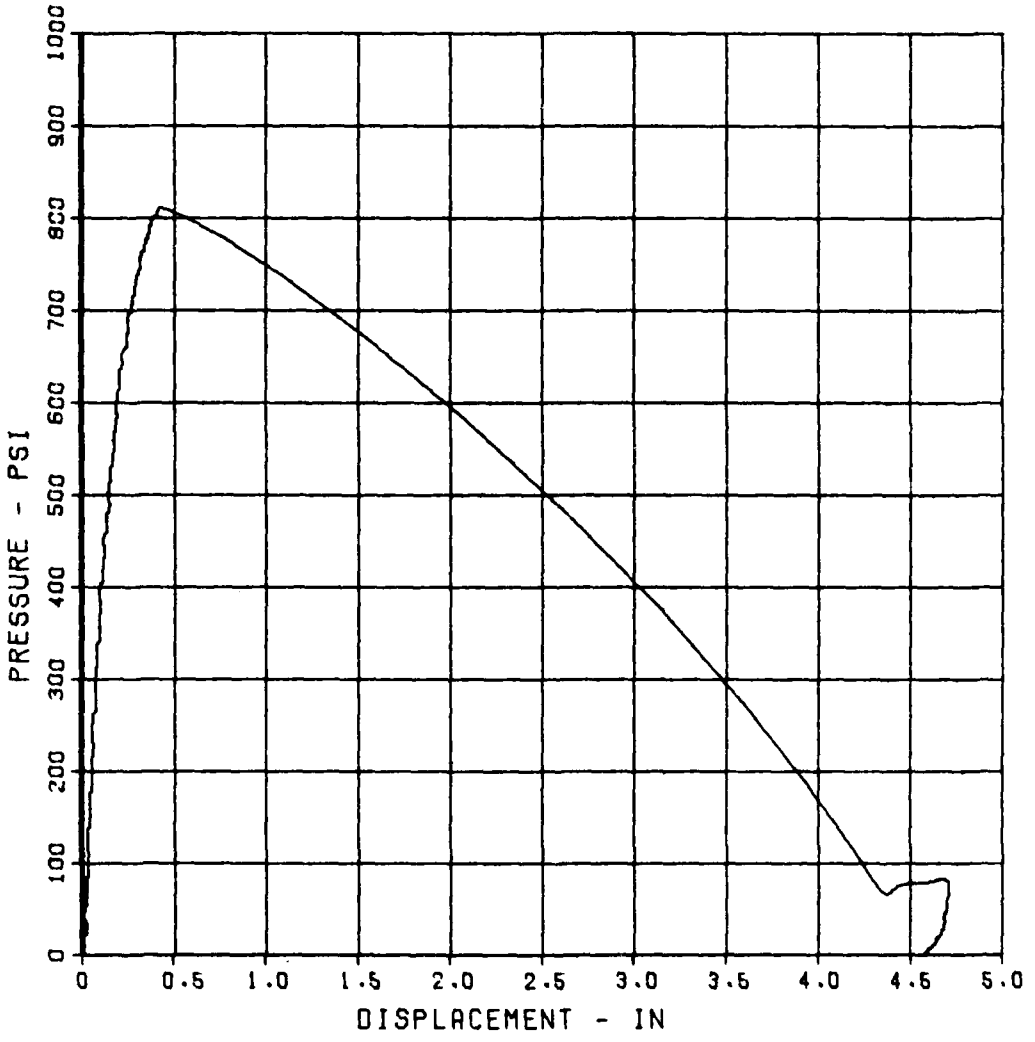

SBS ARCH TEST S-2
D-2

MAXIMUM	SIGMA CAL	CAL VAL
1.6830	2.6172	5.4

CHANNEL NO. 30 19602 1
09/19/86 R0908

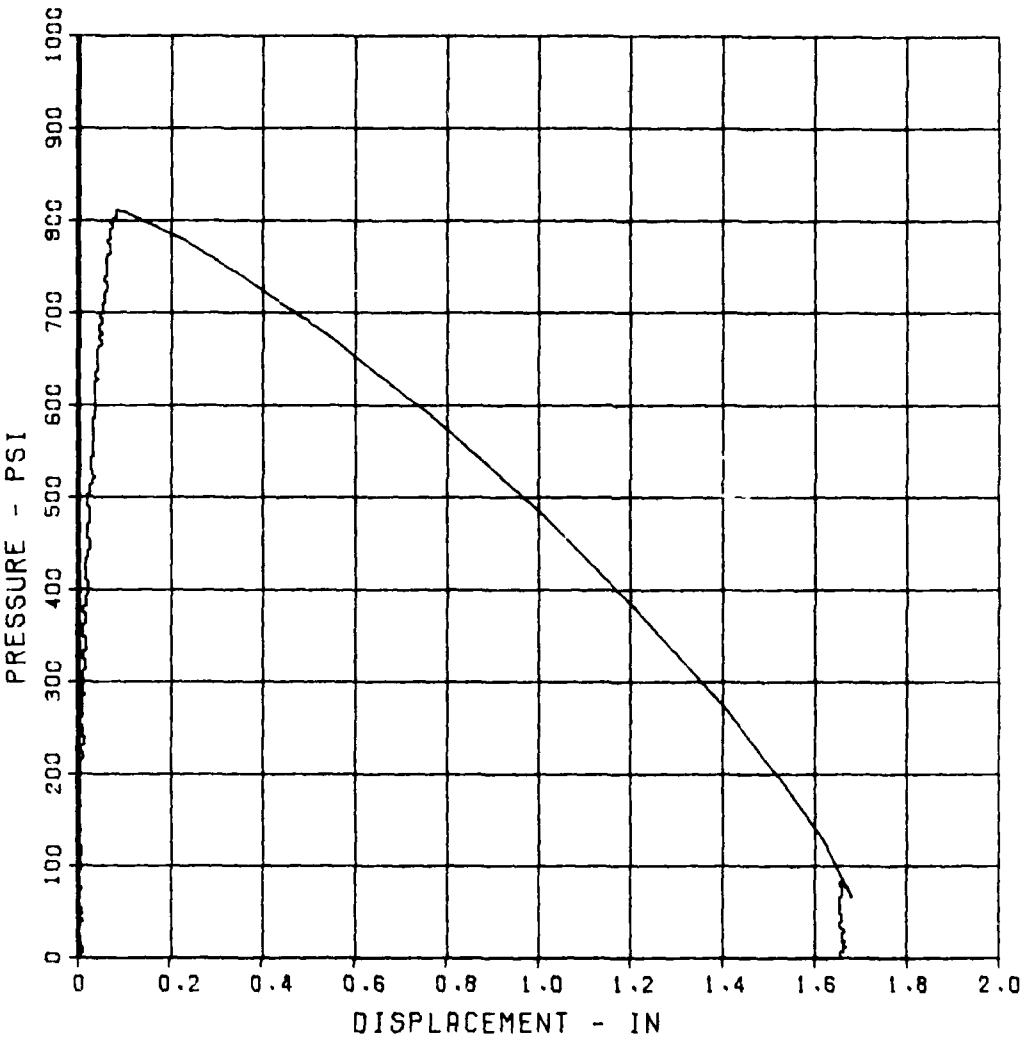

APPENDIX B: COMPUTER PROGRAM

```
      IF (OPT .EQ. 3) THEN
         NCURVS = NCURVS + 1
         CALL OVERLAY(NPTS,NCURVS,T,XM,THRUST)
         CALL PLOT(T,XM,THRUST,TITLE,ANS,NCURVS)
         ELSE
      END IF
      IF (OPT .EQ. 4) GOTO 10
      IF (OPT .EQ. 5) GOTO 20
      IF (OPT .EQ. 6) GOTO 120
      GOTO 105
C
  120 STOP
      END
C
C*********************************************************************
C
C CALCULATES CONCRETE STRESS IN EACH OF 100 LAYERS USING KENT-PARK MODEL
C AND RETURNS VALUES TO SUBROUTINE SUM
      SUBROUTINE CONC (FPC,EC,XINT,IFLAG,SIGC,BPP,SH,RHOS)
      IMPLICIT INTEGER *2(I-N)
C CALCULATE INITIAL TANGENT MODULUS AND UNLOAD SLOPE OF CONCRETE MODEL
      SLOPE = 1000.0*FPC
C
C COMPUTE CONCRETE STRESS (SIGC)
      IF(EC .GT. 0.002) GOTO 10
      SIGC = FPC *(2*EC/0.002-(EC/0.002)**2)
      IF (IFLAG .EQ. 1) RETURN
      GOTO 20
   10 ESOU = (3+0.002*FPC)/(FPC-1000.0)
      IF (RHOS .EQ. 0) THEN
      ESOH = 0.0
      ELSE
      ESOH = 0.75*RHOS*SQRT(BPP/SH)
      END IF
      Z = 0.5/(ESOU+ESOH-0.002)
      SIGC = FPC*(1-Z*(EC-0.002))
      IF (SIGC .LT. 0.20*FPC) SIGC = 0.2*FPC
      IF (IFLAG .EQ. 1) RETURN
   20 EC = EC-XINT
      STRESS = EC*SLOPE
      IF (STRESS .GT. 0.0) GOTO 30
      SIGC = 0.0
      RETURN
   30 IF(STRESS .GT. SIGC) GO TO 40
      SIGC=STRESS
      RETURN
   40 FELAS=0.3*FPC
      IF(XINT.EQ. 0.0 .AND. SIGC.LE. FELAS) RETURN
      XINT=XINT+EC-SIGC/SLOPE
      RETURN
      END
C
C*********************************************************************
C
C READS IN EXPERIMENTAL STRAIN DATA FROM 2 FILES
      SUBROUTINE DATA (TEO,SEO,TEI,SEI,ANS,NPTSO,NPTSI)
      IMPLICIT INTEGER *2 (A-Z)
      CHARACTER*1 ANS
      CHARACTER*10 FLNM1,FLNM2
      REAL TEO,SEO,TEI,SEI
      DIMENSION TEO(100),SEO(100),TEI(100),SEI(100)
C
C  SUBROUTINE TO READ EO & EI DATA FILES
C
      WRITE(6,*)'ENTER EO GAGE FILENAME => '
      READ(5,10) FLNM1
   10 FORMAT(A10)
      OPEN(8,FILE=FLNM1,STATUS='UNKNOWN',ERR=20)
      GOTO 30
   20 WRITE(6,*)'FILE OPEN ERROR: LINE 20'
   30 IF (ANS .EQ. 's' .OR. ANS .EQ. 'S') GOTO 35
      GOTO 50
   35 DO 40 I=1,100
      READ(8,*,END = 70) SEO(I), TEO(I)
   40 CONTINUE
   50 DO 60 I=1,100
      READ(8,*,END=70) TEO(I), SEO(I)
   60 CONTINUE
   70 NPTSO = I-1
      CLOSE (8)
      WRITE(6,*)'ENTER EI FILENAME => '
      READ(5,10) FLNM2
      OPEN (8,FILE=FLNM2,STATUS='UNKNOWN',ERR=20)
      IF (ANS .EQ. 's' .OR. ANS .EQ. 'S') GOTO 75
      GOTO 90
   75 DO 80 I=1,100
      READ (8,*,END=110) SEI(I), TEI(I)
   80 CONTINUE
```

```
   90 DO 100 I=1,100
      READ (8,*,END=110) TEI(I), SEI(I)
  100 CONTINUE
  110 NPTSI = I-1
      CLOSE (8)
      RETURN
      END
C
C*********************************************************************
C
      SUBROUTINE INPUT(FPC,FY,H,D,DP,RHO,IFLAG,ANS,BPP,SH,RHOS)
      IMPLICIT INTEGER *2 (I-N)
      CHARACTER*1 ANS
      WRITE(6,*)' '
      WRITE(6,*)'                    ****************************************.
     &************'
      WRITE(6,*)'                    CODE TO CALCULATE MOMENT-THRUST IN A CONC
     &RETE SECTION'
      WRITE(6,*)'                                FROM EXPERIMENTAL STRAINS'
      WRITE(6,*)'                    ****************************************
     &************'
      WRITE(6,*)' '
      WRITE(6,*)'NOTE: OUTPUT IS FOR A UNIT WIDTH OF THE SECTION '
      WRITE(6,*)' '
      WRITE(6,*)'OVERALL THICKNESS (IN) => '
      READ(5,*) H
      WRITE(6,*)' '
      WRITE(6,*)'EFFECTIVE DEPTH (IN) => '
      READ(5,*) D
      WRITE(6,*)' '
      WRITE(6,*)'STEEL RATIO EACH FACE => '
      READ(5,*) RHO
      WRITE(6,*)' '
      WRITE(6,*)'CONCRETE STRENGTH (PSI) => '
      READ(5,*) FPC
      WRITE(6,*)' '
      WRITE(6,*)'STEEL YIELD STRENGTH (PSI)  => '
      READ(5,*) FY
      WRITE(6,*)' '
      DP=H-D
      WRITE(6,*)'STIRRUP SPACING (ENTER 0 IF NO STIRRUPS) => '
      READ(5,*)SH
      WRITE(6,*)' '
      IF (SH .EQ. 0) GOTO 10
      WRITE(6,*)'WIDTH OF SECTION (IN) => '
      READ(5,*)W
      WRITE(6,*)' '
      WRITE(6,*)'AREA OF STIRRUPS (ONE LEG ONLY), (SQ IN) => '
      READ(5,*)ASTIR
      WRITE(6,*)' '
      WRITE(6,*)'CONCRETE COVER OVER STIRRUPS (IN.) => '
      READ (5,*) COV
      WRITE(6,*)' '
      BPP = W - COV*2
      HPP = H - COV*2
      RHOS = 2*ASTIR*(BPP+HPP)/BPP*HPP*SH
      GOTO 15
   10 RHOS = 0.0
   15 WRITE(6,*)'ENTER "1" TO NEGLECT STRAIN REVERSAL, "2" IF NOT =>
     &'
      READ(5,*) IFLAG
      WRITE(6,*)' '
      WRITE(6,*)'ENTER "D" FOR DYNAMIC OR "S" FOR STATIC DATA => '
      READ(5,'(A)') ANS
      WRITE(6,*)' '
      IF (ANS .EQ. 's' .OR. ANS .EQ. 'S') GOTO 20
      WRITE(6,*)'ENTER DYNAMIC INCREASE FACTOR => '
      READ(5,*)DIF
      WRITE(6,*)' '
      FPC=FPC*DIF
      FY=FY*DIF
   20 RETURN
      END
C
C*********************************************************************
C
      SUBROUTINE INTER(X,XRAY,YRAY,Y,NUM)
      IMPLICIT INTEGER *2 (I-N)
      DIMENSION XRAY(100),YRAY(100)
C
C  SUBROUTINE TO LINEARLY INTERPOLATE FOR Y AT X FOR UP TO
C  100 GIVEN POINTS(XRAY(I),YRAY(I))
C
      N=0
      DO 10 I=1,NUM
      N=N+1
      IF(X .GE. XRAY(I) .AND. X .LT. XRAY(I+1)) GO TO 20
   10 CONTINUE
C
      IF(X .GT. XRAY(NUM)) STOP 'RANGE OF DATA EXCEEDED IN INTER'
   20 Y=YRAY(N)+(X-XRAY(N))*(YRAY(N+1)-YRAY(N))/(XRAY(N+1)-XRAY(N))
      RETURN
      END
```

```
C
C*************************************************************************
C
      SUBROUTINE OVERLAY(NP,NCURVS,T,XM,THRUST)
      IMPLICIT INTEGER *2 (I-N)
      CHARACTER*10 FLNM6
      DIMENSION T(5,100),XM(5,100),THRUST(5,100)
C
      WRITE(6,*)' ENTER MOMENT-THRUST OVERLAY FILENAME => '
      READ(5,10)FLNM6
   10 FORMAT(A10)
      OPEN(8,FILE=FLNM6,STATUS='UNKNOWN',ERR=20)
      GOTO 30
   20 WRITE(6,*)' FILE OPEN ERROR (MOMENT-THRUST OVERLAY)'
   30 DO 40 I=1,NP
      READ(8,*) XM(NCURVS,I), THRUST(NCURVS,I)
   40 CONTINUE
      CLOSE(8)
      WRITE(6,*)' ENTER THRUST-PRESSURE/TIME OVERLAY FILENAME => '
      READ(5,10)FLNM6
      OPEN(8,FILE=FLNM6,STATUS='UNKNOWN',ERR=50)
      GOTO 60
   50 WRITE(6,*)' FILE OPEN ERROR (THRUST OVERLAY)'
   60 DO 70 I=1,NP
      READ(8,*) T(NCURVS,I), THRUST(NCURVS,I)
   70 CONTINUE
      CLOSE(8)
      WRITE(6,*)' ENTER MOMENT-PRESSURE/TIME OVERLAY FILENAME => '
      READ(5,10)FLNM6
      OPEN(8,FILE=FLNM6,STATUS='UNKNOWN',ERR=80)
      GOTO 90
   80 WRITE(6,*)' FILE OPEN ERROR (MOMENT OVERLAY)'
   90 DO 100 I=1,NP
      READ(8,*) T(NCURVS,I), XM(NCURVS,I)
  100 CONTINUE
      CLOSE(8)
      RETURN
      END
C
C*************************************************************************
C
      SUBROUTINE PFILE(NP,T,THRUST,XM,ANS)
C.....CREATES (X,Y) PLOT DATA FILE
      IMPLICIT INTEGER *2 (I-N)
      CHARACTER*1 ANS,ANS2
      CHARACTER*10 FLNM3,FLNM4,FLNM5
      DIMENSION T(5,100),XM(5,100),THRUST(5,100)
C
      WRITE(6,*)' ENTER MOMENT-THRUST OUTPUT FILENAME => '
      READ(5,10) FLNM3
   10 FORMAT (A10)
      OPEN(8,FILE=FLNM3,STATUS='UNKNOWN',ERR=20)
      GOTO 30
   20 WRITE (6,*)' FILE OPEN ERROR (MOMENT-THRUST)'
   30 DO 40 I=1,NP
      WRITE(8,*) XM(1,I), THRUST(1,I)
   40 CONTINUE
      CLOSE(8)
C
      IF (ANS .EQ. 'S' .OR. ANS .EQ. 's') THEN
      WRITE(6,*)' ENTER THRUST-PRESSURE FILENAME => '
      GOTO 50
      ELSE
      WRITE(6,*)' ENTER THRUST-TIME FILENAME => '
      END IF
   50 READ(5,10)FLNM4
      OPEN(8,FILE=FLNM4,STATUS='UNKNOWN',ERR=60)
      GOTO 70
   60 WRITE(6,*) 'FILE OPEN ERROR (THRUST)'
   70 DO 80 I = 1,NP
      WRITE(8,*) T(1,I), THRUST(1,I)
   80 CONTINUE
      CLOSE(8)
C
      IF (ANS .EQ. 'S' .OR. ANS .EQ. 's') THEN
      WRITE(6,*)' ENTER MOMENT-PRESSURE FILENAME => '
      GOTO 90
      ELSE
      WRITE(6,*)' ENTER MOMENT-TIME FILENAME => '
      END IF
   90 READ(5,10)FLNM5
      OPEN(8,FILE=FLNM5,STATUS='UNKNOWN',ERR=100)
      GOTO 110
  100 WRITE(6,*)'FILE OPEN ERROR (MOMENT)'
  110 DO 120 I = 1,NP
      WRITE(8,*) T(1,I),XM(1,I)
  120 CONTINUE
      CLOSE(8)
C
C WRITE TO MOMENT-THRUST TO SCREEN
  130 WRITE(6,*)'**THRUST AND MOMENT VALUES FOR UNIT WIDTH OF SECTION**'
```

```
      WRITE(6,*)' '
      IF (ANS .EQ. 'S' .OR. ANS .EQ. 's') THEN
      WRITE(6,*)'PRESSURE,PSI      THRUST,LBS.      MOMENT,IN-LBS.'
      ELSE
      WRITE(6,*)' TIME,SEC.        THRUST,LBS.      MOMENT,IN-LBS.'
      END IF
      DO 140 I=1,NP,5
      WRITE(6,150) T(1,I), THRUST(1,I), XM(1,I)
  140 CONTINUE
      PAUSE 'PRESS <ENTER> TO CONTINUE'
  150 FORMAT(1X,F10.6,6X,F10.2,6X,F10.2)
      RETURN
      END
C
C*********************************************************************
C
      SUBROUTINE STEEL(IFL,FY,E,RHO,DEP,XINT,F,II,EREF,RELE,STRESS,ORIG)
      IMPLICIT INTEGER *2 (I-N)
      EY=FY/29000000.
C
      IF (II .EQ. 1) RELE = E
      IF (II .EQ. 1) EREF = E
      IF (RELE .LT. 0.0) GOTO 10
      IF (E .LT. EREF) GOTO 30
      GOTO 20
   10 IF (E .GT. EREF) GOTO 30
   20 IF (-.00000001 .LT. ORIG .AND. .0000001 .GT. ORIG) GOTO 25
      RELE = RELE + E - EREF
      GOTO 26
   25 RELE = E
   26 EREF = E
      GOTO 40
   30 PRELE = RELE
      RELE = E-XINT
      IF (EREF .LT. 0.0 .AND. RELE .GT. EY)THEN
      EREF = E
      ORIG = XINT
      ELSE IF (EREF .GT. 0.0 .AND. RELE .LT. -EY)THEN
      EREF = E
      ORIG = XINT
      ELSE IF (EREF .EQ.0.0) THEN
      GOTO 35
      ELSE
      END IF
      GOTO 40
   35 IF (PRELE .LT. 0.0 .AND. RELE .GT. 0.0) GOTO 36
      IF (PRELE .GT. 0.0 .AND. RELE .LT. 0.0) GOTO 36
      GOTO 40
   36 EREF = E
      ORIG = XINT
   40 IF (IFLAG .EQ. 1) RELE = E
C
      ABSE=ABS(RELE)
      IF(ABSE .LE. EY) STRESS=29000000.*ABSE
      IF(ABSE .GT. EY .AND. ABSE .LE. .01) STRESS=FY
      IF(IFLAG .EQ. 2 .AND. EREF .GE. 0.0) GOTO 50
      IF(IFLAG .EQ. 2 .AND. EREF .LE. 0.0) GOTO 60
      GOTO 65
   50 IF(RELE .GT. 0.0 .AND. RELE - (EREF-XINT) .LT. -0.000001) THEN
      STRESS = 29000000.*RELE
      GOTO 70
      ELSE
      END IF
   60 IF(RELE .LT. 0.0 .AND. RELE - (EREF-XINT) .GT. 0.000001) THEN
      STRESS = 29000000. * RELE
      GOTO 70
      ELSE
      END IF
C
C  CALCULATE PARAMETERS FOR NONLINEAR PORTION
   65 D=(0.75-FY/150000.)/4.05/10.**9
      C=-(165000.*D+1./120000.)
      B=FY/150000.+7.05*10.**9*D+11./12.
      A=FY-10000.*B-10000.*10000.*C-10000.**3*D
C
      ABSE = ABSE*1000000.0
      STRES2=A+ABSE*B+ABSE*ABSE*C+ABSE**3*D
      ABSE = ABSE/1000000.0
      IF(ABSE.GT. 0.01 .AND. ABSE.LT. 0.1) STRESS=STRES2
      IF(ABSE .GE.0.1) STRESS=1.6*FY
      IF(RELE .LT. 0.0) STRESS=-STRESS
   70 IF (EREF .EQ. E) XINT = EREF - STRESS/29000000
C-----------------------------------------------------------------
C     WRITE(6,*)'STRESS = ',STRESS
C     WRITE(6,*)'DEP= ',DEP
C-----------------------------------------------------------------
      F=RHO*DEP*STRESS
C
      RETURN
      END
```

```
C
C*********************************************************************
C
      SUBROUTINE SUM(IFLAG,XK,EO,FPC,H,XINTC,FC,XMC,BPP,SH,RHOS)
      IMPLICIT INTEGER *2 (I-N)
      DIMENSION XINTC(100)
      N=0
      DX=H/100
      SUM1=0.
      SUM2=0.
      DO 100 II=1,199,2
      X=II*DX/2.
      N=N+1
      EC=-(EO+XK*X)
      IF(EC.GT.0.0) GO TO 10
      SIGC=0.0
      GO TO 20
   10 CALL CONC(FPC,EC,XINTC(N),IFLAG,SIGC,BPP,SH,RHOS)
   20 SUM1=SUM1+SIGC
      SUM2=SUM2+X*SIGC
  100 CONTINUE
      FC=-SUM1*DX
      XMC=-SUM2*DX
      RETURN
      END
C MENU OF OPTIONS FOR MOMENT-THRUST PROGRAM (27 FEB. 1987)
      SUBROUTINE MTMENU(OPT)
      INTEGER  OPT
      CALL CLRSCR
      WRITE(*,'(/,20X,''        OPTIONS'')')
      WRITE(6,*)' '
      WRITE(*,'(/,20X,''1. Save Values to a Plot File'')')
      WRITE(*,'(/,20X,''2. Plot Curve(s)'')')
      WRITE(*,'(/,20X,''3. Plot Overlay Curve(s)'')')
      WRITE(*,'(/,20X,''4. Run a Complete New Problem'')')
      WRITE(*,'(/,20X,''5. Run With New Strain Data Only'')')
      WRITE(*,'(/,20X,''6. Return to DOS'')')
      WRITE(6,*)' '
      WRITE(6,*)' '
      WRITE(*,'(/,20X,''ENTER OPTION NUMBER => '')')
      READ(5,*)OPT
      CALL CLRSCR
      RETURN
      END
```

APPENDIX C: NOTATION

A_c	Cross-sectional area of concrete
b''	Width of confined core
C_a	Soil arching ratio
D	Outside arch diameter
d	Depth to tension steel
d'	Depth to compression steel
E_h	Strain hardening modulus
E_s	Modulus of elasticity for steel reinforcing
F_c	Force in concrete
F_s	Force in tensile steel
F'_s	Force in compression steel
f'_c	Concrete strength
f_u	Ultimate stress
f_y	Steel yield strength
h	Overall height of the concrete section
K	Lateral earth pressure coefficient
k	Stiffness
k_x	Distance from compression face to F_c
M	Bending Moment
m	Mass
P	Thrust
P_o	Ultimate thrust in pure compression
p	Pressure
q_{y_c}	Ultimate resistance
R	Roughness
R_R	Relative Roughness
r	Arch radius
S_h	Spacing of hoops
T	Natural period
X	Distance to neutral axis
$Y_{elastic}$	Deflection at ultimate resistance
δ	Interface friction angle
Δ	Relative crown displacement
ϵ_c	Concrete strain
ϵ_h	Strain at onset of hardening

ε'_s	Compression steel strain
ε_s	Tensile steel strain
ε_u	Ultimate
θ	Soil friction angle
ρ_s	Ratio of volume of transverse reinforcement to volume of concrete core
ρ_t	Total steel ratio
μ	Coulomb friction coefficient